FERMI LIQUID THEORY OF THE STRONGLY INTERACTING QUANTUM RC CIRCUIT

Michele Filippone

École Normale Supérieure **Département de physique**

laboratoire pierre aigrain
électronique et photonique quantiques

THÈSE DE DOCTORAT

EN VUE DE L'OBTENTION DU GRADE DE

DOCTEUR DE L'ÉCOLE NORMALE SUPÉRIEURE

ÉCOLE DOCTORALE DE PHYSIQUE DE LA RÉGION PARISIENNE - ED 107

SPÉCIALITÉ : PHYSIQUE QUANTIQUE

PRÉSENTÉE ET SOUTENUE PAR:

MICHELE FILIPPONE

LE 13 SEPTEMBRE 2013

TITRE

FERMI LIQUID THEORY OF THE STRONGLY INTERACTING QUANTUM RC CIRCUIT

Unité de recherche : UMR 8551

Membres du jury

M. Christophe Mora	Directeur de Thèse
Mme Janine Splettstößer	Rapporteuse
M. Manuel Houzet	Rapporteur
M. Pascal Simon	Président
M. Thibaut Jonckheere	Examinateur
M. Xavier Leyronas	Examinateur
Mme Karyn Le Hur	Membre invitée

Remerciements

Même si cette thèse a été rédigée en anglais, ce serait quand même dommage de ne pas laisser un petit souvenir de mon fragile français, cause de tant de moments d'hilarité pendant ces belles années passées en France.

Je tiens à remercier tout d'abord les membres du jury pour avoir accepté d'assister à ma soutenance. Merci aux rapporteurs Janine Splettstößer et Manuel Houzet avec lesquels j'ai aimé discuter et qui ont apporté des remarques précieuses sur mon travail et le manuscript. Merci aussi à Xavier Leyronas, qui m'a vraiment touché en rappellant (avant les questions) que le sujet de mon examen à son cours était exactement sur le modèle d'Anderson(!). Merci à Thibaut Jonckheere avec lequel je continue à discuter avec plaisir et à Pascal Simon pour avoir accepté le rôle de président du jury.

Difficile de trouver les paroles de remerciement pour Markus Büttiker, obligé d'annuler sa participation à cause de graves problèmes de santé et dont on a appris avec tristesse le décès. Ce travail de thèse n'aurait même pas été imaginable sans sa formidable contribution à la compréhension des phénomènes de transport mésoscopique. Ça aurait été pour moi un grand honneur de le connaître et de lui présenter mon travail.

Merci à Karyn Le Hur, qui a constamment suivi mon travail de thèse, toujours contribué avec des idées excellentes et soutenu pendant ma recherche de post-doc. La qualité de mon travail aurait été sans doute moindre sans sa contribution.

O Captain! My Captain! Our fearful trip is done! La plus grande reconnaissance va à Christophe Mora, qui m'a véritablement guidé dans un parcours de maturité scientifique et modifié en profondeur mon attitude par rapport à la science. Il a passé tellement de temps à écouter mes délires, qu'il a même commencé à utiliser mes expressions (incorrectes) en français!

Je crois de ne surprendre personne en disant que ça a été une expérience magnifique de faire partie du Laboratoire Pierre Aigrain. C'est un lieu lieu où l'on rencontre des personnes aux grandes qualités tant humaines que scientifiques. Merci à Jean-Marc Berroir pour m'avoir accuelli au sein du labo, organisé le foot et avoir rendu possible tous mes voyages, qui restent les expérience les plus marquantes de ma thèse. Merci à Fabienne Renia et à Anne Matignon, chez qui j'ai toujours aimé papoter sous prétexte de problèmes administratifs . Je suis très fier d'avoir été choisi par Fabienne pour organiser les équipes du tournoi de foot! Merci à Nicolas Regnault: une personne d'une sympathie et hospitalité incroyable et c'est sans doute grâce à lui si tous mes stages, à partir de mon arivée à l'ENS, se sont révélé toujours un très bon choix.

Merci à Takis Kontos, Benjamin Huard, Gwendal Fève et Bernard Plaçais avec lesquels ça a été toujours très stimulant de pouvoir discuter de mon travail.

Maintenant la partie difficile...

Ce que je ne tiens vraiment pas à remercier est le Grand Hall. Faire une thèse en physique théorique à côté d'un rouleau transporteur qui fait un bruit infernal c'est quelque chose de vraiment compliqué. Par contre, je ne peux pas oublier toutes les autres magnifiques personnes qui y ont passé leur temps à le détester avec moi. Merci Antoine Sterdyniak (pas possible sans toi), Simon Huppert (et Leila aussi!), Pierrick Cavalie (qui j'espère va trouver une maison), Camille Ndbeka-Bandou (et les cadeaux du Japon), Jean Maysonave, Matthieu Baillergeau, Cécile Repellin, Julien Madeo, Giovanni Pizzi, Riccardo Cardenas, Dimitri Oustinov et tous les collègues en biophysique! Merci Kenneth Maussang!!! T'as pas raté une seule occasion pour me rappeler que j'arrivais tard au labo le matin et merci aussi à FR Jasnot, Joshua Freeman, Sarah Houver, Sukhdeep Dillon, Philippe Campagne, Emmanuel Flurin, Erwan Bocquillon, Matthieu Delbecq, Jeremy Viennot, Dora Crisan, David Brunel, Vincenzo Ardizzone, Fabien Vialla, Vincent Freulon, Djamal Gacemi et François Mallet.

Merci à Claude Dodray et à Jean-Charles Dumont, qui m'ont supporté dans leur bureau pendant que je blasphémais sur mes feuilles tout seul en italien (j'espère qu'ils n'ont jamais compris ce que je disais). Jean-Charles, qui, pour qui ne le connaît pas, est le génie maléfique derrière toute l'histoire de l'imprimante "en couleur", qui me suivra pour toute ma vie.

Merci à tous les jeunes "séminaristes" condmat Tristan Benoist, Alexander Dobrinievski, Swann Piatecki, Romain Vasseur, Eric Vernier et Sophie Rosay. Je suis vraiment fier de notre petit séminaire en autarcie, que la direction du département a toujours réfusé de financer!

Merci aux copains des repas à "La Montagne" le vendredi midi: Adam Rançon, Florian Haas et Gatien Verley... maintenant que j'y pense... "La Montagne" mérite un merci spéciale pour elle toute seule aussi.

Buffalo! à tous les amis du "master LPA" Benjamin Langlois, Lauriane Chomaz, Romain Hivet, Diego Guenot, Pu Jian, Théo Rybarczik, Raul Teixeira, Alex Baksic.

J'embrasse très très fort aussi les amis de la première heure à l'ENS: Aldo Riello, David Waszeck, Éliane de Larminat, Marine Bellégo, Julius Bonart, Riccardo Barontini et Marco Jalla.

Le plus méchant plaquage au Paris Olympique Rugby Club, mieux nommé le P.O.R.C. !!!! C'est la dédans que j'ai appris à parler français à partir de mes années "porcelettes" et je pense que cela s'entends... mon plus beau souvenir sans doute.

Petite parenthèse pour les amis italiens...

Grazie Matte, Dima e Dave! Vivere con voi è stato fantastico e vedete di venire presto a

Berlino. Forse dovrei anche metterci il buon Carlo Donvito che ha dormito per terra in camera mia per 4 mesi!! Grazie anche a tutti gli amici di Bologna e non: Drogy, Udge, Finch, Palmio, Giovanni, Gabriele, che sono saliti a Parigi solo per mangiare e bere a mie spese (Jenga ti voglio bene anche a te!) Un abbraccio anche a tutti i collegiali sparsi per il mondo: Umberto Marengo, Andrea Garnero, Valentina Montalto, Gianandrea Lanzara, Luca Marcolin, Daniele Pinna, Matteo Morigi e Fabrizio Minganti.

Ovviamente grazie mamma, grazie papà e grazie Alessandra!

Toute cette petite parenthèse linguistique, c'était en réalité pour mettre un peu plus en valeur la toute dernière personne de la liste.Un prodige. On reviendra donc au français, même si elle a toujours préféré que je ne le parle pas correctement...

Merci Nicole.

CONTENTS

INTRODUCTION

Mesoscopic physics can be viewed as the study of transport and manipulation of electrons in solid-state systems in analogy with photons in vacuum. A major goal in this field is to observe and control quantum coherence effects on *macroscopic* quantities, such as the electric current in engineered on-chip devices. The main challenge is to preserve the phase-coherence of electron wave packets when flowing through a conductor. This means that the only effect for the wave packet $|\Phi\rangle$ of an electron traversing the conductor is to add an overall phase $\phi(l)$ depending on the path l which has been covered. The general idea is pictured in Fig. I. As a quantum particle can cover coherently different paths simultaneously, the wave-packet can acquire different phases, engendering interference effects typical of quantum mechanics.

The possibility to realize this situation is non-trivial for electrons propagating in solid-state devices such as semi-conductors. There are various physical effects responsible for the loss of phase-coherence and they are partly pictured on the right part of Fig. I. Decoherence is essentially caused by the interaction of electrons with their environment. This includes interactions with other electrons, magnetic impurities and the phonons corresponding to the vibration modes of the underlying crystal. This does not prevent to define a typical length scale below which electrons keep their phase coherence. This quantity is the *phase coherence length* L_ϕ [1] and defines the *mesoscale*: the domain of validity of all the experimental and theoretical studies carried out in mesoscopic physics. The interest in observing phase-coherent phenomena on electron transport has then spurred the technological progress of these last thirty years in nano-fabrication, to clean samples, and cryogenics, to lower temperatures down to the milli-Kelvin. Electron-electron interactions are a fundamental obstacle to the preservation of coherence in bulk metals at very low temperature. They affect the *coherence time* τ_ϕ of electron wave packets depending on the dimensionality of the system. For

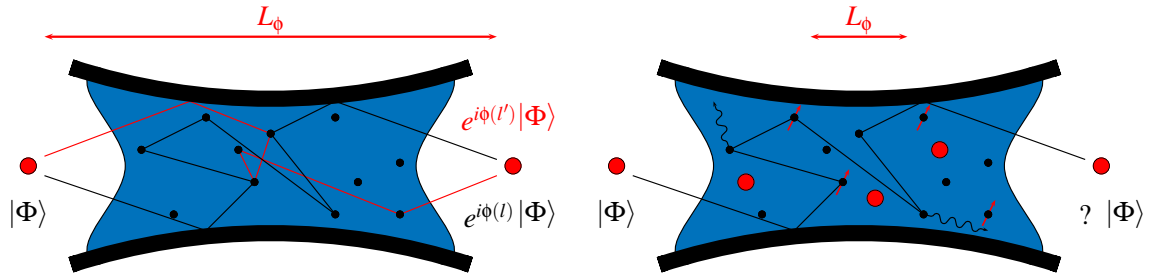

Figure I: Left) Ideal situation of mesoscopic physics. If phase coherence is preserved, the only effect on the wave function $|\Phi\rangle$ of electrons propagating in a solid-state system (here a 2DEG) is to acquire a well-defined phase $\phi(l)$. This phase depends on the path l which has been covered. Quantum particles can cover coherently different paths at the same time, leading to different phases which are responsible for the interference effects typical of quantum mechanics. Right) Effects responsible for the loss of quantum coherence, essentially electron-electron / electron-phonon / electron-magnetic disorder interactions. All these processes cause decoherence on typical length scales L'. It is then possible to define a phase-coherence length $L_\phi \ll L'$ below which electron propagation is phase coherent.

quasi-1D systems the decoherence time scales with the temperature as [2]

$$\frac{1}{\tau_\phi} = AT^{2/3} + BT^3\,, \tag{i}$$

with A and B non-universal parameters depending on the sample. The first term, which dominates at low temperatures, corresponds to the dephasing caused by electron-electron interactions, while the second term, governing the behavior of τ_ϕ at high temperatures, corresponds to the dephasing caused by electron-phonon interactions. The experimental validity of Eq. (i) was proven in Ref. [3] by performing magneto-resistance measurements on quasi-1D metallic wires composed of different metals. The results are reported in Fig. 2(a). The saturation of the coherence time at lower temperatures is caused by the interaction of electrons with magnetic impurities [4, 5, 6], leading to Kondo physics[1], see Fig. 2(b). For disordered samples, the propagation of electron wave packets is diffusive and the phase coherence length is given by the diffusion relation

$$L_\phi = \sqrt{\mathbf{D}\tau_\phi}\,, \tag{ii}$$

where $\mathbf{D} = v_F l_e/d$ is the Einstein relation for the diffusion constant $\mathbf{D}$, with v_F being the Fermi velocity, l_e the mean-free path and d the dimensionality of the sample. Looking at Figs. 2(a) and 2(b), we can consider phase-coherence times of the order $\tau_\phi \sim 10$ ns. In the experiment of Ref. [5], $\mathbf{D} \sim 0.029$ m^2/s and Eq. (ii) sets a phase coherence length $L_\phi \sim 1$ μm.

[1] Kondo physics is a prominent topic of this Thesis and we will discuss it extensively in Chapter 4.

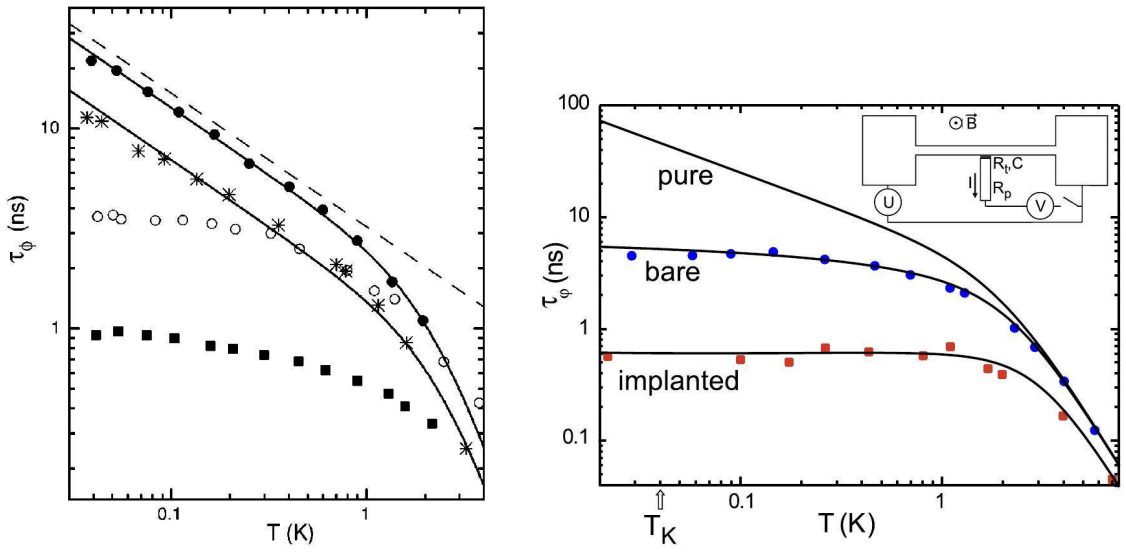

(a) (b)

Figure II: a) Measurements of the phase coherence time τ_ϕ from the magneto-resistance measurements in Ref. [3]. Measurements are carried out for wires composed of silver (•), less pure silver (∘), gold (∗) and copper (■) and they are compared to Eq. (i). *The dashed line plots the first term in Eq.* (i), *while the behavior at large temperatures is governed by the second term in Eq.* (i). *The coherence times are in extremely good agreement with Eq.* (i) *for silver and gold, while sizable deviations are observed at small temperatures for the less pure silver and copper. b) Same measurements from Ref. [5] carried out for different silver wires with different manganese (Mn) doping, "bare" and "implanted" respectively. The behavior of the coherence time is different from the "pure" behavior described by Eq.* (i). *The "bare" and "implanted"solid lines fit the experimental data if the corrections to Eq.* (i) *brought by Kondo correlations are taken into account [4, 6]. T_K is the Kondo temperature.*

For the purposes of this Thesis, the case of the two-dimensional electron gas (2DEG) is especially relevant. It was involved in the first experimental realization of the quantum RC circuit [7, 8], that we address theoretically in this Thesis. For a 2DEG, the first term of Eq. (i) vanishes linearly with the temperature T [9]. For a perfectly clean sample ($k_F l_e \gg 1$) the propagation of electrons is *ballistic* and the phase coherence length is then obtained from the phase coherence time τ_ϕ through the relation

$$L_\phi = v_F \tau_\phi \,. \tag{iii}$$

In the experimental conditions of Refs. [7, 8], at $T = 1$ K, L_ϕ was estimated to be of the order of $\sim 200\ \mu$m, while samples are of the order of $\sim 10\ \mu$m. Below these length scales, the propagation of electrons is phase coherent. One of the first and most striking demonstrations of emergent phase coherent phenomena in the quantum transport of electrons was given by Webb and collaborators in their works starting in 1985. Measuring the conductance of a

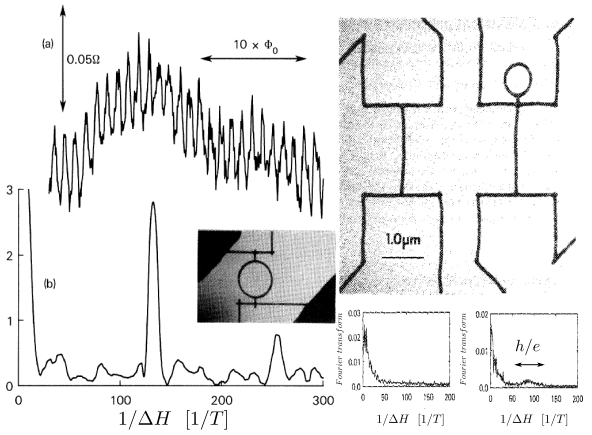

Figure III: Aharonov-Bohm effect on the conductance of a mesoscopic circuit. Left) Experiment of Ref. [11]. The conductance of a gold ring oscillates as a function of the magnetic field, with periodicity fixed by $\Phi_0 = 2\phi_0$, twice the quantum of flux $\phi_0 = h/2e$ through the ring. The oscillations result in a pronounced peak in the Fourier transform. Right) Experiment of Ref. [12]. The peak appears even for a ring external to the circuit, a sign of the non-locality of quantum transport.

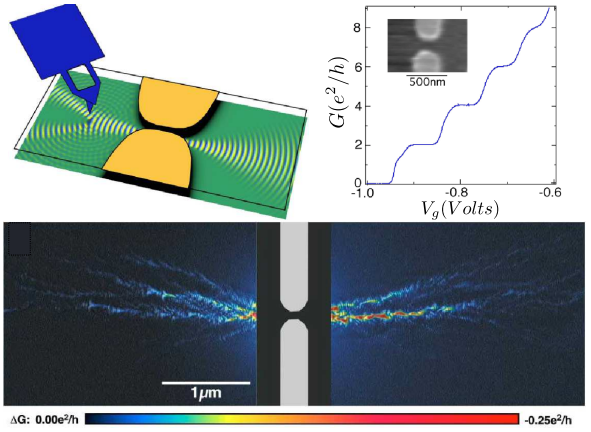

Figure IV: Conductance quantization in 2DEGs connected by a QPC. The conductance increases by finite quanta of $2g_0 = 2 \times e^2/h$ as a function of the applied gate voltage V_g on the QPC. The factor 2 comes from spin degeneracy of electrons. A scanning probe microscope measures the local conductance of electrons, accessing local properties of quantum coherent transport. All images are extracted from Ref. [13].

gold ring as a function of the magnetic field, they observed periodical oscillations by varying the magnetic flux inside the ring [10, 11], see Fig. III. This was a clear consequence of the Aharanov-Bohm effect on the electron transport in the gold wire, an exquisite phase coherent effect. They also pointed out the non-locality of quantum transport. They showed that the conductance of a phase-coherent circuit is sensitive to the magnetic flux through an external connected ring [12], as pictured in Fig. III, which has no classical counterpart. This engendered a real change of paradigm in the theory of quantum circuits with respect to classical ones. The *conductivity*, a local quantity, lost its interest with respect to the *conductance* of the whole device, sensitive to non local effects. We mention in passing that recent experiments, reported in Fig. IV, imaging spatial current paths with scanning probe microscopes [13, 14, 15], motivate a renewed interest in local properties of quantum transport [16].

Another striking manifestation of quantum coherence effects in mesoscopic devices is conductance quantization. The most paradigmatic example involves 2DEGs separated by a quantum point contact (QPC) [17, 18], also illustrated in Fig. IV. 2DEGs are realized by confining electrons along a spatial dimension in the quantum well which can be engineered at the contact between two different hetero-structures (*Ga-As* and *Ga-Al-As* in Refs. [7, 8]). A

QPC is realized by putting on top of the 2DEG two metallic plates as sketched in Fig. IV. When charged with a negative potential, these plates deform the underlying electron gas controlling its shape. The gas can be cut in two and electron transfer is possible only by tunnel effect. These mesoscopic constrictions are much smaller than L_ϕ and current flows through them violating Ohm's law. The conductance of the system does not increase linearly with the applied bias, but by universal quanta of $g_0 = e^2/h$, multiplied by a factor two if electrons are spin degenerate. Analogously, the same phenomenon is observed by gradually opening the QPC at fixed bias, see Fig. IV. Alternative experiments observe the same phenomenon by mechanically breaking the contact between two bulk metals up to reducing it to a single atom [19], in quantum wires [20] and carbon nanotubes [21].

A further remarkable manifestation of the quantum of conductance g_0 arises for the conducting edges of topological insulators [22]. These exotic states of matter are characterized by the non-trivial topology of their band structure, quantified by the Chern invariant [23]. The transition from a topological to a trivial insulator, as the ionic insulator, where all electrons are bond to nuclei, enforces the closing of the gap at the boundaries. A robustly quantized number of zero energy states appears then at the edges. Whereas the bulk remains insulating, they are conducting channels, which were first observed in 2DEGs under strong perpendicular magnetic fields as a manifestation of the integer [24] and fractional [25] quantum Hall effect. The integer quantum Hall edges are pictured in the framework of the quantum RC circuit in Figs. V and VI. Their conductance is g_0 and they are chiral, that is charge carriers can move only in one sense depending on the orientation of the perpendicular magnetic field. The discovery of non trivial topological states of matter in the absence of a magnetic field, giving rise to the quantum spin Hall effect [26, 27], has completely revitalized the field. The restoring of time-reversal symmetry and spin-orbit coupling for electrons are responsible for the appearance of two helical counter-propagating edge modes at the boundaries. In these states electrons of opposite spin flow in opposite directions. Pure spin currents can be observed without a net charge flow. This could provide further implementation of the quantum RC circuit that we outline in the Conclusion.

All these experiments deal with the stationary properties of quantum transport, which is conveniently described by the Landauer-Büttiker scattering theory. This theory describes electron propagation as diffusive wave packets [28, 29, 30] and we illustrate it in Chapter 1. Recent technological progress paved the way to the possibility of controlling and probing in real time the phase-coherent evolution of quantum devices such as quantum dots and superconducting circuits, an important requirement for the implementation of quantum information protocols. The engineering of local Coulomb potentials in semiconductors succeeded in manipulating single electrons and spins confined in the three spatial dimensions. Regions of confinement can reach the order of the nano-meter and behave as highly tunable artificial impurities, so called quantum dots. Quantum dots can be engineered by confining regions of

the order of the μm in 2DEGs [31], or by connecting leads with carbon nanotubes [32] or single atoms [33], see Fig. VII. Since the pioneering proposal by Loss & DiVicenzo [34], coupled single-electron quantum dots have been revealed to be promising candidates to become the building block of a quantum processor. In spite of the stronger coupling of solid-state qubits to their electronic environment, the possibility to perform fast operations (frequencies above the GHz) on these systems [35] allows for the coherent manipulation of coupled electron spins [36]. This same issue is being addressed with different devices in the field of circuit quantum electrodynamics (Circuit-QED). These architectures [37] involve two-level artificial atoms composed of superconducting Josephson junctions coupled to photon resonators. These on-chip systems compete nowadays with experiments performed with real atoms in cavity-QED setups [38, 39]. Coherence and relaxation times of the order of the μ-second have been reached for transmon qubits [40], arbitrary quantum states of light can be synthesized in the resonator [41] and the trajectories of the qubit stabilized relying on quantum feedback [42]. Quantum dot circuits and circuit-QED architectures have been recently cross coupled in new experimental setups. On-chip microwave resonators are coupled to quantum dots, allowing for the simultaneous and entangled measurement of electron and photon transport in phase-coherent nanodevices [43, 44, 45, 46], see also Fig. VIII.

In this framework, it is an important task to investigate the typical time scales governing the dynamics of single electrons in quantum coherent devices. This problem has been directly addressed by the theoretical and experimental study of the *quantum RC circuit*. Its first experimental realization, carried out at the Laboratoire Pierre Aigran (LPA) in 2006 by Gabelli and collaborators [7], is pictured in Fig. V. A two-dimensional electron gas in a strong perpendicular magnetic field is in the integer quantum Hall regime. Only the edge states of the sample allow for electron transport and exchange coherently electrons with a quantum dot through a quantum point contact. A metallic gate is placed on top of the quantum dot without the possibility of exchanging electrons with it. The peculiarity of this system is that it does not allow for the stationary transport of current. A current can be measured only when the system is dynamically driven by a time-dependent gate potential. In Chapter 1, we discuss in detail that, when driven at low frequencies, the system has the same behavior as a classic RC circuit. For this reason, the device of Fig. V is also called the *mesoscopic capacitor*. This device has remarkable properties, predicted in the seminal works by Büttiker and collaborators [48, 49, 50, 51, 52]. It displays a *quantum capacitance* $C_q = e^2\mathcal{N}(E_f)$, proportional to the local density of states $\mathcal{N}(E_F)$ in the quantum dot at the Fermi energy E_F. Its resistance is called the *charge relaxation resistance* and it is universally quantized to $R_q = h/2e^2 \simeq 12.9\ \mathrm{k}\Omega$, see also Figs. 1.5 and 1.6. The interest in this last quantity resides in the fact that its value is different from that observed in direct current (DC) experiments $R_{\mathrm{DC}} = h/De^2$, which depends on the transparency D of the quantum point contact. R_q is then a new fundamental quantity connected to the coherent dynamics of electrons in phase coherent systems. Its appearance

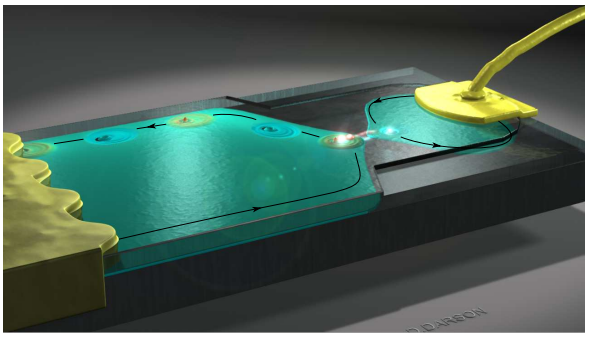

Figure V: Experimental realization of the quantum RC circuit [7]. The integer quantum hall edge states of a two-dimensional electron gas exchange electrons through a quantum point contact with a quantum dot. The quantum dot is coupled capacitively to a top metallic gate driven by the gate voltage V_g. The charge relaxation resistance of the circuit is universally quantized to $R_q = h/2e^2$. Courtesy of David Darson, LPA.

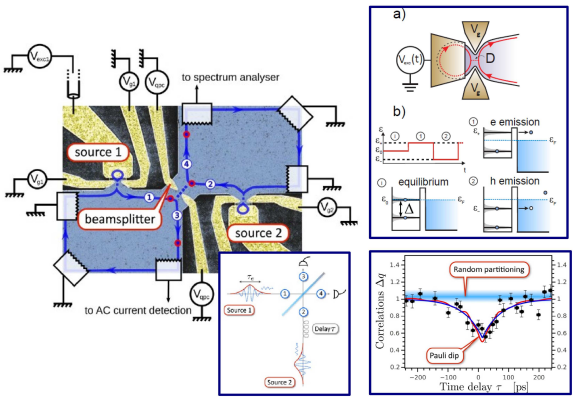

Figure VI: Hong-Ou-Mandel interference experiment from Ref. [47]. In the top-right, the working principle of the quantum RC circuit as a single electron emitter (see main text). Electrons are emitted with a time delay τ on the same QPC working as a beam splitter. In the bottom-right, the fermionic nature of electrons causes a suppression of the current noise when electrons arrive on the QPC at the same time.

is a consequence of the violation of the classical Kirchhoff's laws in phase coherent devices. This is a further example of the non-locality of electron transport in phase-coherent devices: the conductance of a resistive circuit component (the quantum point contact) is different whether the systems is driven by a DC or an AC bias. This device has also been suggested to be relevant for the non-invasive charge readout in quantum dot devices [53] and for the detection of topological excitations [54, 55]. The *RC* time of the circuit provides a time-scale for the electron coherent dynamics. The investigation of the mesoscopic capacitor in the non-linear regime has revealed an efficient tool for the triggered emission of single electron wave packets [56]. Its working principle is illustrated in Fig. VI. A sudden variation of the gate potential V_g quenches the discrete levels of the dot, causing the time-controlled emission of an electron in the nearby integer quantum Hall edge. A variation of the opposite sign of V_g brings the same level below the Fermi energy, ensuring the emission of a hole in the edge. This led to the realization in nanodevices of the electron analog of quantum optics experiments previously done with single quantum particles in the vacuum, that is Hanbury-Brown and Twiss [57, 58] and Hong-Ou-Mandel [47] interference experiments, see Fig. VI.

This Thesis addresses the problem of the effect of electron-electron interactions in the quantum dot on the conduction properties of the quantum RC circuit. Quantum dots are almost zero-dimensional structures in which electrons are close to each other and Coulomb

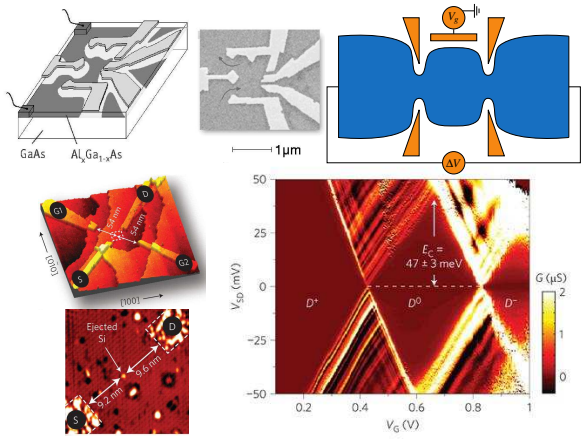

Figure VII: Top) Quantum dots engineered by putting negatively charged metallic plates on top of a 2DEG. The first two images are extracted from Ref. [31]. Bottom) Coulomb blockade observed for the conductance through a quantum dot composed of silicon atoms exchanging electrons with leads [33]. Restricting to the case of small V_{SD} biases, the conductance is completely suppressed for a quantized number of charges on the dot and displays a peak at the charge degeneracy points.

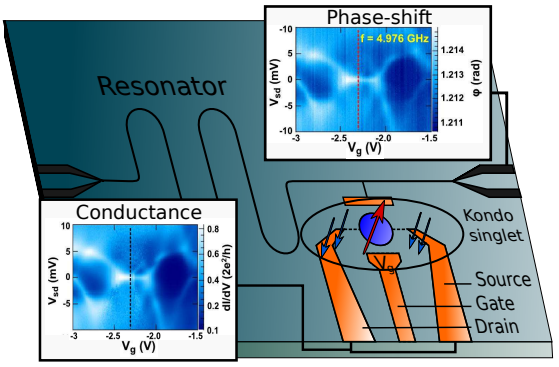

Figure VIII: Kondo effect in direct transport experiments. A Kondo ridge arises at zero bias V_{SD} in the conductance when a single electron is confined in the quantum dot. We signal also the sensitivity of photons to Kondo electronic correlations in quantum dot circuits. The phase-shift of the signal in a microwave resonator capacitively coupled to a quantum dot has the same behavior as the electronic conductance through it (insets from Ref. [43]).

screening is less effective. Interactions on the quantum dot are controlled by the *charging energy* E_c, the energy required to add a charge on the dot. The experimental measurements at the LPA were carried out for $E_c \ll \Delta$, Δ being the energy level spacing on the quantum dot, and driving frequencies $\hbar\omega \sim E_c$. In these conditions a mean-field approach for interactions justifies the original scattering approach of Refs. [48, 49, 50, 51, 52]. The issue of considering strong interactions is promising if we refer to the striking effects they already have on direct transport experiments. The most paradigmatic effect is Coulomb blockade [59]. It arises in quantum dots connected to biased macroscopic electron reservoirs through quantum point contacts, see Fig. VII. The applied gate voltage V_G and strong Coulomb interaction allow to set a quantized number of electrons on the quantum dot [60], see also Fig. 3.1. For temperatures and applied bias voltages much lower than the charging energy E_c, incoming electrons on the quantum dot do not have enough energy to change the charge on the dot. This results in the suppression of the conductance through the device, with the exception of the charge degeneracy points in which two different charge occupations on the dot become degenerate in energy, see Fig. VIII. This phenomenon cannot be explained by the single-body perspective of scattering theory. The charge occupation on the dot triggers the current transfer by electron-electron interactions. A direct treatment of these interactions on the dot is then

required. The quantum RC circuit of Fig. V is described, in the simplified case of spinless electrons, by the Coulomb blockade Hamiltonian [60]

$$H_{\rm CBM} = \sum_{k\sigma} \varepsilon_k c^\dagger_{k\sigma} c_{k\alpha\sigma} + \sum_{l\sigma} \varepsilon_l d^\dagger_{l\sigma} d_{l\sigma} + t \sum_{kl\sigma} \left(c^\dagger_{k\sigma} d_{l\sigma} + d^\dagger_{l\sigma} c_{k\sigma} \right) + E_c \left(\hat{n} - N_0 \right)^2 , \qquad \text{(iv)}$$

where free electrons of dispersion ε_k can tunnel in a multilevel quantum dot through the channel σ. The last term describes the capacitive coupling C_g between the dot and the top metallic gate, controlled by the charging energy $E_c = e^2/2C_g$. For large charging energies, this coupling forces the local quantized number of charges $\hat{n} = \sum_{l\sigma} d^\dagger_{l\sigma} d_{l\sigma}$ to be as close as possible to the classical occupation of the top metallic gate controlled by the gate voltage $N_0 = C_g V_g / e$, see also Fig. 3.1. The extension to the situation with two leads of Fig. VII is readily obtained considering more reservoirs in Eq. (iv).

Even more interesting is the spinful case, giving rise to one of the most paradigmatic many-body phenomena in mesoscopic physics, the Kondo effect [61]. Spin exchange between a single-electron charged quantum dot and itinerant electrons leads to the emergence of many-body Kondo anti-ferromagnetic correlations. The increase of the electronic conductance caused by the opening of the Kondo channel in Coulomb blockade regimes demonstrates the possibility to study many-body phenomena in mesoscopic physics [62, 63, 64], see also Fig. VIII. This phenomenon is captured by the Anderson model

$$H_{\rm An} = \sum_{k\sigma} \varepsilon_{k\sigma} c^\dagger_{k\sigma} c_{k\sigma} + t \sum_{k\sigma} \left(c^\dagger_{k\sigma} d_\sigma + d^\dagger_\sigma c_{k\sigma} \right) + \varepsilon_d \sum_\sigma \hat{n}_\sigma + U \hat{n}_\uparrow \hat{n}_\downarrow , \qquad \text{(v)}$$

describing 1/2 spin electrons tunneling inside a single-level interacting quantum dot. The determination of the admittance of the quantum RC circuit obeying to these Hamiltonians is the purpose of this Thesis. This problem has already received a large attention in recent works. The electron dynamics in the presence of interactions in the dot [65, 66] and its spin/charge separation [67] have been studied. For small metallic islands the problem has been addressed at intermediate temperatures [68] and in the many channel case [69]. In particular, the two-channel case has been argued to exhibit non-Fermi liquid behavior [70, 71]. The universality of R_q still holds if interactions in the dot [72] or not too strong interactions in the lead [73, 74] are taken into account in an exact manner. Increasing the size of the dot results in a mesoscopic crossover for R_q from $h/2e^2$ to h/e^2 [72]. For strong enough interactions in the lead, *i.e.* a Luttinger parameter below 1/2, the system undergoes a Kosterlitz-Thouless phase transition to an incoherent regime where R_q is no longer quantized [73, 74]. The main problem was to understand for which reason the charge relaxation resistance showed the same universal behavior as if interaction did not play any role, recovering, surprisingly, the results of scattering theory even in Coulomb blockade regimes. In this Thesis we provide a general Fermi liquid theory to describe the dynamics of low energy electrons in the quantum RC circuit for systems governed by the Hamiltonians Eq. (iv) and

generalized SU(N) symmetric versions of Eq. (v). Our main achievement is the proof that a generalized Korringa-Shiba relation [75] gives the condition to observe a universal charge relaxation resistance even in the presence of strong interactions on the dot at zero temperature. The study of this formula for spinful electrons in the presence of a magnetic field allows us also to describe analytically the emergence of a giant charge relaxation resistance caused by the destruction of Kondo correlations, in agreement with previous Hartree-Fock [66] and numerical renormalization group results [76]. Moreover, the analytical renormalization group approaches developed in this Thesis can be also extended to more exotic devices displaying SU(4) symmetries. In particular, we derive an analytical expression for the SU(4) Kondo temperature.

Here follows the structure of the Thesis:

Chapter 1 We discuss the original scattering approach of Büttiker and coworkers [48, 49, 50, 51, 52] to describe the quantum RC circuit and make the link with the Hamiltonian approach adopted in this Thesis. This will allow us to define the differential capacitance C_0, connected to the *static* charge susceptibility of the quantum dot, and introduce the link between charge relaxation resistance universality and the Korringa-Shiba relation.

Chapter 2 We give a general and heuristic overview of our approaches and results. In particular, we demonstrate how a Fermi liquid approach consistent with the Friedel sum rule [77] allows us to derive a generalized form of the Korringa-Shiba relation and predict non-universal behaviors for the charge relaxation resistance when both the SU(2) symmetry and the particle-hole symmetry are broken.

Chapter 3 The low energy Fermi liquid fixed point discussed in Chapter 2 is explicitly derived by applying analytical renormalization group techniques and with the help of a new representation of the Coulomb blockade model Eq. (iv) with slave-states.

Chapter 4 The demonstration of Chapter 3 is extended to the Anderson model Eq. (v), with the additional difficulty of dealing correctly with diverging Kondo correlations. Relying on the exact solution of this model provided by the Bethe ansatz [78, 79], we test our Fermi liquid approach in the whole region of parameters and fully characterize the behavior of the giant charge relaxation resistance and the quantum capacitance.

Chapter 5 We extend our Fermi liquid approach to describe the behavior of the charge relaxation resistance in SU(4) symmetric quantum dot circuits in the presence of a magnetic field. We rely on renormalization group techniques to derive the SU(4) Kondo temperature and the dot occupation in the Coulomb blockade regime.

The work presented in this Thesis led to three publications

1. **Filippone Michele**, Le Hur Karyn, Mora Christophe : Giant Charge Relaxation Resistance in the Anderson Model, Physical Review Letters **107**, 176601 (2011) ,
2. **Filippone Michele**, Mora Christophe : Fermi liquid approach to the quantum *RC* circuit: Renormalization group analysis of the Anderson and Coulomb blockade models, Physical Review B **86**, 125311 (2012) ,
3. **Filippone Michele**, Le Hur Karyn, Mora Christophe : Admittance of the SU(2) and SU(4) Anderson quantum RC circuits, Physical Review B **88**, 045302 (2013) .

One more article, corresponding to the results of Chapter 5, is now in preparation.

CHAPTER 1

THEORY OF THE QUANTUM RC CIRCUIT: NON-INTERACTING CASE

Contents

In this chapter the results of the seminal works of Büttiker, Thomas and Prêtre [48, 49, 50, 51, 52] are presented. They were the first to address theoretically the mesoscopic capacitor as the quantum analog of a classical RC circuit, an analogy detailed in Section 1.1. Their work is based on the Landauer-Büttiker scattering formalism [28, 30, 29], discussed in Section 1.2. The scattering approach describes the dynamics of lead electrons and treats the mesoscopic capacitor as a sort of "black box" in which electrons propagate coherently and escape with a well defined phase. Büttiker, Thomas and Prêtre introduced the *quantum capacitance* C_q, a new capacitive contribution in series with the geometrical capacitance C_g. The quantum capacitance reflects the spectral structure of the quantum dot. One of the key results of these authors was to predict a *universal charge relaxation resistance* $R_q = h/2e^2$, regardless of the

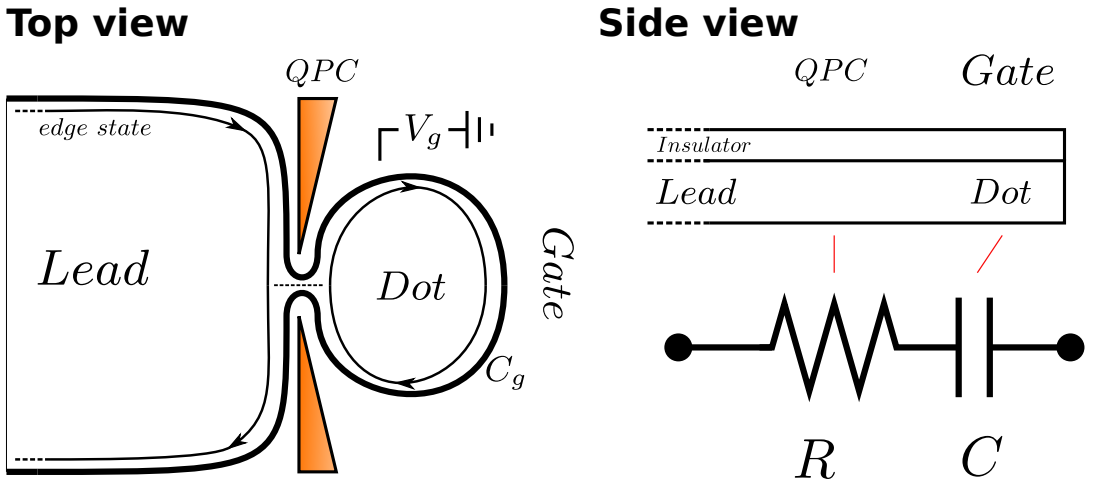

Figure 1.1: Schematic representation of the quantum RC circuit. Left) View from the top: electrons in the edge states of a two dimensional electron gas in the integer quantum Hall regime can tunnel inside a quantum dot through a quantum point contact. The dot is driven by a top metallic gate. Right) The dot and the gate are separated by an insulator. The two components cannot exchange electrons, forming the two plates of a capacitor C. The quantum point contact controls the transmission of electrons, giving rise to a resistance R. These two circuit elements are in series, and define a quantum coherent RC circuit.

opening of the quantum point contact. This result is in striking contrast with the resistance measured in DC experiments. An alternative approach to derive the results of scattering theory is presented in Section 1.3. It is based on the Hamiltonian description of the quantum RC circuit, considering explicitly the internal structure of the quantum dot. In Section 1.3.1, we discuss how linear response theory links the mesoscopic admittance of the quantum RC circuit to the dynamical charge susceptibility $\chi_c(\omega)$ of the quantum dot. We show that the capacitance is actually given by the *differential capacitance* C_0, proportional to the static charge susceptibility of the dot and that charge relaxation universality relies on the Korringa-Shiba relation [75]. Both these results will predict non-trivial behaviors in the interacting case. In Section 1.3.2, we illustrate how these quantities and relations can be readily obtained for a simple non-interacting resonant level model, recovering the results of scattering theory. This allows us to introduce the path integral formalism, largely exploited all along this text.

1.1 Phenomenology

The heuristic argument that motivates the study of the device pictured in Fig. V as the quantum analog of a classical RC circuit is clarified in Fig. 1.1. The metallic gate on top of the quantum dot cannot exchange electrons with it. These two components, the first one de-

scribed by a classical theory and the second one quantum coherent, constitute the two plates of a capacitance on which electrons accumulate following the variation of the gate potential V_g. The value of this capacitance will depend on the geometry of the contact and, in the experiment of Ref. [7], the *geometrical capacitance* C_g was estimated to be of the order of $\sim 10-100$ fF. This capacitance is in series with a quantum point contact. The direct transport measurements [17, 18], discussed in the Introduction, show that this behaves as a resistive element, whose resistance is given by

$$R_{\mathrm{DC}} = \frac{h}{e^2 D}, \tag{1.1}$$

where D is the *transparency*, to be defined through scattering theory in Section 1.2. This quantity depends on the probability r for electrons to be backscattered when arriving at the tunnel barrier constituted by the quantum point contact. D therefore depends on the opening of the quantum point contact. These considerations explain why the device in Fig. 1.1 can be viewed as an RC circuit. The admittance of a classical RC circuit reads

$$G(\omega) = \frac{-i\omega C}{1 - i\omega RC}. \tag{1.2}$$

For the following discussion, it is useful to expand this expression to second order in the frequency ω

$$G(\omega) = -i\omega C\big(1 + i\omega CR\big). \tag{1.3}$$

The question is then to establish whether the admittance of the device in Fig. V respects the RC structure of Eq. (1.3) when quantum coherence effects are considered for electrons. We will see that it is the case.

1.2 Scattering theory of the quantum RC circuit

Coherence effects between electrons, in the absence of interactions, are fully taken into account by scattering theory [28, 30]. The principle of this approach is sketched in Fig. 1.2. Let us consider a two-dimensional spinless electron gas as the one pictured in Fig. 1.2. A difference of potential $\delta V = \mu_L - \mu_R$ is applied between the left and right metallic contacts. It coincides with the difference of their respective chemical potentials $\mu_{\alpha=L,R} = E_F + eV_{L,R}$, E_F being the Fermi energy that, from now on, we fix to zero. It is a fundamental assumption of the scattering formalism to consider the electron reservoirs (the metallic leads) to be at *equilibrium*. This implies that the energy distribution of electrons emitted from the leads obeys the Fermi-Dirac distribution

$$f_\alpha(\varepsilon) = \frac{1}{1 + e^{\beta(\varepsilon - \mu_\alpha)}}. \tag{1.4}$$

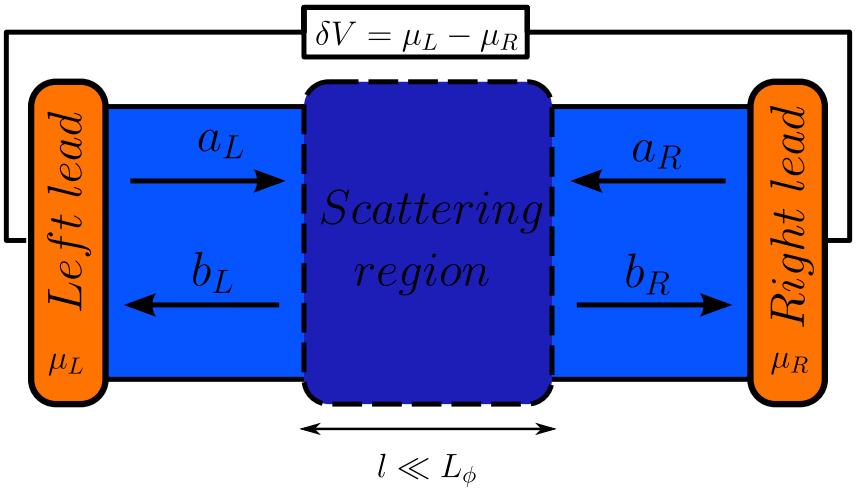

Figure 1.2: Principle of scattering theory for a two-dimensional electron gas. Thermalized leads of chemical potential $\mu_{\alpha=L,R}$ emit electrons towards the phase coherent region smaller than L_ϕ. The operators a_α are associated to the state of these electrons, which are emitted back to the leads in the state b_α as a unitary superposition of the incoming modes.

An operator $a_{\alpha,n}(\varepsilon)$ is associated to every electron in the state n of energy ε, entering the mesoscopic region from the reservoir α. An operator $b_{\alpha,n}(\varepsilon)$ is associated to every mode n of energy ε coming out of the mesoscopic region joining the reservoir α. This assumes implicitly the hypothesis that there exist ideal regions between the mesoscopic scatterer and the reservoirs in which electrons propagate freely without any backscattering in the state n. Scattering theory is characterized by the fundamental assumption that the only effect of the mesoscopic region on incoming states, described by $a_{\alpha,n}(\varepsilon)$, is a unitary evolution. This is formally stated with the help of the scattering matrix $S(\varepsilon)$ defined by

$$\begin{pmatrix} [b_L] \\ [b_R] \end{pmatrix} = \begin{pmatrix} [s_{LL}] & [s_{LR}] \\ [s_{RL}] & [s_{RR}] \end{pmatrix} \begin{pmatrix} [a_L] \\ [a_R] \end{pmatrix}. \tag{1.5}$$

$[a_\alpha]$ and $[b_\alpha]$ are the vectors collecting all the modes n in the ideal region between the reservoir α and the mesoscopic scatterer. Unitary evolution is fulfilled by imposing the unitarity of the scattering matrix $SS^\dagger = S^\dagger S = \mathbb{1}$. We stress that the matrix $S(\varepsilon)$ relates modes with the *same* energy ε. This translates the fact that all processes considered in the mesoscopic scatterer are *elastic*. They do not modify the energy of electrons, excluding the inelastic processes which could be caused by interactions. The expression for the current operator I_α flowing in the reservoir α is readily derived as a difference between the ingoing and outgoing states [1, 80]

$$I_\alpha(x,t) = \frac{e}{h}\int d\varepsilon d\varepsilon' \left[a_\alpha^\dagger(\varepsilon)a_\alpha(\varepsilon') - b_\alpha^\dagger(\varepsilon)b_\alpha(\varepsilon')\right] e^{i(\varepsilon-\varepsilon')(t-x/v_F)/\hbar}, \tag{1.6}$$

with v_F the Fermi velocity. Applying Eq. (1.5) the stationary conductance is given by

$$g_{LR}(\omega=0) = -\frac{\langle I_L\rangle}{\delta V} = \frac{e^2}{h}\int d\varepsilon \mathrm{Tr}\left\{\left[s_{LR}(\varepsilon)\right]^\dagger\left[s_{LR}(\varepsilon)\right]\right\}\cdot\frac{f_L(\varepsilon)-f_R(\varepsilon)}{e\delta V}. \tag{1.7}$$

In the linear regime $\delta V \to 0$ it becomes

$$g_{LR}(\omega=0) = \frac{e^2}{h}\int d\varepsilon \mathrm{Tr}\left\{\left[s_{LR}(\varepsilon)\right]^\dagger\left[s_{LR}(\varepsilon)\right]\right\}\cdot\left(-\frac{\partial f}{\partial\varepsilon}\right) = \frac{e^2}{h}D, \tag{1.8}$$

where we applied the relation $-\partial f/\partial\varepsilon = \delta(\varepsilon - E_F)$, valid at zero temperature. This result provides the formal definition of the transparency D of the scattering region, which we introduced for the DC resistance (the inverse of the DC conductance) in Eq. (1.1)

$$D = \mathrm{Tr}\left\{\left[s_{LR}(E_F)\right]^\dagger\left[s_{LR}(E_F)\right]\right\}. \tag{1.9}$$

This quantity encodes all information about the backscattering and transmission of electrons in the mesoscopic region. Eqs. (1.8) and (1.9) constitute the notorious *Landauer-Büttiker formula*, a powerful tool to describe electron transport in a variety of situations in mesoscopic physics. As an example we discuss the case of the QPC in a 2DEG of Fig. IV. In the single channel case, that is for a single electronic state traversing the QPC, the S-matrix reads

$$S = \begin{pmatrix} r & t \\ t & r \end{pmatrix}, \tag{1.10}$$

where r and t are the back-reflection and transmission amplitudes for electrons coming on the QPC. Eq. (1.9) states that $D = t^2$, the probability for electrons to pass through the QPC. The progressive opening of the QPC governs the transition $D = 0 \to 1$, explaining the transition of the conductance from 0 to e^2/h in Fig. IV. The progressive opening of further channels give rise to the other steps of the conductance always present in Fig. IV.

This formalism can be adapted to the case of the mesoscopic capacitor in Fig. V. A main difference is the "mixed" nature of the quantum RC device, which is highlighted in Fig. 1.3. The quantum RC circuit is composed of a phase-coherent part (the two-dimensional electron gas + the quantum dot) in direct contact to an incoherent one (the top metallic gate). Moreover, these constituents cannot exchange electrons, preventing a direct current. To observe electron transport, the system must be driven dynamically. This is operated by applying a gate potential oscillating periodically in time

$$V_g(t) = V_g + \varepsilon_\omega \cos(\omega\, t). \tag{1.11}$$

For small oscillation amplitudes ε_ω, the Landauer-Büttiker formalism allows for the calculation of the circuit admittance within linear response theory, to be discussed in Section 1.3.1. In the case of a single conduction mode, this reads [49]

$$g_L(\omega) = \frac{e^2}{h}\int d\varepsilon \mathrm{Tr}\left[1 - s^\dagger(\varepsilon)s(\varepsilon+\hbar\omega)\right]\cdot\frac{f(\varepsilon)-f(\varepsilon+\hbar\omega)}{\hbar\omega}. \tag{1.12}$$

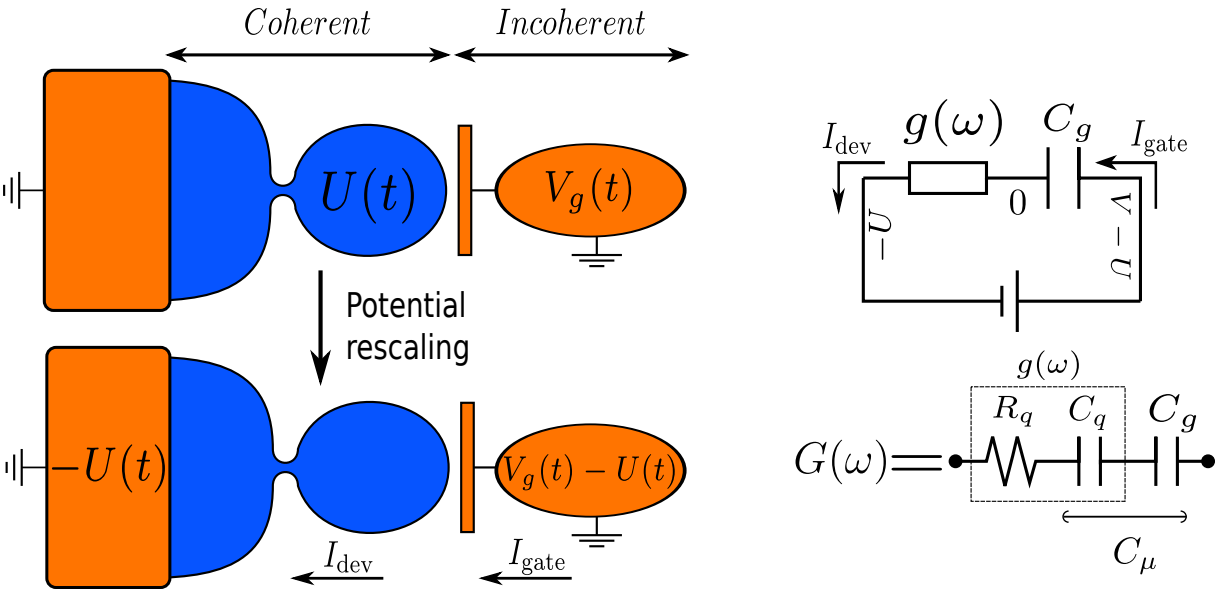

Figure 1.3: The blue region composed of the two-dimensional gas is phase coherent, that is its size $L \ll L_\phi$. The top metallic gate is incoherent and driven by a time-dependent gate potential $V_g(t)$ inducing an unknown uniform potential $U(t)$ on the dot. To compute the admittance of the phase coherent device, all energies have to be shifted by $-U(t)$, allowing for the classical circuit analogy in the top right. The admittance of the whole device results as a series of a charge relaxation resistance R_q and the electrochemical capacitance C_μ, composed of the series of a quantum capacitance C_q and the geometrical capacitance C_g.

For one channel, the matrix $s(\varepsilon)$ reduces to a pure phase $s(\varepsilon) = e^{i\eta(\varepsilon)}$, as the electrons entering the dot come back to the lead with unit probability. This phase is related to the *dwell-time* that electrons typically spend in the quantum dot, defined from the scattering matrix as a Wigner-Smith delay time [81, 82]

$$\frac{\tau(\varepsilon)}{h} = \frac{1}{2\pi i} s^\dagger(\varepsilon) \frac{ds(\varepsilon)}{d\varepsilon} = \frac{1}{2\pi} \frac{d\eta(\varepsilon)}{d\varepsilon}. \tag{1.13}$$

The interpretation of τ as a dwell-time will become clear in a forthcoming example. Applying this definition to the calculation of Eq. (1.12) in the limits $T \to 0$ and $\hbar\omega \to 0$, we find

$$g_L(\omega) = -i\omega \frac{e^2}{h} \left[\tau + \frac{1}{2} i\omega\tau^2 + O(\omega^2) \right]. \tag{1.14}$$

The dwell-time $\tau = \tau(0)$ is considered at the Fermi energy. Notice that this expression has the same structure as Eq. (1.3) for the RC admittance of a classical circuit. Matching Eq. (1.14) with Eq. (1.3), one finds

$$C_q = \frac{e^2}{h}\tau, \qquad R_q = \frac{h}{2e^2}. \tag{1.15}$$

The characteristic time that an electron spends in the quantum dot is given by $\tau = 2R_qC_q$, twice the RC time because it includes the charging and relaxation time of the RC circuit. We notice the emergence of a universally quantized relaxation resistance, regardless of any microscopic detail of the quantum RC circuit, in contrast with the DC formula Eq. (1.1).

Before discussing these two quantities in detail, we would like to stress that the interpretation of the device in Fig. V as a quantum analog of an RC circuit strictly holds at low frequencies. Taking into account higher frequencies forces to introduce inductive constituents if one wants to persevere with a classical circuit analogy [83]. Moreover, when the same system is driven by large pulses of the gate potential as in the single-electron experiments of Ref. [56, 57, 47], discussed in the Introduction, the linear response regime is definitively abandoned and the resistance and capacitance computed here are not relevant anymore.

1.2.1 The quantum capacitance

The effect of the geometrical capacitance C_g has been left aside in the previous discussion of the scattering formalism. The admittance Eq. (1.12) has been derived by applying linear response theory for the driving potential $U(t)$ in the quantum dot, see Fig. 1.3. Electrons getting at different times on the dot are differently phase-shifted, causing a local accumulation of charges responsible for the emergence of quantum capacitive effects, described by C_q. The time delay of the electron phase with respect to the driving potential $U(t)$ are responsible for energy dissipation, controlled by R_q to be discussed in detail in Section 1.2.2. The subtlety, in the presence of the geometrical capacitance C_g, is that the potential $U(t)$ does not coincide with the gate potential $V_g(t)$. The situation is pictured in Fig. 1.3: the geometric capacitance C_g is interposed between the gate and the dot, producing a drop of potential. This potential drop depends on how Coulomb screening effects renormalize the potential felt by electrons on the dot. In a mean-field or Hartree-Fock treatment, the potential on the dot, denoted $U(t)$, is assumed to be uniform for each electron. This is also equivalent as to assume the random phase approximation (RPA) for interactions between electrons in the quantum dot, which can be justified for not too strong interactions or to leading order in a $1/N$ expansion, where N is the number of channels connected to the dot [65]. The potential U can then be determined self-consistently from the constraint of charge/current conservation throughout the whole device. This requires that the current I_{dev} running in the coherent part of the device is the same as the current I_{gate} flowing in the incoherent metallic gate

$$I = I_{\mathrm{dev}} = I_{\mathrm{gate}}\,. \tag{1.16}$$

As all potentials are defined with respect to some constant energy, all energies can be shifted by $-eU(t)$, setting the potential to zero in the quantum dot. In this case the currents in the

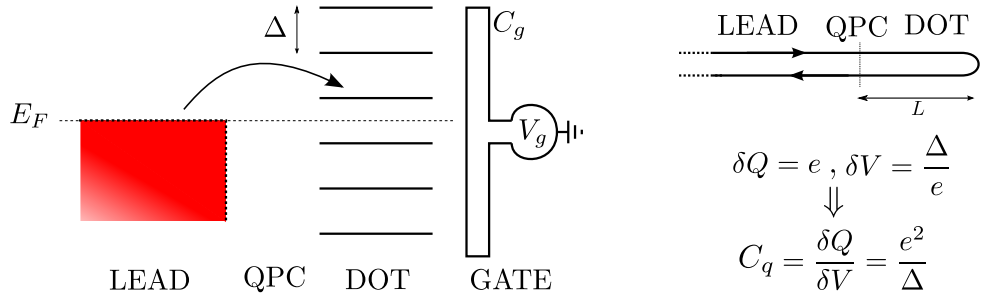

Figure 1.4: Physical mechanism responsible for the arising of the quantum capacitance C_q. The Pauli exclusion forces electrons coming from the lead in the quantum dot to pay a further energy price equal to the local level spacing Δ. The associated capacitance is then $C_q = e^2/\Delta$. On the top-right a one-dimensional representation of the quantum RC circuit is provided, involving a dot of size L.

device and in the metallic gate are given by

$$I_{\text{dev}} = -U(\omega)\, g_L(\omega)\,, \qquad I_{\text{gate}} = -iC_g\omega\big[U(\omega) - V_g(\omega)\big]\,. \tag{1.17}$$

Applying the current conservation condition Eq. (1.16), the potential U is eliminated, leading to the admittance of the total device

$$G(\omega) = -\frac{I}{V_g} = \frac{1}{\frac{1}{g_L(\omega)} + \frac{1}{-i\omega C_g}}\,. \tag{1.18}$$

Recalling that the low frequency behavior of $g_L(\omega)$ in Eq. (1.12) is the same as for a classical RC circuit, given by Eq. (1.3), Eq. (1.18) states that the whole device, including the capacitance C_g, can be viewed as an RC circuit. Albeit with two capacitances in series, Eq. (1.18) nevertheless still gives a universally quantized $R_q = h/2e^2$. The series of C_q and C_g gives the *electro-chemical capacitance* C_μ, see Fig. 1.3. This quantity provides the imaginary part of the RC admittance Eq. (1.3), accessible in experiments. The concept of quantum capacitance and geometric capacitance in series is restricted to a mean-field treatment of interactions. Therefore this circuit description does not hold in the case of interactions.

Once the geometrical capacitance C_g has been included in the formalism, a heuristic argument clarifies the physical origin of the quantum capacitance C_q as a manifestation of the fermionic statistics of electrons, more precisely the Pauli exclusion principle. When an electron is added on the quantum dot, in which energy levels are spaced by Δ, the Pauli exclusion principle does not allow for the filling of an energy state already occupied by an other electron, see Fig. 1.4. The fermionic statistics imposes to pay a further energy price Δ to put a further electron in the dot. The capacitance associated to this process is then

$$C_q = \frac{\delta Q}{\delta V}\,. \tag{1.19}$$

For one electron $\delta Q = e$ and $\delta V = \Delta/e$. Substituting these two expressions in Eq. (1.19), we recover a uniform quantum capacitance

$$C_q = \frac{e^2}{\Delta}. \tag{1.20}$$

This expression establishes that the quantum capacitance is proportional to the density of states in the quantum dot at the Fermi energy $C_q = e^2\mathcal{N}(E_F)$. The level spacing of the quantum dot can be actually estimated and, in the experimental conditions of Ref. [7], it was established to be of the order of $\Delta \sim 15$ GHz, corresponding to a quantum capacitance $C_q \sim 1$ fF. The experimental measurement of C_μ, plotted in Fig. 1.6, gives an estimate also for C_g, showing that $C_q \ll C_g$. This implies that the level spacing Δ was much larger than the charging energy $E_c = e^2/2C_g$, of the order of fractions of the GHz, justifying the mean-field approach to explain the experimental results.

The previous argument applies to the case of perfect transmission $r = 0$, in which the density of states of the completely open dot is uniform accordingly to Eq. (1.20). Finite reflection $r \neq 0$ is responsible for resonant tunneling processes, engendering the oscillatory behavior of the local density of states as a function of the gate potential V_g, in agreement with the experimental findings in Fig. 1.6. All these arguments will be comforted by a quantitative analysis in Sections 1.2.3 and 1.3.2.

1.2.2 The charge relaxation resistance

The predictions from Eq. (1.15) were verified experimentally at the Laboratoire Pierre Aigrain in 2006 [7]. The results are shown in Figs. 1.5 and 1.6. In the quantum coherent regime the charge relaxation resistance is *universal*. It does not depend on the backscattering probability of electrons at the entrance of the quantum dot. As we considered spinless electrons, the 1/2 factor in Eq. (1.15) has nothing to do with spin degeneracy. It comes from the fact that the dot is connected to a *single* reservoir in contrast to the source-drain reservoirs in DC transport. The interpretation of R_q as a Sharvin-Imry contact resistance has been disputed in Refs. [84, 85]. In direct transport, each metallic contact is responsible for a quantized contact resistance $R_c = h/2e^2$, the Sharvin-Imry resistance [86, 87]. Eq. (1.1) should be recast in the form

$$R_{\rm DC} = \frac{h}{2e^2} + \frac{h}{e^2}\frac{1-D}{D} + \frac{h}{2e^2}, \tag{1.21}$$

to highlight the resistive contribution strictly associated to the quantum point contact $R_{\rm QPC} = h/e^2 \cdot (1-D)/D$ and that of the contacts R_c. The reason for the universality of R_q in Eq. (1.15) is that each electron emitted by the unique lead keeps its coherence until it goes back to it. To recover the DC result Eq. (1.21) in an AC measurement, electrons have to loose completely

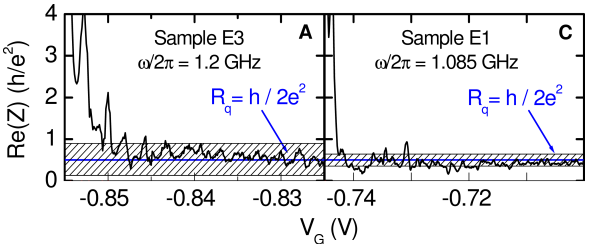

Figure 1.5: Experimental measurement of the charge relaxation resistance (coinciding with the real part of the impedance Z) in two different samples as a function of the quantum point contact potential V, which affects also the gate potential V_g. Measurements were carried out for $T = 30mK$ and $B = 1.3T$. The charge relaxation resistance is shown to be universally fixed to $R_q = h/2e^2$ within the uncertainties indicated by the hatched areas.

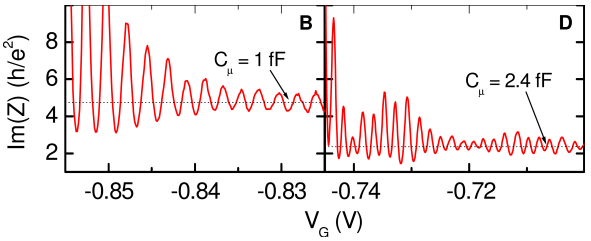

Figure 1.6: Experimental measurements of the electrochemical capacitance C_μ (series of C_g and C_q) for the same samples and the same experimental parameters as in Fig. 1.5. This coincides with the imaginary part of Z. The oscillatory behavior as a function of V_g is related to the density of states in the dot and is qualitatively reproduced in Fig. 1.8. The peaks correspond to the resonance of an internal level of the dot (calibrated by V_g, see Eq. (1.29)*) with the Fermi energy in the lead.*

their phase coherence inside the dot [84, 85]. The high temperature limit $k_B T \gg \Delta$ is not enough to recover Eq. (1.21), giving a charge relaxation resistance $R_q = R_{DC} - h/2e^2$, still reflecting the presence of only one reservoir.

1.2.3 The example of a quantum RC circuit with a 2DEG

We provide in this section an application of the formal concepts of the previous discussion. We consider the case of of Fig. 1.1, in which electrons propagate in the integer quantum Hall edges of the quantum dot. This discussion is inspired from Refs. [7, 8, 88]. If l is the circumference of the part of the edge state that forms the quantum dot and v_d the drift velocity of the electron, $\tau_0 = l/v_d$ is the time needed to cover a tour of the dot. Considering the usual evolution operator $e^{\frac{iHt}{\hbar}}$, acting on eigenfunctions of energy ε, an electric wave of energy ε acquires then a phase $\phi(\varepsilon) = (\varepsilon - eU)\tau_0/\hbar$, when making a tour of the dot. Notice that we had to shift the energy ε of the electron by $-eU$ because of the potential shift schematized in Fig. 1.3. The chiral nature of the edge states allows for a one-dimensional representation of the problem, pictured in the right-top of Fig. 1.4. For a quantum well of size L, close to the Fermi energy, the spectrum can be linearized and the level spacing is constant and given by

$$\Delta = \frac{\pi\hbar v_F}{L}. \tag{1.22}$$

The dwell-time for electrons of velocity v_F is

$$\tau_0 = \frac{2L}{v_F}. \tag{1.23}$$

Substituting Eqs. (1.22) and (1.23) in Eq. (1.15), we find the uniform quantum capacitance, derived heuristically, of Eq. (1.20). If the reflection amplitude at the entrance of the dot is r and $D = 1 - r^2$ the transmission probability, the dot can be viewed as a Fabry-Perot cavity and the phase of the out-coming electron is

$$s(\varepsilon) = r - De^{i\phi(\varepsilon)} \sum_{q=0}^{\infty} r^q e^{iq\phi(\varepsilon)} = \frac{r - e^{i\phi(\varepsilon)}}{1 - re^{i\phi(\varepsilon)}} = e^{i\eta(\varepsilon)}. \tag{1.24}$$

Applying Eq. (1.13) we obtain the local density of states

$$\mathcal{N}(\varepsilon) = \frac{\tau_0}{h} \frac{1 - r^2}{1 - 2r\cos\left[\frac{2\pi}{h}\left(\varepsilon - eU\right)\tau_0\right] + r^2}. \tag{1.25}$$

This is plotted in Fig. 1.8 and reproduces the oscillatory behavior of the capacitance in Fig. 1.6. In the limit of small transmission ($D \ll 1$ and $r \approx 1$), Eq. (1.25) reduces to a sum of Lorentzian peaks of width $\hbar\gamma$, $\gamma = D/\tau_0$:

$$N(\varepsilon) = \frac{2}{\pi\hbar\gamma} \sum_n \frac{1}{1 + \left(\frac{\varepsilon - eU - n\Delta}{\hbar\gamma/2}\right)^2}. \tag{1.26}$$

These peaks are the discrete spectrum of the dot energy levels.

To conclude, we mention that the generalization to N modes is readily obtained. The mesoscopic admittance Eq. (1.12) can be still cast into the form Eq. (1.3) with the difference

$$C_q = \frac{e^2}{h} \sum_{n=1}^{N} \tau_n, \qquad R_q = \frac{h}{2e^2} \frac{\sum_n \tau_n^2}{\left(\sum_n \tau_n\right)^2}, \tag{1.27}$$

in which τ_n are the dwell-times in the quantum dot of electrons in the n-th mode. We discuss now how these same results can be derived from a microscopic approach.

1.3 Hamiltonian description of the quantum RC circuit

The aim of this Thesis is to address the effects of interactions on the quantum capacitance and the charge relaxation resistance. To do this, we cannot look anymore at the quantum dot as a sort of "black-box", but models must be considered that give an exact description of

electron-electron interactions within it. In this section, the results of Section 1.2 are derived from an Hamiltonian approach. We neglect for the moment interactions, which allows for straightforward calculations. We establish the physical origin of the quantum capacitance and the charge relaxation universality from this alternative point of view.

Considering spinless electrons, the Coulomb blockade model Eq. (iv) accounts explicitly for the driving of charges on the dot and interactions. This can be understood by inspecting the part of the Hamiltonian describing the capacitor

$$H_{\text{Capa}} = E_c \left(\hat{n} - N_0\right)^2 . \tag{1.28}$$

If the square is expanded and constant contributions are neglected, it results in a renormalization of orbital energies ε_l in Eq. (iv) and in an interaction term, namely

$$H_{\text{Capa}} = -eV_g(t)\hat{n} + E_c\hat{n}^2 . \tag{1.29}$$

We take into account explicitly the time dependence of the driving gate voltage to stress that it couples to the *charge* occupation of the quantum dot $\hat{Q} = e\hat{n}$. We are interested in calculating the admittance of the system. The current of the whole device is a derivative in time of the charge leaving the quantum dot, the admittance reads then, in Fourier frequency representation,

$$G(\omega) = -i\omega\frac{Q(\omega)}{V_g(\omega)} . \tag{1.30}$$

For "small" oscillations ε_ω of the gate voltage Eq. (1.11), the problem can be studied close to equilibrium, and linear response theory provides the tools to calculate Eq. (1.30).

1.3.1 Linear response theory: basic notions for the quantum RC circuit

Linear response theory [89, 90] addresses the calculation of observables in time-dependent problems which can be written in the form

$$H = H_0 - \lambda f(t)\hat{A} . \tag{1.31}$$

$\hat{A}$ is a generic operator, $f(t)$ any function of time of order 1 and λ a perturbation parameter. To first order in λ, the time-dependent corrections to any observable $\langle\hat{O}\rangle$ can be written as a functional of operators averaged at *equilibrium*

$$\langle\hat{O}\rangle(t) = \langle\hat{O}\rangle_0 + \lambda\int_{-\infty}^{\infty} dt'\chi(t-t')f(t') . \tag{1.32}$$

The notation $\langle\cdot\rangle_0$ means that the averages are carried out by taking traces involving the time-independent part H_0 of the Hamiltonian Eq. (1.31). For instance $\langle\hat{O}\rangle_0 = Z^{-1}\text{Tr}\left[\hat{O}e^{-\beta H_0}\right]$. $Z =$

$\mathrm{Tr}\left[e^{-\beta H_0}\right]$ is the canonical partition function at equilibrium. $\chi(t-t')$ is the *linear response function*

$$\chi(t-t') = \frac{i}{\hbar}\theta(t-t')\left\langle\left[\hat{O}(t),\hat{A}(t')\right]\right\rangle_0, \tag{1.33}$$

where the time dependence of operators is given in the interaction representation

$$\hat{O}(t) = e^{\frac{iH_0t}{\hbar}}\hat{O}e^{-\frac{iH_0t}{\hbar}}. \tag{1.34}$$

The linear response function is then a correlator between $\hat{O}$ and $\hat{A}$ at different times, but always calculated for the equilibrium Hamiltonian H_0. $\theta(t) = 1$ for $t > 0$ and 0 otherwise is the Heaviside function.

Eq. (1.30) states that the admittance is related to the response to gate voltage variations of the charge on the dot. Comparing the time-dependent terms in the Hamiltonians in Eqs. (1.29) and (1.31), with $V_g(t)$ given by Eq. (1.11), all the identifications necessary to map our problem on the language of linear response theory can be done

$$\begin{array}{ccc} \hat{O}(t) & \rightarrow & e\hat{n}(t), \\ \hat{A} & \rightarrow & e\hat{n}, \\ f(t) & \rightarrow & \cos(\omega t), \\ \lambda & \rightarrow & \varepsilon_\omega. \end{array} \tag{1.35}$$

This leads to the following result for the admittance Eq. (1.30)

$$G(\omega) = -i\omega e^2\chi_c(\omega), \tag{1.36}$$

where $\chi_c(\omega)$ is the Fourier transform of the *dynamical charge susceptibility*

$$\chi_c(t-t') = \frac{i}{\hbar}\theta(t-t')\left\langle\left[\hat{n}(t),\hat{n}(t')\right]\right\rangle_0. \tag{1.37}$$

A low frequency expansion of $\chi_c(\omega)$ in Eq. (1.36) provides a different way to define the capacitance and the charge relaxation resistance of the quantum RC circuit. To second order in ω Eq. (1.36) takes the form

$$G(\omega) = -i\omega e^2\left\{\chi_c + i\mathrm{Im}\left[\chi_c(\omega)\right]\right\}, \tag{1.38}$$

where we stress the fact that the even and odd part of the response function Eq. (1.37) coincide respectively with its real and imaginary part, see Appendix A. We also define the *static* charge susceptibility $\chi_c = \chi_c(\omega = 0)$. Identifying term by term Eq. (1.38) with the one for the classical RC circuit Eq. (1.3), we define a *differential capacitance* C_0 and the charge relaxation resistance from microscopic quantities connected to the charge occupation of the dot

$$C_0 = e^2\chi_c = -e^2\frac{\partial\langle\hat{n}\rangle}{\partial\varepsilon_d}, \qquad R_q = \frac{1}{e^2\chi_c^2}\left.\frac{\mathrm{Im}\chi_c(\omega)}{\omega}\right|_{\omega\to 0}. \tag{1.39}$$

The differential capacitance is a quantity that differs from the capacitances considered in the scattering formalism. Experimentally, it is directly measured from the real part of the admittance. In Section 4.1.2.1, in the framework of the Kondo regime of the Anderson model, we discuss how C_0, in the presence of interactions on the dot, cannot be interpreted as the geometrical capacitance C_g in series with the quantum capacitance C_q, proportional to the local density of states of the dot. The differential capacitance is actually proportional to the density of states of the *charge* excitations on the dot, which does not coincide in general to the total density of states if strong interactions are present. The expression for R_q in Eq. (1.39) is also interesting because it provides the general condition for the universal quantization of Eq. (1.15). It is realized when the Korringa-Shiba relation [75]

$$\mathrm{Im}\chi_c(\omega)\big|_{\omega\to 0} = \hbar\pi\omega\chi_c^2 \tag{1.40}$$

holds. The proof of the Korringa-Shiba relation in interacting systems constitutes one of the primary goals of our work. This is achieved through the Fermi liquid approach discussed in Chapter 2. In the following discussion, we proceed with the proof of this formula in a non-interacting systems, recovering the results of scattering theory.

1.3.2 Description of the quantum RC circuit with a resonant level model

In this section, we use a *resonant level* model to describe the quantum dot and the lead

$$H_{\mathrm{Res}} = \sum_k \varepsilon_k c_k^\dagger c_k + t\sum_k \left(c_k^\dagger d + d^\dagger c_k\right) + \varepsilon_d d^\dagger d\,. \tag{1.41}$$

We restrict for simplicity to the single-channel and the single-level case. The generalization of the following calculations to the many-channel case is straightforward. In Appendix B, we carry out explicitly the calculation of the differential capacitance in the multi-level case. The model Eq. (1.41) describes the situation pictured in Fig. 1.4. It constitutes a simplification of the Coulomb blockade model Eq. (iv), where the interacting term of Eq. (1.29) is neglected. This is equivalent to consider $C_g = \infty$, recovering the mean-field analysis of Section 1.2. We take advantage of this section to introduce the notations that we shall use in the path integral formalism in the following chapters. The partition function associated to the Hamiltonian Eq. (1.41) can be written in the form [91]

$$\mathcal{Z} = \int \mathcal{D}\left[c, c^\dagger, d, d^\dagger\right] e^{-S\left[c,c^\dagger,d,d^\dagger\right]}, \tag{1.42}$$

where $S\left[c, c^\dagger, d, d^\dagger\right]$ is the action of the system. The action reads

$$S_{\mathrm{Res}} = \int_0^\beta d\tau \left\{ -\sum_k c_k^\dagger(\tau) G_k^{-1}(\tau) c_k(\tau) - d^\dagger(\tau) D^{-1}(\tau) d(\tau) + t\sum_k \left[c_k^\dagger(\tau) d(\tau) + \mathrm{c.c.}\right]\right\}, \tag{1.43}$$

with the free propagators

$$\begin{aligned} G_k^{-1}(\tau) &= -\partial_\tau - \varepsilon_k\,, \\ D^{-1}(\tau) &= -\partial_\tau - \varepsilon_d\,, \end{aligned} \tag{1.44}$$

The fermionic nature of the operators c_k and d_l in Eq. (1.41) is translated in Eq. (1.43) by the fact that these become Grassmann variables, with the commutation property

$$d_l d_{l'} = -d_{l'} d_l\,, \qquad\qquad d_l^\dagger d_{l'} = -d_{l'} d_l^\dagger\,, \tag{1.45}$$

and they are anti-periodic functions of τ

$$c_k(0) = -c_k(\beta)\,, \qquad\qquad d_l(0) = -d_l(\beta)\,. \tag{1.46}$$

The case of bosons is much simpler: they are described by usual complex scalars which are periodic in the interval $[0,\beta]$. It is practical to do the Fourier transform and switch to a frequency representation of the fields in the action Eq. (1.43). For instance

$$c_{k\sigma}(\tau) = \frac{1}{\beta}\sum_{i\omega_n} e^{-i\omega_n\tau} c_{k\sigma}(i\omega_n)\,, \tag{1.47}$$

where we defined the fermionic Matsubara frequencies $i\omega_n = (2n+1)\pi/\beta$, $n\in\mathbb{Z}$. They satisfy the anti-periodicity property Eq. (1.46). This operation leads to

$$\begin{aligned} S_{\text{Res}} = \sum_{i\omega_n}\Bigg\{ &-\sum_k c_k^\dagger(i\omega_n) G_k^{-1}(i\omega_n) c_k(i\omega_n) - d^\dagger(i\omega_n) D^{-1}(i\omega_n) d(i\omega_n) \\ &+ t\sum_k \left[c_k^\dagger(i\omega_n) d(i\omega_n) + d^\dagger(i\omega_n) c_k(i\omega_n)\right]\Bigg\}\,. \end{aligned} \tag{1.48}$$

The free propagators become diagonal in this representation

$$\begin{aligned} G_k^{-1}(i\omega_n) &= i\omega_n - \varepsilon_k\,, \\ D^{-1}(i\omega_n) &= i\omega_n - \varepsilon_d \end{aligned} \tag{1.49}$$

and they recover the usual retarded/advanced Green's functions if the analytical continuation $i\omega_n \to \omega \pm i0^+$ is done. Reestablishing dimensions, the Fourier transform of the response function Eq. (1.37) in this formalism reads

$$\chi_c(i\nu_n) = \frac{1}{\hbar}\int_0^{\hbar\beta} d(\tau-\tau') e^{i\nu_n(\tau-\tau')} \langle \hat{n}(\tau)\hat{n}(\tau')\rangle_0\,. \tag{1.50}$$

Notice that $\chi_c(i\nu_n)$ is a normal scalar, recovering $\chi_c(\omega)$ by performing the analytical continuation $i\nu \to \omega + i0^+$. This function is periodic in imaginary time and its Fourier transform

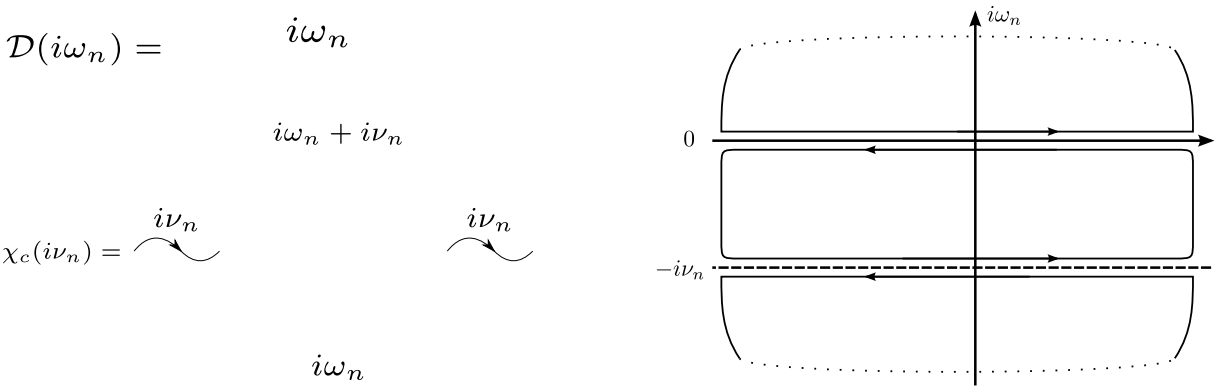

Figure 1.7: Top-Left) Diagrammatic representation of the full quantum dot electron propagator Eq. (1.54). *The arrow represents the creation and annihilation of a mode of frequency $i\omega_n$ in correlators. Bottom-Left) Diagram giving the dynamical charge susceptibility Eq.* (1.51). *Its expression is made explicit in Eq.* (1.55). *The external bosonic lines correspond to the real frequency $\hbar\omega$ pumped in the system by the drive $V_g(t) = V_g + \varepsilon_\omega \cos(\omega t)$. Right) Paths in the complex plane for the calculation of the Matsubara sum Eq.* (1.55).

is a function of the bosonic Matsubara frequencies $i\nu_n = 2n\pi/\beta$. $\hat{n}(\tau) = d^\dagger(\tau)d(\tau)$ counts the number of charges on the dot. The cyclic invariance property of the trace implies that $\langle \hat{n}(\tau)\hat{n}(\tau')\rangle_0 = f(\tau - \tau')$, allowing us to write Eq. (1.50) in the form

$$\chi_c(i\nu_n) = \frac{1}{\beta}\sum_{i\omega_{1,2}} \langle d^\dagger(i\omega_1)d(i\omega_1 + i\nu_n)d^\dagger(i\omega_2)d(i\omega_2 - i\nu_n)\rangle \,. \tag{1.51}$$

To calculate this expression, involving solely the quantum dot fields d, we first integrate the lead modes in Eq. (1.48), a Gaussian integration leading to the effective action S'_{Res} of the resonant level model

$$S'_{\text{Res}} = -\sum_{i\omega_n} d^\dagger(i\omega_n)\mathscr{D}(i\omega_n)d(i\omega_n)\,, \tag{1.52}$$

with

$$\mathscr{D}^{-1}(i\omega_n) = i\omega_n - \varepsilon_d - t^2\sum_k G_k(i\omega_n)\,, \tag{1.53}$$

In the wide-band approximation this propagator reads

$$\mathscr{D}^{-1}(i\omega_n) = i\omega_n - \varepsilon_d + i\Gamma \text{sgn}(\omega_n)\,, \tag{1.54}$$

where we introduced the hybridization constant $\Gamma = \pi\nu_0 t^2$, ν_0 being the density of states of the lead electrons. The action Eq. (1.52) is quadratic and Wick's theorem gives a diagrammatic representation of the four-point correlator Eq. (1.51). For $i\nu_n \neq 0$, this is represented by the diagram pictured in Fig. 1.7. The result reads

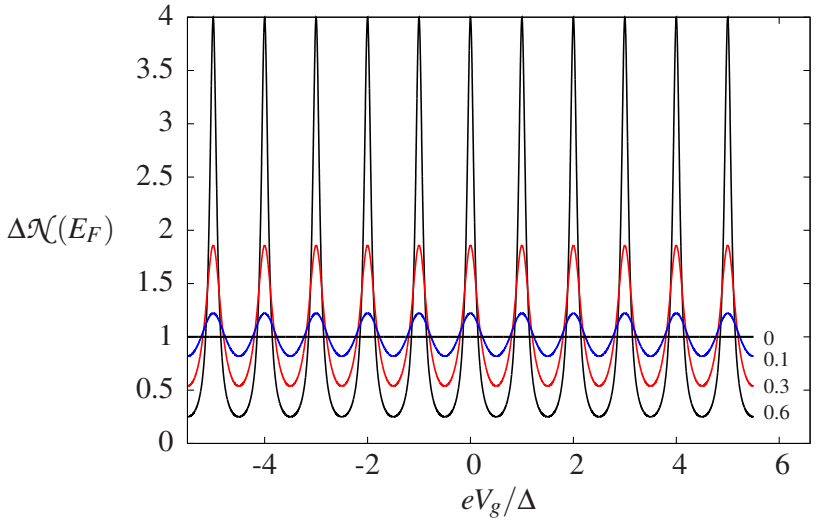

Figure 1.8: Peaked structure of the local density of states $\mathcal{N}(\varepsilon)$ on the dot as a function of the orbital energy shift controlled by the gate potential eV_g from Eq. (1.25). *$\mathcal{N}(E_F)$ is plotted for different values of the backscattering amplitude r. The progressive opening of the dot drives a transition from a Lorentzian to an oscillatory behavior of C_q, coherent with the experimental measurements illustrated in Fig. 1.6. For a completely transparent dot ($r = 0$) the density of states is uniform, which implies $C_0 = e^2/\Delta$.*

$$\begin{aligned}\chi_c(i\nu_n) &= -\frac{1}{\beta}\sum_{i\omega_n}\mathscr{D}(i\omega_n)\mathscr{D}(i\omega_n+i\nu_n)\\ &\to -\frac{1}{\pi\Gamma}\int_{-\infty}^{\infty}dx\,f(\Gamma x+\varepsilon_d)\frac{2x}{(x^2+1)[x^2-(\omega/\Gamma+i)^2]}\,,\end{aligned} \tag{1.55}$$

where the analytical continuation $i\nu \to \omega + i0^+$ has been performed to obtain the second line. At zero temperature, the integral can be calculated analytically

$$\chi_c(\omega) = \frac{1}{\pi\Gamma}\frac{1}{\frac{\omega}{\Gamma}\left(\frac{\omega}{\Gamma}+2i\right)}\ln\frac{\varepsilon_d^2+\Gamma^2}{\varepsilon_d^2-(\omega+i\Gamma)^2}\,. \tag{1.56}$$

Its low frequency expansion matches Eq. (1.3) and accesses the differential capacitance and the charge relaxation resistance. Reestablishing correct dimensions $\omega \to \hbar\omega$, the result recovers Eq. (1.15) obtained within scattering theory

$$C_0 = \frac{e^2}{h}\nu(\varepsilon_d)\,, \qquad\qquad R_q = \frac{h}{2e^2}\,, \tag{1.57}$$

where $\nu(\varepsilon_d)$ is the density of states associated to the single orbital ε_d

$$\nu(\varepsilon_d) = \frac{1}{\pi}\frac{\Gamma}{\varepsilon_d^2+\Gamma^2}\,. \tag{1.58}$$

In Appendix B, we carry out the calculation of the differential capacitance in the multi-level case. Considering a constant level spacing Δ, we can write $\varepsilon_l = -eV_g + l\Delta$ and, for an infinite number of levels, we recover Eq. (1.25), plotted in Fig. 1.8, with the identification

$$\frac{\pi\Gamma}{\Delta} = \frac{(1-r)^2}{1-r^2}\,. \tag{1.59}$$

Notice that, for a single level and one channel, we also recover the universal charge relaxation resistance $R_q = h/2e^2$. This means that the dynamical charge susceptibility Eq. (1.56) fulfills the Korringa-Shiba relation Eq. (1.40). The generalization of the previous calculation to multiple channels is straightforward. The model reads

$$H_{\text{Res-Nch}} = \sum_{k\sigma} \varepsilon_k c^\dagger_{k\sigma} c_{k\sigma} + t\sum_{k\sigma}\left(c^\dagger_{k\sigma} d_\sigma + d^\dagger_\sigma c_{k\sigma}\right) + \sum_\sigma \varepsilon_\sigma d^\dagger_\sigma d_\sigma\,, \tag{1.60}$$

with $\sigma = 1,\ldots,N$ the number of channels. This model readily provides expressions for the differential capacitance and the charge relaxation resistance analog to Eq. (1.27)

$$C_0 = \frac{e^2}{h}\sum_{\sigma=1}^{N} \nu_\sigma\,, \qquad\qquad R_q = \frac{h}{2e^2}\frac{\sum_\sigma \nu_\sigma^2}{\left(\sum_\sigma \nu_\sigma\right)^2}\,, \tag{1.61}$$

where the dwell-times are substituted by the density of states of the channels: $\nu(\varepsilon_\sigma) = \nu(\varepsilon_\sigma)$ from Eq. (1.58).

1.4 Conclusions

In this chapter we discussed the scattering formalism originally adopted by Büttiker, Thomas and Prêtre to explain the dynamical properties of the quantum RC circuit. The main results are the prediction of a quantum capacitance C_q and a charge relaxation resistance R_q, universally quantized in the single channel case. All these results are also derived with an Hamiltonian approach which constitutes the starting point of the forthcoming chapters, where interactions on the dot are addressed. The differential capacitance C_0 has been defined, showing that the capacitance of the quantum RC circuit is actually proportional to the static charge susceptibility of the quantum dot. We established that charge relaxation universality relies on the Korringa-Shiba relation Eq. (1.40). We derived the results of scattering theory from our Hamiltonian study of the quantum RC circuit in the non-interacting case. The following chapters focus on a Fermi liquid method to give a general proof of the Korringa-Shiba relation Eq. (1.40). While the quantum capacitance is a *static* quantity, the proof of the Korringa-Shiba relation requires an understanding of the low-energy dynamics of electrons in strongly interacting systems. This is the main problem to which this Thesis tries to give a comprehensive answer.

CHAPTER 2

A THEORY FOR THE INTERACTING QUANTUM RC CIRCUIT

Contents

In the previous chapter, it has been shown how the dynamical charge susceptibility $\chi_c(\omega)$ of the dot contains information about the conduction properties of the quantum RC circuit. The linear expansion of this quantity in the frequency ω defines, to leading order, the differential capacitance C_0 and, to first order, the charge relaxation resistance R_q. A direct calculation of $\chi_c(\omega)$ is not an easy task in the presence of interactions in the dot. From a formal point of view, the reason is the presence of a non-quadratic term in the Hamiltonian. In the Coulomb blockade and Anderson model, Eqs. (iv) and (v) respectively, this term is controlled by the charging energy E_c, that cannot be treated perturbatively in Coulomb

blockade regimes. The possibility to rely on Wick's theorem, when performing perturbative calculations in the tunneling coupling t, is also forbidden. Switching to a more physical point of view, even if these difficulties are overcome, it remains quite difficult to understand the underlying dissipation mechanisms. For example, the perturbative calculation in Ref. [72] shows that the charge relaxation resistance is universally quantized to $R_q = \frac{h}{2e^2}$, exactly the same value as for non-interacting electrons, while the differential capacitance behaves in a different way. What is the physical reason?

This is the main problem we address in this Thesis. We show that, at low energies, the lead electrons in a rich variety of interacting quantum dot systems are described by an effective non-interacting theory which captures the mechanism underlying energy dissipation, providing the condition for universality. As already discussed in Section 1.3.1, the condition for universality is given by the verification of the Korringa-Shiba relation [75]

$$\mathrm{Im}\chi_c(\omega)\big|_{\omega\to 0} = \hbar\pi\omega\chi_c^2. \tag{2.1}$$

This relation connects in a very specific way the first corrections to adiabaticity of the dynamic charge susceptibility to its zero frequency limit. Its proof requires diagrammatic calculations in the case of the Anderson model [75]. In this chapter, we present the theory describing the dynamics of low energy electrons in these systems. This permits the derivation of even generalized forms of Eq. (2.1), predicting new interesting non-universal behaviors of the charge relaxation resistance within a very simple framework. The main steps for its proof are summarized in Fig. 2.11. The Friedel sum rule [77, 61], discussed in detail in Section 2.1.1, sets the form of the Fermi liquid theory involving the *static* charge susceptibility of the quantum dot $\chi_c = -\partial\langle\hat{n}\rangle/\partial\varepsilon_d$. We recall that, in Chapter 1, we showed that this quantity is proportional to the differential capacitance $C_0 = e^2\chi_c$. This low energy theory is quadratic and the power dissipated when the system is driven by an AC bias $V_g(t)$ is readily calculated. This power is a function of the static charge susceptibility of the dot and has to be matched with the expression derived from the high energy model. Describing the periodic oscillations of the orbital energy around an equilibrium value by $\varepsilon_d(t) = \varepsilon_d^0 + \varepsilon_\omega\cos(\omega t)$, for a small enough amplitude ε_ω, linear response theory applies. In Appendix A, we show that the dissipated power $\mathscr{P}$, obtained from the high energy model, is given by

$$\mathscr{P} = \frac{1}{2}\varepsilon_\omega^2\omega\mathrm{Im}\chi_c(\omega)\,. \tag{2.2}$$

It is proportional to the imaginary part of the dynamical charge susceptibility $\chi_c(\omega)$ which we are interested in. Deriving the result of $\mathscr{P}$ from the low energy model

$$\mathscr{P} = \frac{1}{2}\varepsilon_\omega^2\omega^2\hbar\pi\chi_c^2, \tag{2.3}$$

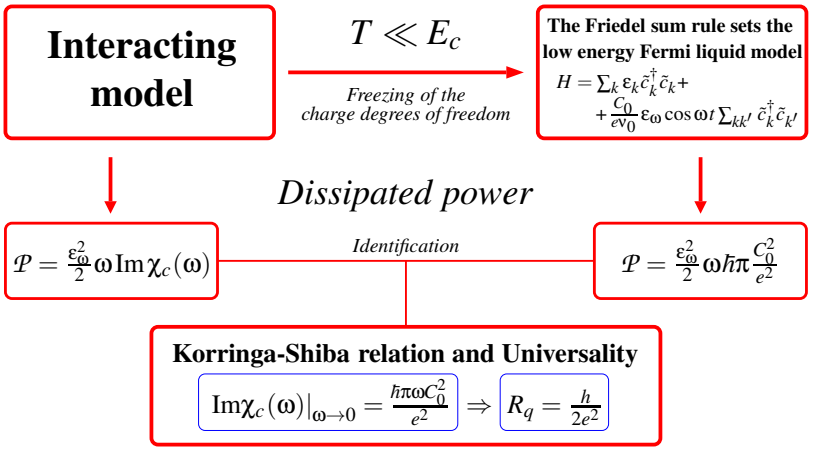

Figure 2.1: Main steps of our approach. For energies much lower than the charging energy E_c, the Friedel sum rule sets the form of the low energy Fermi liquid, whose dissipated power $\mathscr{P}$ is readily calculated. Identifying to the power obtained from the initial interacting model, proportional to the imaginary part of the dynamic charge susceptibility $\chi_c(\omega)$, the Korringa-Shiba relation, responsible for the universality of R_q, is shown.

the Korringa-Shiba relation Eq. (2.1) is readily obtained by identifying Eqs. (2.2) and (2.3). The universality of the charge relaxation resistance quantization $R_q = \frac{h}{2e^2}$ is then shown in the single channel case and in the presence of strong interactions on the dot.

The extension to the N channels case in this approach is straightforward and brings about a slight modification of Eq. (2.1) by a factor N

$$\mathrm{Im}\chi_c(\omega)\big|_{\omega\to 0} = \frac{\hbar\pi\omega\chi_c^2}{N}, \tag{2.4}$$

which also predicts the universality of the charge relaxation resistance to $R_q = h/2Ne^2$. In Section 2.4.1, the continuum limit for the levels in the dot is also discussed in detail predicting the mesoscopic crossover to a doubled value of the charge relaxation resistance [72]. The reason is that the continuum limit allows for energy dissipation inside the quantum dot, which becomes a further reservoir in the system. This results in a factor 2 multiplying the right hand side of Eq. (2.4). Even if the levels on the dot are actually spaced by Δ because of the finite size L of the dot, the condition for having a continuum is defined with respect to the driving frequency

$$\hbar\omega > \Delta. \tag{2.5}$$

This condition simply states that electrons can be excited by the drive also in the dot, creating particle-hole pairs which are responsible for energy dissipation, see also Fig. 2.4.

The universal quantization of R_q relies on the fact that the susceptibility of every channel χ_σ is the same, that is

$$\chi_\sigma = -\frac{\partial \langle n_\sigma \rangle}{\partial \varepsilon_d} = \frac{\chi_c}{N}. \tag{2.6}$$

This implies that the imaginary part of $\chi_c(\omega)$ is proportional to the square of the static charge susceptibility χ_c in Eqs. (2.1) and (2.4). This is the case when the transmission channels are degenerate in energy, but it is not a general feature. This degeneracy can be, for example, lifted by applying a magnetic field for electron with an internal spin degree of freedom. Our approach can be easily extended to this case and a generalized form of Eq. (2.4) is derived

$$\mathrm{Im}\chi_c(\omega)\big|_{\omega\to 0} = \hbar\pi\omega \sum_\sigma \chi_\sigma^2. \tag{2.7}$$

This is responsible for a non-universal expression for the charge relaxation resistance

$$R_q = \frac{h}{2e^2}\frac{\sum_\sigma \chi_\sigma^2}{\left(\sum_\sigma \chi_\sigma\right)^2}. \tag{2.8}$$

This expression is completely similar to that obtained by Büttiker [66] reported in Eq. (1.27) as a function of the densities of states, or dwell-times τ_σ, of the σ channel in the dot, which in our case are replaced by the susceptibilities χ_σ. The single channel case is remarkable in the sense that the numerator simplifies with the denominator in Eq. (2.8), leading to the universal value $h/(2e^2)$. Nothing, except the condition Eq. (2.6), guarantees the universality of Eq. (2.8) and, in Sections 2.5 and 2.6, we discuss how this formula predicts interesting non-universal behaviors of R_q in the presence of a magnetic field. Within the Anderson model, a giant peak arises for the charge relaxation resistance. It is triggered by breaking the Kondo singlet and new scaling regimes described by universal functions are predicted.

In Section 2.1.1 we discuss how a Fermi liquid theory, coherent with the Friedel sum rule, can be derived. In Section 2.2 we give the reason why this theory describes the Coulomb blockade and Anderson models at zero temperature and in Section 2.3 we discuss how the knowledge of the Friedel sum rule and a low energy Fermi liquid behavior allow one to derive the Korringa-Shiba relation, which is generalized to the N channel case in Section 2.4. In Section 2.5, we illustrate our predictions for the loss of universality of the charge relaxation resistance caused by the presence of a magnetic field in the Anderson model and, in Section 2.6, we provide an extension to SU(4) Kondo regimes, showing a further application of our renormalization group analysis to calculate the SU(4) Kondo temperatures.

2.1 The Fermi liquid in the quasi static approximation

As already discussed in Section 1.3.1, linear response theory states the possibility to study a time-dependent problem by looking at dynamical correlators considered at equilibrium. So, neglecting for the moment the time-dependence through $\varepsilon_d(t)$ of our problem, we consider the situation at equilibrium. It is a well established fact that both the Coulomb blockade model [60, 92] and the Anderson model [93] have a Fermi liquid behavior at low energy. We refer to textbooks [94, 95] for a complete review about Fermi liquid theory. What is important for the following discussion is that a fermionic system behaving like a Fermi liquid deploys the same qualitative physics as that of a free Fermi gas. Its constituents are then called *quasi-particles*, which are still fermions whose mass and spectrum are renormalized by the presence of interactions and which still carry the same quanta of charge and spin. The effective Hamiltonian describing the behavior of these quasi-particles has then to be a non-interacting Hamiltonian

$$H_{\mathrm{QP}} = \sum_{k\sigma} \varepsilon_k a^\dagger_{k\sigma} a_{k'\sigma}\,, \tag{2.9}$$

where the operators $a^\dagger_{k\sigma}$ create fermions of momentum k and spin σ. The ground state of this Hamiltonian is a Fermi sea. This feature is relevant for understanding the dynamics of a quantum dot exchanging electrons with the leads. Far from the charge degenerate points, the energy required to modify the charge occupation of the dot is E_c. In the situation that we consider, E_c is far above the temperature and the energy $\hbar\omega$ pumped in the system by the gate. We recall here that this regime differs from the one of the experiment described in Ref. [7], which has been carried for $\hbar\omega \sim E_c < \Delta$ and was the first to measure a universal charge relaxation resistance. As discussed in Ref. [92], it is then clear that a further electron cannot settle permanently in the dot, but it can spend there a (short) time within the uncertainty principle $\hbar/E_c$. At equilibrium, an electron of energy ε entering into the dot must leave it without violating total energy conservation. This can happen by two different kind of processes, which are shown in Fig. 2.2:

- Elastic processes: in this case the electron leaving the quantum dot has the same energy as the incoming one. The presence of the quantum dot affects then by a phase-shift the asymptotic behavior of the single-electron wave function far from the dot;
- Inelastic processes: in this case the electron entering in the quantum dot causes the creation of particle-hole pairs and the emitted electron will have a lower energy than the incoming one.

In the case of systems behaving like a Fermi liquid at low energy, the probability of inelastic processes goes to zero as $(\varepsilon/E_c)^2$ [95]. The Fermi liquid picture implies then that the low energy description of the system maps onto a single-particle problem which has to somewhat

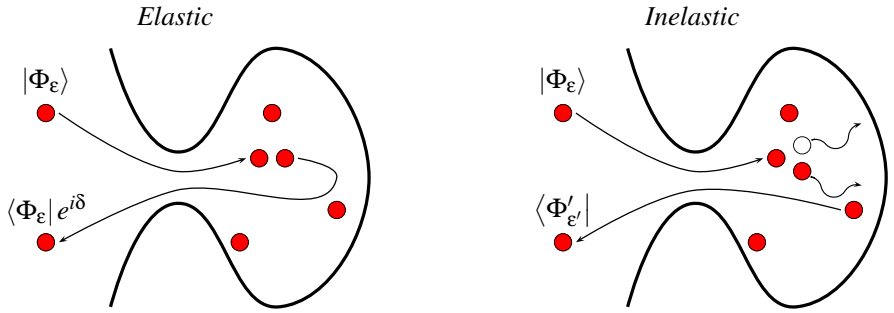

Figure 2.2: Illustration of the difference between elastic (left) and inelastic (right) events for electrons entering and leaving the quantum dot. See main text.

encode the information about the electron scattering with the quantum dot. The simplest model embodying these features is a free Fermi gas with a potential scattering term localized at the entrance of the dot [61]

$$H = \sum_{k\sigma} \varepsilon_k c^\dagger_{k\sigma} c_{k\sigma} + W(\varepsilon_d) \sum_{kk'\sigma} c^\dagger_{k\sigma} c_{k'\sigma} \,. \tag{2.10}$$

In the language of second quantization, the second term in this Hamiltonian describes a delta barrier located in $x = 0$. It is indeed the Fourier transform in the momentum representation of the electron operator $\Psi^\dagger(x=0)\Psi(x=0)$ and it does not conserve the momentum of incoming electrons. This is not particularly surprising as the introduction of a quantum dot breaks the translational invariance of the system and therefore momentum conservation. As a matter of fact, the Hamiltonian Eq. (2.10) is still quadratic and can be always put into the diagonal form Eq. (2.9). The dependence on the orbital energy ε_d of the potential scattering coupling W is explicitly put forward. In Section 2.2, we show that it naturally appears in the models we address, and allows us to understand their time dependence at low energy, as discussed in Section 2.3. The potential scattering coupling W is actually related to the local charge occupation of the quantum dot. The coupling of the dot with the non-interacting leads is responsible for a displacement of electrons. This translates into a local variation of their density and so a variation of their local occupation number $\langle \hat{N} \rangle$. In the following section we show that this variation of the electron number corresponds to the quantum dot occupation and it is a function of the potential scattering coupling W. The relation between the dot occupation and W is set by the Friedel sum rule.

2.1.1 An illustration of the Friedel sum rule for non-interacting electrons

The Friedel sum rule [77] relates the charge occupation of the dot $\langle \hat{n} \rangle$ to the phase-shift $\delta(\varepsilon)$ that the presence of the quantum dot causes on the wave function of the lead electrons at the Fermi surface. It reads

$$\langle \hat{n} \rangle = \frac{\delta(0)}{\pi} \tag{2.11}$$

and the phase-shift is considered at the Fermi energy $E_F = 0$. In this section, we provide an illustration of the Friedel sum-rule for the Anderson model Eq. (v) in the absence of interactions, $U = 0$. The extension to the interacting case is more difficult and it is given in Ref. [96, 97]. As the $\sigma = \uparrow, \downarrow$ spin sectors are decoupled, we can neglect the electron spin and calculate the occupation of the quantum dot described by a resonant level as in Eq. (1.41). To do this, the total electron occupation $\langle \hat{N} \rangle$ of the electron gas has to be calculated. It is given by

$$\langle \hat{N} \rangle = \sum_{\alpha} \int_{-\infty}^{\infty} d\omega A_{\alpha}(\omega) f(\omega) \,, \tag{2.12}$$

the sum on the label α running over all the eigenstates of the Hamiltonian. $A_{\alpha}(\omega)$ is the spectral function of the state α and it is defined as

$$A_{\alpha}(\omega) = -\frac{1}{\pi} \mathrm{Im} G_{\alpha\alpha}(\omega + i0^{+}) \,, \tag{2.13}$$

$G_{\alpha\alpha}$ being the *retarded* Green's function associated to the state α. In this section, we adopt the notation $G_{dk}(t - t') = -i\theta(t - t') \langle d(t) c_k^{\dagger}(t') \rangle$. In the absence of the quantum dot, described by the operators d in the Anderson Hamiltonian Eq. (v), $G_{kk}(\omega + i0^{+}) = (\omega + i0^{+} - \varepsilon_k)^{-1}$ and Eq. (2.12) reduces to a sum over the Fermi function $\sum_k f(\varepsilon_k)$ giving the total number of electrons $\langle \hat{N} \rangle$ composing the system. When the quantum dot is taken into account, a further resonant level is introduced. Working at fixed chemical potential, the total number of electrons Eq. (2.12) will be modified, and the difference with the previous one will give the amount of electrons displaced by the presence of the quantum dot. We already calculated in Section 1.3.2 the retarded Green's function of the quantum dot electrons Eq. (1.54). The retarded Green's function of the lead electrons can be also obtained writing down the equation of motions

$$(\omega - \varepsilon_d) G_{dd}(\omega) = 1 + t \sum_k G_{kd}(\omega) \,, \qquad (\omega - \varepsilon_k) G_{kk'}(\omega) = \delta_{kk'} + t G_{dk'}(\omega) \,, \tag{2.14}$$

$$(\omega - \varepsilon_k) G_{kd}(\omega) = t G_{dd}(\omega) \,, \qquad (\omega - \varepsilon_d) G_{dk} = t \sum_{k'} G_{k'k}(\omega) \,. \tag{2.15}$$

Solving the system, the Green's function for the lead electrons reads

$$G_{kk'}(\omega) = \frac{\delta_{kk'}}{\omega - \varepsilon_k} + \frac{1}{\omega - \varepsilon_k} t^2 G_{dd}(\omega) \frac{1}{\omega - \varepsilon_{k'}} \,. \tag{2.16}$$

The T-matrix of the lead electrons, defined in Appendix C, is then given by

$$T(\omega + i0^+) = t^2 G_{dd}(\omega + i0^+) = \frac{t^2}{\omega - \varepsilon_d + i\Gamma} = \frac{t^2}{\sqrt{(\omega - \varepsilon_d)^2 + \Gamma^2}} e^{i\delta}, \tag{2.17}$$

where we define the *phase-shift*

$$\delta(\omega) = \frac{\pi}{2} - \arctan\left(\frac{\varepsilon_d - \omega}{\Gamma}\right). \tag{2.18}$$

A detailed explanation of the reason why δ can be viewed as the phase-shift of the lead electron wave function is given in the framework of scattering theory in Appendix C. In the wide-band limit, the contribution from the second term in Eq. (2.16) can be neglected in the calculation of $\langle \hat{N} \rangle$ given by Eq. (2.12) [61]. The number of displaced electrons is given solely by the Green's function of the quantum dot d electrons

$$\langle \hat{N} \rangle_{\text{with dot}} - \langle \hat{N} \rangle_{\text{without dot}} = \langle \hat{n} \rangle = -\frac{1}{\pi} \text{Im} \int_{-\infty}^{\infty} d\omega G_{dd}(\omega) f(\omega) = \frac{1}{2} - \frac{1}{\pi} \arctan\left(\frac{\varepsilon_d}{\Gamma}\right), \tag{2.19}$$

what is coherent with Eqs. (2.11) and (2.18). Eq. (2.19) is also meaningful for the two following reasons. 1) In the wide-band approximation, the number of displaced electrons is given by the local Green's function G_{dd} and can then be interpreted as the charge occupation of the quantum dot. 2) The number of displaced electrons by the quantum dot depends on the orbital energy ε_d. This provides a further explanation of how a time dependence of this energy on the gate potential $V_g(t)$ drives a current in the system. A variation of ε_d triggers the displacement of electrons in the leads and it will allow us to access the AC admittance of the system. The generalization of Eq. (2.11) to the N channels case is straightforward

$$\langle \hat{n} \rangle = \sum_{\sigma} \frac{\delta_\sigma(0)}{\pi}, \tag{2.20}$$

with $\sigma = 1, \ldots, N$ labeling channels.

As a final remark, if the Friedel sum rule Eq. (2.11) applies for a system described by the low energy Fermi liquid Hamiltonian Eq. (2.10), the coupling $W(\varepsilon_d)$ is fixed by the quantum dot occupation. In Appendix D, we calculate the phase-shift induced on the low energy quasiparticles of the Fermi liquid by the potential scattering term. It reads

$$\delta_W = -\arctan(\pi \nu_0 W). \tag{2.21}$$

Applying Eq. (2.11), the following correction to the dot occupation is found

$$\langle \hat{n} \rangle = -\frac{1}{\pi} \arctan(\pi \nu_0 W). \tag{2.22}$$

This is an important result, which is involved in the demonstration of the Korringa-Shiba relation in Section 2.3. In the case of the Coulomb blockade Hamiltonian Eq. (iv), there is no formal demonstration of the validity of the Friedel sum rule and we prove it in the large number of channels N limit and for a small tunneling t. We give a flavor of this proof in Section 2.2, extended also to the Anderson Hamiltonian Eq. (v).

2.2 The Schrieffer-Wolff transformation

In this section, we give a simple and more intuitive explanation of why a low energy Hamiltonian such as Eq. (2.10) for the Coulomb blockade and Anderson model is expected. A more formal proof up to higher orders in the tunneling t within the analytical renormalization group will be given in Chapters 3 and 4. We also show the direct dependence of the coupling W on the gate potential V_g, important to understand in Section 2.3 that the creation of particle-hole pairs described by the potential scattering term is responsible for energy dissipation at low energy.

To do this we rely on the Schrieffer-Wolff transformation [98, 95], first devised for the Anderson Hamiltonian [99], to derive the Coqblin-Schrieffer model [100] and that we extend here to the Coulomb blockade model. This procedure has much to do with the idea of renormalization that we will discuss later on. The problem is the following. Far from the charge degeneracy points, the lowest energy charge configuration n is fixed by the gate potential V_g and the possibility to fluctuate to $n \pm 1$ occupations requires an energy of the order of E_c. For temperatures much lower than E_c, the charge degrees of freedom of the quantum dot are frozen, acting but virtually on the low energy behavior of the system. They can be somewhat eliminated and to do this the Hamiltonian in the absence of tunneling can be then separated in a low energy sector, were the charge is fixed to n, and a high energy one where the charge in the dot has different values

$$H_0 = \begin{bmatrix} H_{\text{Low}} & 0 \\ 0 & H_{\text{High}} \end{bmatrix}. \tag{2.23}$$

The presence of the (small) tunneling term couples these different energy sectors, and in this language is then anti-diagonal

$$H_T = \begin{bmatrix} 0 & h_T \\ h_T^\dagger & 0 \end{bmatrix}. \tag{2.24}$$

The Schrieffer-Wolff transformation is nothing more than the unitary transformation generated by the operator U that diagonalizes by blocks this Hamiltonian

$$U\left[H_0 + H_T\right]U^\dagger = \begin{bmatrix} H'_{\text{Low}} & 0 \\ 0 & H'_{\text{High}} \end{bmatrix}, \tag{2.25}$$

including in the low energy sector all the *virtual* excursions in the high energy one induced by the presence of H_T and *vice versa*. It is important to notice that the inclusion of H_T in the Hamiltonian is responsible for the breaking of charge conservation in the dot and n is not a good quantum number anymore.

For interacting systems, this diagonalization can be performed exactly only in principle, but practically only by a perturbative approach. Unitarity allows one to write $U = e^{iS}$, where

S is a Hermitian operator. As S has to be at least of order t, we can expand the exponential and find to the leading order

$$H' = H_0 + H_T + i\,[S, H_0] + O\left(t^2\right). \tag{2.26}$$

This Hamiltonian is then block diagonal if the following condition is fulfilled

$$i\,H_T = [S, H_0]\,. \tag{2.27}$$

The fact that H' is block diagonal and coincides formally with H_0 should not give the wrong impression that different sectors can be defined where the charge in the dot is still quantized to integer values given by $\langle \sum_\alpha d_\alpha^\dagger d_\alpha \rangle = n$, α being any label (including spin) for electrons in the dot. This is not possible anymore, as the hybridization H_T has been taken into account and it does not commute with the operator $\sum_\alpha d_\alpha^\dagger d_\alpha$, giving the electron occupation on the quantum dot. The transformation Eq. (2.25) implies a change of basis and the new operators d_α and $d_\alpha^\dagger$ in H' do not describe the electrons in the quantum dot anymore, but an excitation very close to them hybridized with the lead electrons. This is a way to understand how the concept of quasi-particle arises in many-body systems.

Even if the condition Eq. (2.27) takes into account the first charge fluctuations in the dot, it is not enough to obtain the residual interaction between lead and dot electrons induced by the presence of the hybridization term H_T. The term of second order in t in Eq. (2.26) must be considered and Eq. (2.27) implies

$$H' = H_0 + \frac{i}{2}\,[S, H_T]\,, \tag{2.28}$$

which can be always put into a block diagonal form. We show in the following sections that this correction gives the potential scattering contribution to the low energy Hamiltonian Eq. (2.10).

2.2.1 Coulomb blockade model

Following Grabert [101, 102], to perform the operations required by the Schrieffer-Wolff transformation sketched in the previous section, it is useful to decouple the charge occupation of the dot from the fermionic degrees of freedom of the electrons in it. This can be done by adding to the Coulomb blockade Hamiltonian Eq. (iv) a new operator $\hat{n}$, giving the occupation number on the dot fixed by the gate voltage. The fermionic operators d_l and $d_l^\dagger$ in Eq. (iv) are replaced by new operators (that we shall also call d_l and $d_l^\dagger$) describing only a free electron gas in the dot and charge fluctuations are now taken into account by a new expression of the hybridization term

$$H_T = t \sum_{n,k,l} \left[d_l^\dagger c_k \,|n+1\rangle \langle n| + c_k^\dagger d_l \,|n-1\rangle \langle n| \right]. \tag{2.29}$$

The operator $S = s + s^\dagger$ fulfilling Eq. (2.27) is given by

$$s = it \sum_{k,l,n} s_{kln} c_k^\dagger d_l \, |n-1\rangle \langle n| \,, \tag{2.30a}$$

$$s_{kln} = \frac{1}{\varepsilon_l - \varepsilon_k + E_c(2n-1) + \varepsilon_d}. \tag{2.30b}$$

This operator, when substituted into Eq. (2.28) to obtain the effective quasi-particle interaction, is responsible for a coupling between sectors of charge n and $n \pm 2$. This coupling can be eliminated by performing a further Schrieffer-Wolff transformation, giving further corrections of order t^3 irrelevant for the purposes of the current discussion. The Hamiltonian becomes then block diagonal in the sectors given by different values of n. For $-E_c < \varepsilon_d < E_c$, the lowest energy sector corresponds to $n = 0$ and the effective Hamiltonian reads $H'_{\rm CBM} = H_0 + H_B$, with

$$H_{\rm B} = \frac{t^2}{2} \sum_{kk'll'} \left(s_{kl0} d_{l'}^\dagger c_{k'} c_k^\dagger d_l - s_{kl1} c_k^\dagger d_l d_{l'}^\dagger c_{k'} + \text{h.c.} \right). \tag{2.31}$$

This interaction can be simplified by a mean-field treatment

$$d_l^\dagger c_k c_{k'}^\dagger d_{l'} = \langle d_l^\dagger d_{l'} \rangle \, c_k c_{k'}^\dagger + \langle c_k c_{k'}^\dagger \rangle \, d_l^\dagger d_{l'} = \delta_{ll'} \theta(-\varepsilon_l) c_k c_{k'}^\dagger + \delta_{kk'} \theta(\varepsilon_k) d_l^\dagger d_{l'} \,, \tag{2.32}$$

which is justified in the renormalization group framework [1]. We are then left with marginal operators giving a potential scattering contribution which corresponds to the backscattering of electrons at the lead-dot boundary. After the simplification in Eq. (2.32) we can carry out part of the sums in Eq. (2.31) and obtain, for example, for the first term in Eq. (2.32)

$$\begin{aligned} \frac{t^2}{2} \sum_{kk'} c_{k'} c_k^\dagger \sum_{ll'} \delta_{ll'} \theta(-\varepsilon_l) s_{kl0} = \\ = \sum_{kk'} c_{k'} c_k^\dagger \frac{\nu_0 t^2}{2} \int_{-D_0}^{0} \frac{d\varepsilon_l}{\varepsilon_l - \varepsilon_k - E_c + \varepsilon_d} = \\ = \sum_{kk'} c_k^\dagger c_{k'} \frac{\nu_0 t^2}{2} \ln \left(\frac{\varepsilon_k + E_c - \varepsilon_d + D_0}{\varepsilon_k + E_c - \varepsilon_d} \right). \end{aligned} \tag{2.34}$$

We inserted a high energy cut-off D_0 which is sent to infinity without any divergence at the end of calculations. As we are concerned only with electrons close to the Fermi surface, the

[1] As a matter of fact, this expansion is justified by the RG flow of operators. To classify them one must look at the normal ordered form

$$d_l^\dagger c_k c_{k'}^\dagger d_{l'} = \delta_{ll'} \theta(-\varepsilon_l) c_k c_{k'}^\dagger + \delta_{kk'} \theta(\varepsilon_k) d_l^\dagger d_{l'} + : d_l^\dagger c_k c_{k'}^\dagger d_{l'} : , \tag{2.33}$$

where the last normal ordered operator describing interaction between electrons is irrelevant at low energy and then neglected in Eq. (2.32). The terms kept are marginal in the RG sense. A formal discussion of the operator classification in the RG flow is given within the path-integral formalism in Chapter 3.

energies $\varepsilon_{k,l}$ appearing in the logarithm can be sent consistently to zero. In Section 3.3.3, we discuss in detail that all the corrections to this approximation, being energy dependent, are irrelevant at low energy in the RG flow, and can then be neglected. Summing up all the contributions, D_0 can be safely sent to infinity. The effective low energy model, to leading order in the dimensionless conductance $g = (\nu_0 t)^2$, is obtained

$$H'_{\mathrm{CBM}} = H_0 + \frac{g}{\nu_0} \ln\left(\frac{E_c - \varepsilon_d}{E_c + \varepsilon_d}\right) \left[\sum_{ll'} d_l^\dagger d_{l'} - \sum_{kk'} c_k^\dagger c_{k'}\right]. \tag{2.35}$$

This expression of the Hamiltonian describes two Fermi gases completely decoupled, but affected by potential scattering interactions with opposite amplitudes. This is the feature responsible for the mesoscopic crossover to a double universal charge relaxation resistance $R_q = h/e^2$ in the continuum limit of the dot, and it will be discussed in Section 2.4.1. The model then recovers the Hamiltonian (2.10) for the lead electrons. The phase-shift δ_W is given by Eq. (2.21) and the charge occupation of the dot is calculated to leading order by applying the Friedel sum rule Eq. (2.11)

$$\langle \hat{n} \rangle = \frac{\delta}{\pi} = g \ln\left(\frac{E_c - \varepsilon_d}{E_c + \varepsilon_d}\right). \tag{2.36}$$

This result is in complete agreement with a direct perturbative calculation of the charge on the dot [60, 101, 102]. The extension to the N channel case is trivial and one has to simply substitute $g \to N(\nu_0 t)^2$ in Eq. (2.36).

As previously claimed, the potential scattering coupling W in Eq. (2.35) directly depends on the orbital energy ε_d and therefore on the gate potential V_g, which tunes it. This is the requirement setting the dissipation term in the quasi static approximation of Section 2.3. We switch now to the spin-full case for a single level. The system is described by the Anderson model and the mapping onto Eq. (2.10) will present further difficulties because of the emerging of Kondo correlations.

2.2.2 Anderson model

As already mentioned, the Schrieffer-Wolff transformation has been expressly devised for the Anderson Hamiltonian to better understand the behavior of localized moments in dilute alloys [103]. The main result of Ref. [99] is the mapping of the Anderson Hamiltonian onto the Kondo Hamiltonian including a potential scattering term out of particle-hole symmetry

$$H'_{\mathrm{AM}} = H_0 + J_0 \mathbf{S} \cdot \mathbf{s} + W_0 \sum_{kk'\sigma} c_{k\sigma}^\dagger c_{k'\sigma}. \tag{2.37}$$

This mapping applies for a single electron occupying the dot at energies lower than E_c. This requires $-U \ll \varepsilon_d \ll 0$, as it can be seen in the phase diagram of the isolated quantum dot, pictured in Fig. 4.1. The spin of the electron in the quantum dot $\mathbf{S}$ is coupled anti-ferromagnetically to the local spin of the lead electrons $\mathbf{s} = \sum_{kk'\tau\tau'} c^\dagger_{k\sigma} \frac{\sigma_{\tau\tau'}}{2} c_{k'\sigma'}$, with $\sigma_{\tau\tau'}$ the vector composed of the Pauli matrices, and

$$J_0 = 2t^2 \left(\frac{1}{\varepsilon_d + U} - \frac{1}{\varepsilon_d} \right), \tag{2.38}$$

$$W_0 = -\frac{t^2}{2} \left(\frac{1}{\varepsilon_d + U} + \frac{1}{\varepsilon_d} \right). \tag{2.39}$$

$W_0 = 0$ at the particle-hole symmetric point $\varepsilon_d = -U/2$ and, if we forget for the moment the Kondo anti-ferromagnetic coupling controlled by J_0, we recover again the Hamiltonian Eq. (2.10) with a potential scattering coupling which depends on the energy of the dot occupation ε_d. In Chapter 4, we show that the anti-ferromagnetic coupling in Eq. (2.37) can

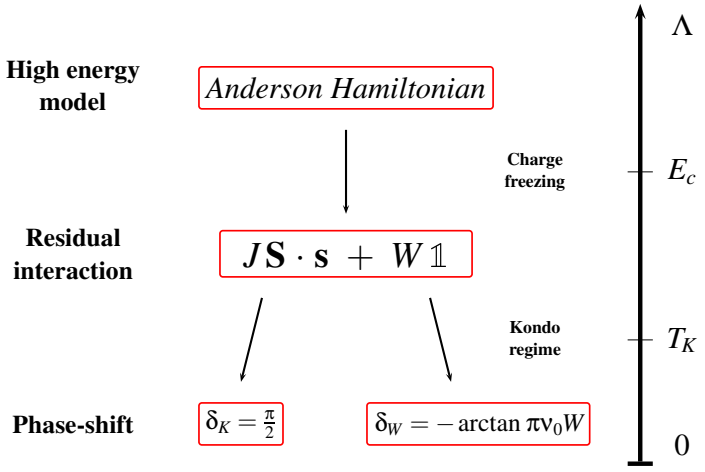

Figure 2.3: Sketch of the renormalization behavior of the Anderson Hamiltonian. For energy scales Λ for the lead electrons below the charging energy E_c, the charge degrees of freedom of the quantum dot are frozen. The lead electrons interact anti-ferromagnetically with the spin of the electron in the dot and also feel a potential backscattering. In the zero energy limit, below the Kondo crossover, these two terms are responsible for different phase-shifts δ_K and δ_W for the lead electrons, which can be calculated independently.

be actually ignored following the renormalization scheme sketched in Fig. 2.3. The anti-ferromagnetic coupling is exclusively responsible for a $\delta_K = \pi/2$ phase-shift of the low energy quasi-particles of the system. The actual origin of this phase-shift will be discussed in Section 4.2.3, but we can understand it by simple considerations. As already mentioned, the Friedel sum rule applies for the Anderson Hamiltonian [96]. At particle-hole symmetry, the charge

on the dot is fixed to one by symmetry, W in Eq. (2.39) is zero and then only the Kondo coupling in Eq. (2.37) is responsible for the phase-shift of the low energy quasi-particles. Then, in the absence of any magnetic field, the two opposite spin channels are symmetric and the Friedel sum rule states

$$\langle \hat{n} \rangle = 2\frac{\delta_K}{\pi}. \tag{2.40}$$

The fact that $\langle \hat{n} \rangle = 1$ sets $\delta_K = \pi/2$. Relying on the works by Cragg and Lloyd [104, 105, 106], which addressed a Kondo Hamiltonian corrected by a potential scattering contribution as in Eq. (2.37), it is possible to show that the phase-shift δ_W, caused by the potential scattering term on the low energy quasi-particles, is *additive* to δ_K:

$$\delta = \delta_K + \delta_W, \tag{2.41}$$

and can then be calculated independently. This can be verified to leading order in t with the Schrieffer-Wolff transformation Eqs. (2.37), (2.38) and (2.39). Eq. (2.21) gives the phase-shift caused by the potential scattering term for every spin channel

$$\delta_W = -\arctan(\pi \nu_0 W_0) \tag{2.42}$$

and the Friedel sum rule provides the correction to the charge in the dot to the leading order

$$\langle \hat{n} \rangle = \frac{2}{\pi}\left[\delta_K - \arctan(\pi \nu_0 W)\right] = 1 + \frac{\Gamma}{\pi}\left(\frac{1}{\varepsilon_d + U} + \frac{1}{\varepsilon_d}\right). \tag{2.43}$$

The validity of this expression can be tested and compared to the static charge susceptibility χ_c obtained with Bethe ansatz calculations at particle-hole symmetry [107]

$$\chi_c = -\frac{\partial \langle \hat{n} \rangle}{\partial \varepsilon_d}\bigg|_{\varepsilon_d = -\frac{U}{2}} = \frac{8\Gamma}{\pi U^2}\left(1 + \frac{12\Gamma}{\pi U} + \ldots\right). \tag{2.44}$$

The equations (2.43) and (2.44) are coherent and written as an expansion in powers of Γ/U. Our approach provides, through the Schrieffer-Wolff transformation, the static susceptibility even out of particle-hole symmetry:

$$\chi_c = \frac{\Gamma}{\pi}\left[\frac{1}{(\varepsilon_d + U)^2} + \frac{1}{\varepsilon_d^2}\right]. \tag{2.45}$$

In Chapter 4, more extended expressions of Eqs. (2.43) and (2.45) are provided, including the next to leading order corrections in the tunneling t. These are verified to be coherent with Eq. (2.44), showing the validity of our approach. Moreover, the analytical knowledge of χ_c out of particle-hole symmetry is a completely new result, turning out to be useful to determine the analytic expression of the envelope of the giant peak of R_q, to be discussed in Sections 2.5.1 (briefly) and 4.4.1 (in more detail).

2.3 The quasi static approximation

In the previous discussion, we showed that the potential scattering coupling W of the low energy Fermi liquid Hamiltonian Eq. (2.10) is a direct function of the orbital energy of the dot ε_d. As discussed in Chapter 1, this energy is renormalized by the gate potential $\varepsilon_d \to \varepsilon_d - eV_g(t)$, see Eq. (1.29). For an AC bias, this is a periodic function of time oscillating at the frequency ω, given by

$$\varepsilon_d(t) = \varepsilon_d^0 + \varepsilon_\omega \cos\left(\omega t\right). \tag{2.46}$$

The *quasi-static approximation* consists in substituting Eq. (2.46) directly in Eq. (2.10). This condition assumes that the low energy Hamiltonian Eq. (2.10), derived for the equilibrium problem, follows, without any delay, the orbital oscillations given in the high energy theory. The quasi-static approximation is then a statement about a behavior close to adiabaticity and requires that the energy $\hbar\omega$ pumped in the system is much smaller than all the other energy scales of the problem.

If this condition is satisfied, the linear response regime allows for an expansion in ε_ω of the coupling $W(\varepsilon_d)$. Restricting ourselves to the single channel case (the extension to the multi-channel case is straightforward)

$$H = \sum_k \varepsilon_k c_k^\dagger c_k + \left[W(\varepsilon_d^0) + W'(\varepsilon_d^0)\varepsilon_\omega \cos\left(\omega t\right)\right] \sum_{kk'} c_k^\dagger c_{k'}'. \tag{2.47}$$

The time independent part of this Hamiltonian can be diagonalized, leading to [108]

$$H = \sum_{kk'} \varepsilon_k a_k^\dagger a_k + \frac{W'(\varepsilon_d^0)}{1 + \left[\pi\nu_0 W(\varepsilon_d^0)\right]^2} \varepsilon_\omega \cos\left(\omega t\right) \sum_{kk'} a_k^\dagger a_{k'}, \tag{2.48}$$

where the operators a and $a^\dagger$ describe the new quasi-particles diagonalizing the time independent part of the Hamiltonian (2.47). The renormalization of the bulk spectrum ε_k can be neglected in the following calculations. Realizing that the Friedel sum rule, in the form Eq. (2.22) for the potential scattering Hamiltonian, sets

$$\chi_c = \frac{\nu_0 W'(\varepsilon_d^0)}{1 + \left[\pi\nu_0 W(\varepsilon_d^0)\right]^2}, \tag{2.49}$$

the Hamiltonian (2.48) can be cast in the more compact and transparent form

$$H = \sum_{kk'} \varepsilon_k a_k^\dagger a_k + \frac{\chi_c}{\nu_0} \varepsilon_\omega \cos\left(\omega t\right) \sum_{kk'} a_k^\dagger a_{k'}. \tag{2.50}$$

This Hamiltonian shows which mechanism is responsible for energy dissipation at low energy for a rich variety of strong interacting systems satisfying the Friedel sum rule and a Fermi

liquid behavior at low energy. The time dependent term pumps energy in the system, which is then dissipated by the creation of *free* particle-hole pairs controlled by the static charge susceptibility χ_c of the quantum dot. The non-interacting Hamiltonian Eq. (2.50) explains why the scattering formalism, discussed in Chapter 1, predicts the correct universal charge relaxation resistance also in the presence of interactions on the quantum dot, the dissipation mechanism being that of a non-interacting system.

2.4 Generalized form of the Korringa-Shiba relation

The Hamiltonian (2.50), devised for the low energy behavior of the lead electrons in devices including quantum dots, is easy to handle. Recalling the results of Appendix A, the time dependent Hamiltonian Eq. (2.50) dissipates the power

$$\mathscr{P} = \frac{1}{2}\varepsilon_\omega^2 \omega \mathrm{Im}\chi_{\hat{A}}(\omega)\,, \tag{2.51}$$

where the linear response function

$$\chi_{\hat{A}}(t-t') = \frac{i}{\hbar}\theta(t-t')\left\langle\left[\hat{A}(t),\hat{A}(t')\right]\right\rangle_0 \tag{2.52}$$

is a correlator at different times of the potential scattering operator

$$\hat{A} = \frac{\chi_c}{\nu_0}\sum_{kk'} a_k^\dagger a_{k'}\,, \tag{2.53}$$

responsible for the creation of particle-hole pairs. As we are interested only in the zero temperature limit, the calculation is conveniently performed directly in real time, differently than in Section 1.3.2. Nevertheless, comparing to the calculation in the Matsubara formalism remains an instructive exercise and we sketch it in parallel [2]. The Fourier transform of

[2]The expression of the Fourier transform of the response function Eq. (2.52) in the Matsubara formalism follows from that given in Eq. (1.50)

$$\chi_{\hat{A}}(i\nu_n) = \frac{1}{\hbar}\int_0^{\hbar\beta} d(\tau-\tau')e^{i\nu_n(\tau-\tau')}\langle\hat{A}(\tau)\hat{A}(\tau')\rangle_0\,. \tag{2.54}$$

All the steps in the main text can be repeated with the substitution $it \to \tau$ in Eq. (2.57). The main difference is given by the fact that the commutator in Eq. (2.56) has been replaced by an upper bound $\hbar\beta$ in the imaginary time integral. The repetition of the steps in the main text leads to the formula

$$\chi_{\hat{A}}(\omega) = \frac{1}{\hbar}\frac{\chi_c^2}{\nu_0^2}\sum_{pp'} f_p(1-f_{p'})\frac{1}{i\nu_n + \frac{\varepsilon_{p'}-\varepsilon_p}{\hbar}}\left(e^{\beta(\varepsilon_p-\varepsilon_{p'})}-1\right), \tag{2.55}$$

which recovers Eq. (2.58) if the analytical continuation $i\nu_n \to \omega + i0^+$ is done and the zero temperature limit is taken.

the response function Eq. (2.52) reads

$$\chi_{\hat{A}}(\omega) = \frac{i}{\hbar}\int_0^\infty d(t-t')e^{i(t-t')(\omega+i0^+)}\left\langle\left[\hat{A}(t),\hat{A}(t')\right]\right\rangle_0 . \tag{2.56}$$

The time dependence of the operators a and $a^\dagger$ is easily obtained in the Heisenberg representation

$$a_k(t) = a_k e^{-\frac{i}{\hbar}t\varepsilon_k}, \qquad a_k^\dagger(t) = a_k^\dagger e^{\frac{i}{\hbar}t\varepsilon_k}. \tag{2.57}$$

Applying Wick's theorem and that $\langle a_p^\dagger a_k\rangle_0 = \delta_{pk}f(\varepsilon_p)$ and $\langle a_k a_p^\dagger\rangle_0 = \delta_{kp}[1-f(\varepsilon_p)]$ one can transform Eq. (2.56) into the form

$$\chi_{\hat{A}}(\omega) = -\frac{1}{\hbar}\frac{\chi_c^2}{\nu_0^2}\sum_{pp'}\theta(-\varepsilon_p)\theta(\varepsilon_{p'})\left[\frac{1}{\omega+\frac{\varepsilon_p-\varepsilon_{p'}}{\hbar}+i0^+}-\frac{1}{\omega+\frac{\varepsilon_{p'}-\varepsilon_p}{\hbar}+i0^+}\right], \tag{2.58}$$

where the zero temperature limit for the Fermi distribution has been carried out. Taking the imaginary part and the continuum limit

$$\mathrm{Im}\chi_{\hat{A}}(\omega) = \pi\chi_c^2\int_{-\infty}^\infty d\varepsilon d\varepsilon'\theta(-\varepsilon)\theta(\varepsilon')\left[\delta(\hbar\omega+\varepsilon-\varepsilon')-\delta(\hbar\omega+\varepsilon'-\varepsilon)\right]. \tag{2.59}$$

This expression is easily integrated and gives

$$\mathrm{Im}\chi_{\hat{A}}(\omega) = \pi\hbar\omega\chi_c^2. \tag{2.60}$$

Identifying with the dissipated power expected from the initial model Eq. (2.2), the Korringa-Shiba relation

$$\mathrm{Im}\chi_c(\omega) = \pi\hbar\omega\chi_c^2 \tag{2.61}$$

is proven, predicting a universal value for the charge relaxation resistance

$$R_q = \frac{h}{2e^2}. \tag{2.62}$$

This result holds then even in the presence of strong interactions in the dot, provided a Fermi liquid low energy behavior, effectively non-interacting. This reasoning can be easily extended to the N channel case leading to a Korringa-Shiba relation of the form Eq. (2.4) and $E_Q = h/2Ne^2$.

2.4.1 A continuum in the dot

In Section 2.2.1, we argued that the Fermi liquid picture still applies to a large dot described by the Coulomb blockade model Eq. (iv). The subtlety is that dot and lead constitute two

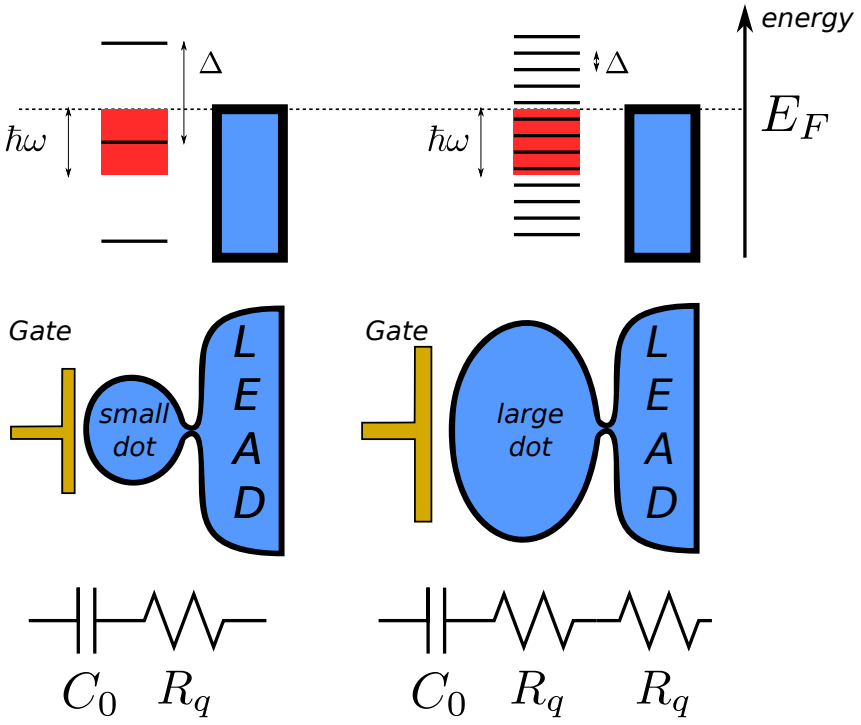

Figure 2.4: Mesoscopic crossover in the charge relaxation resistance. Left) In a small dot, the level spacing Δ is larger than the driving energy $\hbar\omega$ and energy levels in the dot are not excited. The universal resistance $R_q = h/2e^2$ of the equivalent RC circuit is furnished exclusively by the lead electron reservoir. Right) Excitation of energy levels inside the dot are permitted in the large dot limit, which acts as a further reservoir in series to the lead.

separate Fermi liquids, one describing the electrons in the lead and the other the electrons in the quantum dot, see Eq. (2.35). At first glance, it may seem that the quantum dot simply adds an additional channel for dissipation so that $R_q = h/2Ne^2$ would apply with $N = 2$. The situation is actually different. The energy cost E_c to modify the dot occupation prevents at low energy the transfer of electrons between the dot and the lead [92]. The electrons of both these gases are then only backscattered at the lead/dot boundary with opposite amplitudes. In the quasi-static approximation, all the steps carried in the previous discussion can be repeated for the Hamiltonian Eq. (2.35). The main difference is that the time variation of the orbital energy ε_d couples also to the residual fermionic degrees of freedom of the electrons in the dot. The operator responsible for energy dissipation becomes

$$\hat{A} = \frac{\chi_c}{\nu_0}\left(\sum_{kk'} c_k^\dagger c_{k'} - \sum_{ll'} d_l^\dagger d_{l'}\right), \tag{2.63}$$

where we remember that the operators $c_k^\dagger$ and $d_l^\dagger$ create lead and dot electrons of energy $\varepsilon_{k,l}$ respectively. The presence of this further element in the operator $\hat{A}$ adds a further contribu-

tion to Eq. (2.58), completely analog to the contribution of particle-hole pairs excited in the lead Eq. (2.58),

$$-\frac{1}{\hbar}\frac{\chi_c^2}{\nu_0^2}\sum_{ll'}\theta(-\varepsilon_l)\theta(\varepsilon_{l'})\left[\frac{1}{\omega+\frac{\varepsilon_l-\varepsilon_{l'}}{\hbar}+i0^+}-\frac{1}{\omega+\frac{\varepsilon_{l'}-\varepsilon_l}{\hbar}+i0^+}\right]. \tag{2.64}$$

The continuum limit $\Delta \to 0$ for a large dot had been already taken to obtain the low energy Hamiltonian Eq. (2.35). In Eq. (2.64) the limits $\omega \to 0$ and $\Delta \to 0$ do not actually commute, giving a result equal to zero if the frequency is sent to zero before the level spacing. If the opposite limit is taken the condition Eq. (2.5) is fulfilled and the delta functions that are present also in Eq. (2.59) give a non zero contribution exactly equal to Eq. (2.60). The Korringa-Shiba relation is then modified by a factor two

$$\mathrm{Im}\chi_c(\omega) = 2\pi\hbar\omega\chi_c^2, \tag{2.65}$$

which implies a new universal value for the charge relaxation resistance in the single channel case

$$R_q = \frac{h}{e^2}. \tag{2.66}$$

The extension to N channels remains straightforward and give $R_q = h/Ne^2$. The above discussion is summarized in Fig. 2.4. Driving at a frequency higher than the dot level spacing induces the creation of particle/hole pairs inside the dot, enhancing energy dissipation with respect to the small dot limit $\hbar\omega < \Delta$. The result is a charge relaxation resistance which coincides with a series of two contact resistances. The dot acts effectively as a further reservoir in the system in series with the lead.

2.5 The loss of universality

The discussion of the previous sections provides a quite general understanding of why interacting quantum dots behave as non-interacting ones, at least for what concerns the charge relaxation resistance R_q. The generalization to the N channel case, $R_q = h/(2Ne^2)$, is however not general. This result requires an effective Hamiltonian similar to Eq. (2.50)

$$H = \sum_{kk'\sigma}\varepsilon_k a^\dagger_{k\sigma}a_{k\sigma} + \frac{\chi_c}{N\nu_0}\varepsilon_\omega\cos\omega t\sum_{kk'\sigma}a^\dagger_{k\sigma}a_{k'\sigma}, \tag{2.67}$$

with the assumption of a complete symmetry between the channels, see Eq. (2.6). In the case of spinful electrons, for example, this symmetry is broken in the presence of a magnetic field and the more general form holds at low energy

$$H = \sum_{kk'\sigma}\varepsilon_k a^\dagger_{k\sigma}a_{k\sigma} + \varepsilon_\omega\cos\omega t\sum_\sigma\frac{\chi_\sigma}{\nu_0}\sum_{kk'}a^\dagger_{k\sigma}a_{k'\sigma}, \tag{2.68}$$

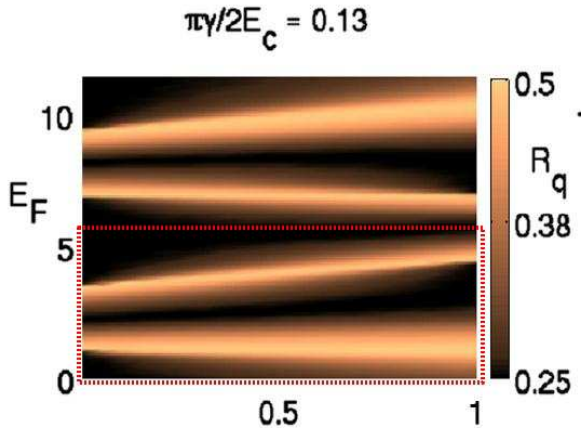

Figure 2.5: Behavior of R_q as a function of the Zeeman splitting Δ_Z in Ref. [66], within the Hartree-Fock approximation for interactions in the dot. γ corresponds to the hybridization constant Γ. In the inset delimited by the red rectangle we indicate the zone described by the Anderson Hamiltonian. All the energies are given in units of the bare level spacing Δ and R_q of h/e^2.

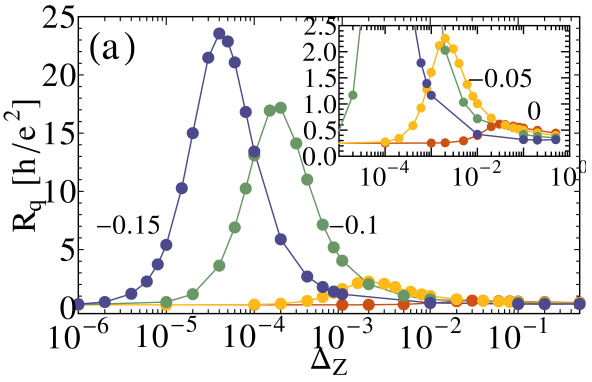

Figure 2.6: Dependence of R_q on the Zeeman splitting Δ_Z in the Kondo regime from Ref. [76]. These results have been obtained by numerical renormalization group calculations with $\Gamma = 0.02$ and $E_c = 0.2$. They show that for Zeeman energies of the order of the Kondo temperature a giant non-universal peak appear in the charge relaxation resistance.

where

$$\chi_\sigma = -\frac{\partial \langle \hat{n}_\sigma \rangle}{\partial \varepsilon_d}, \tag{2.69}$$

is the susceptibility of the occupation of every single level σ in the dot. The channel symmetry corresponds to $\chi_\sigma = \chi_c/N, \forall \sigma$. In the asymmetric case, the model (2.68) results in the new generalized form of the Korringa-Shiba relation Eq. (2.7), corresponding to the non-universal charge relaxation resistance Eq. (2.8).

2.5.1 Dependence of R_q on the magnetic field: giant and universal peaks.

Lifting the orbital level degeneracy by a magnetic field breaks the channel symmetry and the charge relaxation resistance is no longer universal. As shown in Fig. 2.5, in the Hartree-Fock approximation for interactions in the dot, it is possible to predict a peak at $R_q \simeq h/(2e^2)$ at the resonance between different spin populations driven by the magnetic field [66]. It is also interesting to notice that, for certain values of the orbital energy ε_d (E_F in Fig. 2.5), R_q is insensitive to the magnetic field.

The Hartree-Fock approximation does not describe properly the strong correlations brought by the Kondo singlet to be discussed in Chapter 4. This can be addressed, for instance, using

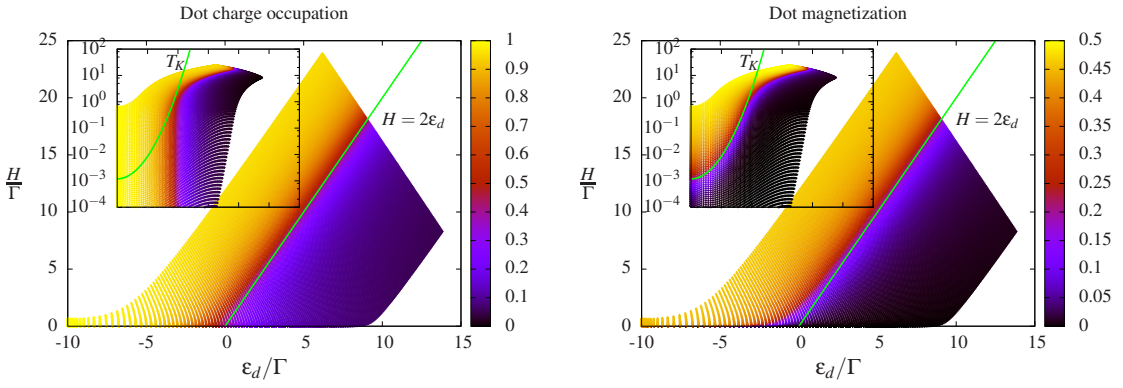

(a) (b)

Figure 2.7: Charge occupation and magnetization of the dot. Both quantities reproduce quite well the phase diagram of the isolated dot in Fig. 4.1. The insets show the same quantities on a logarithmic scale. The charge is not sensitive to the formation of the Kondo singlet for Zeeman energies below the Kondo temperature, while the magnetization becomes zero.

the numerical renormalization group (NRG) [109, 110, 108]. The charge relaxation resistance has then been calculated for the Anderson model in Ref. [76] showing that, for Zeeman splittings of the order of the Kondo temperature, the charge relaxation resistance can reach up to 100 times the universal value of the charge relaxation resistance in the two-fold spin degenerate case $R_q = h/(4e^2)$. In the next sections, we show that the Fermi liquid approach developed in this Thesis provides a general framework to predict and explain these behaviors analytically. We show how particle-hole symmetry protects the charge relaxation resistance universality even when the SU(2) symmetry is broken and *vice versa*. We then exhibit scaling behaviors for the peak of the charge relaxation resistance both in the Kondo and in the mixed valence regime, described by universal analytical functions.

2.5.1.1 The giant peak of the charge relaxation resistance

Expression (2.8) for the charge relaxation resistance does not give explicitly the reasons for universality in the many channel case. One of these is surely the symmetry between channels ensuring $\chi_\sigma = \chi_c/N$ and so $R_q = h/(2Ne^2)$. In the case of two spin channels and an interacting dot, described by the Anderson Hamiltonian, Eq. (2.8) can be actually recast in the more expressive form

$$R_q = \frac{h}{4e^2}\left(1 + \frac{\chi_m^2}{\chi_c^2}\right), \tag{2.70}$$

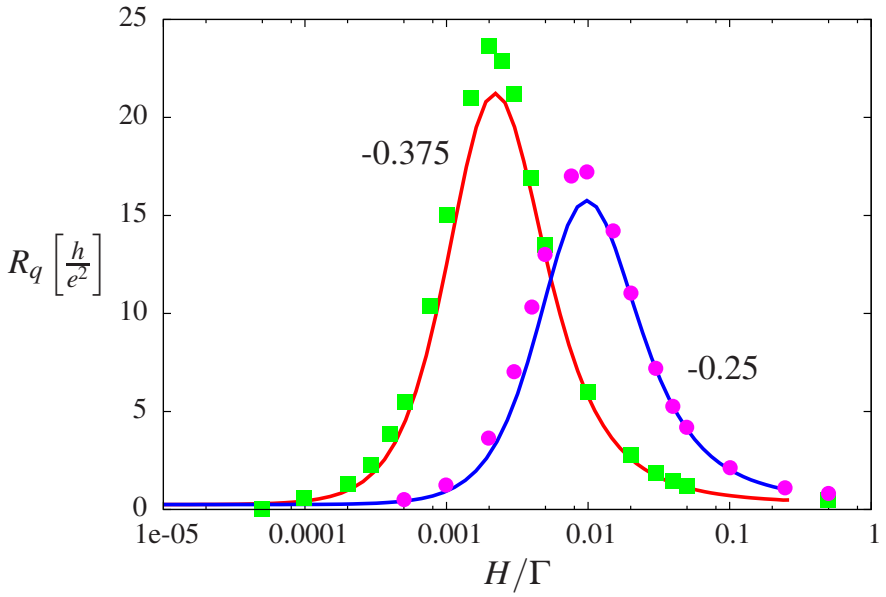

Figure 2.8: Comparison of R_q as a function of the magnetic field between NRG calculations (dots) (extracted from Ref. [76]) and our Bethe Ansatz results (solid lines) for different ε_d/U and $U/\Gamma = 20$, showing good agreement.

where the *charge-magneto* susceptibility

$$\chi_m = -2\frac{\partial \langle \hat{m} \rangle}{\partial \varepsilon_d} \tag{2.71}$$

has been defined. This is twice the derivative of the dot magnetization $\langle \hat{m} \rangle = (\langle \hat{n}_\uparrow \rangle - \langle \hat{n}_\downarrow \rangle)/2$, with respect to the orbital energy ε_d. This quantity is quite atypical in the framework of quantum dot systems, where the *magnetic* susceptibility $\chi_H = -\partial \langle \hat{m} \rangle / \partial H$ is usually studied to obtain information about the sensitivity of the local moment of the quantum dot to a local variation of the magnetic field H. Moreover, Eq. (2.70) states that the susceptibility of the *magnetization* of the dot, and not its total charge, is responsible for the departure from the universal quantization to $h/(4e^2)$ for the charge relaxation resistance. Eq. (2.70) is also remarkable as it separates explicitly the charge and spin degrees of freedom of the electrons in the quantum dot. They can display very different behaviors in 1D systems and a manifestation of it can be observed in Fig. 2.7.

Indeed the Bethe ansatz, presented in Appendix G, diagonalizes the Anderson Hamiltonian and provides, through coupled integral equations, the physical properties of the ground state. As we will discuss in Chapter 4, these equations can be solved numerically for any parameter of the Anderson Hamiltonian and the numerical solutions for the charge and the magnetization are plotted in Fig. 2.7. A detailed discussion of the different behaviors and

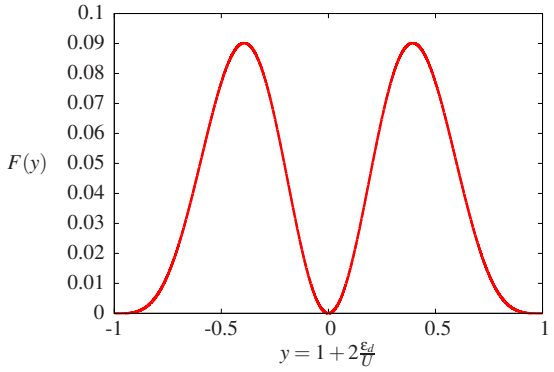

Figure 2.9: Scaling limit of the envelope function of the peak as an exclusive function of the asymmetry parameter y. Notice that the function is zero at particle-hole symmetry.

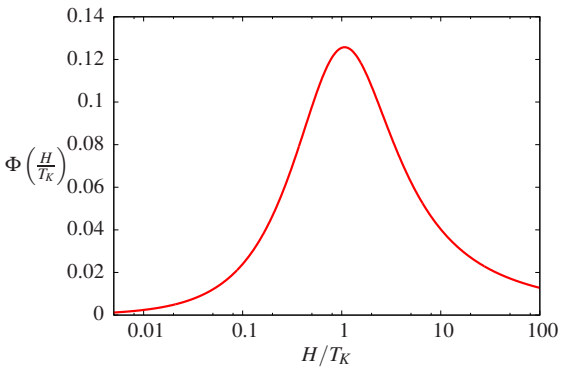

Figure 2.10: Universal function $\Phi_0(H/T_K)$ describing the peak in R_q in the Kondo scaling limit. The maximum is at $H/T_K = 1.0697$ and signals then the breaking of the Kondo singlet.

regimes, that can be identified by inspecting the respective behavior of the dot charge and magnetization, is given in Section 4.1. For the present discussion, it is enough to notice that these two quantities exhibit different behaviors, especially in the Kondo regime, defined for one charge blocked on the dot and Zeeman energies below the Kondo temperature [78, 79, 93, 111]

$$T_K = 2\sqrt{\frac{U\Gamma}{\pi e}}\, e^{\frac{\pi\epsilon_d(\epsilon_d+U)}{2U\Gamma}}. \tag{2.72}$$

Kondo physics strongly affects the magnetization of the dot, but not its charge occupation. χ_c and χ_m are computed numerically and they are plotted in Fig. 4.2. The points where χ_m behaves differently from χ_c give a non-universal value of the charge relaxation resistance. In Fig. 2.8, the values obtained by our approach are compared to those obtained by numerical renormalization group calculations [76]. The agreement between the two consolidates the validity of our low energy Fermi liquid model Eq. (2.68). A main achievement of our work is to give also an exact analytical description of this peak in the Kondo regime and in the valence-fluctuation region. The Kondo scaling limit corresponds to $U/\Gamma \gg 1$, $\varepsilon_d^*/\Gamma \ll 1$ and $H/\Gamma \ll 1$, where $\varepsilon_d^* = \varepsilon_d + \Gamma/\pi \ln(\pi e U/4\Gamma)$ is the renormalization of orbital energy because of the presence of interactions [78, 93]. In this limit, the charge relaxation resistance assumes the following form

$$R_q = \frac{h}{4e^2}\left[1 + \left(\frac{U}{\Gamma}\right)^4 F_0(y)\Phi_0^2\left(\frac{H}{T_K}\right)\right], \tag{2.73}$$

where $y = 1 + 2\varepsilon_d/U$ is the *asymmetry parameter*, simply describing the distance to particle-hole symmetry. The scaling functions Φ_0 and F_0 are universal and they are plotted in Figs. 2.9 and 2.10. They describe respectively the shape and the envelope of the peak as a function of the magnetic field and the particle-hole asymmetry parameter. These analytical functions

actually capture the behavior of the giant peak in the whole Kondo regime, even far from the scaling limit. This is discussed in detail in Section 4.4.1, where the NRG results of Ref. [76] are compared to our numerical solution of the Bethe ansatz equations.

The behavior of the scaling function in Eq. (2.73) conveys an interesting message about charge relaxation universality in strongly correlated systems. First of all it indicates that the universal quantization $R_q = h/(4e^2)$ is protected by particle-hole symmetry. For $\varepsilon_d = -U/2$, the envelope function F_0 is zero and the charge relaxation resistance does not feel the presence of a magnetic field. Additionally, breaking particle-hole symmetry alone is not sufficient to destroy universality. A simultaneous breaking of the SU(2) and particle-hole symmetry is required to observe an increase of the charge relaxation resistance and the emergence of a giant peak. This scales as the 4th power of U/Γ and appears for Zeeman splittings of the order of the Kondo temperature. This physically means that breaking the Kondo singlet by a magnetic field activates spin-flip processes of the quantum dot that dissipate energy through the creation of particle-hole pairs [76].

2.5.1.2 A universal peak in the mixed-valence region

The behavior of the envelope function F_0 in Fig. 2.9 predicts, with Eq. (2.73), that the charge relaxation resistance universal quantization to $h/4e^2$ should be restored for any magnetic field for $\varepsilon_d = 0$ and $-U$. These points correspond to the transitions between different charge occupations of the quantum dot, see Section 4.1. Actually this is not true and the analytical description devised for the Kondo regime breaks down close to the mixed-valence region, defined for $\varepsilon_d^* \sim 0$. This is the subject of the discussion in Section 4.4.2.1. The fate of the peak out of the Kondo regime can already be guessed by looking at Fig. 2.5 and the inset of Fig. 2.6, where R_q varies from $h/4e^2$ to $h/2e^2$ as a function of the magnetic field. We provided an exact analytical description of R_q by performing perturbation calculation to second order in the tunneling t. The Fermi liquid formula Eq. (2.70) remains valid also in this regime and, as shown in Fig. 2.11, only the states $|1,\uparrow\rangle$ and $|0\rangle$ are now competing for the ground state of the quantum dot, such that Kondo correlations are no longer present. For $H = 2\varepsilon_d$ these two states become resonant and the spin down state of the quantum dot can be initially neglected, discarding also the double occupied state $|2\rangle$. The model of the system becomes then a single resonant level model

$$H = \sum_k \varepsilon_k c_{k\uparrow}^\dagger c_{k\uparrow} + \varepsilon_{d\uparrow} d_\uparrow^\dagger d_\uparrow + t \sum_k \left(c_{k\uparrow}^\dagger d_\uparrow + d_\uparrow^\dagger c_{k\uparrow} \right), \tag{2.74}$$

which gives $R_q = h/2e^2$ as we discussed in Section 1.3.2. This is the reason why, in the scaling limit $\varepsilon_d \gg \Gamma$, at the resonance between the $|0\rangle$ and $|1,\uparrow\rangle$ states, the charge relaxation resistance is twice the 2 channel value $h/4e^2$. The dependence of the charge relaxation resistance

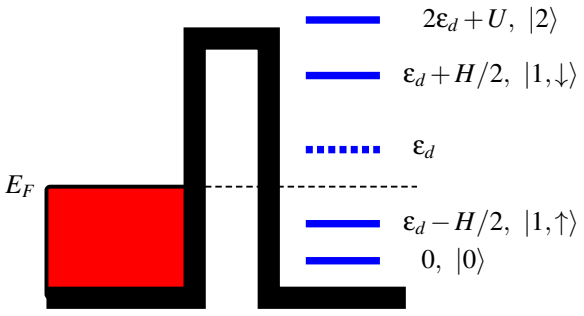

Figure 2.11: Spectrum of the Anderson dot isolated from the lead on the left. For a positive ε_d in the presence of a magnetic field, only the states $|0\rangle$ and $|1,\uparrow\rangle$ compete in the low energy sector.

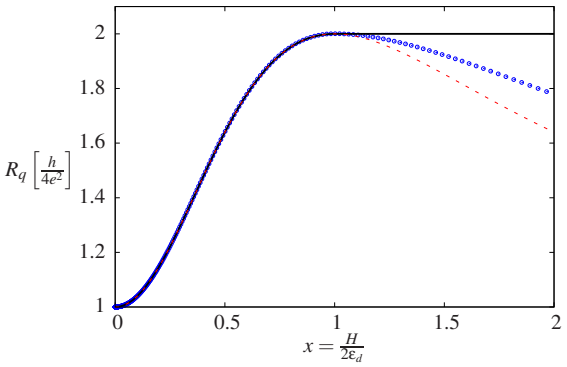

Figure 2.12: Scaling form of the charge relaxation resistance R_q in the limits $\Gamma \ll \varepsilon_d \ll U$ (solid line) and $\Gamma \ll U \ll \varepsilon_d$ (dashed line). In circles, the resistance R_q is plotted for $U = \varepsilon_d$.

on the magnetic field is determined by allowing spin fluctuations, that is taking into account the spin down state of the quantum dot. The behavior of the peak is captured by considering the first order correction to the ground state in the tunneling term

$$H_{T\downarrow} = t \sum_k \left(c^\dagger_{k\downarrow} d_\downarrow + d^\dagger_\downarrow c_{k\downarrow} \right). \tag{2.75}$$

This term activates the interaction energy U when virtual fluctuation to the doubly occupied state $|2\rangle$ are considered. This calculation, discussed in Section 4.4.3, is in full agreement with the results obtained by Bethe ansatz as shown in Fig. 4.14. Two interesting scaling limits in the $\varepsilon_d \gg \Gamma$ limit are found. They are plotted in Fig. 2.12. Before the resonance, that is for $x = H/2\varepsilon_d < 1$, the crossing between $h/4e^2$ and $h/2e^2$ is universally described by the formula

$$R_q = \frac{h}{4e^2} \left[1 + \frac{4x^2}{(x^2+1)^2} \right], \tag{2.76}$$

independently of the value of the interaction U. This is because, in the limit $\Gamma \to 0$, the ground state is $|0\rangle$ and, to first order in t, it cannot fluctuate to the double occupation $|2\rangle$. Once $x > 1$ the ground state becomes $|1,\uparrow\rangle$, which can fluctuate with both the empty and the doubly occupied states. In the $U \to \infty$ limit any fluctuation to the $|2\rangle$ state is forbidden again and the system remains described solely by Eq. (2.74), corresponding to $R_q = h/2e^2$ irrespective of the magnetic field. In the opposite scaling limit $\Gamma \ll U \ll \varepsilon_d$, Eq. (2.76) also holds for Zeeman energies $H > 2\varepsilon_d$, describing a progressive decrease of R_q towards $h/4e^2$.

2.6 The SU(4) Anderson model

As a further demonstration of the generality of our approach, we also consider the electron dynamics in the case of a further orbital degree of freedom for the quantum dot. A twofold orbital degeneracy is responsible for more exotic manifestations of SU(4) Kondo regimes [112, 113, 114, 115, 116], see Fig. 2.13. This has been experimentally demonstrated in systems where the role of the quantum dot is played by a finite size carbon nanotubes [117, 118] (see Fig. 2.14) or in single dopant Silicium devices [119, 120].

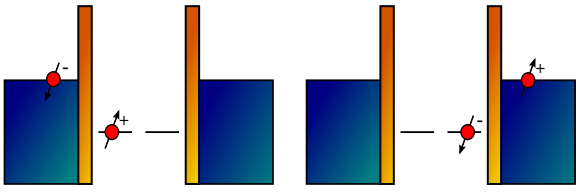

Figure 2.13: The fourfold degeneracy of the quantum dot allows for flipping at the same time the spin and orbital state of the lead electrons, giving rise to SU(4) Kondo processes.

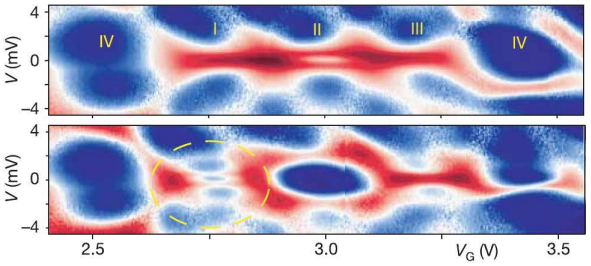

Figure 2.14: Fourfold splitting of the DC conductance peak as observed in Ref. [117] for a finite size carbon nanotube dot in the presence of a magnetic field. This is a demonstration of SU(4) Kondo behaviors.

The dot states can be labelled by $|+,\uparrow\rangle$, $|+,\downarrow\rangle$, $|-,\uparrow\rangle$ and $|-,\downarrow\rangle$, where $\pm$ stand for the orbital degrees of freedom and $\uparrow,\downarrow$ for the spin ones. Without any loss of generality, we can label these states by a new quantum number $\nu = 1,\ldots,4$ and the system is described by a generalized SU(4) version of the Anderson Hamiltonian

$$H = \sum_{k\nu} \varepsilon_k c^\dagger_{k\nu} c_{k\nu} + t \sum_{k\nu} \left(c^\dagger_{k\nu} d_\nu + d^\dagger_\nu c_{k\nu} \right) + \varepsilon_d \sum_\nu \hat{n}_\nu + U \sum_{\nu<\nu'} \hat{n}_\nu \hat{n}_{\nu'} \,. \tag{2.77}$$

In the case where the charge is fixed to $q = 1$, 2 or 3, a Schrieffer-Wolff transformation [121] maps Eq. (2.77) onto a Kondo Hamiltonian like Eq. (2.37) with couplings

$$J_q = -2t^2 \left(\frac{1}{\varepsilon_d + (q-1)U} - \frac{1}{\varepsilon_d + qU} \right), \tag{2.78}$$

$$W_q = -\frac{t^2}{N} \left(\frac{q}{\varepsilon_d + (q-1)U} + \frac{N-q}{\varepsilon_d + qU} \right). \tag{2.79}$$

Here the "spin" operators $\mathbf{S} = \sum_{\nu\nu'} d^\dagger_\nu \frac{\lambda_{\nu\nu'}}{2} d_{\nu'}$ and $\mathbf{s} = \sum_{kk'\nu\nu'} c^\dagger_{k\nu} \frac{\lambda_{\nu\nu'}}{2} c_{k'\nu'}$ are generated by the 15 matrices λ composing the 4×4 fundamental representation of the SU(4) group, see Appendix E. The generalization to the SU(N) case of Eqs. (2.77), (2.78) and (2.79) is straightforward.

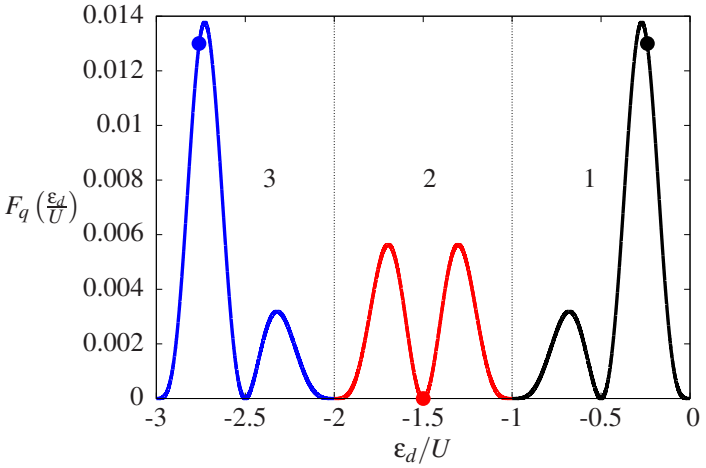

Figure 2.15: Envelope functions F_q in the sectors where the charge is frozen to 1, 2 or 3, that is when $\varepsilon_d/U \in$ [-1,0], [-2,-1] or [-3,-2] respectively. The function becomes zero in the middle of the Coulomb valleys, while the circles correspond to the values of ε_d/U for which the potential scattering couplings W_q in Eq. (2.79) becomes zero.

In Section 5.1 we show that steps completely analog to those outlined in Section 2.5.1.1, can be repeated with slight modifications to predict again a Kondo scaling behavior for the charge relaxation resistance of the form

$$R_q = \frac{h}{8e^2}\left[1+\left(\frac{U}{\Gamma}\right)^4 F_q\left(y_q\right)\Phi_q^2\left(\frac{H}{T_K^q}\right)\right], \tag{2.80}$$

where now $y_q = 2\varepsilon_d/u + 2q - 1$ gives the deviations from the centers of the Coulomb valleys where the charge is fixed to $q = 1$, 2 or 3. The form of the envelope is given in Fig. 2.15, while that of the peak is analog to that plotted in Fig. 2.10, valid in the SU(2) case. Interestingly, the function F_q for $q = 2$ coincides with the function of the envelope in the SU(2) case examined in Section 2.5.1.1. But for $q = 1$ and 3 this function is strongly asymmetric and would permit to distinguish between a SU(4) and a SU(2) Kondo regime in nanodevices. Moreover, we also notice that the values of ε_d/U for which $F_{1,3}$ becomes zero do not coincide with the values for which the potential scattering correction to the SU(4) Kondo mapping Eq. (2.79) is absent. These values imply the cancellation of the couplings W_q in Eq. (2.79) and are represented by the circles in Fig. 2.15. We suppose that the approach to the scaling behavior described by the function Φ_q will be faster at these points. By coincidence, the envelope at these points is closer to its maxima instead of zero, a remark of experimental relevance.

2.6.1 Determination of the SU(4) Kondo temperature

In this introductory presentation of our results, we did not pay a particular attention to the renormalization group techniques we developed to show the low energy Hamiltonian beyond Schrieffer-Wolff calculations. These techniques allow us to exactly determine the form of the fixed point potential scattering interaction in Eq. (2.10) and then to extract the charge on the dot through the Friedel sum rule Eq. (2.22). These calculations are presented in Sections 3.4, 4.3 and 5.2 for all the models considered in this work. Actually it is also of interest to describe here these calculations as they also allowed for the achievement of further fundamental results in determining analytically the SU(4) Kondo temperatures in different charge sectors, previously unknown.

In the presence of SU(N) Kondo physics, all the information about the interaction in the system at low energy is embodied by the renormalized vertex of the theory $\mathcal{V}^R$ [122, 123]. This is a physical quantity, which can be directly measured and that we define for the Coulomb blockade and the Anderson model in Chapters 3 and 4. We show that for the SU(N) Anderson Hamiltonian Eq. (2.77), it assumes the same form as in the SU(2) case [104, 105, 106, 124]

$$\mathcal{V}^R = \mathcal{V}_J^R \mathbf{S}\cdot\mathbf{s} + \mathcal{V}_W^R \mathbb{1}. \tag{2.81}$$

In this equation, $\mathbf{S}$ and $\mathbf{s}$ are the vectors composed of the N^2-1 matrices of the fundamental representation of the SU(N) group acting respectively on the subspace of the quantum dot and of the lead electrons. To one loop calculation, $\mathcal{V}_J^R$ assumes the following form [125, 126]

$$\mathcal{V}_J^R = J - \frac{N\nu_0}{2} J^2 \ln\frac{\Lambda}{D} + \dots \tag{2.82}$$

where D is the bandwidth and Λ is an infra-red cut-off. This last quantity must be introduced to avoid the divergencies caused by the ill definition of a perturbation approach in the coupling J. The Kondo model being a renormalizable theory [127], the choice of the couple of parameters (J, D) is actually arbitrary. This can be seen by considering Eq. (2.82) which is invariant, to second order in J, under the following transformation

$$\begin{aligned} J &\to J + aJ^2, \\ D &\to D e^{\frac{2a}{N\nu_0}}. \end{aligned} \tag{2.83}$$

This is a particular transformation, but, in general, all the possible choices of (J, D) giving the same value of $\mathcal{V}_J^R$ belong to the same universality class which is defined by the Kondo temperature [122, 123]

$$T_K = D \sqrt[N]{\frac{N\nu_0 J}{2}} e^{-\frac{2}{N\nu_0 J}}, \tag{2.84}$$

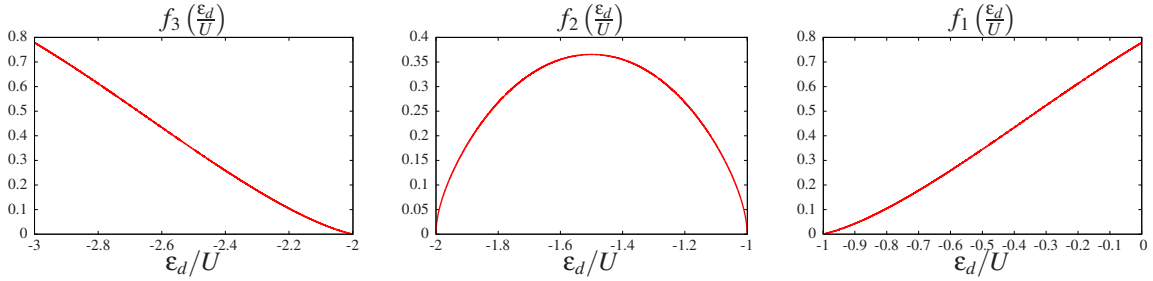

Figure 2.16: Functions $f_q(\varepsilon_d/U)$ in Eq. (2.85) plotted for q=3, 2 and 1 (left to right).

which is also invariant under the transformation Eq. (2.83). Notice that for Λ of the order of T_K, the second order correction in Eq. (2.82) becomes of the same order as the leading contribution J. T_K defines the energy scale at which a perturbative approach in J breaks down. As we will discuss in Chapter 4, the Kondo temperature is the energy scale at which Kondo correlations appear because of the formation of the Kondo singlet. It is a quantity of experimental relevance and its exact dependence on the orbital and charging energy in SU(4) regimes is unknown.

Calculating the renormalized vertex $\mathcal{V}^R$ up to fourth order in t within the SU(4) Anderson model Eq. (2.77) and rewriting it in the form Eq. (2.81) allows one to fix the high energy cut-off D in Eq. (2.82) as a function of the charge and orbital energy E_c and ε_d. In Section 5.2 we perform this calculation and provide an analytical expression for the Kondo temperature in the form

$$T_K^q = \sqrt[4]{\frac{4\Gamma U^3}{\pi}} f_q\left(\frac{\varepsilon_d}{U}\right) e^{-\frac{1}{2\nu_0 J_q}}, \tag{2.85}$$

where the functions $f_q(x)$ are plotted in Fig. (2.16).

CHAPTER 3

EFFECTIVE THEORY OF THE COULOMB BLOCKADE MODEL

Contents

In this section, we develop a renormalization group approach to show that the action describing the low energy quasi-particles in the Coulomb blockade model corresponds to the

Fermi liquid Hamiltonian Eq. (2.35), that is

$$S = \int_0^\beta d\tau \left\{ -\sum_{k\sigma} c^\dagger_{k\sigma}(\tau)\left(\partial_\tau - \varepsilon_k\right) c_{k\sigma}(\tau) - \sum_{l\sigma} d^\dagger_{l\sigma}(\tau)\left(\partial_\tau - \varepsilon_l\right) d_{l\sigma}(\tau) + \right. \\ \left. + \mathcal{V}^R \left[\sum_{kk'\sigma} c^\dagger_{k\sigma}(\tau) c_{k'\sigma}(\tau) - \sum_{ll'\sigma} d^\dagger_{l\sigma}(\tau) d_{l'\sigma}(\tau) \right] \right\}. \quad (3.1)$$

To prove the Friedel sum rule to fourth order in t, we calculate the potential scattering coupling in the limit of a large number of channels N. It reads

$$\mathcal{V}^R = \nu_0 t^2 \ln \frac{E_c + \varepsilon_d}{E_c - \varepsilon_d} + N\nu_0^3 t^4 \left(A[\varepsilon_d] - A[\varepsilon_d] \right), \quad (3.2)$$

with

$$A[\varepsilon_d] = \frac{-\varepsilon_d}{2E_c}\left(\frac{4\pi^2}{3} + \ln^2 \frac{E_c+\varepsilon_d}{E_c-\varepsilon_d}\right) + \frac{8\left(2E_c^2 - 2E_c\varepsilon_d - \varepsilon_d^2\right)}{(3E_c+\varepsilon_d)(E_c-\varepsilon_d)} \ln \frac{E_c+\varepsilon_d}{E_c} + \\ \frac{(2E_c+\varepsilon_d)}{E_c}\left[\ln^2 \frac{E_c+\varepsilon_d}{4E_c+2\varepsilon_d} + 2Li_2\left(\frac{3E_c+\varepsilon_d}{4E_c+2\varepsilon_d}\right) - \frac{4E_c(2E_c+\varepsilon_d)}{(E_c+\varepsilon_d)(3E_c+\varepsilon_d)} \ln \frac{4E_c+2\varepsilon_d}{E_c} \right] \quad (3.3)$$

where $Li_2(x)$ is the dilogarithm function

$$Li_2(x) = \int_x^0 dt \frac{\ln(1-t)}{t}. \quad (3.4)$$

$\mathcal{V}^R$ in Eq. (3.2) is the *renormalized vertex* of the theory, to be defined in Section 3.4. Eqs. (3.1) and (3.2) allow to readily show the validity of the Friedel sum rule Eq. (2.11) in the Coulomb blockade model. The potential scattering term, in the second line of Eq. (3.1), is responsible for a phase-shift of the lead electrons. Its expression is obtained from Eq. (2.21)

$$\delta = -\arctan\left(\pi\nu_0 \mathcal{V}^R\right). \quad (3.5)$$

Inserting this result in the Friedel sum rule Eq. (2.11), we verify that it provides the correct value for the charge occupation of the quantum dot

$$\langle \hat{n} \rangle = g \ln \frac{E_c - \varepsilon_d}{E_c + \varepsilon_d} - g^2 \left(A[\varepsilon_d] - A[-\varepsilon_d] \right). \quad (3.6)$$

The validity of this result is tested by comparing to previous calculations carried out by Grabert [101, 102] in the large-N limit, using a completely different perturbative approach. These corrections describe the smearing of the coulomb staircase close to charge degeneracy and they are plotted in Fig. 3.1. Notice that Eq. (3.6) actually diverges for $\varepsilon_d/E_c = \pm 1$,

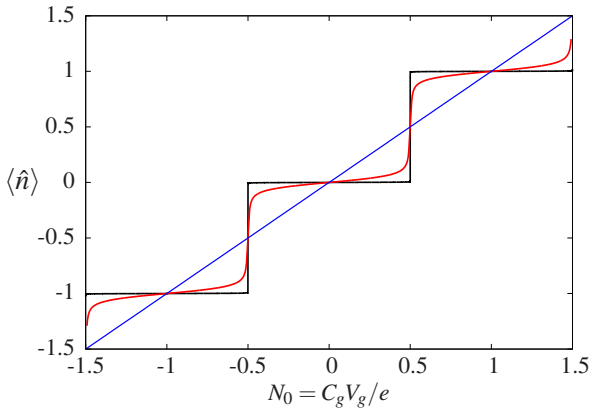

Figure 3.1: Smearing of the Coulomb staircase for the charge $\langle \hat{n} \rangle$ on the quantum dot. The black and red lines are obtained for $g = 0.001$ and $g = 0.03$ respectively from the formula provided by Grabert in Ref. [102]. It interpolates between Eq. (3.6)*, describing the charge blocked on the dot, and the behavior close to charge degeneracy derived by Matveev Eq.* (3.7)*. The blue straight line describes the limit of an open dot, in which the charge on the dot is continuous.*

corresponding to the charge degeneracy points $N_0 = C_g V_g / e = \pm 1/2$. The behavior of the charge on the dot close to these points has been derived by Matveev in Ref. [60]. It reads

$$\langle \hat{n} \rangle = \frac{-g^* \ln \zeta^*}{1 - 2g^* \ln \zeta^*} + \mathrm{O}(\zeta) \,, \tag{3.7}$$

with $g^* = g[1 + 6g + O(g^2)]$ and $\zeta^* = \zeta[1 + 9.7762g + O(g^2)]$ [102]. $\zeta = 1/2 - N_0$ is the distance from the charge degeneracy point $N_0 = 1/2$. Eq. (3.7), interpolated with Eq. (3.6), allows one to obtain the finite results plotted in Fig. 3.1.

To perform renormalization group calculations, we develop a new path integral formulation of the Coulomb blockade Hamiltonian introducing bosonic slave-states. The theory is projected back to the original (and physical) Hilbert space by applying the Abrikosov's projection technique [122, 123], exposed in Section 3.1. In this slave-boson representation, the action is quadratic and, in Section 3.2, the high energy charge sectors are integrated, providing an alternative tool to the Schrieffer-Wolff transformation. In Section 3.3, we illustrate the renormalization group arguments justifying the mapping onto the low-energy action Eq. (3.1) and the need of calculating the renormalized vertex $\mathcal{V}^R$ to obtain the potential scattering coupling. In the slave-boson formalism, Wick's theorem applies and, in Section 3.4, we carry out the diagrammatic calculation of $\mathcal{V}^R$.

3.1 Slave states and Abrikosov's projection technique

The states $|n\rangle$, adopted by Grabert [101, 102] and introduced in Eq. (2.29) to decouple charge and fermionic degrees of freedom on the quantum dot, do not find a convenient formulation in the path integral formalism. We circumvent this problem by introducing slave-boson fields. The procedure is sketched in Tab. 3.1. A slave-state is an accessory degree of freedom

Charge Occupation	$\mathbf{E_n}$	**Grabert's basis**	**Slave-boson basis**
...	...	...	...
2	$4E_c + 2\varepsilon_d$	$\|2\rangle$	$b_2^\dagger \|0\rangle_b$
1	$E_c + \varepsilon_d$	$\|1\rangle$	$b_1^\dagger \|0\rangle_b$
0	0	$\|0\rangle$	$b_0^\dagger \|0\rangle_b$
-1	$E_c - \varepsilon_d$	$\|-1\rangle$	$b_{-1}^\dagger \|0\rangle_b$
-2	$4E_c - 2\varepsilon_d$	$\|-2\rangle$	$b_{-2}^\dagger \|0\rangle_b$
...	...	...	...

Table 3.1: Representation of the states describing the charge occupation on the dot and their energy within Grabert's and the slave-boson representation.

which is introduced to simplify calculations. The price to pay is that unphysical states are added to the Hilbert space spanned by the new Hamiltonian and a projection technique is required to obtain correct results. Further examples of analog approaches can be found in Refs. [125, 128, 129, 130] for the $U \to \infty$ limit in the Anderson model. In our case, to every Fock state $|n\rangle$, describing the occupation by n charges on the dot, we associate a bosonic operator $b_n^\dagger$ which creates a state of energy $E_n = E_c n^2 + \varepsilon_d n$ when acting on a new vacuum called $|0\rangle_b$. This vacuum must be distinguished from the zero charge state, which is given by $b_0^\dagger|0\rangle_b$ in this new representation. $|0\rangle_b$ is a fictitious state where the quantum dot does not even exist. A quantum dot occupied by n charges is described by the state $b_n^\dagger|0\rangle_b$. The redefinition of the tunneling Hamiltonian Eq. (2.29) in this representation is readily obtained

$$H_T = t \sum_{kl\sigma n} \left(c_{k\sigma}^\dagger d_{l\sigma} b_{n-1}^\dagger b_n + d_{l\sigma}^\dagger c_{k\sigma} b_{n+1}^\dagger b_n \right) \tag{3.8}$$

and the Hamiltonian without this tunneling term is quadratic

$$H_0 = \sum_{k\sigma} \varepsilon_k c_{k\sigma}^\dagger c_{k\sigma} + \sum_{l\sigma} \varepsilon_l d_{l\sigma}^\dagger d_{l\sigma} + \sum_n E_n b_n^\dagger b_n \,. \tag{3.9}$$

An infinite series of free slave-bosons replaces the interaction term of Eq. (iv). The interest of this slave-boson representation is that Wick's theorem applies, diagrammatic calculations

are possible and the higher energy modes can be integrated, as illustrated in the following section. The action corresponding to Eqs. (3.8) and (3.9) reads

$$S_{\mathrm{CBM}} = \int_0^\beta d\tau \left\{ -\sum_{k\sigma} c^\dagger_{k\sigma}(\tau) G_k^{-1} c_{k\sigma}(\tau) - \sum_{l\sigma} d^\dagger_{l\sigma}(\tau) D_k^{-1} d_{l\sigma}(\tau) - \right.$$
$$\left. -\sum_n b^\dagger_n(\tau) F_n^{-1} b_n(\tau) + t \sum_{kl\sigma n} \left[c^\dagger_{k\sigma}(\tau) d_{l\sigma}(\tau) b^\dagger_{n-1}(\tau) b_n(\tau) + d^\dagger_{l\sigma}(\tau) c_{k\sigma}(\tau) b^\dagger_{n+1}(\tau) b_n(\tau) \right] \right\}, \quad (3.10)$$

in which the free Green's operators have been defined

$$G_k^{-1}(\tau) = -\partial_\tau - \varepsilon_k\,, \quad (3.11)$$
$$D_l^{-1}(\tau) = -\partial_\tau - \varepsilon_l\,, \quad (3.12)$$
$$F_n^{-1}(\tau) = -\partial_\tau - E_n - \lambda\,. \quad (3.13)$$

The introduction of the *para-energy* λ in Eq. (3.13) is necessary to project our theory back to the physical space. The theory Eq. (3.10) contains unphysical states as, for instance, $b^\dagger_n b^\dagger_m |0\rangle_b$, describing the simultaneous existence of two dots occupied by n and m charges respectively. The elimination of these states requires the implementation of the following constraint

$$\hat{N}_b = \sum_n b^\dagger_n b_n = 1\,, \quad (3.14)$$

which is realized sending λ to infinity at the end of calculations. This is the Abrikosov's projection technique [122], first devised for the fermionic representation of the dot spin in the Kondo problem, to be discussed in Section 4.2.1. The introduction of λ in Eq. (3.13) corresponds to adding a chemical potential associated to the number of slave-bosons $\hat{N}_b$ in Eq. (3.9). This operator commutes with the rest of the Hamiltonian, which can then be block-diagonalized in sectors with fixed number n of slave-bosons. Any trace involving the Boltzmann weight $e^{-\beta H}$ and physical observables $\mathcal{O}$, which must commute with $\hat{N}_b$, can then be written into the form

$$\mathrm{Tr}\left[\mathcal{O} e^{-\beta H - \beta\lambda \hat{N}_b}\right] = \mathrm{Tr}_0\left[\mathcal{O} e^{-\beta H}\right] + e^{-\beta\lambda}\mathrm{Tr}_1\left[\mathcal{O} e^{-\beta H}\right] + e^{-2\beta\lambda}\mathrm{Tr}_2\left[\mathcal{O} e^{-\beta H}\right] \ldots \quad (3.15)$$

The notation $\mathrm{Tr}_n[\cdot]$ means that the trace is carried out in the Hilbert sector in which $\langle \hat{N}_b \rangle = n$. In this notation, the physical average of the operator $\mathcal{O}$ reads

$$\langle \mathcal{O} \rangle = \frac{\mathrm{Tr}_1\left[\mathcal{O} e^{-\beta H}\right]}{\mathrm{Tr}_1\left[e^{-\beta H}\right]}\,. \quad (3.16)$$

Calling $\langle \mathcal{O} \rangle_\lambda = \mathrm{Tr}[\mathcal{O} e^{-\beta H - \beta\lambda \hat{N}_b}]/\mathrm{Tr}[e^{-\beta H - \beta\lambda \hat{N}_b}]$ the expectation value of the operator $\mathcal{O}$ in the whole Hilbert space spanned by the action Eq. (3.10), Eq. (3.16) is recovered by the following

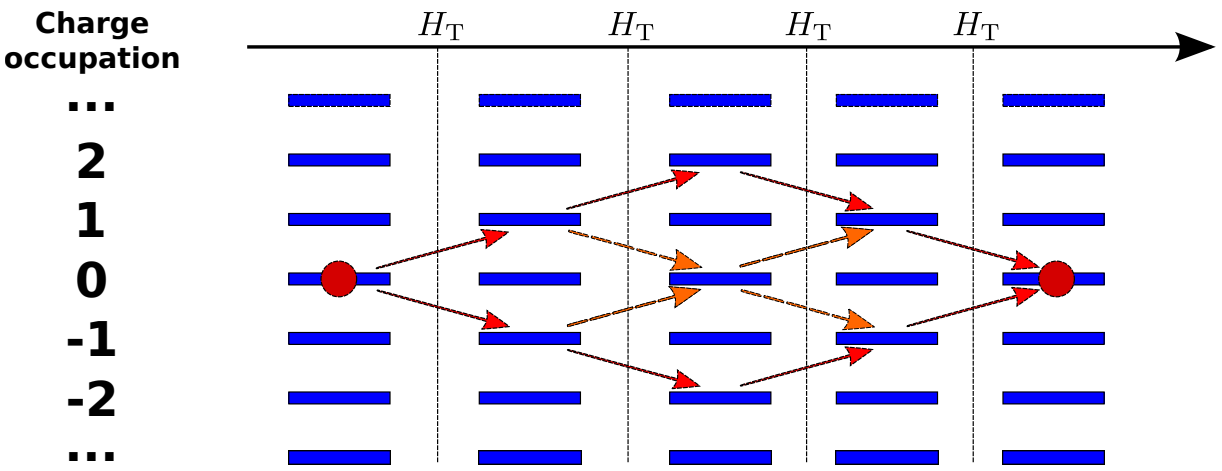

Figure 3.2: Virtual path of the charge occupation of the dot back and forth from the lowest energy sector. This is defined by zero charges on the quantum dot if $-E_c \ll \varepsilon_d \ll E_c$. The arrows indicate the effect of the repeated action of the tunneling term Eq. (3.8) *on this state. To fourth order in the tunnel coupling t, only virtual excursions up to the occupations ± 2 have to be taken into account.*

prescription [68]

$$\begin{aligned} Z &= \lim_{\lambda\to\infty} \frac{\partial}{\partial e^{-\beta\lambda}} Z_\lambda \,, \\ \langle \mathcal{O} \rangle &= \lim_{\lambda\to\infty} \left[\langle \mathcal{O} \rangle_\lambda + \frac{Z_\lambda}{Z} \frac{\partial}{e^{-\beta\lambda}} \langle \mathcal{O} \rangle_\lambda \right] , \end{aligned} \tag{3.17}$$

where $Z = \mathrm{Tr}_1 \left[e^{-\beta H} \right]$ is the *physical* partition function associated to the Coulomb blockade Hamiltonian.

3.2 Integration of the high energy charge sectors

Assuming $-E_c \ll \varepsilon_d \ll E_c$, the lowest energy sector corresponds to the zero charge occupation of the dot. The translational symmetry between charge sectors makes this choice irrelevant and what we discuss applies to any charge sector. As shown in Fig. 3.2, perturbative calculations to fourth order in t involve virtual occupations on the dot from -2 to $+2$ charges. All the bosonic degrees of freedom associated to $|n| > 2$ appearing in Eq. (3.10) can then be discarded to this order. In Coulomb blockade regimes, charge fluctuations are frozen, what suggests the integration of the bosonic modes $b_{\pm 1}$ and $b_{\pm 2}$. The action Eq. (3.10) being quadratic, the integrations over the fields $b_{\pm 2}$ are Gaussian, bringing the following contribu-

tions to the effective action

$$\begin{aligned} S_2 &= t^2 \sum_{kk'll'\sigma\sigma'} \mathrm{Tr}\left[c^\dagger_{k\sigma} d_{l\sigma} b^\dagger_1 F_2 d^\dagger_{l'\sigma'} c_{k'\sigma'} b_1\right], \\ S_{-2} &= t^2 \sum_{kk'll'\sigma\sigma'} \mathrm{Tr}\left[d^\dagger_{l\sigma} c_{k\sigma} b^\dagger_{-1} F_{-2} c^\dagger_{k'\sigma'} d_{l'\sigma'} b_{-1}\right]. \end{aligned} \tag{3.18}$$

In these expressions, we adopted a formulation independent from the specific representation of the fields in imaginary time or Matsubara frequencies. By writing

$$\mathrm{Tr}\left[c^\dagger_{k\sigma} G^{-1}_k c_{k\sigma}\right], \tag{3.19}$$

we mean from now on equally

$$\int_0^\beta d\tau\, c^\dagger_{k\sigma}(\tau) G^{-1}_k(\tau) c_{k\sigma}(\tau) \;\text{ or }\; \sum_{i\omega_n} c^\dagger_{k\sigma}(i\omega_n) G^{-1}_k(i\omega_n) c_{k\sigma}(i\omega_n). \tag{3.20}$$

This choice simplifies the integration and the expansion in t of operators, which becomes clear in the following calculations. Eqs. (3.18) renormalize the slave-boson propagators $F_{\pm1}$. The resulting action can be cast in the form $S'_{\mathrm{CBM}} = S_0 + S_1 + S_{-1}$ with

$$\begin{aligned} S_0 &= \sum_{k\sigma} \mathrm{Tr}\left[c^\dagger_{k\sigma} G^{-1}_k c_{k\sigma}\right] + \sum_{l\sigma} \mathrm{Tr}\left[d^\dagger_{l\sigma} D^{-1}_l d_{l\sigma}\right] + \mathrm{Tr}\left[b^\dagger_0 F^{-1}_0 b_0\right], \\ S_1 &= -\mathrm{Tr}\left[b^\dagger_1 \Phi^{-1}_1 b_1\right] + \sum_{kl\sigma} \mathrm{Tr}\left[c^\dagger_{k\sigma} d_{l\sigma} b^\dagger_0 b_1 + d^\dagger_{l\sigma} c_{k\sigma} b^\dagger_1 b_0\right], \\ S_{-1} &= -\mathrm{Tr}\left[b^\dagger_{-1} \Phi^{-1}_{-1} b_{-1}\right] + \sum_{kl\sigma} \mathrm{Tr}\left[c^\dagger_{k\sigma} d_{l\sigma} b^\dagger_{-1} b_0 + d^\dagger_{l\sigma} c_{k\sigma} b^\dagger_0 b_{-1}\right], \end{aligned} \tag{3.21}$$

and

$$\begin{aligned} \Phi^{-1}_1 &= F^{-1}_1 - t^2 \sum_{kk'll'\sigma\sigma'} c^\dagger_{k\sigma} d_{l\sigma} F_2 d^\dagger_{l'\sigma'} c_{k'\sigma'}, \\ \Phi^{-1}_1 &= F^{-1}_{-1} - t^2 \sum_{kk'll'\sigma\sigma'} d^\dagger_{l\sigma} c_{k\sigma} F_{-2} c^\dagger_{k'\sigma'} d_{l'\sigma'}. \end{aligned} \tag{3.22}$$

The integration of the $b_{\pm1}$ modes is also Gaussian and leads to the following action

$$S''_{\mathrm{CBM}} = S_0 + t^2 \sum_{kk'll'\sigma\sigma'} \mathrm{Tr}\left[c^\dagger_{k\sigma} d_{l\sigma} b^\dagger_0 \Phi_1 d^\dagger_{l'\sigma'} c_{k'\sigma'} b_0 + d^\dagger_{l\sigma} c_{k\sigma} b^\dagger_0 \Phi_{-1} c^\dagger_{k'\sigma'} d_{l'\sigma'} b_0\right]. \tag{3.23}$$

The operators $\Phi_{\pm1}$ can be linearly expanded in the tunneling t

$$\begin{aligned} \Phi_1 &= F_1 + t^2 \sum_{kk'll'\sigma\sigma'} F_1 c^\dagger_{k\sigma} d_{l\sigma} F_2 d^\dagger_{l'\sigma'} c_{k'\sigma'} F_1, \\ \Phi_{-1} &= F_{-1} + t^2 \sum_{kk'll'\sigma\sigma'} F_{-1} d^\dagger_{l\sigma} c_{k\sigma} F_{-2} c^\dagger_{k'\sigma'} d_{l'\sigma'} F_{-1}, \end{aligned} \tag{3.24}$$

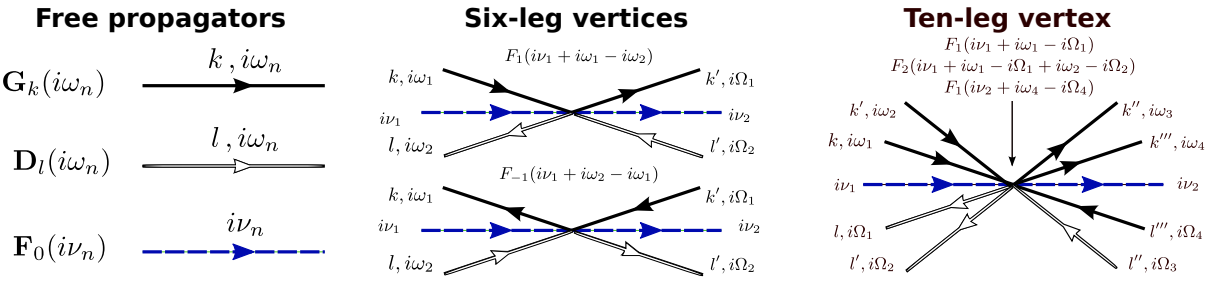

Figure 3.3: Vertex structure of the effective theory Eq. (3.25). The free propagators G_k, D_l and F_0 describe lead, dot and slave-bosons respectively. We give their representation in the Matsubara frequency domain. The six- and ten-leg bare vertices correspond to the t^2 and t^4 order interactions in Eq. (3.25). The ten-leg vertex representing the last line in Eq. (3.25) *is omitted. Energy must be conserved, implying that the sum of all the external frequencies is zero. The smallest arrows pointing to the center of these vertices indicate the frequency dependence of the high-energy propagators included in the interaction.*

leading to the final form of the effective action

$$\begin{aligned} S'''_{\mathrm{CBM}} = S_0 + t^2 \sum_{\substack{kk'll' \\ \sigma\sigma'}} \mathrm{Tr}\Big[& c^\dagger_{k\sigma} d_{l\sigma} b^\dagger_0 F_1 d^\dagger_{l'\sigma'} c_{k'\sigma'} b_0 + d^\dagger_{l\sigma} c_{k\sigma} b^\dagger_0 F_{-1} c^\dagger_{k'\sigma'} d_{l'\sigma'} b_0 \\ & + t^2 \sum_{\substack{k''k'''l''l''' \\ \sigma''\sigma'''}} c^\dagger_{k\sigma} d_{l\sigma} b^\dagger_0 F_1 c^\dagger_{k''\sigma''} d_{l''\sigma''} F_2 d^\dagger_{l'''\sigma'''} c_{k'''\sigma'''} F_1 d^\dagger_{l'\sigma'} c_{k'\sigma'} b_0 \\ & + t^2 \sum_{\substack{k''k'''l''l''' \\ \sigma''\sigma'''}} d^\dagger_{l\sigma} c_{k\sigma} b^\dagger_0 F_{-1} d^\dagger_{l''\sigma''} c_{k''\sigma''} F_{-2} c^\dagger_{k'''\sigma'''} d_{l'''\sigma'''} F_{-1} c^\dagger_{k'\sigma'} d_{l'\sigma'} b_0 \Big]. \end{aligned} \tag{3.25}$$

This action describes the Coulomb blockade regime with zero charges on the dot. All charge fluctuations are frozen and do not appear in the action anymore. They affect virtually the effective interaction between the lead and dot electrons. This is manifested by the presence in Eq. (3.25) of the propagators $F_{\pm 1}$ and $F_{\pm 2}$. The only residual slave-boson is b_0. The diagrammatic structure of the theory Eq. (3.25) is pictured in Fig. 3.3. Virtual fluctuations to charge sectors differing by $|n|$ with the low energy sector are responsible for an effective interaction of order $t^{2|n|}$. The exponent corresponds to the number of times the tunneling Eq. (3.8) must operate to go back and forth from the low energy charge sector as in the paths shown in Fig. 3.2. This is a sensible difference to the SU(2) Anderson model, where the high energy charge occupations can differ a maximum of one from the single charge occupation of the dot. As we discuss in Section 4.2.1, only an effective t^2 order interaction is found for the SU(2) Anderson model, while a contribution to t^4 order is found again in the SU(4) case, where larger charge fluctuations are permitted again.

3.3 The renormalization group

The effective action Eq. (3.25) is quite different from that corresponding to a Fermi liquid Eq. (3.1). In this section we illustrate the arguments, derived from the renormalization group, which allow for the mapping of the Coulomb blockade model, in the zero temperature limit, to a non-interacting Fermi liquid.

The renormalization group was originally formulated, in the context of Condensed Matter Physics, by Kenneth G. Wilson [109]. It provided a comprehensive description of critical phenomena and paved the way to the solution of a huge class of difficult problems in which perturbative approaches revealed unsuccessful because of the appearance of logarithmic divergences $\propto \ln E/E_F$, when the low energy limit $E \to 0$ was investigated. An example is the logarithmic divergence of Eq. (3.6) at the charge degeneracy points. The presence of an infinite number of degrees of freedom, like the lead/dot electrons interacting with each other described by Eq. (3.25), is responsible for the failure of perturbative calculations. The smallness of the coupling constants, say the tunnel coupling t in Eq. (3.25), is not a sufficient condition to justify a perturbative approach with the associated operator. One must look indeed at the large number of degrees of freedom that it correlates in the regime which one is interested in. The renormalization group directly addresses this question. It is defined by the steps summarized in Fig. 3.4, which we apply here to determine the low energy action corresponding to the Coulomb blockade model.

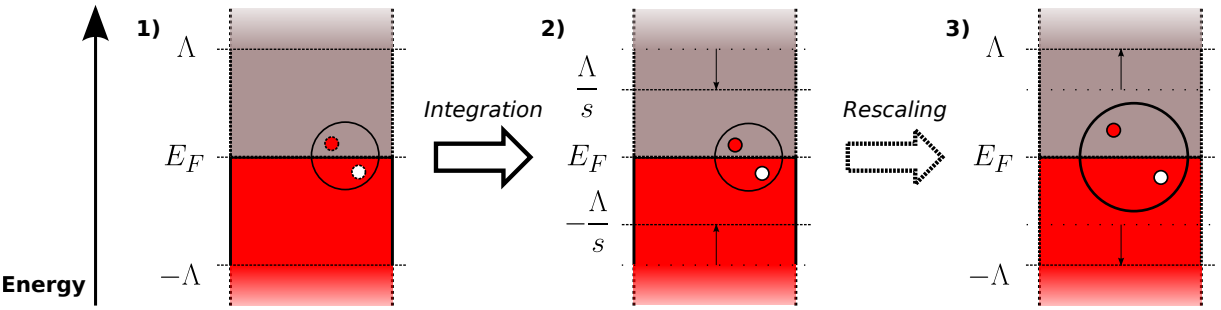

Figure 3.4: Steps defining the renormalization group analysis. 1) Integration of the modes above the running energy scale Λ, 2) progressive reduction of the running energy scale and 3) rescaling to the initial Λ. This works as a sort of zoom of the low energy processes.

3.3.1 Integration of high energy degrees of freedom

The first step has the deepest physical intuition. It has analogies with the Schrieffer-Wolff transformation [99] and with the integration of the high energy slave-bosons of the previous

section. Close to zero temperature, much smaller than an arbitrary *running energy scale* Λ, it is a reasonable assumption to think that particle or hole excitations do not play any relevant role if their energy is larger than Λ. The path integral formulation allows one to get correctly rid of these excitations by integrating them and derive an effective action. In the case of Eq. (3.25), this assumes the form $S^\Lambda = S_0^\Lambda + S_1^\Lambda$ [131, 132], with

$$\begin{aligned} S_0^\Lambda &= -\sum_{k\sigma i\omega_n}^{<\Lambda} c_{k\sigma}^\dagger \left[\mathscr{G}_k^\Lambda\right]^{-1} c_{k\sigma} - \sum_{l\sigma i\omega_n}^{<\Lambda} d_{l\sigma}^\dagger \left[\mathscr{D}_l^\Lambda\right]^{-1} d_{l\sigma} - \sum_{i\nu_n}^{<\Lambda} b_0^\dagger \left[\mathscr{F}_0^\Lambda\right]^{-1} b_0 \,, \\ S_1^\Lambda &= \sum_{kk'\sigma,i\omega,i\nu}^{<\Lambda} \mathscr{V}_c^\Lambda c_{k\sigma}^\dagger c_{k'\sigma} b_0^\dagger b_0 + \sum_{ll'\sigma,i\omega,i\nu}^{<\Lambda} \mathscr{V}_d^\Lambda d_{l\sigma}^\dagger d_{l'\sigma} b_0^\dagger b_0 + \ldots \end{aligned} \tag{3.26}$$

The notation $\sum^{<\Lambda}$ means that the summations run over Matsubara frequencies and momenta whose absolute value is smaller than Λ. We omit the field dependence on Matsubara frequencies only to simplify notations, but it must be always considered in calculations and respect energy conservation. $\mathscr{G}_k^\Lambda$, $\mathscr{D}_l^\Lambda$ and $\mathscr{F}_0^\Lambda$ are the full propagators associated to the fields $c_{k\sigma}$, $d_{l\sigma}$ and b_0 respectively. Their exact expression is given by the Dyson equation. For instance, in the case of the lead electrons, this reads

$$\mathscr{G}_k^\Lambda(i\omega_n) = \frac{1}{G_k(i\omega_n)^{-1} - \Sigma^\Lambda(i\omega_n)} \,. \tag{3.27}$$

Σ^Λ denotes the *self-energy*, composed of the series of irreducible diagrams appearing in the diagrammatic expansion of the propagator [133], as those that are calculated in Fig. 3.5 for the slave-boson self-energy. The superscript Λ means that all the internal lines of the diagrams, contributing to the self-energy Σ^Λ, are integrated for frequencies and momenta larger than the running energy scale Λ. The importance of this prescription will become manifest when we will encounter the Kondo infra-red divergencies in Section 4.3. The same applies for the vertex functions $\mathscr{V}^\Lambda$. Restricting us to the case of lead electrons, this reads [133]

$$\mathscr{V}_c^\Lambda(k, i\omega_1, i\nu_1; k' i\omega_2, i\nu_2) = -\beta \frac{\langle c_{k\sigma}(i\omega_1) b_0(i\nu_1) b_0^\dagger(i\nu_2) c_{k'\sigma}^\dagger(i\omega_2)\rangle\Big|_c}{G_k(i\omega_1) G_{k'}(i\omega_2) F_0(i\nu_1) F_0(i\nu_2)} \,. \tag{3.28}$$

The denominator cuts away the external lines of the two-particle Green's functions, appearing in the numerator. The notation $\langle\cdot\rangle_c$ means that only connected irreducible diagrams, as those from Fig. 3.6 to 3.10, are considered. In Section 3.4.5, we shall discuss that total charge conservation implies

$$\mathscr{V}_c^\Lambda = -\mathscr{V}_d^\Lambda \,, \tag{3.29}$$

in close connection with the Friedel sum rule and in strict analogy with Eq. (2.35), obtained by applying the Schrieffer-Wolff transformation on the Coulomb blockade model. All the terms omitted in the second line of Eq. (3.26) involve further interactions with more dot/lead operators. They can be neglected by applying scaling arguments, provided by the remaining steps of Wilson's renormalization approach.

3.3.2 Rescaling

The second step involves the concept of *rescaling*. Integrating all the modes with an energy belonging to the interval $[\Lambda/s, \Lambda]$ with $s > 1$, Eq. (3.26) remains unchanged, but with the substitution $\Lambda \to \Lambda/s$. To know the effect of this operation on the couplings in the action, we have to compare with the initial action and *rescale* the energy shell to its initial value, that is reestablishing $\Lambda/s \to \Lambda$, see Fig. 3.4. This is not equivalent to come back to the initial action with running energy scale Λ, because some high energy modes have been integrated in the meanwhile and so irremediably lost. The $T \to 0$ limit justifies the continuum limit also for the Matsubara frequencies and this rescaling can be done by making the substitutions

$$\begin{aligned} i\omega' &= s\, i\omega\,, \\ \varepsilon'_k &= s\,\varepsilon_k\,. \end{aligned} \tag{3.30}$$

As we are interested in exploring the possibility of having a free electron gas at low energy, we wish to know if free quasi-particles are "stable" upon this operation. Quantum dots in nanodevices have only a local effect on the wave function of bulk electrons, typically the phase-shift controlled by the Friedel sum rule discussed in Section 2.1.1. The integration of the high energy modes presented in Section 3.3.1 has then no effect on the Green's functions of bulk electrons, which remain that of a free Fermi gas, that is $\mathscr{G}_k = G_k$ and $\mathscr{D}_l = D_l$ in Eq. (3.26). We give an explicit proof of it in Section 3.4.2. The stability of a free electron gas can then be explored leaving invariant the non-interacting part of the action Eq. (3.26). The transformation Eq. (3.30) forces then the choice to *rescale* lead/dot fields according to the following transformation

$$\begin{aligned} c' &= s^{-3/2} c\,, & d' &= s^{-3/2} d\,, \\ c'^{\dagger} &= s^{-3/2} c^{\dagger}\,, & d'^{\dagger} &= s^{-3/2} d^{\dagger}\,. \end{aligned} \tag{3.31}$$

The rescaling of the free fields and energies gives the criterion to establish which perturbation to the free Fermi liquid must be taken into account or not.

3.3.3 Relevant, irrelevant and marginal operators

For instance, let us consider one of the operators neglected in the second line of Eq. (3.26), namely

$$\int_{kk'll'}^{<\Lambda} \mathcal{V}^{\Lambda}_{cd} c^{\dagger}_k c_{k'} d^{\dagger}_l d_{l'}\,, \tag{3.32}$$

where $\mathcal{V}^{\Lambda}_{cd}$ is defined like in Eq. (3.28), substituting the slave-boson operators b_0 with the quantum dot electron operators d_l. The interaction Eq. (3.32) is completely local and describes lead/dot interactions at the boundary between them, that we fix at $x = 0$. Longer

range interactions, like Coulomb electron-electron interactions, would involve less sums over momenta, with different conclusions that will not be discussed here, see Ref. [131] for a general discussion. As we are interested in the low energy behavior, we expand the vertex function $\mathcal{V}_{cd}^{\Lambda}$ close to $i\omega = 0$ and $k = k_F$, both for lead and dot electrons. The first contribution is then given by a constant and exits from the integral in Eq. (3.32). Once the scaling steps Eqs. (3.30) and (3.31) are performed, Eq. (3.32) transforms to

$$\frac{\mathcal{V}_{cd}^{\Lambda}}{s}\int_{kk'll'}^{<\Lambda} c_k^{\prime\dagger} c_{k'}^{\prime} d_l^{\prime\dagger} d_{l'}^{\prime}\,. \tag{3.33}$$

The fact that $s > 1$ implies that $\mathcal{V}_{cd}^{\Lambda}/s$ is smaller than the initial coupling $\mathcal{V}_{cd}^{\Lambda}$. The importance of this operator decreases when lowering the running energy scale Λ. It vanishes in the limit $\Lambda \to 0$ and it is called for this reason an *irrelevant* operator, as it does not affect the free Fermi gas behavior of the lead/dot electrons. This is the reason why, in Chapter 2, the normal ordered operators could be neglected to the fourth order in t to obtain the effective interaction Eq. (2.32). The frequency corrections to Eq. (3.33), coming from the frequency/momentum expansion of $\mathcal{V}_c$, can be also neglected as they scale even faster to zero. Operators whose coupling increases with the scaling analysis are called *relevant* operators. They tell that a free Fermi gas is actually unstable with respect to these operators and one must look for different low energy behaviors. The arising of the superconducting phase, because of long-range attractive electron-electron interaction, is a typical example [131]. Operators that remain unchanged upon the scaling transformation are called *marginal* and they turn out to be the only ones affecting the Fermi liquid in the Coulomb blockade model. The operators involving slave-boson fields kept in Eq. (3.26) are marginal. The scaling analysis of these fields is more subtle and deserves a separate discussion.

The slave-boson fields b_0 are completely different from the lead/dot ones, mainly for two reasons. Firstly, they are not associated to a continuum, but to a set of well discretized levels. Secondly, they are subject to the constraint Eq. (3.14), setting the number of slave-states in the $\lambda \to \infty$ limit. It is a non-trivial issue to establish how this prescription evolves once some of the slave-states entering in Eq. (3.14) are integrated. This question has been addressed in Refs. [134, 135] dealing with the Bose-Fermi Kondo model and in Ref. [68] for the Kondo model, even in out of equilibrium contexts [136]. To define the renormalization of local slave-fields one must look at the behavior of the slave-boson propagator $\mathscr{F}_0$ upon decreasing the energy shell Λ of the lead/dot electrons. The slave-boson propagator also obeys to the Dyson relation

$$\mathscr{F}_0(i\nu_n) = \frac{1}{F_0^{-1}(i\nu_n) - \Sigma_0(i\nu_n)}\,. \tag{3.34}$$

Notice that we omit the superscript Λ. In the Coulomb blockade model all the internal lines in diagrams can be integrated up to zero energies for $\Lambda \to 0$, what is assumed in all the calculations carried in Section 3.4. To appreciate how the slave-boson evolves in the scaling

analysis, Eq. (3.34) must be compared to the initial free propagator F_0. This can be done expanding Eq. (3.34) close to its pole, defined by the implicit equation

$$i\nu_n - \lambda - \Sigma_0(i\nu_n) = 0\,. \tag{3.35}$$

This is solved, to leading order, by

$$i\nu_n = \tilde{E}_0 = \lambda + \Sigma_0\,, \tag{3.36}$$

where we defined $\Sigma_0 = \Sigma_0(i\nu_n \to \lambda)$, to stress that Σ_0 does not depend on λ. This is verified in Eq. (3.45) and it is relevant for the following discussion. Expanding Eq. (3.34) close to $\tilde{E}_0$, this can be cast into the form

$$\mathscr{F}_0 = \frac{\mathscr{Z}_0}{i\nu - \tilde{E}_0}\,, \tag{3.37}$$

with

$$\mathscr{Z}_0 = \frac{1}{1 - \partial_\omega \Sigma_0}\,. \tag{3.38}$$

This is the slave-boson *quasi-particle* weight. We precise also that $\partial_\omega \Sigma_0 = \partial_\omega \Sigma(\omega)|_{\omega\to\lambda}$ does not depend on λ, which is verified in Eq. (3.46). Through Eq. (3.37), $\mathscr{Z}_0$ appears to be the renormalization of the slave-boson wave function, while $\tilde{E}_0$ is the renormalized energy of the slave-boson. To complete the mapping onto the free propagator, a different rescaling of the fields is necessary

$$b_0' \to \frac{b_0}{\sqrt{\mathscr{Z}_0}}\,, \qquad\qquad b_0'^\dagger \to \frac{b_0^\dagger}{\sqrt{\mathscr{Z}_0}}\,. \tag{3.39}$$

Eq. (3.26) transforms to

$$\begin{aligned} S_0' =& -\sum_{k\sigma i\omega_n} c_{k\sigma}^\dagger G_k^{-1} c_{k\sigma} - \sum_{l\sigma i\omega_n} d_{l\sigma}^\dagger D_l^{-1} d_{l\sigma} - \sum_{i\nu_n} b_0'^\dagger \left(i\nu_n - \tilde{E}_0\right) b_0'\,, \\ S_{\mathrm{I}}' =& \mathscr{V}^R \sum_{i\nu_n} \left(\sum_{kk'\sigma, i\omega} c_{k\sigma}^\dagger c_{k'\sigma} - \sum_{ll'\sigma, i\omega_n} d_l^\dagger d_{l'} \right) b_0'^\dagger b_0'\,, \end{aligned} \tag{3.40}$$

where we defined the *renormalized vertex*

$$\mathscr{V}^R = \mathscr{Z}_0 \cdot \mathscr{V}_c\,. \tag{3.41}$$

Also in this case, the frequencies of the vertex function are fixed to the renormalized poles of the propagators ($i\omega \to 0$, $k \to k_F$ and $i\nu \to \tilde{E}_0$), all the corrections to this approximation give irrelevant contributions which can be discarded. The steps 2) and 3) of the scaling analysis of Fig. 3.4 can be repeated for the Coulomb blockade model. They leave invariant the free quadratic part of the action Eq. (3.26), which is only affected by the marginal interaction in

Eq. (3.40). The renormalization group can be performed up to $\Lambda \to 0$ and the action recovered in this limit is the *fixed point* describing the zero temperature behavior of the Coulomb blockade Hamiltonian.

The Hamiltonian Eq. (3.40) corresponds to the Fermi liquid action Eq. (3.1) To see it, we switch back to the imaginary-time representation, in which Eq. (3.40) reads

$$\begin{aligned} S_0' &= \int_0^\beta d\tau \left\{ \sum_{k\sigma} c_{k\sigma}^\dagger \big(\partial_\tau + \varepsilon_k\big) c_{k\sigma} + \sum_{l\sigma} d_{k\sigma}^\dagger \big(\partial_\tau + \varepsilon_l\big) d_{l\sigma} + b_0^\dagger \big(\partial_\tau + \lambda + \Sigma_0\big) b_0 \right\}, \\ S_{\rm I}' &= \mathcal{V}^R \int_0^\beta d\tau \left(\sum_{kk'\sigma} c_{k\sigma}^\dagger c_{k'\sigma} - \sum_{ll'\sigma} d_{l\sigma}^\dagger d_{l'\sigma} \right) b_0'^\dagger b_0', \end{aligned} \tag{3.42}$$

where all fields are taken at the same imaginary time τ. The presence of the para-energy λ in Eq. (3.42) still works as an effective chemical potential setting the constraint [68, 136]

$$b_0'^\dagger b_0' = 1, \tag{3.43}$$

when λ is sent to infinity, as it was discussed in Section 3.1. We recover then the Fermi liquid action Eq. (3.1). In the following sections, we calculate the renormalized vertex Eq. (3.2), showing that it is in agreement with the Friedel sum rule.

3.4 Calculation of the vertex

The proof of the Friedel sum rule to higher orders in the tunneling coupling t requires the calculation of the renormalized vertex $\mathcal{V}^R$. In this section we carry out all the calculations necessary to this purpose.

3.4.1 Slave-boson self-energy

The leading contributions to Σ_0 are given by the diagrams illustrated in Fig. 3.5. Their expression is readily obtained in the zero temperature limit

$$\begin{aligned} \Sigma_0(i\nu_n) &= -\frac{t^2}{\beta^2} \sum_{kl\sigma i\omega_{1,2}} G_k(i\omega_1) D_l(i\omega_2) \left[F_1(i\nu_n + i\omega_1 - i\omega_2) + F_{-1}(i\nu_n + i\omega_2 - i\omega_1) \right] \\ &= -N(\nu_0 t)^2 \int d\varepsilon_1 d\varepsilon_2 \left[\frac{\theta(\varepsilon_1)\theta(\varepsilon_2)}{\varepsilon_1 + \varepsilon_2 + E_1 + \lambda - i\nu_n} + \frac{\theta(\varepsilon_1)\theta(\varepsilon_2)}{\varepsilon_1 + \varepsilon_2 + E_{-1} + \lambda - i\nu_n} \right]. \end{aligned} \tag{3.44}$$

The pole renormalization is then obtained from Eq. (3.36)

$$\tilde{E}_0 = \lambda - N(\nu_0 t)^2 \int d\varepsilon_1 d\varepsilon_2 \left[\frac{\theta(\varepsilon_1)\theta(\varepsilon_2)}{\varepsilon_1 + \varepsilon_2 + E_1} + \frac{\theta(\varepsilon_1)\theta(\varepsilon_2)}{\varepsilon_1 + \varepsilon_2 + E_{-1}} \right], \tag{3.45}$$

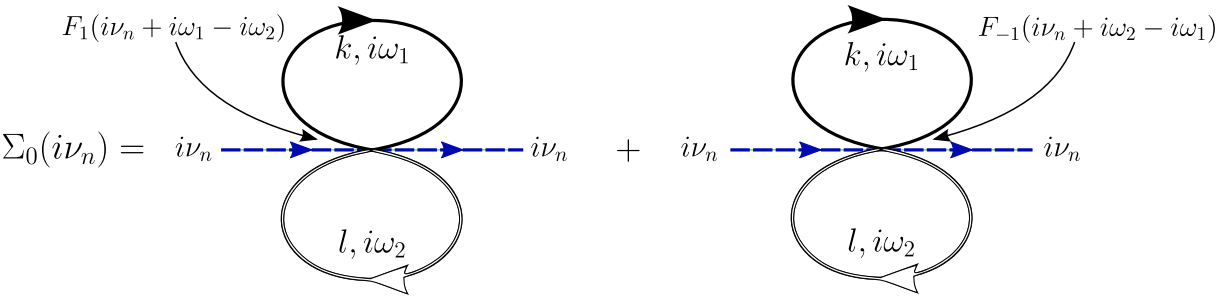

Figure 3.5: Leading order diagrams for the slave-boson self-energy.

with the quasi-particle weight from Eq. (3.38)

$$\mathcal{Z}_0 = 1 - N(\nu_0 t)^2 \int d\varepsilon_1 d\varepsilon_2 \left[\frac{\theta(\varepsilon_1)\theta(\varepsilon_2)}{(\varepsilon_1+\varepsilon_2+E_1)^2} + \frac{\theta(\varepsilon_1)\theta(\varepsilon_2)}{(\varepsilon_1+\varepsilon_2+E_{-1})^2} \right]. \tag{3.46}$$

All these integrals are divergent. Adopting a "sharp" ultra-violet (UV) cutoff D_0 for the integrals $\propto \int_{-D_0}^{D_0} d\varepsilon$, they scale as $\sim D_0 \ln D_0$. The summation of all the contributions to fourth order in t to the renormalized vertex $\mathcal{V}^R$ allows one to safely perform the $D_0 \to \infty$ limit at the end of calculations. This is discussed in Appendix F. The divergence of Σ_0 affects both the renormalized energy $\tilde{E}_0$ and the quasi-particle weight $\mathcal{Z}_0$, which is only logarithmically divergent. Their contribution to the renormalized vertex $\mathcal{V}^R$ appears as t^4 order corrections to the one-loop diagrams that we calculate in Section 3.4.3. We stress again that the corrections in the tunnel coupling t in Eqs. (3.45) and (3.46) do not depend on λ, verifying the assumptions used to derive the fixed-point action Eq. (3.42).

3.4.2 Lead/dot electrons self-energy

The diagrams giving the leading contributions to the lead/dot electrons self-energy are similar to those illustrated in Fig. 3.5, with the difference that the slave-boson lines are contracted instead of the dot/lead ones. The self-energy of the lead electrons reads

$$\begin{aligned}\Sigma_c(i\omega_n) &= -\frac{t^2}{\beta^2} \sum_{l,i\nu_n,i\omega_1} F_0(i\nu_n) D_l(i\omega_1) \left[F_1\left(i\nu_n + i\omega_n - i\omega_1\right) + F_{-1}\left(i\nu_n + i\omega_1 - i\omega_n\right)\right] \\ &= \frac{t^2}{\beta} \sum_{l,i\omega_1} D_l(i\omega_1) \left[b(\lambda) \left(\frac{1}{i\omega_n - i\omega_1 - E_1} + \frac{1}{i\omega_1 - i\omega_n - E_{-1}} \right) + \right. \\ &\qquad \left. + \frac{b(\lambda+E_1)}{i\omega_1 - i\omega_n} + \frac{b(\lambda+E_{-1})}{i\omega_n - i\omega_1 + E_{-1}} \right],\end{aligned} \tag{3.47}$$

with $b(\varepsilon) = \left(e^{\beta\varepsilon} - 1\right)^{-1}$ the Bose-Einstein distribution. In the projection limit $\lambda \to \infty$ this expression vanishes and can then be neglected. This proves the validity of the assumption of

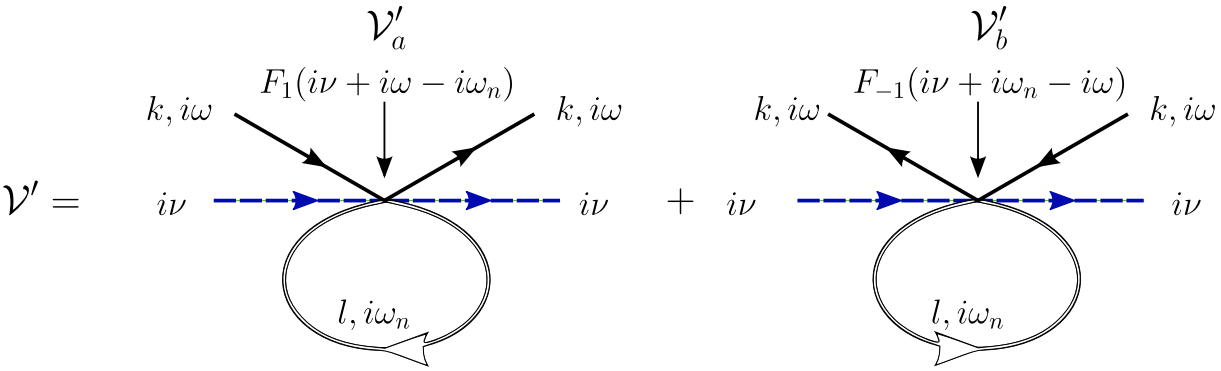

Figure 3.6: Illustration of the one-loop contribution to the vertex.

Section 3.3.2, stating the invariance of the bulk Green's functions upon the integration of the high energy modes for a local interaction. The calculation in the case of the dot electrons is completely similar and leads to the same result.

3.4.3 One-loop diagrams

The one-loop diagrams in Fig. 3.6, are the leading contribution to the vertex function Eq. (3.28). They are similar to those giving the self-energy in Fig. 3.5, but without the contraction of the lead electrons lines. They read

$$\begin{aligned} \mathcal{V}'_a &= -\frac{t^2}{\beta}\sum_{l,i\omega_n} D_l(i\omega_n)F_1(i\nu+i\omega-i\omega_n) & \mathcal{V}'_b &= -\frac{t^2}{\beta}\sum_{l,i\omega_n} D_l(i\omega_n)F_{-1}(i\nu+i\omega_n-i\omega) \\ &= -\nu_0 t^2\int d\varepsilon \frac{1-f(\varepsilon)}{\varepsilon+E_1-\Sigma_0(\lambda)}, & &= -\nu_0 t^2\int d\varepsilon \frac{f(\varepsilon)}{\varepsilon-E_{-1}+\Sigma_0(\lambda)}. \end{aligned} \tag{3.48}$$

The analytical continuations $i\omega \to 0$ and $i\nu \to \tilde{E}_0$ must be taken *after* the summation over the Matsubara frequencies to deal correctly with the analytic structure of the free Green's functions. The continuum limit has been taken for the summation running over the bandwidth. In the zero temperature limit, the summation of the two contributions $\mathcal{V}' = \mathcal{V}'_a + \mathcal{V}'_b$, expanded to second order in t^2, reads

$$\mathcal{V}' = \nu_0 t^2 \ln\frac{E_1}{E_{-1}} + N\nu_0^3 t^4 \int_{\varepsilon_{1,2,3}>0} d\varepsilon_{1,2,3}\left(\sum_{s=\pm1}\frac{1}{\varepsilon_1+\varepsilon_2+E_s}\right)\left[\sum_{s\pm1}\frac{s}{(\varepsilon_3+E_s)^2}\right]. \tag{3.49}$$

The first term of this expression makes the connection with the Schrieffer-Wolff transformation that we applied in Section 2.2. The second contribution exhibits a divergence essentially coming from the renormalized pole Eq. (3.45). The number of variables in the integral can

be reduced switching to the exponential regularization $\int_0^{D_0} d\varepsilon \to \int_0^{\infty} d\varepsilon e^{-\varepsilon/D_0}$. Following the change of variable $\varepsilon_1+\varepsilon_2 \to \varepsilon_1$, ε_2 can be integrated obtaining

$$\mathcal{V}' = \nu_0 t^2 \ln\frac{E_1}{E_{-1}} + N\nu_0^3 t^4 \int_{\varepsilon_{1,3}>0} d\varepsilon_{1,3} \left(\sum_{s=\pm1} \frac{\varepsilon_1}{\varepsilon_1+E_s}\right)\left[\sum_{s\pm1} \frac{s}{(\varepsilon_3+E_s)^2}\right] e^{-\frac{\varepsilon_1+\varepsilon_3}{D_0}}. \tag{3.50}$$

We can switch back again to the sharp regularization, what allows one to calculate the remaining integrals as shown in Appendix F. This procedure must be carried out in the same way for all diverging integrals to obtain the correct result and it is tacitly assumed in the following. Notice that the first term in Eq. (3.50) provides the leading contribution to Eq. (3.2), corresponding to the Schrieffer-Wolff transformation.

The necessity to multiply the vertex function by the slave-boson quasi-particle weight $\mathcal{Z}_0$, required by Eq. (3.41), provides a further contribution to fourth order in t

$$\mathcal{V}'' = -N\nu_0^3 t^4 \ln\frac{E_1}{E_{-1}} \int_{\varepsilon>0} d\varepsilon \sum_{s=\pm1} \frac{\varepsilon}{(\varepsilon+E_s)^2}. \tag{3.51}$$

3.4.4 The large-N limit and second order diagrams

We consider now the genuine second order diagrammatic contributions to the vertex function Eq. (3.28). They can be divided in two classes. The first ones are discussed in Section 3.4.4.1 and involve the repeated action of the bare interaction of order t^2 in Eq. (3.10) reported as six-leg vertices in Fig. 3.3. The second ones imply different contractions of the lead or dot lines in the bare interaction of order t^4 in the action Eq. (3.10). They are reported in Fig. 3.3 as ten-leg vertices and their contribution is discussed in Section 3.4.4.2. The calculation can be further simplified by considering the limit of a large number of channels N, where certain diagrams are eliminated. Nevertheless our approach remains valid for any value of N.

3.4.4.1 Diagrams from combinations of the six-leg vertex

Part of the diagrams contributing to the vertex function Eq. (3.28) are listed in Fig. 3.7. They are built by combining two six-leg vertices from Fig. 3.3. These contributions are all of order $N\nu_0^3 t^4$ and dominate in the large-N limit. In Fig. 3.8, we show which diagrams are neglected in this approximation. They result from the contraction of the quantum dot electron d lines within the same six-leg vertex.

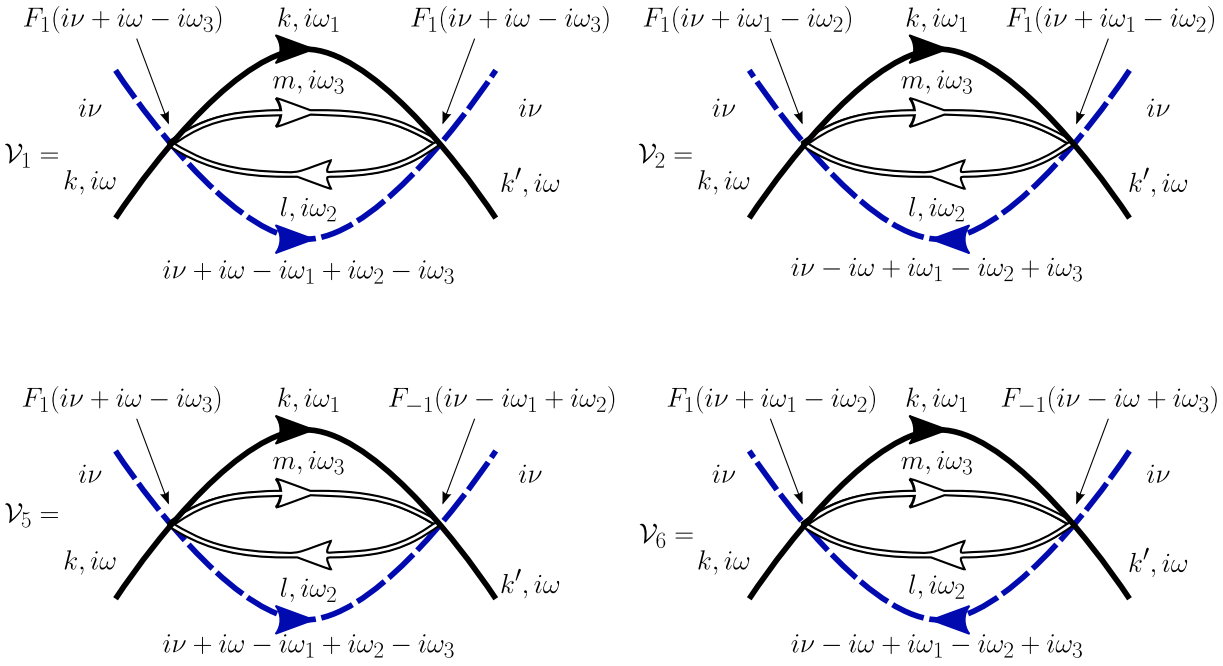

Figure 3.7: Diagrams of order Nt^4 derived by the repeated action of the six-leg vertices in Fig. 3.3. The diagrams $\mathcal{V}_{3,4}$, particle-hole symmetric to $\mathcal{V}_{1,2}$, are readily obtained by inverting the overall signs and making the substitution $E_n \to E_{-n}$.

To give a general illustration of how calculations work, only the calculation of the diagram $\mathcal{V}_1$ is explicitly provided, the others being similar. This reads

$$\mathcal{V}_1 = \frac{Nt^4}{\beta^3} \sum_{klm, i\omega_{1,2,3}} G_k(-i\omega_1) D_l(i\omega_2) D_m(-i\omega_3) \times \\ F_1^2(i\nu+i\omega+i\omega_3) F_0(i\nu+i\omega+i\omega_1+i\omega_2+i\omega_3) . \quad (3.52)$$

The choice of the signs of the Matsubara frequencies inside the free propagators is different from that, more natural, illustrated in Fig. 3.7. This choice is actually arbitrary, but it is useful to simplify calculations. Positive signs for the frequencies in the argument of the bosonic propagators $F_{0,1}$ allow one to automatically discard all the contributions from their poles, proportional to $+\lambda$. For instance, when performing the summation over $i\omega_1$, the pole of F_0 is responsible for a contribution proportional to $f(\lambda)$, which vanishes in the $\lambda \to \infty$ limit. This is similar to what happens for the lead/dot electron self-energies in Eq. (3.47). Only poles coming from lead/dot fermion propagators give non zero contributions. The result

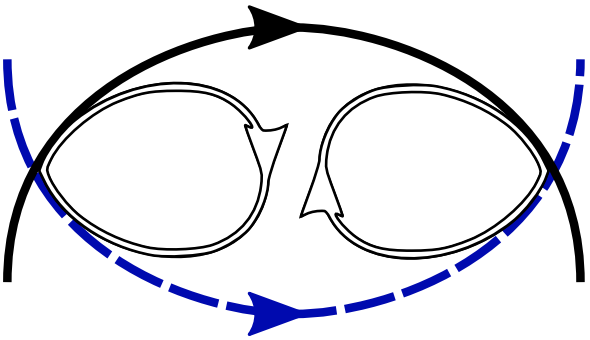

Figure 3.8: Example of diagram derived from the repeated action of the six-leg vertex in Fig. 3.3 which is neglected in the large-N limit.

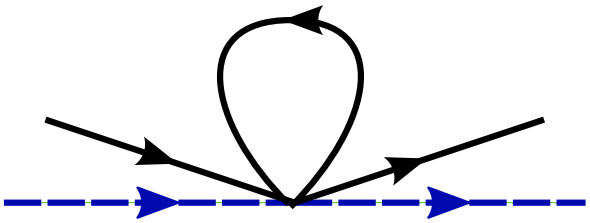

Figure 3.9: Example of diagram derived from the ten-leg interaction in Fig. 3.3 which is neglected in the large-N limit.

reads

$$\begin{aligned}\mathcal{V}_1 &= Nt^4 \sum_{klm} \frac{f(-\varepsilon_k) f(\varepsilon_l) f(-\varepsilon_m)}{(\varepsilon_m + E_1)^2 (\varepsilon_l - \varepsilon_k - \varepsilon_m)} \\ &= -N\nu_0^3 t^4 \int_{\varepsilon_{1,2}>0} d\varepsilon_{1,2} \frac{\varepsilon_1}{(\varepsilon_2 + E_1)^2 (\varepsilon_1 + \varepsilon_2)} .\end{aligned} \tag{3.53}$$

It can be checked that a different choice for the frequency sign in Eq. (3.52) leads to the same result. In Fig. 3.7 the diagrams $\mathcal{V}_3$ and $\mathcal{V}_4$ are omitted. These terms are the particle-hole symmetric of the diagrams $\mathcal{V}_1$ and $\mathcal{V}_2$. They are readily obtained by inverting the overall sign of these contributions and making the substitution $E_n \to E_{-n}$ and they are reported in Appendix F. Notice that, to order t^4, the corrections to the pole Eq. (3.44) and the quasi-particle weight $\mathcal{Z}_0$ are subleading and one can safely make the analytical continuation $i\nu \to \lambda$.

3.4.4.2 Diagrams from the ten-leg vertex

Most of the previous considerations also apply to the diagrammatic contributions involving the ten-leg interaction of order t^4 in the action Eq. (3.10). The diagrams dominating in the large-N limit are plotted in Fig. 3.10. Only "particle" contributions are illustrated. Their particle-hole symmetric equivalents $\mathcal{V}_{10,11,12}$ are obtained in the same way as in the previous section, that is by inverting the overall sign and making the substitution $E_n \to E_{-n}$. The results are summarized in Appendix F. In Fig. 3.9 we report, as an example, a diagram which is neglected in the large-N limit.

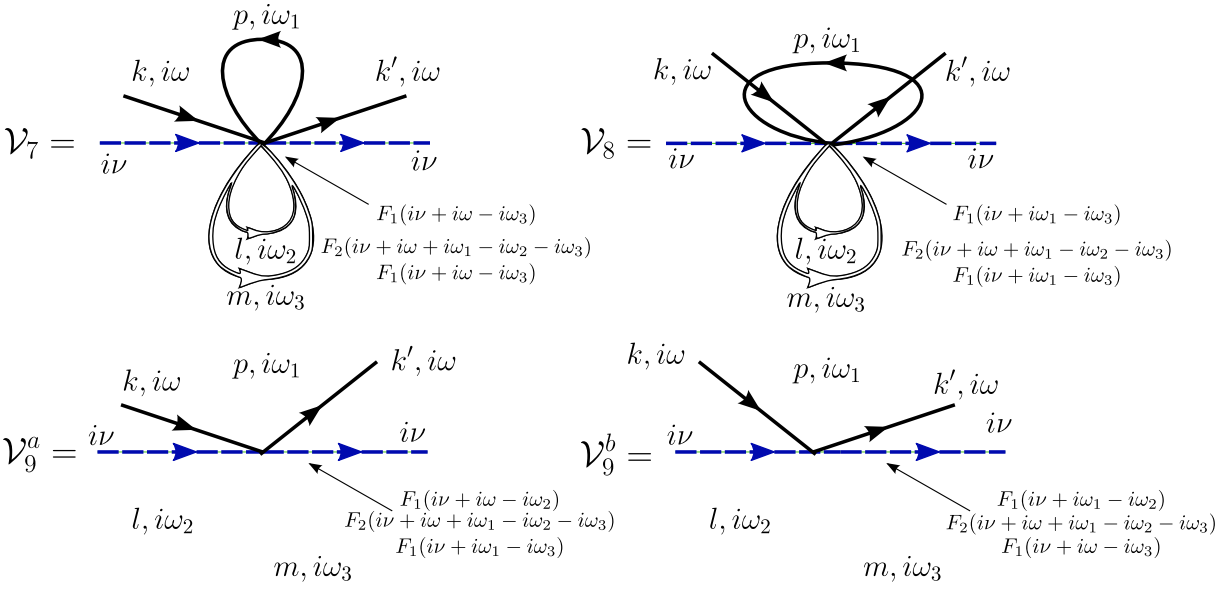

Figure 3.10: Contributions to the vertex from the ten-leg interaction of order t^4 in Fig. 3.3. Also in this case we omit $\mathcal{V}_{10,11,12}$. These diagrams can be readily obtained by inverting the sign and making the substitution $E_n \to E_{-n}$. Notice $\mathcal{V}_9 = \mathcal{V}_9^a + \mathcal{V}_9^b = 2\mathcal{V}_9^a$.

The summation, carried out in Appendix F, of all the leading contributions in the large-N limit to fourth order in t results in Eqs. (3.2) and (3.3), in agreement with the Friedel sum rule.

3.4.5 Total charge conservation and the Friedel sum rule

We come back to Eq. (3.29). All the calculations performed for the vertex function $\mathcal{V}_c$ can be repeated for $\mathcal{V}_d$ in Eq. (3.26), with the result that $\mathcal{V}_d = -\mathcal{V}_c$. The proof of the Friedel sum rule gives more physical insight on why Eq. (3.29) holds. Using the fact that the total number of electrons in the system $\hat{N}_t$ is conserved by the Hamiltonian, one can replace $\hat{n} = \hat{N}_t - \hat{n}_L$, $\hat{n}_L$ being the number of electrons in the lead, and transfer the Coulomb interaction to the lead. Therefore, the low energy model for the dot is the same as for the lead, namely Eq. (2.35), but the strength of the scattering potential for dot electrons, noted $\mathcal{V}_d(\varepsilon_d)$, is now given by the Friedel sum rule

$$\hat{N}_t - \langle\hat{n}\rangle = \langle\hat{n}_L\rangle = -\frac{1}{\pi}\arctan\left[\pi\nu_0\mathcal{V}_d(\varepsilon_d)\right] = N_t - \left(-\frac{1}{\pi}\arctan\left[\pi\nu_0\mathcal{V}_c(\varepsilon_d)\right]\right). \tag{3.54}$$

An alternative formulation is that the phase shift accumulated after backscattering at the boundary is $\delta(\varepsilon_d)$ for lead electrons and $\delta_t - \delta(\varepsilon_d)$ for dot electrons, where $\delta_t = \hat{N}_t/\pi$.

3.5 Conclusions

In this chapter, we illustrated in detail the renormalization group arguments which allow us to determine the low energy Fermi liquid fixed point of the Coulomb blockade Hamiltonian Eq. (iv). The result was checked to fulfill the Friedel sum rule. The ability to integrate the high energy modes and rely on diagrammatic techniques to carry out perturbative calculation in the tunnel coupling t, motivated our introduction of slave-bosons corresponding to the charge occupation of the quantum dot. The integration of the high energy slave-bosons is a first step to obtain the effective action in Coulomb blockade regimes. It provides a general method to obtain precise results more easily than with the Schrieffer-Wolff transformation. Diagrammatic calculations to fourth order in the tunnel coupling t are then carried out to calculate the renormalized vertex of the Coulomb blockade theory. This provides the potential scattering coupling affecting, with opposite amplitudes, lead and dot electrons, coherently with the Friedel sum rule.

This chapter also has the merit of introducing part of the techniques adopted in the following chapters where spinful electrons are considered. This case is more difficult because of the emergence of Kondo correlations. But, despite these complications, the final result is essentially the same, that is the validity of the Korringa-Shiba relation, leading to charge relaxation resistance universality.

CHAPTER 4

THE ANDERSON MODEL AND THE KONDO REGIME

Contents

In this chapter we develop the analytical methods to obtain the behavior of the differential capacitance and the charge relaxation resistance in a quantum RC circuit described by the Anderson model. The attested Fermi liquid behavior at low energy [93] and the validity of the Friedel sum rule [96] for the Anderson model are actually sufficient to ensure the validity

of the low energy effective Hamiltonian Eq. (2.10). As illustrated in Section 2.5, this allows us to show the generalized Korringa-Shiba relation Eq. (2.7), leading to Eq. (2.8). For a number of channels $N = 2$, this formula predicts universality of the charge relaxation resistance $R_q = h/4e^2$. The possibility to break channel-symmetry Eq. (2.6) by switching on a magnetic field is responsible for the loss of universality out of particle-hole symmetry. Eq. (2.70) describes this loss and requires the knowledge of the charge occupation and magnetization of the quantum dot. In this chapter, we illustrate a variety of analytical methods to calculate exactly these quantities. In Section 4.1, the numerical solution of the Bethe ansatz equations for the ground state of the Anderson model is presented. The behavior of the charge and charge-magneto susceptibilities, χ_c and χ_m respectively, is obtained for the whole phase diagram of the Anderson Hamiltonian Eq. (v). The validity of the Fermi liquid approach is tested and compared to numerical renormalization group calculations [76], as previously shown in Fig. 2.8. In Section 4.2, switching to the path-integral formalism we show that the introduction of slave-states allows for an exact mapping of the Anderson model onto the Kondo Hamiltonian. The difficulties peculiar to Kondo physics and its solution within a Fermi liquid theory are discussed. In Section 4.3, renormalization group methods, similar to those presented in the previous chapter for the Coulomb blockade model, are applied to derive the low energy Fermi liquid Hamiltonian Eq. (2.10). Relying on previous works by Cragg and Lloyd [104, 105, 106], the low energy Fermi liquid action is shown to read

$$S = \int_0^\beta d\tau \left\{ \sum_{k\sigma} c^\dagger_{k\sigma}(\tau)\left(\partial_\tau + \varepsilon_k\right) c_{k\sigma}(\tau) + \mathcal{V}_W^R \sum_{kk'\sigma} c^\dagger_{k\sigma}(\tau) c_{k'\sigma}(\tau) \right\}. \tag{4.1}$$

The proof that this action describes the low energy quasi-particles in the lead is interesting for essentially two reasons. On one hand, it applies to any order in t and extends the proof of the low energy potential scattering Hamiltonian provided in Section 2.2.2. On the other hand, it has a practical interest. The calculation to the fourth order in t of $\mathcal{V}_W^R$ in Eq. (4.1) provides, with the Friedel sum rule, an analytical formula for the charge susceptibility of the dot out of particle-hole symmetry in the Kondo regime

$$\begin{aligned}\chi_c = \frac{\Gamma}{\pi}\Bigg\{ &\frac{1}{(\varepsilon_d+U)^2} + \frac{1}{\varepsilon_d^2} + \frac{2\Gamma}{\pi}\cdot\left[\frac{1}{(\varepsilon_d+U)^3} - \frac{1}{\varepsilon_d^3}\right] + \\ &+ \frac{\Gamma}{\pi}\left[\left(\frac{1}{\varepsilon_d+U} - \frac{1}{\varepsilon_d}\right)^3 + 2\left(\frac{1}{\varepsilon_d+U} - \frac{1}{\varepsilon_d}\right)\left(\frac{1}{\varepsilon_d^2} - \frac{1}{(\varepsilon_d+U)^2}\right)\ln\frac{\varepsilon_d+U}{-\varepsilon_d}\right]\Bigg\}. \end{aligned} \tag{4.2}$$

This expression extends previous analytical results obtained by Bethe ansatz at particle-hole symmetry [107] and it is useful to carry out the analytical description of the giant charge relaxation resistance, to be discussed in Section 4.4.

An important point of the following discussion is that $\mathcal{V}_W^R$ in Eq. (4.1) is only a part of the total renormalized vertex, to be defined in a similar way as in Section 3.3.1. The total

renormalized vertex reads, see Eq. (2.81),

$$\mathcal{V}^R = \mathcal{V}_J^R \mathbf{S}\cdot\mathbf{s} + \mathcal{V}_W^R \mathbb{1}, \tag{4.3}$$

with **S** and **s** the vector composed of the SU(2) Pauli matrices acting on the spin of the quantum dot and that of the conduction electrons and $\mathbb{1} = \delta_{\sigma\sigma'}\delta_{\tau\tau'}$ is the diagonal matrix. Eq. (4.3) includes a spin-exchange and a potential scattering contribution, $\mathcal{V}_J^R$ and $\mathcal{V}_W^R$ respectively. The fate of the spin-exchange part has been already sketched in Fig. 2.3, being responsible for the universal phase-shift $\delta_K = \pi/2$ of the low energy quasi-particles. The rigorous argument for the additivity of the spin-exchange and potential scattering phase-shifts Eq. (2.41) is discussed in Section 4.2.4.

4.1 The Bethe ansatz solution of the Anderson model

In this section the zero temperature behavior at equilibrium of a quantum dot described by the Anderson Hamiltonian is illustrated. We exploit the integrability of this model through the Bethe ansatz. We observe the manifestations of Kondo physics, which cannot be addressed by perturbative approaches.

4.1.0.1 Phase diagram

The phase diagram in Fig. 4.1 represents the state of the isolated quantum dot in the Anderson model as a function of the orbital energy ε_d and the Zeeman energy H. It is readily obtained by diagonalizing the last two terms in Eq. (v) and describes the atomic limit, in which the dot is decoupled from the lead. The Hilbert space of the quantum dot is composed of four states defined by the charge occupation n and spin σ of electrons on the dot, see Fig. 4.5. Charge and spin symmetry allow us to confine to the colored region of Fig. 4.1, the same that is spanned by the Bethe ansatz equations. One could expect that a small hybridization ($\Gamma \ll U$), between the quantum dot and itinerant electrons in the leads, does not critically modify the phase diagram of the isolated quantum dot, the only important effect being to smoothen the transitions between different states of the dot. We already mentioned in Chapter 2, looking at Fig. 2.7, that this is not the case, in particular for what concerns the quantum dot magnetization. It vanishes in the single charge region for Zeeman energies below the Kondo temperature T_K associated to the Anderson model [93, 111, 79, 78]

$$T_K = 2\sqrt{\frac{U\Gamma}{\pi e}}\, e^{\frac{\pi\varepsilon_d(\varepsilon_d+U)}{2U\Gamma}}. \tag{4.4}$$

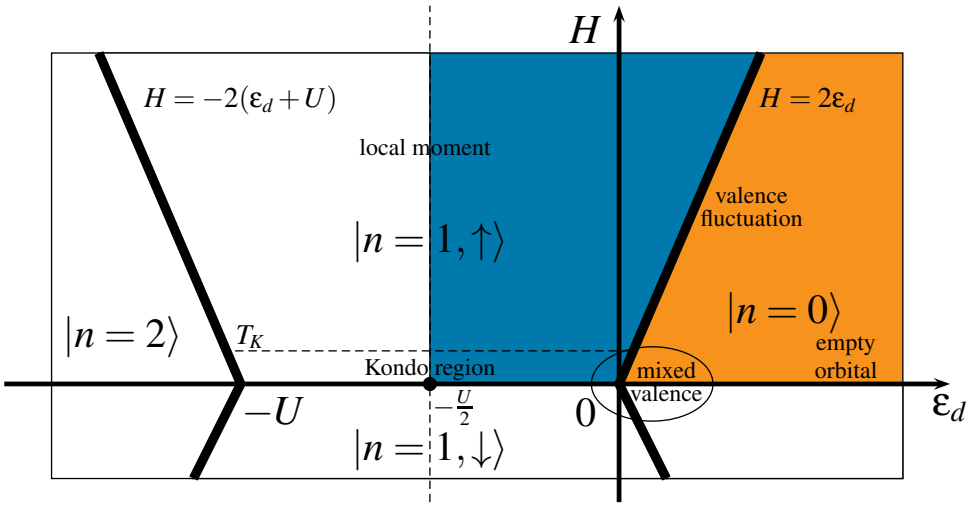

Figure 4.1: Phase diagram of the isolated dot in the presence of a magnetic field for the Anderson model Eq. (v). The colored region is that spanned by the Bethe ansatz equations.

This reduced magnetization at low field is a signature of the formation of the Kondo singlet to be discussed in detail in Section 4.2.3.

Outside the single charge region, strong spin-exchange correlations are suppressed and the phase diagram of the dot weakly hybridized with the lead electrons follows that of the isolated dot in Fig. 4.1, see also Fig. 2.7. $H < 2\varepsilon_d$ and $\varepsilon_d \gg \Gamma$ define the *empty orbital* region, where there are zero charges on the dot. Zeeman energies lower than $H_1 = \Gamma U/(U + 2\varepsilon_d)$ and $|\varepsilon_d| \sim \Gamma$ define the *mixed-valence* region. This is the transient region from an empty to a single-occupied quantum dot, in which Kondo correlations start setting up. Nevertheless, the transition from an empty to a single occupied orbital out of the mixed-valence region (H and $2\varepsilon_d > H_1$) lacks of Kondo correlations. This defines the *valence fluctuation* region and can be addressed by perturbative approaches as it is shown in Section 4.4.3. The region in which the charge on the dot is one and $H > T_K$ is the *local moment* region, first studied by Anderson to explain the appearance of local moments in metals [103]. We start by discussing the Kondo regime of the quantum dot.

4.1.1 The Bethe ansatz equations

The emergence of Kondo correlations can be understood by considering the mapping of the Anderson Hamiltonian onto the Kondo Hamiltonian Eq. (2.37), that was obtained within the Schrieffer-Wolff transformation [99] in Section 2.2.2. We showed that perturbative calculations give the behavior of the charge on the dot out of particle-hole symmetry, see Eq. (2.43).

The validity of these perturbative calculations does not extend to observables related to the spin of the quantum dot. Let us assume particle-hole symmetry, $W_0 = 0$ in Eq. (2.39) and the problem is mapped onto a pure Kondo Hamiltonian. We recall here that it reads

$$H_{\text{Kondo}} = \sum_{k\sigma} \varepsilon_k c^\dagger_{k\sigma} c_{k\sigma} + J\mathbf{S}\cdot\mathbf{s}, \tag{4.5}$$

with $\mathbf{S}$ the vector composed of the operators acting on the projections of the 1/2 spin of the quantum dot in the three spatial dimensions and $\mathbf{s} = \sum_{kk'\tau\tau'}(c^\dagger_{k\tau}\sigma_{\tau\tau'}c_{k'\tau'})/2$, with $\sigma_{\tau\tau'}$ the matrix elements of the vector composed of the Pauli matrices. A perturbative calculation in J of the magnetic susceptibility diverges logarithmically for temperatures going to zero [137]

$$\chi_H = \frac{\partial\langle m\rangle}{\partial H} = \frac{1}{4T}\left[1 - \nu_0 J + (\nu_0 J)^2 \ln\frac{2\pi T}{De^{C+\frac{3}{4}}} + \ldots\right], \tag{4.6}$$

where $C = 0.5772\ldots$ is Euler's constant. This expression gives the physical interpretation of the Kondo energy scale discussed in Section 2.6.1. If Eq. (4.6) is cast into the form

$$\chi_H = \frac{\partial\langle m\rangle}{\partial H} = \frac{1}{4T}\left[1 - \left(\ln\frac{T}{T_K}\right)^{-1} + \ldots\right], \tag{4.7}$$

this expression diverges for $T = T_K$, giving the energy scale at which a perturbative approach fails. The identification with Eq. (4.6) gives

$$T_K = \frac{D}{2\pi} e^{C+\frac{3}{4}} e^{-\frac{1}{\nu_0 J}} \tag{4.8}$$

and, performing calculations to higher orders in J, one obtains [61]

$$T_K = \frac{D}{2\pi} e^{C+\frac{3}{4}} \sqrt{\nu_0 J} e^{-\frac{1}{\nu_0 J}} \tag{4.9}$$

in the SU(2) case. There are different ways to define the Kondo temperature [61]. They differ by meaningless prefactors, as the definition given in Eq. (2.84) obtained from the expression of the renormalized vertex. The necessity of mentioning these different definitions of T_K will become manifest in Section 4.3.1. Eq. (4.6) shows that it is not possible to obtain the zero temperature expression of the quantum dot magnetization from perturbative calculations. Eq. (2.70), proven in Section 2.5.1 for R_q in the Anderson model, requires the knowledge of the charge-magneto susceptibility χ_m to study the charge relaxation resistance. This motivates the search for methods alternative to perturbation theory, as the solution of the Bethe ansatz equations for the ground state of the Anderson Hamiltonian.

The Bethe ansatz technique provides exact solutions for integrable one-dimensional problems. In the case of the Anderson Hamiltonian, it was devised by Wiegmann and Tsvelick [78, 79, 138] and Okiji and Kawakami [139, 140]. The ground state is described using two

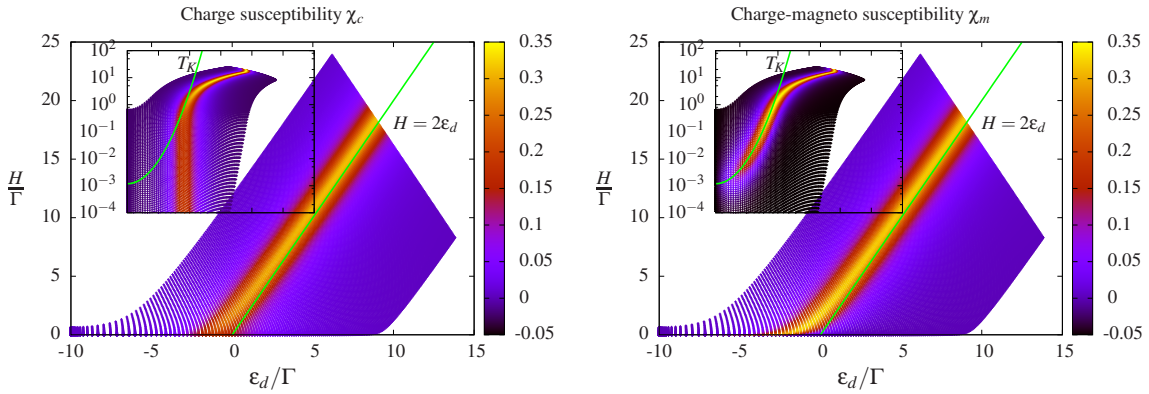

Figure 4.2: Charge susceptibility (left) and charge-magneto susceptibility (right) as a function of the orbital energy ε_d and the Zeeman energy H. The susceptibilities are in units of $1/\Gamma$. In the insets the same quantities are plotted on a logarithmic scale and the zone of appearance of the giant peak of the charge relaxation resistance can be appreciated. It is the region, following T_K, in which χ_c is close to zero, while χ_m acquires important values because of the formation of the Kondo singlet.

separate spin and charge excitations called *spinons* and *holons*, carrying respectively a quantum of spin 1/2 and charge e. Their respective distribution functions $\rho(k)$ and $\sigma(\lambda)$ satisfy a system of coupled integral equations detailed in Appendix G. Analytical results from this approach are possible only at particle-hole symmetry or in the absence of a magnetic field in the mixed-valence region. We take advantage of them in Section 4.4.1, to obtain the scaling limit Eq. (2.73) for the charge relaxation resistance in the Kondo regime. The numerical solution of the Bethe ansatz equations provides the charge occupation and magnetization of the quantum dot as functions of the orbital energy ε_d and the magnetic field H. An example is given in Fig. 2.7 for $U/\Gamma = 20$. Focusing on the logarithmic insets of Fig. 2.7, we observe markedly different behaviors for the charge and spin responses of the system, as a consequence of spin-charge separation in the solution of the model. The charge still reproduces a behavior which is coherent with the phase diagram of the isolated dot in Fig. 4.1, except that the position of the Coulomb peak of the static charge susceptibility χ_c, expected at $\varepsilon_d = 0$, is strongly renormalized and given by $\varepsilon_d^* = 0$, see Fig. 4.3. We recall that $\varepsilon_d^* = \varepsilon_d + \Gamma/\pi \ln(\pi e U/4\Gamma)$ [78, 93]. This is not the case for the magnetization. The zero magnetization regime penetrates in the local moment region for Zeeman energies which are lower than the Kondo temperature Eq. (4.4). This is plotted in green in the insets of Figs. 2.7 and 4.2.

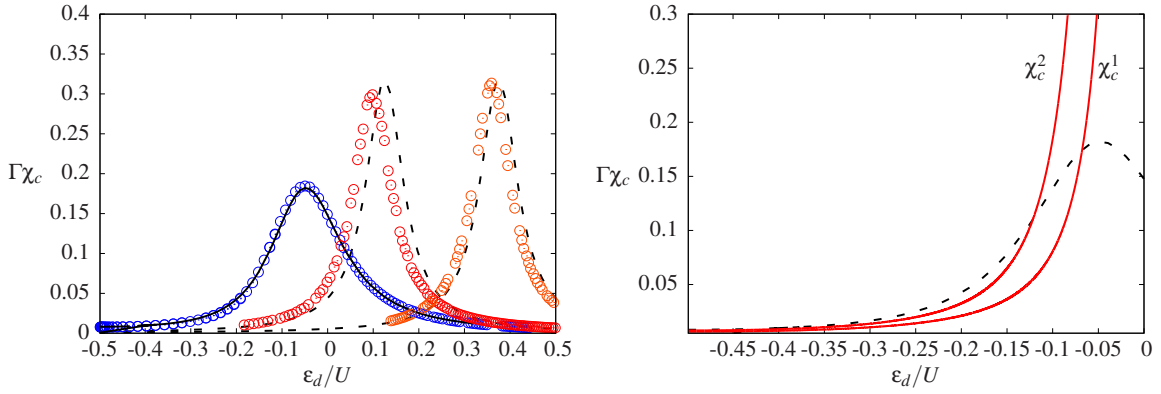

Figure 4.3: Left) Charge susceptibility χ_c for $U/\Gamma = 20$. The circles (left to right) correspond to $H/\Gamma =$ 0.1, 5 and 15 respectively and show the displacement of the Coulomb peak, also visible in Fig. 4.2. The solid line is obtained for $H/\Gamma = 0.0001$ and almost coincides with $H/\Gamma = 0.1$, showing the very weak dependence of χ_c on the magnetic field in the Kondo regime. For higher Zeeman energies, $H/\Gamma = 5$ and 15, χ_c converges to the Lorentzian form Eq. (4.62) (dashed lines) derived in the valence-fluctuation region. Right) Comparison of χ_c obtained at zero magnetic field with Bethe ansatz (dashed lines) and analytical calculations (solid lines). χ_c^1 is the leading contribution Eq. (2.45), while χ_c^2 the corrected version Eq. (4.2). These two functions diverge for $\varepsilon_d = 0$, where the Coulomb peak appears and the perturbation approach to derive Eqs. (2.45) and (4.2) breaks down.

4.1.2 Preliminary considerations on C_0 and R_q

From the numerical calculation of the charge occupation and magnetization of the quantum dot in Fig. 2.7, the susceptibilities χ_c and χ_m are readily obtained, see Fig. 4.2. Considering Eq. (2.70) for the charge relaxation resistance, the presence of a peak along T_K for χ_m, in a region in which χ_c is almost constant, is responsible for the giant charge relaxation resistance, discussed in detail in Section 4.4.1. Otherwise the two quantities have the same behavior for large magnetic fields along the $H = 2\varepsilon_d$ line. Looking at Eq. (2.70), this feature gives a hint of the asymptotic behavior of $R_q = h/2e^2$, to be discussed in detail in Section 4.4.3.

We recall here Eq. (1.39), stating that the differential capacitance C_0 coincides with $e^2\chi_c$. The numerical calculation by Bethe ansatz and the analytical expression Eq. (4.2) of the charge susceptibility χ_c allow us to study the differential capacitance in the Anderson quantum RC circuit. We focus especially on the insensitivity of χ_c to the magnetic field in the region of appearance of the Kondo peak of χ_m. This is proven in Fig. 4.3, where χ_c is plotted as a function of the orbital energy ε_d for different magnetic fields. χ_c displays a Coulomb peak for $\varepsilon_d^* = 0$ which starts moving following the line $H = 2\varepsilon_d$. At large fields and asymmetries (H and $2\varepsilon_d \gg H_1$), χ_c assumes the Lorentzian shape Eq. (4.62), that we shall obtain

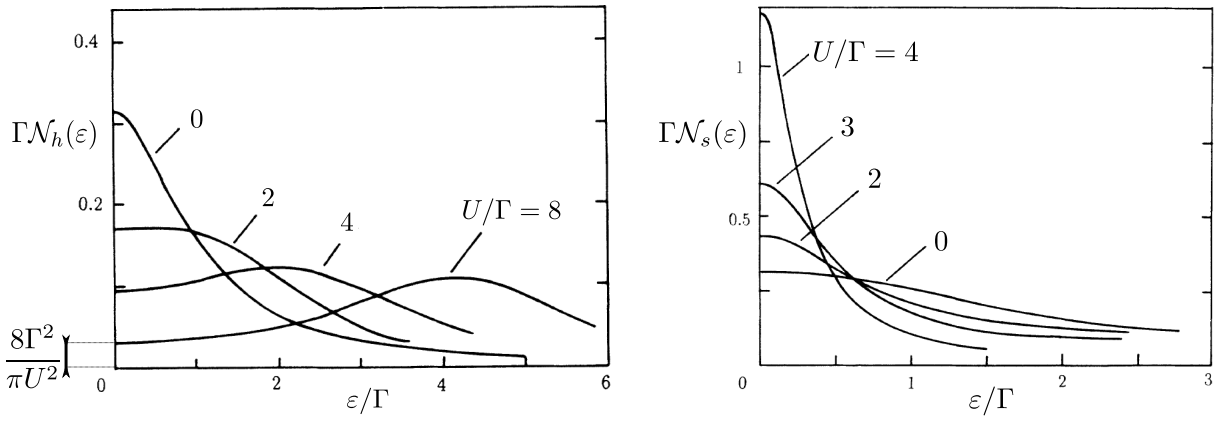

Figure 4.4: Left) Density of states of local holons on the dot $\mathcal{N}_h(\varepsilon)$. ε is the excitation energy. A Coulomb peak emerges increasing the interaction parameter U/Γ and vanishes at zero energy as $8\Gamma/\pi U^2$. This quantity is the same as χ_c [141], which is plotted in Fig. 4.3. Right) Density of states of local spinons $\mathcal{N}_s(\varepsilon)$. It behaves as the holonic one for $U/\Gamma = 0$ and develops the Abrikosov-Suhl resonance at zero energy, the signature of the formation of the strongly correlated Kondo singlet state.

by a direct perturbative calculation in Section 4.4.3. A comparison with the analytical formula Eq. (4.2), valid in the single charge region, is also plotted in Fig. 4.3. We notice that the next-to-leading order corrections are important in the Kondo regime to obtain a quantitative agreement. The divergence of Eq. (4.2) at $\varepsilon_d = 0$ signals the transition to the empty orbital regime.

4.1.2.1 The differential capacitance C_0 is proportional to the *charge* density of states

In Chapter 1, in the case of weak electron-electron interactions on the dot, we gave the interpretation of the quantum capacitance C_q as the contribution, in series with the geometrical C_g, caused by the fermionic statistics of electrons. We also showed that C_q, in the absence of interactions, is proportional to the local density of states of the dot and so the differential capacitance C_0. The spin/charge separation arising in the Anderson model has deep consequences on the physical interpretation of the differential capacitance in strongly interacting systems. We recall that charge and spin on the dot are carried by different dressed particles, called holons and spinons respectively. We report in Fig. 4.4 the density of states of these excitations in the particle-hole symmetric case $\varepsilon_d = -U/2$. In the absence of interactions ($U/\Gamma = 0$) they have the same shape, but their behavior becomes considerably different with the increasing of the interaction parameter U/Γ. Both develop well pronounced peaks but for different excitation energies, signaling the appearance of separated charge and spin states. In the case of the holons, the excited charge state appears for energies close to

$\varepsilon = U/2$, exactly the energy required to change the charge on the dot at particle-hole symmetry. In Ref. [141], it is shown that the density of states of the holons is equal to the static charge susceptibility χ_c, giving then the differential capacitance C_0. At particle-hole symmetry, this quantity scales to zero as $8\Gamma/\pi U^2$, see Eq. (4.2). This in striking contrast to what happens for the spinon density of states: a huge peak appears at zero energy as a signature of the strongly correlated Kondo singlet. It is called the Abrikosov-Suhl resonance [142]. The differential capacitance C_0 is completely insensitive to this peak, which strongly affects the *total* density of states on the dot.

4.2 Kondo physics in the Anderson model

In this section we illustrate a renormalization group analysis of the Anderson model. We discuss the reason for the failure of perturbative approaches in the Kondo regime within a renormalization group framework and its solution with a Fermi liquid theory. As for the Coulomb blockade model, the introduction of slave-states provides a platform to perform systematic perturbative computations. We adopt Barnes' formulation of the Anderson Hamiltonian [143]: slave-bosons and para-fermions are introduced to describe the Hilbert space of the quantum dot. For a single electron on the dot, the high energy sectors, corresponding to zero and two charges on the dot, can be integrated, which gives a rigorous mapping of the Anderson model onto the Kondo Hamiltonian.

4.2.1 Path integral approach with slave states and link to the Schrieffer-Wolff transformation

In Fig. 4.5, the basis introduced by Barnes is illustrated. The states describing a single spin σ electron on the dot are created by *para-fermion* operators $f_\sigma^\dagger$ acting on a new vacuum called $|0\rangle_\lambda$. The empty and doubly occupied states of the quantum dot orbital are created by slave-boson operators $b_0^\dagger$ and $b_2^\dagger$ respectively. The original quantum dot operators d_σ can then be expressed as a function of these new operators

$$d_\sigma = b_0^\dagger f_\sigma + \sigma f_{-\sigma}^\dagger b_2 \,. \tag{4.10}$$

The factor σ is necessary to respect the fermionic commutation relations of the original quantum dot operators d_σ. The action corresponding to this new representation is readily

obtained

$$S_{\mathrm{AM}} = -\sum_{i\omega_n k\sigma} c^\dagger_{k\sigma}(i\omega_n) G^{-1}_{k\sigma}(i\omega_n) c_{k\sigma}(i\omega_n) - \sum_{i\omega_n \sigma} f^\dagger_\sigma(i\omega_n) F^{-1}_\sigma(i\omega_n) f_\sigma(i\omega_n)$$
$$- \sum_{i\nu_n} \left(b^\dagger_0(i\nu_n) F^{-1}_0(i\nu_n) b_0(i\nu_n) + b^\dagger_2(i\nu_n) F^{-1}_2(i\nu_n) b_2(i\nu_n) \right)$$
$$+ \frac{t}{\sqrt{\beta}} \sum_{\substack{i\omega_n i\nu_n \\ k\sigma}} \left(c^\dagger_{k\sigma}(i\omega_n) b^\dagger_0(i\nu_n) f_\sigma(i\nu_n + i\omega_n) + \sigma c^\dagger_{k\sigma}(i\omega_n) f^\dagger_{-\sigma}(i\nu_n - i\omega_n) b_2(i\nu_n) + \mathrm{c.c.} \right), \quad (4.11)$$

with the free propagators

$$G^{-1}_{k\sigma}(i\omega_n) = i\omega_n - \varepsilon_k, \quad (4.12a)$$
$$F^{-1}_\sigma(i\omega_n) = i\omega_n - \lambda, \quad (4.12b)$$
$$F^{-1}_0(i\nu_n) = i\nu_n + \varepsilon_d - \lambda, \quad (4.12c)$$
$$F^{-1}_2(i\nu_n) = i\nu_n - \varepsilon_d - U - \lambda. \quad (4.12d)$$

Notice that the para-energy λ has been inserted to perform Abrikosov's projection, discussed in Section 3.1. It eliminates unphysical states like, for instance, $f^\dagger_\sigma f^\dagger_{-\sigma}|0\rangle_\lambda$. All the energies of the dot slave-states have been shifted by $-\varepsilon_d$ for practical purposes. For $-U \ll \varepsilon_d \ll 0$, one charge is fixed on the dot and the quadratic form of the action Eq. (4.11) allows for the exact integration of the high energy charge sectors associated to the slave-boson fields b_0 and b_2. A mapping onto a Kondo action plus a potential scattering term is obtained

$$S'_{\mathrm{AM}} = -\sum_{i\omega_n k\sigma} c^\dagger_{k\sigma}(i\omega_n) G^{-1}_{k\sigma}(i\omega_n) c_{k\sigma}(i\omega_n) - \sum_{i\omega_n \sigma} f^\dagger_\sigma(i\omega_n) F^{-1}_\sigma(i\omega_n) f_\sigma(i\omega_n) +$$
$$\frac{1}{\beta} \sum_{\substack{kk'\sigma\sigma'\tau\tau' \\ i\omega_1 i\omega_2 i\nu_n}} \left[\mathscr{J} \mathbf{S}_{\tau\tau'} \cdot \mathbf{s}_{\sigma\sigma'} + \mathscr{W} \delta_{\sigma\sigma'} \delta_{\tau\tau'} \right] c^\dagger_{k\sigma}(i\omega_1) c_{k'\sigma'}(i\omega_2) f^\dagger_\tau(i\nu_n + i\omega_2) f_{\tau'}(i\nu_n + i\omega_1), \quad (4.13)$$

Energy		1st quantization	2nd quantization	Barnes' representation
$2\varepsilon_d + U$		$\|2\rangle$	$d^\dagger_\uparrow d^\dagger_\downarrow \|0\rangle$	$b^\dagger_2 \|0\rangle_\lambda$
ε_d		$\|1,\sigma\rangle$	$d^\dagger_\sigma \|0\rangle$	$f^\dagger_\sigma \|0\rangle_\lambda$
0		$\|0\rangle$	$\|0\rangle$	$b^\dagger_0 \|0\rangle_\lambda$

Figure 4.5: Different representations of the Hilbert space of the quantum dot. The energies are given for an isolated dot.

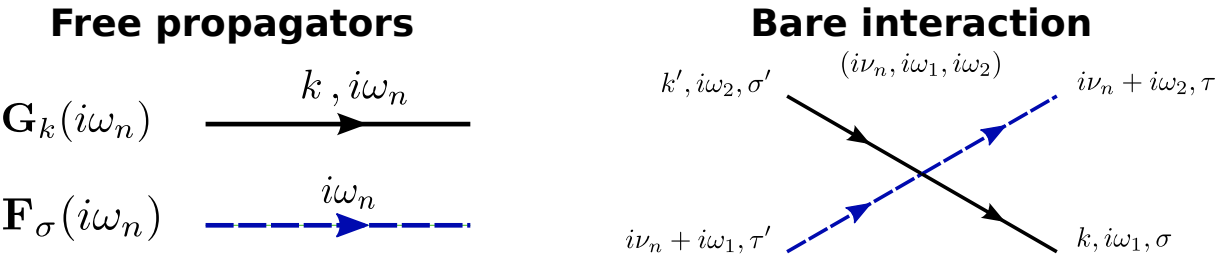

Figure 4.6: Diagrammatic structure of the Anderson model. The arrow pointing to the center of the vertex gives the values of the Matsubara frequencies in Eqs. (4.14) *and* (4.15).

with

$$\mathscr{J} = -2t^2\left[F_2(i\nu_n + i\omega_1 + i\omega_2) + F_0(i\nu_n)\right], \tag{4.14}$$

$$\mathscr{W} = \frac{t^2}{2}\left[F_2(i\nu_n + i\omega_1 + i\omega_2) - F_0(i\nu_n)\right]. \tag{4.15}$$

The diagrammatic structure of the theory is pictured in Fig. 4.6. Recalling the discussion of Section 3.3, to leading order in t, it is possible to discard the frequency dependence of the couplings and the results of the Schrieffer-Wolff transformation Eqs. (2.37), (2.38) and (2.39) are readily obtained. The poles of the free propagators Eqs. (4.12a) and (4.12b) define the low energy fixed point to the leading order. Performing the substitutions $i\omega_{1,2} \to 0$ and $i\nu_n \to \lambda$, Eqs. (4.14) and (4.15) recover Eqs. (2.38) and (2.39). Before repeating the steps performed for the vertex calculations for the Coulomb blockade Hamiltonian in Section 3.4, the problems raised by the anti-ferromagnetic Kondo coupling in Eq. (4.13) deserve a separate discussion.

4.2.2 The failure of a perturbative approach

The perturbative calculations in J leading to Eq. (4.6) have been carried out taking as unperturbed ground state a spin **S** on the dot disconnected from the lead electrons. The divergence at low energies of Eq. (4.6) reveals that the real ground state is considerably different from it. The spin-exchange interaction in Eq. (4.5) correlates an infinite number of degrees of freedom in the lead with the spin on the dot. This is a signature of the emergence at low energy of strong Kondo correlations. This could seem in contradiction with the scaling analysis presented in Section 3.3, classifying both the potential scattering and the spin-exchange coupling as marginal interactions and then not really critical for the low energy physics. Indeed, we did not specify that the scaling analysis actually describes the renormalization flow of operators only to leading order (0-loop). Next-to-leading order corrections must be taken into account to fully determine the behavior of marginal operators. Abrikosov [122, 123] was the

first to introduce para-fermion states for the path-integral description of the Kondo model

$$S_{\rm K} = \int_0^\beta d\tau \left\{ \sum_{k\sigma} c^\dagger_{k\sigma}(\partial_\tau + \varepsilon_k) c_{k\sigma} + \sum_\sigma f^\dagger_\sigma (\partial_\tau + \lambda) f_\sigma + J \sum_{\substack{\sigma\sigma'\tau\tau' \\ kk'}} \left(c^\dagger_{k\sigma} \mathbf{s}_{\sigma\sigma'} c_{k'\sigma'} \right) \cdot \left(f^\dagger_\tau \mathbf{S}_{\tau\tau'} f_{\tau'} \right) \right\} \quad (4.16)$$

and calculate the next-to-leading corrections to the vertex function, defined in a similar way as in Eq. (3.28),

$$\mathcal{V}^\Lambda_{\sigma\sigma',\tau\tau'}(k, i\omega_1, i\Omega_1; k' i\omega_2, i\Omega_2) = -\beta \frac{\langle c_{k\sigma}(i\omega_1) f_\tau(i\Omega_1) f^\dagger_{\tau'}(i\Omega_2) c^\dagger_{k'\sigma'}(i\omega_2)\rangle \Big|_c}{G_k(i\omega_1) G_{k'}(i\omega_2) F_\tau(i\Omega_1) F_{\tau'}(i\Omega_2)} . \quad (4.17)$$

This reads

$$\mathcal{V}^\Lambda_J = \mathbf{S}_{\tau\tau'} \cdot \mathbf{s}_{\sigma\sigma'} \left(J - \frac{\nu_0 J^2}{2} \ln \frac{\Lambda}{D} + \ldots \right) \quad (4.18)$$

and diverges logarithmically for $\Lambda \to 0$. The anti-ferromagnetic coupling of the Kondo Hamiltonian, even if marginal according to the scaling analysis, increases logarithmically lowering the running scale energy. The spin-exchange coupling is then a *marginally relevant* contribution, that strongly affects the low energy quasi-particles of the system. We mention that this is also the case for the BCS pairing, leading to superconductivity [131].

4.2.3 A Fermi liquid theory for the Kondo Hamiltonian

The proof of the Fermi liquid behavior at low energy for the Kondo Hamiltonian has required a huge effort and has been definitively demonstrated with the numerical renormalization group devised by Wilson. The interested reader can find a comprehensive review in Refs. [61, 109]. A more intuitive explanation of his conclusions is given by the following argument by Nozières [95, 144]. A spatial representation of the Kondo problem is pictured in Fig. 4.7 and it is described by the Hamiltonian

$$H = t \sum_{i=0,\sigma}^{\infty} c^\dagger_{i,\sigma} c_{i+1,\sigma} + J \sum_{\sigma\sigma'} \mathbf{S} \cdot \left(c^\dagger_{0\sigma} \mathbf{s}_{\sigma\sigma'} c_{0\sigma'} \right) , \quad (4.19)$$

with t the hopping constant and a the lattice spacing. Only electrons adjacent to the impurity interact with the spin of the quantum dot. At half-filling, the asymptotic behavior of the wave-function for low energy electrons far from the dot is $\psi(x) \propto \sin(k_F x)$, with $k_F = \pi/2a$. The wave-function has to vanish at the boundary of the chain $x = 0$, defined by the quantum dot site. The discussion of the previous section predicts that a *strong coupling regime* appears for energies $\Lambda \sim T_K$ and the effective coupling $\mathcal{V}^\Lambda_J$ cannot be treated perturbatively anymore. This situation is described by taking $J = \infty$ in Eq. (4.19). Minimizing the anti-ferromagnetic

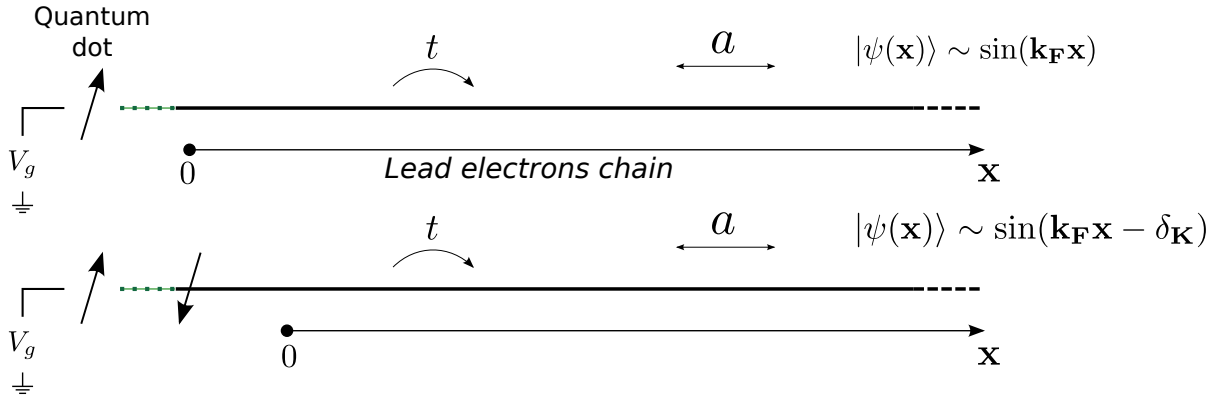

Figure 4.7: Spatial representation of the Kondo problem in the quantum RC circuit. In the strong coupling limit, the adjacent electron to the quantum dot screens its spin preserving the Fermi liquid behavior at long distance of the quasi-particles, phase-shifted by $\delta_K = \pi/2$.

coupling requires just one conduction electron in $x = 0$ with a spin opposite to that of the electron in the quantum dot. An electron is then trapped close to the dot to screen its spin, which becomes invisible to the others electrons in the one-dimensional chain. This situation is pictured in the lower part of Fig. 4.7 and it is equivalent to eliminate one site from the lead electron chain. Here, the lead electron wave-function has to vanish in $x = a$ instead of $x = 0$, what implies a phase-shift of the lead electrons by $\delta_K = \pi/2$. This is exactly the Kondo phase-shift previously derived by symmetry considerations in Section 2.2.2. This discussion points out that the wave-function of the lead electrons remains that of free quasi-particles, justifying the Fermi liquid behavior at low energy.

4.2.4 Cragg & Lloyd's argument for the potential scattering correction

How this kind of considerations is affected by the presence of a potential scattering term, breaking particle-hole symmetry, was addressed by Cragg and Lloyd [104, 105, 106]. They realized the additivity of the Kondo phase-shift δ_K with the phase-shift caused by potential scattering, summarized by Eq. (2.41). What is remarkable about this relation is that the two phase-shifts can be calculated independently. The strong Kondo coupling limit for the low energy quasi-particles forces δ_K to equal $\pi/2$, regardless of the value of the spin-exchange coupling J. This is a manifestation of the universality of the Kondo problem. The potential scattering term in Eq. (2.37) can be diagonalized by defining new operators [145, 146]

$$q^\dagger_{k\sigma} = c^\dagger_{k\sigma} + \sum_{k'} c^\dagger_{k'\sigma} \frac{\langle k'|T_W|k\rangle}{k - k' + i0^+}, \tag{4.20}$$

leading to

$$H = \sum_{k\sigma} \varepsilon_k q^\dagger_{k\sigma} q_{k\sigma} + \sum_{kk'\sigma\sigma'} J_{kk'} \mathbf{S} \cdot \left(q^\dagger_{k\sigma} \mathbf{s}_{\sigma\sigma'} q_{k'\sigma'} \right), \tag{4.21}$$

with

$$J_{kk'} = J |\Gamma(k)|^2 , \tag{4.22}$$

$$\Gamma(k) = \sum_k \left[\delta(k-k') + \frac{\langle k'|T_W|k\rangle}{k-k'+i0^+} \right] . \tag{4.23}$$

T_W is the T-matrix associated to the potential scattering interaction, see Appendix C. As the low energy theory is that of a Fermi liquid, some quasi-particle operators $a^\dagger_{k\sigma}$ must exist to fully diagonalize Eq. (2.37) and not only the potential scattering term. A transformation like Eq. (4.20) should apply with the whole T-matrix T instead of T_W

$$a^\dagger_{k\sigma} = c^\dagger_{k\sigma} + \sum_{k'} c^\dagger_{k'\sigma} \frac{\langle k'|T|k\rangle}{k-k'+i0^+} , \tag{4.24}$$

leading to a full diagonal Fermi liquid Hamiltonian like Eq. (2.9)

$$H' = \sum_{k\sigma} \varepsilon_k a^\dagger_{k\sigma} a_{k'\sigma} . \tag{4.25}$$

At the same time, also Eq. (4.21) is diagonalized by an analog transformation

$$a^\dagger_{k\sigma} = q^\dagger_{k\sigma} + \sum_{k'} q^\dagger_{k'\sigma} \frac{\langle k'|T_J|k\rangle}{k-k'+i0^+} , \tag{4.26}$$

involving T_J, the T-matrix associated to the spin-exchange interaction in Eq. (4.21). Eqs. (4.20), (4.24) and (4.26) lead to the following relation [106]

$$\langle k|T|k\rangle = \langle k|T_W|k\rangle + \langle k|T_J|k\rangle - 2\pi i \langle k|T_W|k\rangle \langle k|T_J|k\rangle . \tag{4.27}$$

Applying Eq. (C.9) the additivity of the phase-shifts δ_K and δ_W claimed in Eq. (2.41) is readily checked and has been verified with numerical renormalization group calculations [104]. The contribution to the total phase-shift given by the potential scattering term is non-universal and gives the corrections to the charge occupation of the quantum dot out of particle-hole symmetry thanks to the Friedel sum rule, as we show in the following discussion.

4.3 Calculation of the vertex in the Anderson model

The steps required for the calculation of the renormalized vertex to fourth order in t in the Anderson model recover those carried in Section 3.4 for the Coulomb blockade model. There

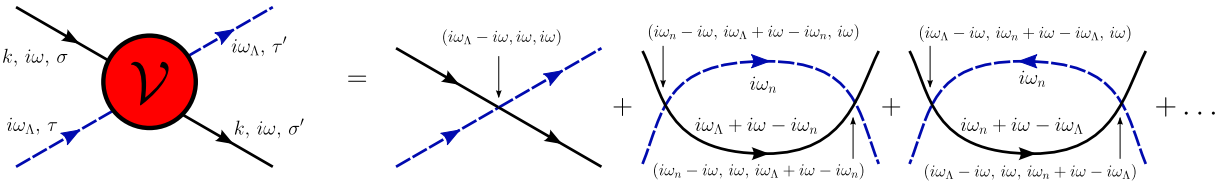

Figure 4.8: Diagrammatic series for the vertex function Eq. (4.17).

are essentially two differences. The first one is that the limit $\Lambda \to 0$ cannot be carried out for $\mathcal{V}_J^R$ in Eq. (4.3) because of the appearance of infra-red logarithmic divergencies. The second one is that less diagrams have to be calculated because of the smaller number of vertices associated to the action Eq. (4.13), see Fig. 4.6 and Fig. 4.8.

In a similar way as in Section 3.4, the expression of the full para-fermion propagator can be written with the help of a Dyson equation

$$\mathscr{F}_\sigma(i\omega_n) = -\langle f_\sigma(i\omega_n) f_\sigma^\dagger(i\omega_n)\rangle = \frac{\mathcal{Z}_0}{i\omega_n - \Sigma(i\omega_n)}\,. \tag{4.28}$$

The self-energy is given, to leading order, by the one-loop diagram in Fig. 4.9, whose corresponding expression is

$$\begin{aligned}\Sigma(i\omega_n) &= \frac{2}{\beta}\sum_{k,i\Omega_n} G_k(i\Omega_n)\mathscr{W}(i\omega_n - i\Omega_n, i\Omega_n, i\Omega_n) \\ &= t^2\sum_k\left[\frac{f(\varepsilon_k)+b(\varepsilon_d+U+\lambda)}{i\omega_n+\varepsilon_k-\varepsilon_d-U-\lambda} - \frac{f(\varepsilon_k)+b(-\lambda+\varepsilon_d)}{i\omega_n-\varepsilon_k-\lambda+\varepsilon_d s}\right].\end{aligned} \tag{4.29}$$

Notice that the spin-exchange part of the interaction in Eq. (4.13) does not give any contribution to the self-energy. This is a direct consequence of the antisymmetric properties of the SU(2) Pauli matrices, whose trace is zero. The limit $\lambda \to \infty$ can be taken with the continuum limit for the summation over momenta with a sharp cutoff D_0

$$\Sigma(i\omega_n) = \frac{\Gamma}{\pi}\left[\ln\frac{\varepsilon_d+U+\lambda-i\omega_n}{D_0} + \ln\frac{\lambda-\varepsilon_d-i\omega_n}{D_0}\right]. \tag{4.30}$$

The self-energy is logarithmically divergent in the cutoff D_0, which must be adopted in intermediate calculations, but it can be sent safely to infinity when computing observables. The corrections to the para-fermion pole and its quasi-particle weight are readily found

$$\tilde{\varepsilon}_d = \lambda + \frac{\Gamma}{\pi}\left(\ln\frac{\varepsilon_d+U}{D_0} + \ln\frac{-\varepsilon_d}{D_0}\right), \tag{4.31}$$

$$\mathcal{Z}_0 = 1 - \frac{\Gamma}{\pi}\left(\frac{1}{\varepsilon_d+U} - \frac{1}{\varepsilon_d}\right) = 1 - \frac{\nu_0}{2}J_0\,. \tag{4.32}$$

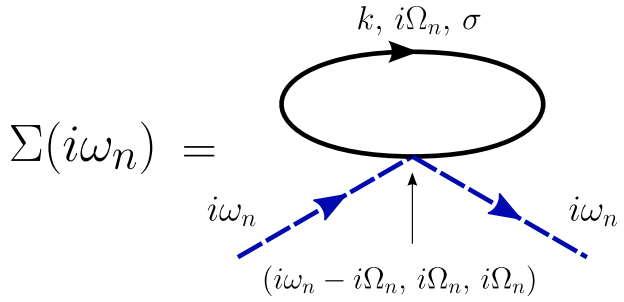

Figure 4.9: One-loop contribution to the self-energy of the para-fermions.

J_0 is the spin-exchange coupling obtained within the Schrieffer-Wolff transformation [99] in Eq. (2.38). We recall that the Kondo regime in the Anderson model requires $-U < \varepsilon_d < 0$, implying that the arguments of the logarithms in Eq. (4.31) are positive. Notice also that the quasi-particle weight, differently than in the Coulomb blockade model, does not diverge in the $D_0 \to \infty$ limit. The diagrammatic series for the four-point vertex function Eq. (4.17) is illustrated in Fig. 4.8. The renormalized vertex, defined as in Eq. (3.41), can then be written as the sum of four contribution $\mathcal{V}^R = \mathcal{Z}_0 \mathcal{V} = \mathcal{V}_1 + \mathcal{V}_Z + \mathcal{V}^a + \mathcal{V}^b$. $\mathcal{V}_1$ is given by the leading contributions in Fig. 4.8 and it can be put into the form

$$\mathcal{V}_1 = \mathbf{S}\cdot\mathbf{s} J_0 + \mathbb{1} W_0 , \tag{4.33}$$

with J_0 and W_0 given by the Schrieffer-Wolff transformation, Eqs. (2.38) and (2.39). The corrections to this contribution given by the renormalized pole, Eq. (4.31), and the quasi-particle weight, Eq. (4.32), are collected in $\mathcal{V}_Z$, namely

$$\mathcal{V}_Z = \mathbf{S}\cdot\mathbf{s}\left[\nu_0\left(\frac{J_0^2}{4}+4W_0^2\right)\left(\ln\frac{-\varepsilon_d(\varepsilon_d+U)}{D_0^2}\right)-\frac{\nu_0 J_0^2}{2}\right]+\mathbb{1}\frac{\nu_0 J_0 W_0}{2}\left[\ln\frac{-\varepsilon_d(\varepsilon_d+U)}{D_0^2}-1\right]. \tag{4.34}$$

The contributions $\mathcal{V}^a$ and $\mathcal{V}^b$ correspond to the two last diagrams in Fig. 4.8. Only the calculation of $\mathcal{V}^a$ needs to be illustrated, that of $\mathcal{V}^b$ being similar:

$$\begin{aligned}\mathcal{V}^a = -\frac{1}{\beta}\sum_{k,i\omega_n} & F_\sigma(i\omega_n)G_k(i\omega_\Lambda + i\omega - i\omega_n)\times \\ & \left[\mathbf{S}_{\beta\tau}\cdot\mathbf{s}_{\alpha\sigma}\mathcal{J}_{i\omega_n - i\omega, i\omega_\Lambda + i\omega - i\omega_n, i\omega} + \delta_{\beta\tau}\delta_{\alpha\sigma}\mathcal{W}_{i\omega_n - i\omega, i\omega_\Lambda + i\omega - i\omega_n, i\omega}\right]\times \\ & \left[\mathbf{S}_{\tau'\beta}\cdot\mathbf{s}_{\sigma'\alpha}\mathcal{J}_{i\omega_n - i\omega, i\omega, i\omega_\Lambda + i\omega - i\omega_n} + \delta_{\beta\tau'}\delta_{\alpha\sigma'}\mathcal{W}_{i\omega_n - i\omega, i\omega, i\omega_\Lambda + i\omega - i\omega_n}\right].\end{aligned} \tag{4.35}$$

Applying Eq. (E.6), for $N = 2$, the relation

$$\left(\mathbf{S}_{\beta\tau}\cdot\mathbf{s}_{\alpha\sigma}\right)\left(\mathbf{S}_{\tau'\beta}\cdot\mathbf{s}_{\sigma'\alpha}\right) = -\frac{1}{2}\mathbf{S}_{\tau'\tau}\cdot\mathbf{s}_{\sigma'\sigma} + \frac{3}{16}\delta_{\tau\tau'}\delta_{\sigma\sigma'}, \tag{4.36}$$

allows one to readily cast $\mathcal{V}^a$ in the form of Eq. (4.3), with

$$\mathcal{V}_J^a = 4\frac{t^4}{\beta}\sum_{k,i\omega_n} F(i\omega_n)G_k(i\omega_\Lambda + i\omega - i\omega_n)\times \\ \left[F_2^2(i\omega_\Lambda + i\omega) + F_2(i\omega_\Lambda + i\omega)F_0(i\omega_n - i\omega)\right], \quad (4.37)$$

$$\mathcal{V}_W^a = -\frac{t^4}{\beta}\sum_{k,i\omega_n} F(i\omega_n)G_k(i\omega_\Lambda + i\omega - i\omega_n)\times \\ \left[F_0^2(i\omega_n - i\omega) + F_2^2(i\omega_\Lambda + i\omega) + F_0(i\omega_n - i\omega)F_2(i\omega_\Lambda + i\omega)\right]. \quad (4.38)$$

The Matsubara sums are carried out as in the previous chapter. Here we notice that logarithmic divergences prevent to perform the limit $\Lambda \to 0$. These divergences are circumvented by performing integrals over momenta within the interval $\Lambda < |\varepsilon| < D_0$. This is equivalent to modify the analytical continuations of the external frequencies in the diagrams, following Solyom [124]

$$\begin{aligned} i\omega_\Lambda &\to \tilde{\varepsilon}_d - \Lambda, \\ i\omega &\to 0. \end{aligned} \quad (4.39)$$

The result reads

$$\mathcal{V}_J^a = -4\nu_0 t^4\left[\frac{1}{(\varepsilon_d+U)^2}\ln\frac{\Lambda}{D_0} + \frac{1}{\varepsilon_d(\varepsilon_d+U)}\left(\ln\frac{-\varepsilon_d}{D_0} - \ln\frac{\Lambda}{D_0}\right)\right], \quad (4.40a)$$

$$\mathcal{V}_W^a = \nu_0 t^4\left[\frac{1}{\varepsilon_d^2}\left(1 - \ln\frac{-\varepsilon_d}{D_0} + \ln\frac{\Lambda}{D_0}\right) + \frac{1}{\varepsilon_d(\varepsilon_d+U)}\left(\ln\frac{-\varepsilon_d}{D_0} - \ln\frac{\Lambda}{D_0}\right) + \frac{1}{(\varepsilon_d+U)^2}\ln\frac{\Lambda}{D_0}\right]. \quad (4.40b)$$

The same kind of considerations can be carried for $\mathcal{V}^b$, reading

$$\mathcal{V}^b = -\frac{1}{\beta}\sum_{k,i\omega_n} F_\sigma(i\omega_n)G_k(i\omega_n + i\omega - i\omega_\Lambda)\times \\ \left[\mathbf{S}_{\tau'\beta}\cdot\mathbf{s}_{\alpha\sigma}\mathcal{J}_{i\omega_\Lambda - i\omega, i\omega_n + i\omega - i\omega_\Lambda, i\omega} + \delta_{\beta\tau'}\delta_{\alpha\sigma}\mathcal{W}_{i\omega_\Lambda - i\omega, i\omega_n + i\omega - i\omega_\Lambda, i\omega}\right]\times \\ \left[\mathbf{S}_{\beta\tau}\cdot\mathbf{s}_{\sigma'\alpha}\mathcal{J}_{i\omega_\Lambda - i\omega, i\omega, i\omega_n + i\omega - i\omega_\Lambda} + \delta_{\beta\tau}\delta_{\alpha\sigma'}\mathcal{W}_{i\omega_\Lambda - i\omega, i\omega, i\omega_n + i\omega - i\omega_\Lambda}\right]. \quad (4.41)$$

The relation dual to Eq. (4.36)

$$\left(\mathbf{S}_{\tau'\beta}\cdot\mathbf{s}_{\alpha\sigma}\right)\left(\mathbf{S}_{\beta\tau}\cdot\mathbf{s}_{\alpha\sigma'}\right) = +\frac{1}{2}\mathbf{S}_{\tau'\tau}\cdot\mathbf{s}_{\sigma'\sigma} + \frac{3}{16}\delta_{\tau\tau'}\delta_{\sigma\sigma'}, \quad (4.42)$$

is applied to obtain the final result in the form of Eq. (4.3), with

$$\mathcal{V}_J^b = -4\nu_0 t^4 \left[\frac{1}{\varepsilon_d^2} \ln \frac{\Lambda}{D_0} + \frac{1}{\varepsilon_d(\varepsilon_d+U)} \left(\ln \frac{\varepsilon_d+U}{D_0} - \ln \frac{\Lambda}{D_0} \right) \right], \tag{4.43a}$$

$$\mathcal{V}_W^b = -\nu_0 t^4 \left[\frac{1}{(\varepsilon_d+U)^2} \left(1 + \ln \frac{\Lambda}{D_0} - \ln \frac{\varepsilon_d+U}{D_0} \right) + \frac{1}{\varepsilon_d(\varepsilon_d+U)} \left(\ln \frac{\varepsilon_d+U}{D_0} - \ln \frac{\Lambda}{D_0} \right) + \frac{1}{\varepsilon_d^2} \ln \frac{\Lambda}{D_0} \right]. \tag{4.43b}$$

The summation of all the contributions from Eqs. (4.33), (4.34), (4.40) and (4.43) leads to the final result

$$\mathcal{V}_J^R = J_0 - \frac{\nu_0}{2} J_0^2 - \nu_0 J_0^2 \ln \left(\frac{\Lambda}{\sqrt{-\varepsilon_d(\varepsilon_d+U)}} \right), \tag{4.44a}$$

$$\mathcal{V}_W^R = W_0 + \frac{\nu_0}{2} J_0 W_0 + \frac{\nu_0}{8} J_0^2 \ln \left(\frac{\varepsilon_d+U}{-\varepsilon_d} \right). \tag{4.44b}$$

Notice that the UV cutoff D_0 is absent from these equations and can be sent to infinity. The potential scattering contribution Eq. (4.44b) becomes zero for $\varepsilon_d = -U/2$, according to particle-hole symmetry. Moreover, the invariance property of the theory to transformations like Eqs. (2.83) is not valid anymore for both Eqs. (4.44a) and (4.44b). In the Anderson model, the choice of the couple (J, D) is not arbitrary and physically meaningless, as in the case of a pure Kondo model, see Section 2.6.1.

4.3.1 Kondo temperature and agreement with the Friedel sum rule

The calculation of the spin-exchange contribution Eq. (4.44a) provides an alternative way to obtain the Kondo temperature for the Anderson model. This was first obtained by Haldane [93, 111], by calculating the magnetic susceptibility for the Anderson model and matching it with Eq. (4.7). The resulting expression for the Kondo temperature was found to be

$$T_K = \frac{e^{\frac{1}{4}+C}}{2\pi} \sqrt{\frac{2\Gamma U}{\pi}} e^{\frac{\pi\varepsilon_d(\varepsilon_d+U)}{2U\Gamma}}. \tag{4.45}$$

This same result can be obtained by matching Eq. (4.44a) to the corresponding expression Eq. (4.18) for a pure Kondo model. Choosing arbitrarily the high energy cutoff

$$\mathscr{D} = \sqrt{-\varepsilon_d(\varepsilon_d+U)}, \tag{4.46}$$

we obtain the corresponding value for the effective spin-exchange coupling constant $J = J_0 - (\nu_0/2)J_0^2$

$$\nu_0 J = -\frac{2\Gamma U}{\pi\varepsilon_d(\varepsilon_d+U)} - \frac{2\Gamma^2 U^2}{\pi^2\varepsilon_d^2(\varepsilon_d+U)^2}. \tag{4.47}$$

Inserting Eqs. (4.46) and (4.47) into expression Eq. (4.9), we find Eq. (4.45)[1]. In the Anderson model, the cutoff divergence is eliminated by the charging energy, a physical quantity, which acts as an effective cutoff of the theory, setting the Kondo universality class through the Kondo temperature Eq. (4.45).

A further test of the validity of our approach is obtained by verifying the compatibility of Eq. (4.44b) with the Friedel sum rule. Relying on Cragg and Lloyd's study of the Kondo problem, the Fermi liquid action Eq. (4.1) describes the low energy quasi-particles of the system. Applying the Friedel sum rule Eq. (2.20) and the additivity of the phase-sifts Eq. (2.41), one finds the charge occupation on the dot to fourth order in t

$$\langle \hat{n} \rangle = 1 - 2\nu_0 \mathcal{V}_W^R . \tag{4.48}$$

Its derivative gives the charge susceptibility Eq. (4.2). For $\varepsilon_d = -U/2$, the results coincides with Eq. (2.44) obtained from the Bethe ansatz analytical solution at particle-hole symmetry.

To summarize, Cragg and Lloyd's argument, exposed in Section 4.2.4, allows us to completely forget about the spin exchange interaction in the initial action Eq. (4.13). At zero temperature this is responsible of a $\delta_k = \pi/2$ of the low energy quasi-particles in the leads. We consider then exclusively the renormalization of the potential scattering coupling looking at the renormalized vertex. As previously done in Section 3.3 for the Coulomb blockade model, we get rid of the residual para-fermions fields f_σ by switching back to the imaginary time representation and setting the constraint $\sum_\sigma f_\sigma^\dagger f_\sigma = 1$, imposed by sending the para-energy λ to infinity. The mapping onto the effective Fermi liquid action Eq. (4.1) is eventually obtained, giving a formal proof of the approach carried out in Chapter 2.

4.4 A (giant) peak for the charge relaxation resistance

The analytical results of the preceding analysis show that the Fermi liquid action Eq. (4.1) describes the low energy quasi-particles of the Anderson quantum RC circuit and it is coherent with the Friedel sum rule. The approach illustrated in Section 2.4 then applies to calculate the charge relaxation resistance, leading in particular to Eq. (2.70). In this section, we give a comprehensive study of the behaviors predicted by Eq. (2.70) in the Kondo and in the mixed valence regime.

[1] A different choice for the cutoff $\mathscr{D}$ implies a different expression for J from Eq. (4.44a). However the combination of $\mathscr{D}$ and J always leads to the same expression for T_K given by Eq. (4.45). This is a consequence of the renormalizability of the Kondo model [123, 127].

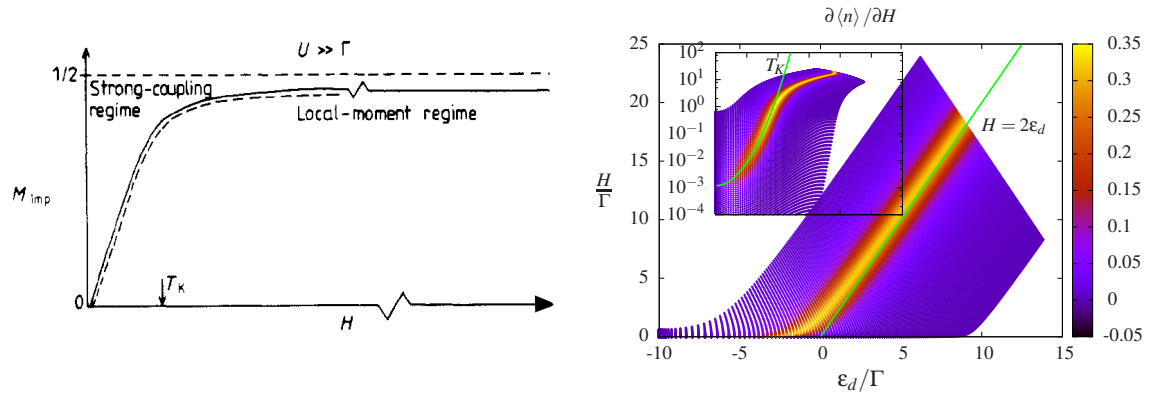

Figure 4.10: Left) Universal shape of the magnetization as a function of H from Ref. [147]. T_K sets the transition from the strong coupling (Kondo) regime to the local moment regime. Right) $\partial\langle n\rangle/\partial H$ as a function of the orbital energy ε_d and the Zeeman energy H. It has exactly the same behavior as χ_m in Fig. 4.2 and verifies Eq. (4.58).

4.4.1 The giant charge relaxation resistance in the Kondo regime

The Kondo scaling limit coincides with the symmetric limit for the Anderson model $(U/2+\varepsilon_d)/\sqrt{U\Gamma} \ll 1$ [79]. It means that the analytical solution of the charge-magneto susceptibility χ_m can be obtained from the analytical solution of the Bethe ansatz equations at particle-hole symmetry [79]. It is possible to show that all physical quantities, in particular the magnetization, are universal functions of H/T_K [147, 148]

$$\langle\hat{m}\rangle = f\left(\frac{H}{T_K}\right), \tag{4.49}$$

with T_K a function of the orbital energy ε_d given by Eq. (4.4). The magnetization is plotted in Fig. 4.10. Its asymptotic behaviors are

$$f(x) = \begin{cases} \frac{x}{\sqrt{2\pi e}} & x \ll 1 \\ \frac{1}{2} - \frac{1}{4\ln x} & x \gg 1 \end{cases}. \tag{4.50}$$

In this limit the charge-magneto susceptibility Eq. (2.71) is readily obtained. We recall that this quantity is defined as $\chi_m = -2\partial\langle\hat{m}\rangle/\partial\varepsilon_d$. Assuming the scaling form for the magnetization Eq. (4.49), this leads to

$$\chi_m = 2\frac{\partial \ln T_K}{\partial \varepsilon_d}\frac{H}{T_K}f'\left(\frac{H}{T_K}\right). \tag{4.51}$$

Substituting Eq. (4.4) for the Kondo temperature, we obtain

$$\chi_m = \frac{\pi}{\Gamma}\frac{2\varepsilon_d + U}{U}\Phi_0\left(\frac{H}{T_K}\right), \tag{4.52}$$

with $\Phi_0(x) = xf'(x)$, plotted in Fig. 2.10. Its maximum is given for $x_0 = 1.0697$ and $\Phi_0(x_0) = 0.1257$.

Switching to χ_c, assuming $U/\Gamma \gg 1$, only the leading contribution Eq. (2.45) is taken into account for the charge susceptibility Eq. (4.2). Furthermore, Fig. 4.3 shows that any dependence of χ_c on the magnetic field can be neglected in this regime. The peak of Φ_0 raises for Zeeman energies of the order of T_K, which is much smaller than Γ close to particle-hole symmetry. Together with Eq. (4.52), Eq. (2.70) for the charge relaxation resistance can be expressed in the scaling form first presented in Eq. (2.73)

$$R_q = \frac{h}{4e^2}\left[1 + \left(\frac{U}{\Gamma}\right)^4 F_0(y)\Phi_0^2\left(\frac{H}{T_K}\right)\right]. \tag{4.53}$$

The universal function of the envelope is plotted in Fig. 2.9 and reads

$$F_0(y) = \left(\frac{\pi^2}{8}\right)^2 \frac{y^2(y^2-1)^4}{(y^2+1)^2}. \tag{4.54}$$

We recall here that $y = 1 + 2\varepsilon_d/U$ is the asymmetry parameter, vanishing at particle-hole symmetry.

4.4.2 Corrections to the Kondo scaling limit: a numerical approach

The numerical solution of the Bethe ansatz equations allows one to test the relevance of the analytical scaling solution Eq. (4.53) out of the scaling limit, which is of interest to understand how quantitative it is for real systems. In Fig. 2.8, we plot the behavior of the charge relaxation resistance obtained from Eq. (2.70) by calculating numerically χ_c and χ_m from the Bethe ansatz. The results agree with numerical renormalization group calculations [76] and prove the validity of our Fermi liquid approach. To test the quantitative relevance of the analytical scaling Eq. (4.53), we extend the definition of the envelope and peak functions

$$F = \left(\frac{\Gamma}{U}\right)^4 \left(\frac{\pi y}{\Gamma\chi_c}\right)^2, \qquad \Phi = \frac{\Gamma\chi_m}{\pi y}, \tag{4.55}$$

such that they coincide with F_0 and Φ_0 in the scaling limit. F and Φ do not depend only on $y = 1+2\varepsilon_d/U$ and H/T_K respectively, but on all the energy scales of the problem U, ε_d, Γ and H.

4.4.2.1 Persistence of the peak in the function Φ

In Fig. 4.11 the comparison of the analytical scaling limit Φ_0 (also plotted in Fig. 2.10) is done with the numerical solution of the Bethe ansatz equations for different U/Γ. This numerical analysis permits to distinguish between two regimes separated by the interaction value

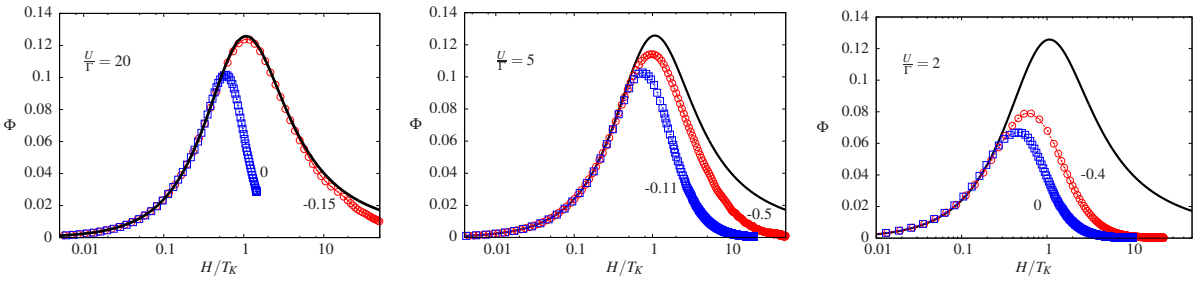

Figure 4.11: Function Φ *defined in Eq.* (4.55) *for different* ε_d/U *(squares and circles) and* U/Γ *obtained from the numerical solution of the Bethe ansatz. The results are compared with the universal scaling* Φ_0 *(solid line). The values of* T_K *for the numerical data are fixed by matching the values of* Φ *at low fields to the linear behavior of* Φ_0*. These are plotted in Fig. 4.12.*

$U/\Gamma = 5$. For $U/\Gamma > 5$, the scaling limit shows to be robust against the breaking of particle-hole symmetry. The shape of the analytical scaling limit is reproduced faithfully by numerical calculations until $\varepsilon_d \sim \Gamma$, that is when the Coulomb peaks of the differential capacitance $C_0 = e^2\chi_c$ are approached, see Fig. 4.3. A good measure of this robustness is the numerical verification of the Kondo temperature according to Eq. (4.4). The numerical definition of T_K is operated by matching the behavior of Φ at low fields with that of the analytical scaling

$$\Phi_0\left(\frac{H}{T_K}\right) = \frac{H/T_K}{\sqrt{2\pi e}}, \quad \text{for} \quad \frac{H}{T_K} \ll 1. \tag{4.56}$$

The results are illustrated in Fig. 4.12. For $U/\Gamma = 20$ the agreement is perfect. For $U/\Gamma \leq 5$, Kondo physics starts to fade out. This is manifested by the fact that the peak of the function Φ Eq. (4.55) is less pronounced than the one of the scaling limit Φ_0, even close to particle-hole symmetry. Furthermore, the quantitative disagreement with Eq. (4.4) becomes manifest.

4.4.2.2 The $\frac{\Gamma}{U}$ corrections to the envelope function F

In Fig. 4.13(a) NRG, BA and analytical calculations are compared showing a good agreement between each other. The next to leading order corrections to χ_c in Eq. (4.2) are taken into account to have quantitative agreement. In Fig. 4.13(b) the convergence of F onto the scaling limit F_0 Eq. (4.54) is illustrated, showing that a good quantitative agreement is reached only for interactions of the order $U/\Gamma \sim 100$. The analytical expression of F obtained through Eq. (4.2) converges to the BA numerical results for interactions of the order of $U/\Gamma \sim 50$, illustrating a slow convergence to the scaling limit.

This last discussion completes our analytical study of the giant charge relaxation resistance in the Kondo regime of the Anderson model.

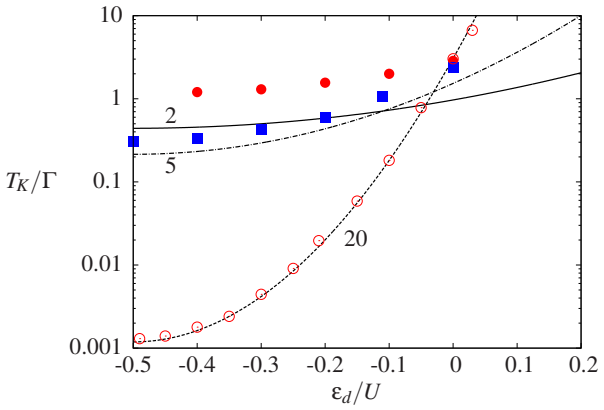

Figure 4.12: Numerical values of T_K obtained (see main text) from the BA equations for $U/\Gamma = 2$, 5 and 20 (full circles, squares and empty circles respectively). They are compared to the analytical formula Eq. (4.45) *(solid lines).*

4.4.2.3 Identity between χ_m and $\frac{\partial\langle\hat{n}\rangle}{\partial H}$

The fact that the derivatives of the average over the Hamiltonian $\langle H\rangle$ give the value of the magnetization and the charge occupation of the dot

$$\langle\hat{m}\rangle = -\frac{\partial\langle H\rangle}{\partial H} \qquad \text{and} \qquad \langle\hat{n}\rangle = \frac{\partial\langle H\rangle}{\partial\varepsilon_d} \tag{4.57}$$

implies

$$\frac{\partial\langle\hat{n}\rangle}{\partial H} = \chi_m\,. \tag{4.58}$$

This seems to be in contradiction with the fact the χ_m acquires "large" values, while $\partial\langle\hat{n}\rangle/\partial H$ should remain small because $\langle\hat{n}\rangle$ is weakly dependent on the magnetic field in the Kondo regime. This is however not the case. As previously stated, in the Kondo regime, all physical quantities, $\langle\hat{n}\rangle$ included, are universal function of H/T_K [79]

$$\langle\hat{n}\rangle = 1 + \alpha g\left(\frac{H}{T_K}\right) + \ldots \tag{4.59}$$

We assume that the function g is of order one and α has to be a small parameter in agreement with the fact that $\langle\hat{n}\rangle$ depends weakly on the magnetic field. If we take the derivative in the magnetic field and consider adimensional quantities, we obtain

$$\Gamma\frac{\partial\langle\hat{n}\rangle}{\partial H} = \frac{\Gamma}{T_K}\alpha g'\left(\frac{H}{T_K}\right). \tag{4.60}$$

Assuming that $g'(x)$ is also of order one, the small coupling α is multiplied by Γ/T_K , which is much larger than one, see Fig. 4.12. This implies that the left-hand-side of Eq. (4.58) can

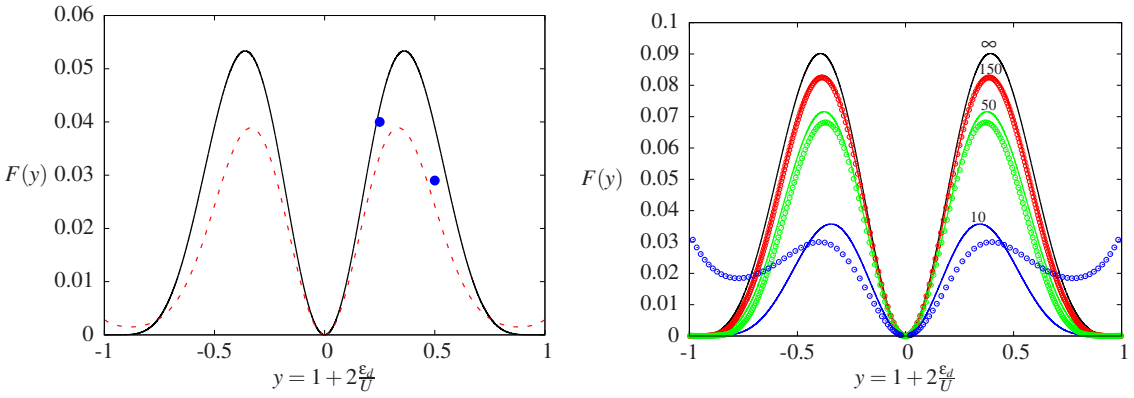

Figure 4.13: a) Comparison of NRG (points extracted from the results of Ref. [76]), BA (dashed line) and analytical (solid line) results for the function F with $U/\Gamma = 20$. b) Approach to the scaling limit F_0 Eq. (4.54) for different U/Γ. The dotted lines are obtained by BA while the solid ones correspond to the analytical result Eq. (4.2).

also acquire "large" values, accordingly to the behavior of χ_m. The numerical verification of this statement, proving Eq. (4.58) is shown in Fig. 4.10, in which $\partial\langle\hat{n}\rangle/\partial H$ displays exactly the same behavior as χ_m in Fig. 4.2.

4.4.3 Universal scaling behaviors in the valence-fluctuation regime

The scaling limit for the charge relaxation resistance Eq. (4.53) is meaningless when the Coulomb peaks of the charge are approached. In Fig. 4.11 it is shown that, for any value of the interaction strength U/Γ, the peak decreases abandoning the scaling limit Φ_0. To build an intuition of what happens to the charge relaxation resistance once the Kondo regime is left, one has to look at the phase diagram of the isolated quantum dot in Fig. 4.1. If $\varepsilon_d > 0$, a positive magnetic field drives a transition between an empty orbital $|0\rangle$ and a polarized spin in the dot $|1,\uparrow\rangle$, see Fig. 2.11. These states become resonant at $H = 2\varepsilon_d$ and the suppression of spin-exchange Kondo correlations allows for a perturbative approach. We consider the perturbation in the spin down tunneling term Eq. (2.75) to the ground state $|\psi_0\rangle$ of the resonant level Hamiltonian Eq. (2.74) confined to the spin up sector. $|\psi_0\rangle$ is characterized by the charge occupation of a resonant level model

$$\langle\hat{n}_\uparrow\rangle_0 = \langle\psi_0|\,\hat{n}\,|\psi_0\rangle = \frac{1}{2} - \frac{1}{\pi}\arctan\left(\frac{\varepsilon_d - \frac{H}{2}}{\Gamma}\right) \tag{4.61}$$

and $\langle \hat{n}_\downarrow \rangle_0 = 0$. In this case the charge and the charge-magneto susceptibilities have the same Lorentzian behavior

$$\chi_c^0 = \chi_m^0 = \chi_\uparrow^0 = \frac{\Gamma}{\pi} \frac{1}{(\varepsilon_d - H/2)^2 + \Gamma^2} . \tag{4.62}$$

Considering Eq. (2.70) this is coherent with a charge relaxation resistance quantized to $R_q = h/2e^2$, but also with the discussion about the resonant level model in Chapter 1. The Lorentzian Eq. (4.62) reproduces the behavior of the charge susceptibility for $\varepsilon_d \gg \Gamma$, as shown in Fig. 4.3. Including the spin down sector to first order in t, the corrections to the resonant level ground state $|\psi_0\rangle$ are readily obtained

$$|\psi_1\rangle = t \sum_k \left(\frac{1}{\varepsilon_k - U - \varepsilon_d - \frac{H}{2}} d_\downarrow^\dagger c_{k\downarrow} \hat{n}_\uparrow + \frac{1}{\varepsilon_k - \varepsilon_d - \frac{H}{2}} d_\downarrow^\dagger c_{k\downarrow} (1 - \hat{n}_\uparrow) \right) |\psi_0\rangle . \tag{4.63}$$

The projectors $\hat{n}_\uparrow$ and $1 - \hat{n}_\uparrow$ are necessary to determine the sectors in which $|\psi_0\rangle$ is occupied by a spin up electron or not, implying the presence/absence of the interaction energy U in the denominators. The populations $\langle \hat{n}_\sigma \rangle$ of the quantum dot are then calculated for the state $|\psi_0\rangle + |\psi_1\rangle$, leading to

$$\begin{aligned} \langle \hat{n}_\uparrow \rangle &= \langle \hat{n}_\uparrow \rangle^0 - \frac{\Gamma}{\pi} \frac{U \langle \hat{n}_\uparrow \rangle^0 (1 - \langle \hat{n}_\uparrow \rangle^0)}{(U + \varepsilon_d + \frac{H}{2})(\varepsilon_d + \frac{H}{2})} , \\ \langle \hat{n}_\downarrow \rangle &= \frac{\Gamma}{\pi} \left(\frac{1 - \langle \hat{n}_\uparrow \rangle^0}{\varepsilon_d + \frac{H}{2}} + \frac{\langle \hat{n}_\uparrow \rangle^0}{\varepsilon_d + U + \frac{H}{2}} \right) , \end{aligned} \tag{4.64}$$

corresponding to the static susceptibilities

$$\begin{aligned} \chi_\uparrow =& \chi_\uparrow^0 - \frac{\Gamma}{\pi} \frac{\chi_\uparrow^0 (1 - 2\langle \hat{n}_\uparrow \rangle^0) U}{(\varepsilon_d + U + H/2)(\varepsilon_d + H/2)} - \frac{\Gamma}{\pi} \frac{\langle \hat{n}_\uparrow \rangle^0 (1 - \langle \hat{n}_\uparrow \rangle^0)[U^2 + 2U(\varepsilon_d + H/2)]}{(\varepsilon_d + U + H/2)^2 (\varepsilon_d + H/2)^2} , \\ \chi_\downarrow =& \frac{\Gamma}{\pi} \left[\frac{1 - \langle \hat{n}_\uparrow \rangle^0}{(\varepsilon_d + \frac{H}{2})^2} + \frac{\langle \hat{n}_\uparrow \rangle^0}{(\varepsilon_d + \frac{H}{2} + U)^2} + \chi_\uparrow^0 \left(\frac{1}{\varepsilon_d + \frac{H}{2} + U} - \frac{1}{\varepsilon_d + \frac{H}{2}} \right) \right] . \end{aligned} \tag{4.65}$$

Their combination gives both $\chi_c = \chi_\uparrow + \chi_\downarrow$ and $\chi_m = \chi_\uparrow - \chi_\downarrow$ and provides an analytical expression for the charge relaxation resistance through Eq. (2.70). This is found to be in excellent agreement with the numerical solution of the Bethe ansatz equations, as illustrated in Fig. 4.14. The analytical solution Eq. (4.65) allows one to carry out the limit $\varepsilon_d \gg \Gamma$ and find the scaling limits discussed in Section 2.5.1.2 and plotted in Fig. 2.12. A clearer intuition of how these scaling limits are recovered is possible by following the progressive increasing of the orbital energy ε_d. For $\Gamma \ll \varepsilon_d \ll U$, the position of the maximum of R_q can be found perturbatively

$$\frac{H}{2\varepsilon_d} = 1 - \frac{\Gamma}{\pi \varepsilon_d} \frac{U(4\varepsilon_d + U)}{(2\varepsilon_d + U)^2} , \tag{4.66}$$

$$R_q = \frac{h}{2e^2} \left(1 + \frac{\Gamma}{\pi \varepsilon_d} \frac{U}{2\varepsilon_d + U} \right) . \tag{4.67}$$

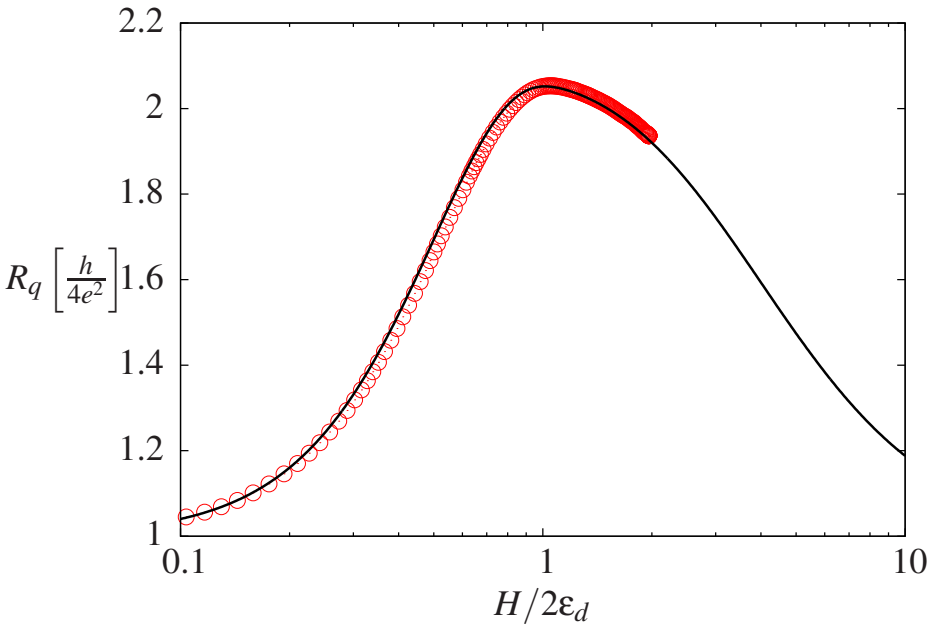

Figure 4.14: Comparison between R_q obtained from the analytical results Eqs. (4.65) *(solid line) and the numerical solution of the BA equations (circles) for $U/\Gamma = 20$ and $\varepsilon_d/\Gamma = 6$.*

Going towards the scaling limit, this maximum sets at $H/2\varepsilon_d = 1$ and, at the same time, the solid line plotted in Fig. 2.12 is recovered with $R_q = h/2e^2$ for all $H > 2\varepsilon_d$. Only when ε_d becomes of the order of the charging energy U, the right part of this scaling starts lowering and recovers the scaling limit obtained for $\Gamma \ll U \ll \varepsilon_d$.

4.5 Conclusions

In this chapter we gave a further demonstration of a path-integral RG approach to determine the low energy Fermi liquid action of a quantum RC circuit described by the Anderson model and coherent with the Friedel sum rule. In contrast with the Coulomb blockade model, spin-exchange processes are responsible for logarithmic Kondo divergencies in the renormalized vertex, preventing to directly carry out the $\Lambda \to 0$ limit. This problem is circumvented relying on Cragg and Lloyd's proof of the additivity of the universal Kondo phase-shift $\delta_K = \pi/2$ with the shift δ_W caused by the potential scattering interaction. We study the effects of a magnetic field on the charge relaxation resistance given by Eq. (2.70). This requires the calculation of the static susceptibilities χ_c and χ_m with analytical approaches and the numerical solution of the Bethe ansatz equations for the ground state of the Anderson model. Our Fermi liquid approach is in agreement with previous NRG calculations [76] and provides a comprehen-

sive analytic description of the behavior of the charge relaxation resistance both in the Kondo regime, where a giant peak arises, and in the mixed valence regime, where R_q follows a universal curve connecting $h/4e^2$ to $h/2e^2$ as a function of the magnetic field. The analytical calculation of the vertex through the introduction of slave-states provides an alternative way to access the charge occupation of the dot and the Kondo temperature, which is of interest in the framework of SU(4) Kondo regimes discussed in the following chapter.

As a concluding remark, one may wonder why in our discussion, for magnetic fields larger than any other energy scale in the problem, we do not recover the single-channel value of the charge relaxation resistance $R_q = h/2e^2$, corresponding to a polarized gas, but the one associated to two spin channels $R_q = h/4e^2$. This relies on the fact that we assumed the hybridization constant $\Gamma = \pi\nu_0 t^2$ to be independent of the magnetic field. For QPCs in 2DEGs, this approximation is justified as the tunneling becomes sensitive to the magnetic field when the Zeeman splitting of the transverse modes in the QPC becomes of the order of their level spacing, which is larger than T_K [149]. The regime studied in Section 4.4.3 is then relevant for setups where the tunneling is weakly dependent on the magnetic field, as for carbon nanotube dots. We neglect this dependence here, but it must be kept in mind that it controls the closing of the anti-parallel spin channel bringing R_q back to $h/2e^2$ in the large magnetic field limit.

CHAPTER 5

THE SU(4) ANDERSON MODEL

Contents

The renormalization group approaches devised in the previous chapters find an important extension to generalized versions of the Anderson Hamiltonian Eq. (2.77), displaying SU(N) symmetries. We focus on the case $N = 4$, which can be observed in quantum dots with further orbital degeneracy [112, 113, 114, 115, 116]. Our Fermi liquid approach allows for the investigation of the charge relaxation resistance in recent carbon nanotube devices displaying this symmetry [117, 118, 119, 120]. In Section 5.1, we address new manifestations of the giant charge relaxation resistance caused by the breaking of the SU(4) Kondo singlet by a magnetic field. In Section 5.2, we extend the representation of the quantum dot Hilbert space with slave-bosons and para-fermions to the SU(4) case. This provides a more practical path-integral representation of the action and paves the way to the calculation of the next to leading order corrections to the renormalized vertex Eq. (2.81). New fundamental results in the framework of impurity problems are obtained. We provide the analytical expression of the SU(4) Kondo temperature in the form Eq. (2.85). Relying on the Friedel sum rule and on the assumption that Cragg and Lloyd's argument also applies in the SU(4) case, we obtain the analytical expression for the charge occupation of the quantum dot in the Coulomb blockade regions. In Section 5.3, we discuss a possible generalization of our results to the SU(N) case.

5.1 A new giant peak for the charge relaxation resistance

The Fermi liquid nature of the ground state of the SU(4) Anderson model [126, 150, 151] provides a further application for the field-theoretical methods developed in Chapter 4. The discussion recovers the steps for the SU(2) Anderson model. For $\varepsilon_{d0} = (1-q-q/N)U$ the potential scattering coupling W_q in Eq. (2.79) vanishes and the Hamiltonian Eq. (2.77) is mapped onto a pure Kondo model with $J_q = \frac{2t^2}{U}\frac{N^2}{q(N-q)}$. Also in this case the Friedel sum rule sets the value of the Kondo phase-shift at strong coupling, $\mathcal{V}_J^R \to \infty$,

$$\delta_K = \frac{q}{N}\pi\,. \tag{5.1}$$

Relying on Cragg and Lloyd's argument, illustrated in Section 4.2.4, the potential scattering coupling W_q Eq. (2.79) adds a further phase-shift

$$\delta_{W_q} = -\arctan\left(\pi\nu_0 W_q\right) \tag{5.2}$$

to Eq. (5.1), see also Eq. (2.21). We showed that this has to be coherent with the Friedel sum rule. The model Eq. (2.68) applies then to describe the low energy quasi-particles and, for the charge relaxation resistance, leads to

$$R_q = \frac{h}{2e^2}\frac{\sum_\nu \chi_\nu^2}{\left(\sum_\nu \chi_\nu\right)^2}\,. \tag{5.3}$$

As in the SU(2) Kondo model, the appearance of infra-red logarithmic divergences prevents a perturbative investigation of the single population susceptibilities $\chi_\nu = -\partial\langle\hat{n}_\nu\rangle/\partial\varepsilon_d$. To circumvent this problem, the separation between spin, charge and orbital degrees of freedom in the SU(4) Anderson Hamiltonian is made explicit by the following change of basis

$$\begin{pmatrix} \chi_c \\ \chi_m \\ \chi_\nu \\ \chi_{m\nu} \end{pmatrix} = \begin{pmatrix} 1 & 1 & 1 & 1 \\ 1 & -1 & 1 & -1 \\ 1 & 1 & -1 & -1 \\ 1 & 1 & -1 & -1 \end{pmatrix} \begin{pmatrix} \chi_1 \\ \chi_2 \\ \chi_3 \\ \chi_4 \end{pmatrix}. \tag{5.4}$$

This transformation defines the analog of the charge χ_c and the charge-magneto susceptibility χ_m for the SU(4) Anderson model. χ_ν is a new quantity that measures the sensitivity of the orbital magnetization to a change in the gate voltage. $\chi_{m\nu}$ is given by the difference between the spin magnetization of the two orbital states. The new expression for the charge relaxation resistance becomes

$$R_q = \frac{h}{8e^2}\left(1 + \frac{\chi_m^2 + \chi_\nu^2 + \chi_{m\nu}^2}{\chi_c^2}\right). \tag{5.5}$$

This formula gives the condition for the non-quantization of the charge relaxation resistance, that is when either χ_m, χ_v or χ_{mv} is non-vanishing. If spin and orbital degeneracies in the quantum dot are not broken, we have $\chi_m = \chi_v = \chi_{mv} = 0$ and $R_q = h/8e^2$. The breaking of the SU(2) symmetry by a magnetic field concerns only spin degeneracy, so χ_v and χ_{vm} remain zero. Eq. (5.5) then recovers Eq. (2.70) up to a factor 2, caused by the participation of four channels to transport instead of two. The Kondo scaling limit can be studied again. For $U \gg \Gamma$ and for Zeeman energies of the order of the SU(4) Kondo temperature, any dependence of the charge susceptibility on the magnetic field is negligible. The charge susceptibility can be analytically derived to leading order in t^2 from Eq. (2.79) by applying the Friedel sum rule

$$\chi_c^q = 4\nu_0 \frac{\partial W_q}{\partial \varepsilon_d} = \frac{\Gamma}{\pi}\left[\frac{q}{(\varepsilon_d + (q-1)U)^2} + \frac{4-q}{(\varepsilon_d + qU)^2}\right]. \tag{5.6}$$

The charge-magneto susceptibility can be also derived from scaling arguments. The definition of the magnetization is

$$\langle \hat{m} \rangle = \frac{1}{2}\sum_{l,\sigma} \sigma \langle \hat{n}_{l,\sigma} \rangle , \tag{5.7}$$

where $l = \pm 1$ and $\sigma = \uparrow, \downarrow$ labels correspond to the orbital and the spin of electrons in the dot. In the Kondo scaling limit, the mapping onto the SU(4) Kondo Hamiltonian Eq. (2.37) becomes exact. This is given by $H/\Gamma \ll 1$ and $U/\Gamma \gg 1$ and far enough from charge degeneracy. The SU(N) version of the model Eq. (2.37), also called Coqblin-Schrieffer model [100], has been solved by Bethe ansatz [126, 152], showing that the magnetization Eq. (5.7) is a smooth and universal function $f_q\left(H/T_K^q\right)$ going from 0 to 1/2 for $q = 1$ and 3 or from 0 to 1 for $q = 2$. The charge-magneto susceptibility then assumes the form

$$\chi_m = 2\frac{\partial \ln T_K^q}{\partial \varepsilon_d}\Phi_q\left(\frac{H}{T_k^q}\right), \tag{5.8}$$

where we defined the dimensionless functions $\Phi_q(x) = x f_q'(x)$. From the general form of the functions $f_q(x)$ we expect $\Phi_q(x)$ to develop a peaked shape for Zeeman energies of the order of T_K^q in a similar way as $\Phi_0(x)$ in the SU(2) case, see Fig. 2.10. The analytical determination of Eq. (5.8) requires also the knowledge of the exact expression for the Kondo temperatures T_K^q, which motivates our vertex calculation in Section 5.2. The form of the SU(4) Kondo temperature is, see Eq. (2.84),

$$T_K^q = \mathscr{D}\sqrt[4]{2\nu_0 J_q}\, e^{-\frac{1}{2\nu_0 J_q}}. \tag{5.9}$$

Eq. (5.8) involves the derivative of the prefactor to the exponential in Eq. (5.9). In Section 5.2.1, we carry out the calculation to second order in J_q of the spin-exchange part of the renormalized vertex and access the effective cutoff $\mathscr{D}$. In the SU(4) case, we show that, in contrast to the SU(2) case, see Eq. (4.4), the whole prefactor to the exponential in Eq. (5.9)

depends on the orbital energy ε_d. Its derivative provides subleading corrections which can be neglected in the $U \gg \Gamma$ limit. The result is

$$\chi_m^q = \frac{\pi}{2\Gamma} \frac{2\varepsilon_d + (2q-1)U}{U} \Phi_q \left(\frac{H}{T_K^q} \right). \tag{5.10}$$

Combining Eqs. (5.5), (5.6) and (5.10), the scaling form for the charge relaxation resistance Eq. (2.80) is obtained. We recall here its expression

$$R_q = \frac{h}{8e^2} \left[1 + \left(\frac{U}{\Gamma} \right)^4 F_q\left(y_q\right) \Phi_q^2 \left(\frac{H}{T_K^q} \right) \right], \tag{5.11}$$

It also predicts a giant peak for the charge relaxation resistance scaling as $(U/\Gamma)^4$, for Zeeman splittings of the order of T_K^q. The envelope of the peak is given by the analog, in the SU(4) case, of the envelope function $F_0(y)$ Eq. (4.54). This function is plotted in Fig. 2.15 as a function of ε_d/U and reads

$$F_q(y_q) = \left(\frac{\pi^2}{32} \right)^2 \frac{y_q^2 (y_q^2 - 1)^4}{\left[1 + y_q^2 + y_q (q-2) \right]^2}. \tag{5.12}$$

This expression depends on the number of charges blocked on the quantum dot q and on the asymmetry parameter

$$y_q = 2\frac{\varepsilon_d}{U} + 2q - 1. \tag{5.13}$$

This is defined such that $y_q = \pm 1$ at the location of the Coulomb peaks, defining the transition between different charge occupations of the quantum dot, and $y_q = 0$ in the middle of the Coulomb valleys. Interestingly, the function F_2 coincides with the envelope function F_0 of the SU(2) case Eq. (4.54) up to the multiplicative factor 16. F_1 and F_3 are instead asymmetric and can provide an experimental signature to distinguish between SU(2) and SU(4) regimes. Notice that Eq. (5.12) always vanishes in the middle of the Coulomb valleys, see also Fig. 2.15. In the SU(2) Anderson model, the vanishing of the envelope function, due to particle-hole symmetry, establishes the quantization of the charge relaxation resistance. The SU(4) Anderson model is particle-hole symmetric only for $\varepsilon_d = -3U/2$. Why then the envelop function $F_q(y_q)$ vanishes also at $\varepsilon_d = -U/2$ and $\varepsilon_d = -5U/2$, where the system is not particle-hole symmetric? This is an artifact of the scaling limit $U \gg \Gamma$. Looking at Fig. 5.1, we notice that, at the center of the Coulomb valleys, the two energy sectors closer to the ground-state are degenerate. In the scaling limit, only the leading contributions in the tunnel coupling t to χ_c and T_K^q are considered. They involve virtual fluctuations only to the closest charge states and excursions to farther ones are neglected, see also Fig. 5.3. This approximation gives an effective particle-hole symmetry to the problem and implies a vanishing envelope function in the middle of the Coulomb valleys. The subleading corrections

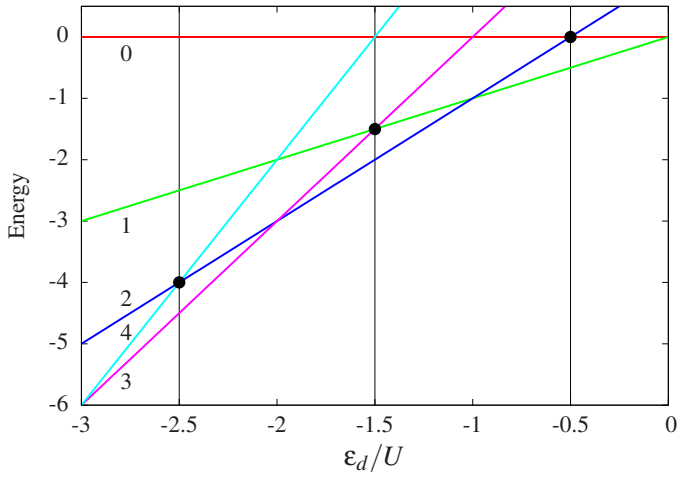

Figure 5.1: Spectrum of the isolated quantum dot. The energies associated to different charge occupations are plotted as functions of ε_d/U. The vertical lines signal the middle of the Coulomb valleys in which $q = 1$, 2 or 3 charges are blocked on the dot (right to left respectively). The dots highlight the degeneracy of the two closest energy sectors, providing effective particle-hole symmetry to leading order in Γ/U, see main text.

to the Kondo temperature, obtained in the following sections, take into account the virtual processes breaking particle-hole symmetry. This can be appreciated by inspecting the behaviors of the prefactors $f_q(\varepsilon_d/U)$ of the Kondo temperature Eq. (2.85), plotted in Fig. 2.16. Their derivatives are different from zero in the middle of the Coulomb valleys for $q = 1$ and 3, implying in particular non-zero corrections to the envelope function at $\varepsilon_d = -U/2$ and $\varepsilon_d = -5U/2$, in contrast with the particle-hole symmetric point at $\varepsilon_d = -3U/2$, where the derivative vanishes to all order in Γ/U. Notice also that the middle of the Coulomb valleys does not coincide wiht the points ε^q_{d0} for which the potential scattering coupling Eq. (2.79) vanishes. These points are signaled in Fig. 2.15 by circles. These are close to the maxima of the envelope function for q =1 and 3. We expect that the approach to the Kondo scaling behavior is faster at these points, what would allow one to observe more easily the giant charge relaxation resistance than in the $q = 2$ region, in which this point coincides with the zero of the envelope function, and is protected by particle-hole symmetry.

5.2 Path integral formulation of the SU(4) Anderson model

The representation *via* slave-states of the Hilbert space of a SU(4) symmetric quantum dot is illustrated in Fig. 5.2. Slave-bosons are associated to states of the quantum dot involving

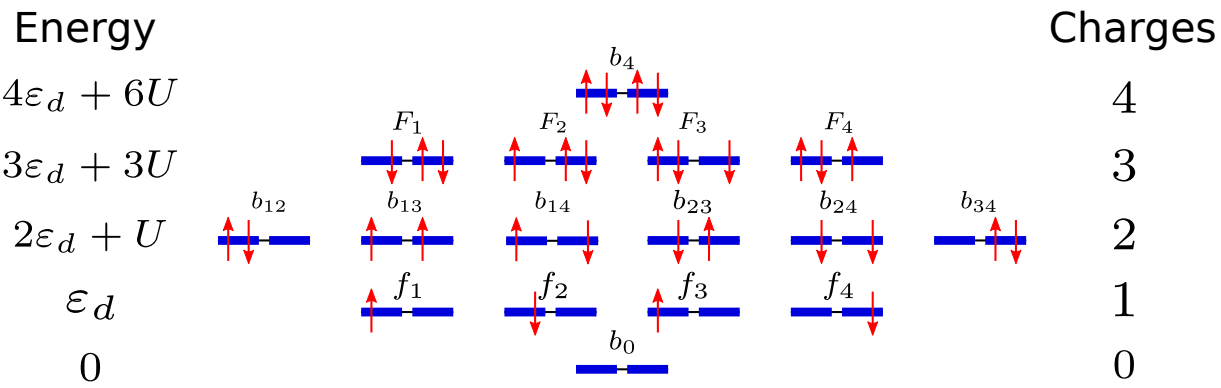

Figure 5.2: Representation of the SU(4) quantum dot Hilbert space with slave-boson and para-fermions. The spin and valley occupation are represented with their energy and the total charge occupation. To every configuration a slave-field is associated: bosons for even occupations of the dot and fermions for odd occupations.

an even number of charges. $b_0^\dagger$ and $b_4^\dagger$ create the empty and completely filled quantum dot respectively. In the case of two charges on the quantum dot, the occupied levels must be specified and the operators $b_{\nu\nu'}^\dagger$ describe a quantum dot occupied by two charges set in the states ν and ν'. Para-fermions are associated to odd occupations of the quantum dot, either one or three charges. $f_\nu^\dagger$ creates an electron in the state ν, while the complementary operator $F_\nu^\dagger$ creates the state with three electrons filling all the dot states except the one labeled by ν. In this new basis, the expressions of the original quantum dot fermionic operators $d_\nu^\dagger$ read

$$\begin{aligned}
d_1^\dagger &= f_1^\dagger b_0 + b_{12}^\dagger f_2 + b_{13}^\dagger f_3 + b_{14}^\dagger f_4 + b_4^\dagger F_1 - F_2^\dagger b_{34} + F_3^\dagger b_{24} - F_4^\dagger b_{23}\,,\\
d_2^\dagger &= f_2^\dagger b_0 - b_{12}^\dagger f_1 + b_{23}^\dagger f_3 + b_{24}^\dagger f_4 + b_4^\dagger F_2 + F_1^\dagger b_{34} - F_3^\dagger b_{14} + F_4^\dagger b_{13}\,,\\
d_3^\dagger &= f_3^\dagger b_0 - b_{13}^\dagger f_1 - b_{23}^\dagger f_2 + b_{34}^\dagger f_4 + b_4^\dagger F_3 - F_1^\dagger b_{24} + F_2^\dagger b_{14} - F_4^\dagger b_{12}\,,\\
d_4^\dagger &= f_4^\dagger b_0 - b_{14}^\dagger f_1 - b_{24}^\dagger f_2 - b_{34}^\dagger f_3 + b_4^\dagger F_4 + F_1^\dagger b_{23} - F_2^\dagger b_{13} + F_3^\dagger b_{12}\,.
\end{aligned} \tag{5.14}$$

The choice of the signs is fixed to preserve the fermionic commutation relations $\left\{d_\nu^\dagger, d_{\nu'}\right\} = \delta_{\nu\nu'}$ and $\left\{d_\nu^\dagger, d_{\nu'}^\dagger\right\} = 0$ between original operators. The action of the system is readily written in this new basis in the form $S_{\mathrm{SU(4)}} = S_0 + S_T$, where

$$S_0 = -\int_0^\beta d\tau \left\{c_{k\nu}^\dagger G_k^{-1} c_{k\nu} + f_\nu^\dagger D_1^{-1} f_\nu + F_\nu^\dagger D_3^{-1} F_\nu + b_0^\dagger B_0^{-1} b_0 + b_{\nu\nu'}^\dagger B_2^{-1} b_{\nu\nu'} + b_4^\dagger B_4^{-1} b_4\right\}, \tag{5.15}$$

with

$$G_k^{-1} = -\partial_\tau - \varepsilon_k\,, \tag{5.16a}$$
$$B_0^{-1} = -\partial_\tau - \lambda\,, \tag{5.16b}$$
$$D_1^{-1} = -\partial_\tau - \varepsilon_d - \lambda\,, \tag{5.16c}$$
$$B_2^{-1} = -\partial_\tau - 2\varepsilon_d - U - \lambda\,, \tag{5.16d}$$
$$D_3^{-1} = -\partial_\tau - 3\varepsilon_d - 3U - \lambda\,, \tag{5.16e}$$
$$B_4^{-1} = -\partial_\tau - 4\varepsilon_d - 6U - \lambda\,. \tag{5.16f}$$

In Eq. (5.15), repeated labels are summed up with the prescription $\nu < \nu'$. The para-energy λ has been introduced in free slave-state propagators to perform Abrikosov's projection onto the physical sector. This is defined by the constraint

$$b_0^\dagger b_0 + \sum_\nu f_\nu^\dagger f_\nu + \sum_{\nu'>\nu} b_{\nu\nu'}^\dagger b_{\nu\nu'} + \sum_\nu F_\nu^\dagger F_\nu + b_4^\dagger b_4 = 1\,. \tag{5.17}$$

In Eqs. (5.16), we stress the difference between para-fermion and slave-boson propagators by labeling them with different letters, D and B respectively. They depend respectively on fermionic and bosonic Matsubara frequencies $i\omega$ or $i\nu$. The tunneling contribution to the action reads

$$S_T = \int_0^\beta d\tau\, t \sum_{k\nu} \left(c_{k\nu}^\dagger d_\nu + d_\nu^\dagger c_{k\nu} \right), \tag{5.18}$$

in which the transformation Eq. (5.14) is assumed implicitly. In the following, the calculation of the renormalized vertex is carried out in all the three charge sectors $q = 1, 2, 3$. The steps are the same for all the three sectors and recover those already illustrated for the SU(2) Anderson model in Chapter 4. Firstly, we integrate all the high energy sectors relevant to fourth order in t and show that the effective interaction can always be cast in the form

$$S_{\mathrm{SU(4)}} = \frac{1}{\beta} \sum_{kk'} c_{k\mu}^\dagger(i\omega_1) c_{k'\mu'}(i\omega_2) g_\nu^\dagger(i\nu + i\omega_2) g_{\nu'}(i\nu + i\omega_1) \times \\ \left[\mathscr{J}(i\omega_1, i\omega_2, i\nu) \mathbf{S}_{\nu\nu'} \cdot \mathbf{T}_{\mu\mu'} + \mathbb{1} \mathscr{W}(i\omega_1, i\omega_2, i\nu) \right]. \tag{5.19}$$

This involves a SU(4) spin-exchange and a potential scattering interaction. The fermionic fields g_ν are differently defined, depending on the charge sector q. All spin labels are summed up and run from one to four. **S** and **T** are the vectors composed of the fundamental representation of the SU(4) group illustrated in Appendix E. The renormalized vertex is then calculated as in Section 4.3. We show that it assumes the form of Eq. (2.81), allowing us to access the SU(4) Kondo temperatures and the charge occupation of the quantum dot.

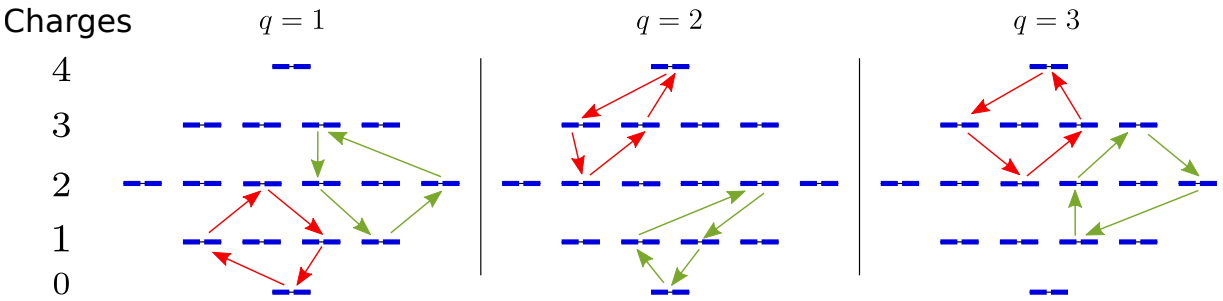

Figure 5.3: Virtual paths in the SU(4) Anderson model to fourth order in the tunnel coupling t, for different Coulomb blockade regimes $q = 1$, 2 and 3. The circles signal the departure state to which one has to come back in Coulomb blockade regimes. We emphasize graphically the symmetry between the sectors $q = 1$ and 3. Notice that, for $q = 1$ and 3, the charge sectors 4 and 0 can be respectively neglected to fourth order in t.

5.2.1 The calculation of the SU(4) renormalized vertices

In this section we give a fully detailed illustration of the calculation of the renormalized vertex to fourth order in t only for the sector of charge $q = 1$. Only the major differences arising in the other charge sectors will be discussed, but there is no need to repeat in detail all calculations, whose main steps are summarized in Appendix H.

5.2.1.1 Sector of charge $q = 1$

The quantum dot hosts a single charge if $-U < \varepsilon_d < 0$. In Fig. 5.3 we show that virtual processes to fourth order in the tunneling t do not involve the charge sector occupied by four charges, which can be neglected. The action of the system can then be written in the form $S = S_0 + S_{01} + S_{12} + S_{23}$, where S_0 is the quadratic action Eq. (5.15) without the b_4 field and the notation S_{nm} stands for the terms in Eq. (5.18) which hybridize the slave-fields associated to n and m charges on the quantum dot. We first consider the simpler Gaussian integration concerning the single mode b_0, associated to the empty orbital sector. Adopting the general notation with traces defined in Eqs. (3.19) and (3.20), S_{01} reads

$$S_{01} = t\,\mathrm{Tr}\left[b_0^\dagger \sum_{kv} c_{kv}^\dagger d_v + \mathrm{h.c.} \right] . \tag{5.20}$$

The integration of the b_0 slave-field leads to an the effective interaction, recovering the form Eq. (5.19)

$$\begin{aligned} S'_{01} &= -\frac{t^2}{\beta}\sum_{kk'\nu\nu'} B_0(i\nu)c^\dagger_{k\nu}(i\omega_1)c_{k'\nu'}(i\omega_2)f^\dagger_{\nu'}(i\nu+i\omega_2)f_\nu(i\nu+i\omega_1) \\ &= -\frac{t^2}{\beta}\sum_{kk'\mu\mu'\nu\nu'} B_0(i\nu)c^\dagger_{k\mu}(i\omega_1)c_{k'\mu'}(i\omega_2)f^\dagger_{\nu}(i\nu+i\omega_2)f_{\nu'}(i\nu+i\omega_1)\left[2\mathbf{S}_{\nu\nu'}\cdot\mathbf{T}_{\mu\mu'}-\frac{1}{4}\mathbb{1}\right]. \end{aligned} \tag{5.21}$$

To pass from the first to the second expression, Eq. (E.2) with $q=1$ has been applied. The integration of the remaining high energy fields is trickier. In a similar way as for the Coulomb blockade model, the integration of the F_ν modes renormalizes the $b_{\nu\nu'}$ slave-bosons, but more effort is required to write the effective interaction between the fields $c_{k\nu}$ and f_ν in the form Eq. (5.19). We start with the integration of the highest energy slave-modes F_ν. The action S_{23} can be expressed in the following algebraic form

$$S_{23} = t\,\mathrm{Tr}\left[\mathbf{F}^\dagger\cdot\mathbf{C}\cdot\mathbf{b}\right]+\mathrm{h.c.} \tag{5.22}$$

with[1]

$$\mathbf{F}=\begin{pmatrix}F_1\\F_2\\F_3\\F_4\end{pmatrix},\qquad \mathbf{b}=\begin{pmatrix}b_{12}\\b_{13}\\b_{14}\\b_{23}\\b_{24}\\b_{34}\end{pmatrix}\quad\text{and}\quad \mathbf{C}=\begin{pmatrix}0&0&0&c_4&-c_3&c_2\\0&-c_4&c_3&0&0&-c_1\\c_4&0&-c_2&0&c_1&0\\-c_3&c_2&0&-c_1&0&0\end{pmatrix}. \tag{5.23}$$

The integration of the para-fermions F_ν leads to the following effective interaction

$$S'_{23} = t^2\,\mathrm{Tr}\left[\mathbf{b}^\dagger\cdot\mathbf{A}_2\cdot\mathbf{b}\right], \tag{5.24}$$

with $\mathbf{A}_2=\mathbf{C}^\dagger\cdot D_3\mathbb{1}_4\cdot\mathbf{C}$, $\mathbb{1}_4$ the 4×4 identity matrix and D_3 given by Eq. (5.16e). This term renormalizes the quadratic part of the action Eq. (5.15) and the interacting part Eq. (5.18), involving the $b_{\nu\nu'}$ slave-bosons,

$$S_{12}+S'_{23} = -\mathrm{Tr}\left[\mathbf{b}^\dagger\cdot\Phi_2^{-1}\cdot\mathbf{b}\right]+t\,\mathrm{Tr}\left[\mathbf{b}^\dagger\cdot\mathbf{w}+\mathbf{w}^\dagger\cdot\mathbf{b}\right], \tag{5.25}$$

where

$$\Phi_2^{-1}=B_2^{-1}\mathbb{1}_6-t^2\mathbf{A}_2\qquad\text{and}\qquad \mathbf{w}=\begin{pmatrix}f_2c_1-f_1c_2\\f_3c_1-f_1c_3\\f_4c_1-f_1c_4\\f_3c_2-f_2c_3\\f_4c_2-f_2c_4\\f_4c_3-f_3c_4\end{pmatrix}. \tag{5.26}$$

[1] To keep simple notations, we omit in the following the sum on the momentum index k for lead electrons.

Eq. (5.25) is quadratic in $\mathbf{b}$ and its integration is also Gaussian. It leads to

$$S'_{12} = t^2 \mathrm{Tr}\left[\mathbf{w}^\dagger \cdot \Phi_2 \cdot \mathbf{w}\right] = t^2 \mathrm{Tr}\left[\mathbf{w}^\dagger \cdot B_2 \mathbb{1}_6 \cdot \mathbf{w}\right] + t^4 \mathrm{Tr}\left[\mathbf{w}^\dagger \cdot B_2 \cdot \mathbf{A}_2 \cdot B_2 \cdot \mathbf{w}\right], \tag{5.27}$$

where, in the last equality, we expanded in t the operator Φ_2. The mapping of the first term of Eq. (5.27) onto Eq. (5.19) is possible considering the following identity

$$\mathbf{w}^\dagger \cdot \mathbf{w} = \sum_{\nu \neq \nu'} c^\dagger_\nu c_\nu f^\dagger_{\nu'} f_{\nu'} - \sum_{\nu \neq \nu'} c^\dagger_\nu c_{\nu'} f^\dagger_{\nu'} f_\nu = \sum_{\mu\mu'\nu\nu'} c^\dagger_\mu c_{\mu'} f^\dagger_\mu f_{\nu'} \left[\frac{3}{4}\delta_{\mu\mu'}\delta_{\nu\nu'} - 2\mathbf{S}_{\nu\nu'} \cdot \mathbf{T}_{\mu\mu'}\right]. \tag{5.28}$$

The last equality is obtained applying the relation

$$\sum_{\nu \neq \nu'} f^\dagger_\nu f_\nu = 1 - f^\dagger_{\nu'} f_{\nu'}. \tag{5.29}$$

This is a direct consequence of the constraint Eq. (5.17). All the slave-states participating to it, with the exception of the para-fermions f_ν, have been integrated out. In the effective action, only the residual slave-fermion f_ν is controlled by the para-chemical potential λ, which, when sent to infinity, sets the constraint $\sum_\nu f^\dagger_\nu f_\nu = 1$, responsible for Eq. (5.29). The effective action can be finally cast into the form

$$S'_1 = S'_0 + S_{\mathrm{SU}(4)} + t^4 \mathrm{Tr}\left[\mathbf{w}^\dagger \cdot B_2 \cdot \mathbf{A}_2 \cdot B_2 \cdot \mathbf{w}\right], \tag{5.30}$$

with S'_0 composed of the two first terms of Eq. (5.15). The frequency dependent couplings in $S_{\mathrm{SU}(4)}$ read

$$\mathscr{J}_1 = -2t^2 \left[B_0(i\nu) + B_2(i\nu + i\omega_1 + i\omega_2)\right], \quad \mathscr{W}_1 = -\frac{t^2}{4}\left[B_0(i\nu) - 3B_2(i\nu + i\omega_1 + i\omega_2)\right]. \tag{5.31}$$

These two expressions recover the couplings obtained by the Schrieffer-Wolff transformation Eqs. (2.78) and (2.79), for $q = 1$. This can be verified by substituting the frequencies of Eq. (5.31) with the poles of G_k and F_1 in Eq. (5.16), $i\nu \to \varepsilon_d + \lambda$ and $i\omega_{1,2} \to 0$.

A mean-field treatment of the quartic term in Eq. (5.30) provides the exact contribution to fourth order in t to the four-point vertex function that we define as in Eq. (4.17)

$$\mathscr{V}^\Lambda_{\sigma\sigma',\tau\tau'}(k, i\omega_1, i\Omega_1; k' i\omega_2, i\Omega_2) = -\beta \frac{\langle c_{k\sigma}(i\omega_1) f_\tau(i\Omega_1) f^\dagger_{\tau'}(i\Omega_2) c^\dagger_{k'\sigma'}(i\omega_2)\rangle\Big|_c}{G_k(i\omega_1) G_{k'}(i\omega_2) D_1(i\Omega_1) D_1(i\Omega_2)}. \tag{5.32}$$

One can realize, that the mean-field treatment of the four point interaction $\left(c^\dagger c\right)^2$, as already carried out in Section 2.2.1 for the Coulomb blockade model, permits to map this interaction

onto Eq. (5.19). The calculations are quite tedious and they are detailed in Appendix H. The last term in Eq. (5.30) can then be cast into the form

$$t^4 \sum_{kk'\mu\mu'\nu\nu'} \mathrm{Tr}\left\{\left[(8A_1-4A_0-4A_2)\,\mathbf{S}_{\nu\nu'}\cdot\mathbf{T}_{\mu\mu'}+\left(\frac{3}{2}A_0+\frac{3}{2}A_2-3A_1\right)\delta_{\mu\mu'}\delta_{\nu\nu'}\right] c^\dagger_{k\mu}c_{k'\mu'}f^\dagger_\nu f_{\nu'}\right\}, \tag{5.33}$$

with the coefficients A_n also listed in Appendix H.

The calculation of the renormalized vertex involves the usual steps of the two previous chapters. These are the calculation of the full renormalized para-fermion propagator, with the corrections to the pole and its quasi-particle weight, and the calculation of all diagrams up to fourth order in t contributing to the vertex function Eq. (5.32). All the details about these calculations are given in Appendix H. The renormalized vertex is cast in the form Eq. (2.81). The spin-exchange coupling reads

$$\mathcal{V}^R_{J_1} = J_1 + 2\nu_0 J_1^2 g_1\left(\frac{\varepsilon_d}{U}\right) - 2\nu_0 J_1^2 \ln\frac{\Lambda}{\sqrt[4]{-\varepsilon_d(\varepsilon_d+U)^3}}, \tag{5.34}$$

with

$$g_1(x) = \frac{1}{4}\frac{3x-2}{x+2} - \frac{1}{2}\frac{x^2(x^2+3x+3)}{(2+x)^2}\ln\frac{2x+3}{x+1}. \tag{5.35}$$

The part concerning the potential scattering coupling is given by

$$\mathcal{V}^R_{W_1} = W_1 + \frac{1}{\nu_0}\left(\frac{\Gamma}{\pi U}\right)^2 h_1\left(\frac{\varepsilon_d}{U}\right), \tag{5.36}$$

where

$$\begin{aligned} h_1(x) = {} & \frac{3}{4}\left(\frac{1}{x^2}+\frac{1}{(x+1)^2}\right) + \frac{1}{x^2}\ln\frac{\sqrt[4]{-x(x+1)}}{-x} + \frac{3}{(x+1)^2}\ln\frac{\sqrt{(x+1)(2x+3)}}{\sqrt[4]{-x(x+1)}} + \\ & \frac{3}{2}\frac{1}{x(x+1)}\ln\frac{-x}{x+1} + 3\left[\frac{1}{(x+2)^2}\ln\sqrt{\frac{2x+3}{x+1}} - \frac{1}{(x+1)(x+2)}\left(\frac{1}{2}+\ln\frac{2x+3}{x+1}\right)\right]. \end{aligned} \tag{5.37}$$

One checks at this point that W_1 vanishes in the middle of the Coulomb valley for $\varepsilon_d = -U/2$ but not h_1, a consequence of the absence of particle-hole symmetry in this sector. Eq. (5.34) can be mapped onto Eq. (2.82) with the choice for the effective cutoff

$$\mathscr{D}_1 = \sqrt[4]{-\varepsilon_d(\varepsilon_d+U)^3}. \tag{5.38}$$

This sets the choice of the corresponding spin-exchange coupling constant, that is the first two terms in Eq. (5.34)

$$J = J_1 + 2\nu_0 J_1^2 g_1\left(\frac{\varepsilon_d}{U}\right). \tag{5.39}$$

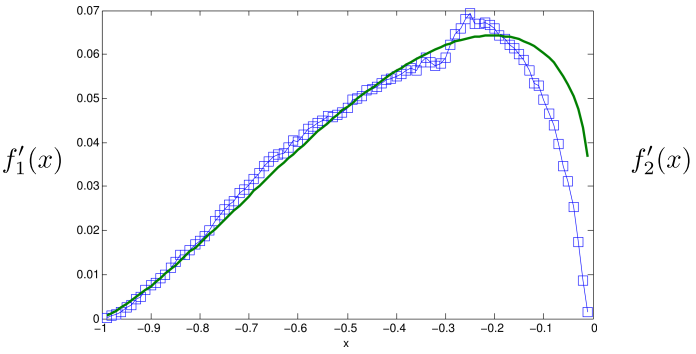

Figure 5.4: Comparison between the analytical prefactor $f_1(x)$ Eq. (5.40) *and $f_2(x)$ Eq.* (5.54) *(solid line) with numerical renormalization group calculations (points) [153]. The points were obtained by a different procedure leaving invariant J_1 in Eq.* (2.78) *and U and varying ε_d/U and Γ/U, which implies a different definition of the prefactors $f_1 \to f_1'$. The same for the charge sector $q=2$. The sector associated to $q=3$ is obtained by symmetry from $q=1$.*

From this definition the Kondo temperature Eq. (2.85) is found for $q=1$, with

$$f_1(x) = \sqrt{1+x}\, e^{g_1(x)}\,, \tag{5.40}$$

plotted in Fig. 2.16. Applying the Friedel sum rule, the dot occupation reads

$$\langle \hat{n}_1 \rangle = 1 - 4\nu_0 \mathcal{V}_{W_1}^R\,. \tag{5.41}$$

To check the validity of our approach we report in Fig. 5.4 the comparison of our analytic formula of the prefactor $f_1(x)$ in Eq. (2.85) to that obtained by numerical renormalization group calculations [153].

5.2.1.2 Sector of charge $q=2$

In this section, the discussion is limited to the main differences arising from the calculation of the renormalized vertex in the case of two charges blocked on the dot. All further difficulties with respect to the previous calculations come essentially from the fact that the local modes describing the charge on the dot are not four para-fermions, what is the usual representation of the SU(N) Kondo interaction Eq. (E.2) [154], but slave-bosons. They require some further effort to make explicit the mapping onto the SU(4) para-fermionic effective interaction Eq. (5.19).

For $-2U < \varepsilon_d < -U$, two charges are frozen at low energy on the dot. To fourth order in the tunneling t, all the other charge sectors of the quantum dot contribute to the effective

action describing this regime, see Fig. 5.3. None of the slave-states introduced in the new representation Eq. (5.14) can then be neglected. The farthest charge modes in energy b_0 and b_4 are integrated first and the effective action can be written in the following form

$$S_2 = -\mathrm{Tr}\left[\mathbf{b}^\dagger \cdot B_2^{-1}\mathbb{1}_6 \cdot \mathbf{b}\right] - \mathrm{Tr}\left[\mathbf{f}^\dagger \cdot \Phi_1^{-1} \cdot \mathbf{f}\right] - \mathrm{Tr}\left[\mathbf{F}^\dagger \cdot \Phi_3^{-1} \cdot \mathbf{F}\right] + t\,\mathrm{Tr}\left[\mathbf{B}_1^\dagger \cdot \mathbf{f} + \mathbf{f}^\dagger \cdot \mathbf{B}_1 + \mathbf{B}_3^\dagger \cdot \mathbf{F} + \mathbf{F}^\dagger \cdot \mathbf{B}_3\right]. \tag{5.42}$$

The vectors **F** and **b** are the same as in Eq. (5.23), and we defined the new vectors

$$\mathbf{f} = \begin{pmatrix} f_1 \\ f_2 \\ f_3 \\ f_4 \end{pmatrix}, \quad \mathbf{B}_1 = \begin{pmatrix} c_2^\dagger b_{12} + c_3^\dagger b_{13} + c_4^\dagger b_{14} \\ -c_1^\dagger b_{12} + c_3^\dagger b_{23} + c_4^\dagger b_{24} \\ -c_1^\dagger b_{13} - c_2^\dagger b_{23} + c_4^\dagger b_{34} \\ -c_1^\dagger b_{14} - c_2^\dagger b_{24} - c_3^\dagger b_{34} \end{pmatrix}, \quad \mathbf{B}_3 = \begin{pmatrix} b_{34}c_2 - b_{24}c_3 + b_{23}c_4 \\ -b_{34}c_1 + b_{14}c_3 - b_{13}c_4 \\ b_{24}c_1 - b_{14}c_2 + b_{12}c_4 \\ -b_{23}c_1 + b_{13}c_2 - b_{12}c_3 \end{pmatrix}, \tag{5.43}$$

and the renormalized propagators

$$\Phi_1^{-1} = F_1^{-1}\mathbb{1}_4 - t^2\mathbf{A}_1\,, \tag{5.44a}$$
$$\Phi_3^{-1} = F_3^{-1}\mathbb{1}_4 - t^2\mathbf{A}_3\,, \tag{5.44b}$$

with

$$\mathbf{A}_1 = \begin{pmatrix} c_1 \\ c_2 \\ c_3 \\ c_4 \end{pmatrix} \cdot B_0\mathbb{1}_4 \cdot \begin{pmatrix} c_1^\dagger & c_2^\dagger & c_3^\dagger & c_4^\dagger \end{pmatrix}, \qquad \mathbf{A}_3 = \begin{pmatrix} c_1^\dagger \\ c_2^\dagger \\ c_3^\dagger \\ c_4^\dagger \end{pmatrix} \cdot B_4\mathbb{1}_4 \cdot \begin{pmatrix} c_1 & c_2 & c_3 & c_4 \end{pmatrix}. \tag{5.45}$$

Also in this case, the integration of the remaining para-fermions collected in the vectors **f** and **F** is Gaussian and leads to the following effective action

$$S_2' = -\mathrm{Tr}\left[\mathbf{b}^\dagger \cdot B_2^{-1} \cdot \mathbf{b}\right] + \mathrm{Tr}\left[\mathscr{J}_2\left(\mathbf{b}^\dagger \cdot \mathbf{S} \cdot \mathbf{b}\right) \cdot \left(\mathbf{c}^\dagger \cdot \mathbf{T} \cdot \mathbf{c}\right) + \mathscr{W}_2\left(\mathbf{b}^\dagger \cdot \mathbb{1}_6 \cdot \mathbf{b}\right)\left(\mathbf{c}^\dagger \mathbb{1}_4 \mathbf{c}\right)\right] + \\ + t^4\mathrm{Tr}\left[\mathbf{B}_1^\dagger \cdot D_1 \cdot \mathbf{A}_1 \cdot D_1 \cdot \mathbf{B}_1\right] + t^4\mathrm{Tr}\left[\mathbf{B}_3^\dagger \cdot D_3 \cdot \mathbf{A}_3 \cdot D_3 \cdot \mathbf{B}_3\right], \tag{5.46}$$

with

$$\mathscr{J}_2 = -2t^2\left[D_1(i\nu - i\omega_1) + D_3(i\nu + i\omega_2)\right], \quad \mathscr{W}_2 = -\frac{t^2}{2}\left[D_1(i\nu - i\omega_1) - D_3(i\nu + i\omega_2)\right]. \tag{5.47}$$

Taking the analytical continuations $i\nu \to 2\varepsilon_d + U + \lambda$ and $i\omega_{1,2} \to 0$, these expressions recover the Schrieffer-Wolff couplings Eqs. (2.78) and (2.79) for $q = 2$. The SU(4) representation of the interaction $\left(\mathbf{b}^\dagger \cdot \mathbf{S} \cdot \mathbf{b}\right)\left(\mathbf{c}^\dagger \cdot \mathbf{T} \cdot \mathbf{c}\right)$ deserves a specific discussion. The vector **b** has six components and this implies that the matrices composing the invariant SU(4) vector **S** are not

those of the fundamental representation Eq. (E.1) in Appendix E. The explicit expression of the product in Eq. (5.46) reads

$$\begin{aligned}
2\left(\mathbf{b}^\dagger\cdot\mathbf{S}\cdot\mathbf{b}\right)\left(\mathbf{c}^\dagger\cdot\mathbf{T}\cdot\mathbf{c}\right) = & c_1^\dagger c_2\left(b_{24}^\dagger b_{14}+b_{23}^\dagger b_{13}\right)+c_1^\dagger c_3\left(b_{34}^\dagger b_{14}-b_{23}^\dagger b_{12}\right)+\\
& c_1^\dagger c_4\left(-b_{34}^\dagger b_{13}-b_{24}^\dagger b_{12}\right)+c_2^\dagger c_3\left(b_{34}^\dagger b_{24}+b_{13}^\dagger b_{12}\right)+\\
& c_2^\dagger c_4\left(-b_{34}^\dagger b_{23}+b_{14}^\dagger b_{12}\right)+c_3^\dagger c_4\left(b_{24}^\dagger b_{23}+b_{14}^\dagger b_{13}\right)+\text{h.c.}\\
& \frac{1}{2}c_1^\dagger c_1\left(b_{12}^\dagger b_{12}+b_{13}^\dagger b_{13}+b_{14}^\dagger b_{14}-b_{23}^\dagger b_{23}-b_{24}^\dagger b_{24}-b_{34}^\dagger b_{34}\right)+\\
& \frac{1}{2}c_2^\dagger c_2\left(b_{12}^\dagger b_{12}+b_{23}^\dagger b_{23}+b_{24}^\dagger b_{24}-b_{13}^\dagger b_{13}-b_{14}^\dagger b_{14}-b_{34}^\dagger b_{34}\right)+\\
& \frac{1}{2}c_3^\dagger c_3\left(b_{13}^\dagger b_{13}+b_{23}^\dagger b_{23}+b_{34}^\dagger b_{34}-b_{12}^\dagger b_{12}-b_{14}^\dagger b_{14}-b_{24}^\dagger b_{24}\right)+\\
& \frac{1}{2}c_4^\dagger c_4\left(b_{14}^\dagger b_{14}+b_{24}^\dagger b_{24}+b_{34}^\dagger b_{34}-b_{12}^\dagger b_{12}-b_{13}^\dagger b_{13}-b_{23}^\dagger b_{23}\right).
\end{aligned} \tag{5.48}$$

We stress that this expression is obtained by applying the constraint $\sum_{\nu'>\nu} b_{\nu\nu'}^\dagger b_{\nu\nu'}=1$ and not Eq. (5.17), because all the other fields have been integrated to obtain the effective action Eq. (5.46). To obtain the mapping onto Eq. (5.19) one has to switch back to a fermionic basis. The slave-bosons $b_{\tau\tau'}$ are associated to a two-electron state, which can also be described within a fermionic representation

$$b_{\nu\nu'}^\dagger = g_\nu^\dagger g_{\nu'}^\dagger . \tag{5.49}$$

The g_ν are para-fermions fields obeying the constraint

$$\sum_\nu g_\nu^\dagger g_\nu = 2 . \tag{5.50}$$

Substituting Eq. (5.49) in Eq. (5.48) and applying Eq. (5.50), one proves the mapping onto the usual SU(4) symmetric form Eq. (5.19), more precisely we recover Eq. (E.2) for $q=2$. For our purposes, it is much simpler to calculate the vertex function for the slave-bosons, defined similarly as in Eq. (3.28)

$$\mathcal{V}^\Lambda_{\mu\mu';\nu\nu',\nu\nu'}(k,i\omega_1,i\nu_1;k'i\omega_2,i\nu_2) = -\beta\frac{\langle c_{k\mu}(i\omega_1)b_{\nu\nu'}(i\nu_1)b_{\nu\nu'}^\dagger(i\nu_2)c_{k'\mu'}^\dagger(i\omega_2)\rangle\Big|_c}{G_k(i\omega_1)G_{k'}(i\omega_2)B_2(i\nu_1)B_2(i\nu_2)} . \tag{5.51}$$

This takes the form Eq. (2.81), but the components of the vector $\mathbf{S}$ are the 6×6 matrices in Eq. (5.46) leading to Eq. (5.48). The details of the calculation of this function and then of the renormalized vertex are illustrated in Appendix H. The mean-field treatment of the last two terms in Eq. (5.46) also maps onto Eq. (5.19) and gives a t^4 order contribution to the vertex function. This is also illustrated in Appendix H. The complete calculation leads to a renormalized vertex of the form Eq. (2.81). The spin-exchange coupling reads

$$\mathcal{V}_{J_2}^R = J_2 + 2\nu_0 J_2^2 g_2\left(\frac{\varepsilon_d}{U}\right) - 2\nu_0 J_2^2 \ln\frac{\Lambda}{e^{-\frac{1}{2}}\sqrt{(-\varepsilon_d-U)(\varepsilon_d+2U)}} , \tag{5.52}$$

where

$$g_2(x) = \frac{(x+2)^2}{4x^2}\left[x + \ln\frac{x+1}{2x+1}\right] + \frac{(x+1)^2}{4(x+3)^2}\left[-x-3+\ln\frac{x+2}{2x+5}\right], \tag{5.53}$$

This allows to determine the function $f_2(x)$ in Eq. (2.85)

$$f_2(x) = \sqrt[4]{\frac{(-1-x)(x+2)}{e^2}}\, e^{g_2(x)}. \tag{5.54}$$

The potential scattering term reads

$$\mathcal{V}^R_{W_2} = W_2 + \frac{1}{\nu_0}\left(\frac{\Gamma}{\pi U}\right)^2 h_2\left(\frac{\varepsilon_d}{U}\right), \tag{5.55}$$

with

$$\begin{aligned} h_2(x) = \frac{1}{4}\frac{4x+1}{x(x+1)^2} - \frac{1}{4}\frac{4x+11}{(x+3)(x+2)^2} - \frac{1}{2}\frac{1}{(x+1)(x+2)}\ln\frac{x+2}{-x-1} + \\ \frac{1}{2}\frac{1-x}{(x+1)x^2}\ln\frac{x+1}{2x+2} + \frac{1}{2}\frac{x+4}{(x+2)(x+3)^2}\ln\frac{x+2}{2x+5} + \\ \frac{3-2x}{(x+1)^2(x+2)^2}\ln\frac{x+2}{\sqrt{(-x-1)(2x+5)}}. \end{aligned} \tag{5.56}$$

Notice also that $\mathcal{V}^R_W$ Eq. (5.55) vanishes at particle-hole symmetry $x\varepsilon_d/U = -3/2$, which coincides with the middle of the Coulomb valley, in contrast with the $q = 1$ case, see Eq. (5.36). The corrections to the charge on the quantum dot are also found with the help of the Friedel sum rule

$$\langle \hat{n}_2 \rangle = 2 - 4\nu_0 \mathcal{V}^R_{W_2}. \tag{5.57}$$

5.2.1.3 Sector of charge $q = 3$

This last section is dedicated to the discussion of how all the previous calculations can be repeated for three charges blocked on the dot. Actually, the fact that the $q = 3$ sector is the particle-hole symmetric to that defined by $q = 1$ allows us to readily derive all the desired results by making the following set of substitutions in all the expressions derived in Section 5.2.1.1

$$\mathbf{q = 1} \qquad\qquad \mathbf{q = 3} \tag{5.58a}$$

$$E_0 - E_1 = -\varepsilon_d \quad \rightarrow \quad E_4 - E_3 = \varepsilon_d + 2U, \tag{5.58b}$$

$$E_2 - E_1 = \varepsilon_d + U \quad \rightarrow \quad E_2 - E_3 = -\varepsilon_d - 3U, \tag{5.58c}$$

$$E_3 - E_1 = 2\varepsilon_d + 3U \quad \rightarrow \quad E_1 - E_3 = -2\varepsilon - 3U. \tag{5.58d}$$

The only point deserving a specific discussion is the derivation of the effective SU(4) symmetric action Eq. (5.19) from the para-fermion representation of the quantum dot states with the fields F_ν. We recall that the constraint Eq. (5.17) must be adapted upon the integration of the high energy slave-fields. In this case

$$\sum_\nu F_\nu^\dagger F_\nu = 1\,. \tag{5.59}$$

In this representation, the spin-exchange interaction reads

$$2\mathbf{S}\cdot\mathbf{s} = -\sum_{\nu\nu'} c_{k\nu}^\dagger c_{k'\nu'}\left(F_\nu^\dagger F_{\nu'} - \frac{1}{4}\delta_{\nu\nu'}\right). \tag{5.60}$$

This expression recovers the canonical one Eq. (E.2) with $q = 3$ if we use the substitution $F_\nu^\dagger F_{\nu'} = -g_{\nu'}^\dagger g_\nu$, where these last fermionic fields are submitted to the constraint

$$\sum_\nu g_\nu^\dagger g_\nu = 3\,. \tag{5.61}$$

5.3 Generalization to SU(N)

One may wonder whether it is possible to generalize Eq. (5.5) to the general SU(N) case. The SU(N) generalization of Eq. (5.3) states that charge relaxation resistance universality to $h/2Ne^2$ holds if all channels are symmetric, namely

$$\chi_\nu = \frac{\chi_c}{N}, \quad \forall\ \nu\,. \tag{5.62}$$

$\chi_c = \sum_\nu \chi_\nu$ is the usual total charge susceptibility and appears in the denominator of Eq. (5.3). The transformation Eq. (5.4) is then extended in the following way

$$\begin{pmatrix} \chi_c \\ \chi_1' \\ \vdots \\ \chi_{N-1}' \end{pmatrix} = \begin{pmatrix} 1 & 1 & \dots & \dots & 1 \\ & & \upsilon_1 & & \\ & & \vdots & & \\ & & \upsilon_{N-1} & & \end{pmatrix} \begin{pmatrix} \chi_1 \\ \chi_2 \\ \vdots \\ \chi_N \end{pmatrix}. \tag{5.63}$$

The first row vector $(1,1,\dots,1)$ of the transformation matrix gives χ_c and all the remaining vectors υ_i are orthogonal to it and normalized to N. The υ_i vectors define new susceptibilities χ_i' whose physical meaning cannot be determined a priori, but case by case depending on the physical problem in which SU(N) effective low energy symmetry appears. The resulting expression for the charge relaxation resistance reads

$$R_q = \frac{h}{2Ne^2}\left(1 + \frac{\sum_{i=1}^{N-1}\chi_i'^2}{\chi_c^2}\right). \tag{5.64}$$

The orthogonality of the υ_i vectors to $(1,1,\dots,1)$ ensures that every $\chi_i' = 0$ if the condition Eq. (5.62) applies, leading to the universal quantization of R_q.

5.4 Conclusions

In this chapter we illustrated a further application of our Fermi liquid approach to study the charge relaxation resistance in interacting systems displaying more exotic SU(4) symmetries. The possible generalization to the SU(N) case is also provided. Moreover, we show that it is possible to extend the slave-state representation of the quantum dot Hilbert space to carry out the calculation of the Kondo temperature and the dot charge occupation in SU(4) Kondo regimes. The results illustrate the generality of our approach, a tool for studying static and dynamical quantities in a variety of strongly interacting systems that cannot be accessed by perturbative calculations.

CONCLUSIONS AND PERSPECTIVES

In this Thesis, I addressed the electron dynamics of the quantum RC circuit considering the presence of strong electron-electron interactions on the quantum dot. We showed that, for a variety of situations, the low energy behavior of the quasi-particles of the system is governed by a time-dependent Fermi liquid Hamiltonian. This has to be coherent with the Friedel sum rule, establishing a connection between the phase acquired by electrons scattering on the dot and its charge occupation. We gave a formal proof of the derivation of the low energy effective Hamiltonian by devising path integral representations of these systems with the help of slave-states, allowing for diagrammatic calculations. This gave us a direct derivation of the low energy effective action by applying the analytical renormalization group. The main result of this study is the proof of a generalized Korringa-Shiba relation [75] leading to the many-channel formula Eq. (2.8) for the charge relaxation resistance in interacting systems. This formula provides a general explanation for the universal quantization of R_q. This holds if either particle-hole or SU(2) symmetry are not broken. This formula is also powerful as it allows for the investigation of R_q by calculating *static* quantities. It allowed us to predict and describe analytically the appearance of a giant peak in the charge relaxation resistance caused by the breaking of the Kondo singlet by a magnetic field. We characterized this peak in the full region of parameters solving numerically the Bethe ansatz equations for the ground state of the Anderson model. We extended then the renormalization group approach to the SU(4) Anderson model, predicting new behaviors of the giant charge relaxation resistance caused by the breaking of the SU(4) Kondo singlet by a magnetic field. Moreover our slave-state approach was also applied to access the analytical expression of the SU(4) Kondo temperature and the charge occupation of the quantum dot.

A problem which remains essentially open and not addressed by our work is the study of the effect of finite temperatures on the charge relaxation resistance in interacting quantum

dot circuits. What is expected is that, in the high temperature limit, coherence is progressively lost so that the universal quantization for the charge relaxation resistance is abandoned. This is verified in the non-interacting case in the framework of scattering theory [84]. How this situation is modified in the presence of interactions is a completely open issue. One of the main problems is that, at finite temperature, the $\omega \to 0$ and the $t \to 0$ limits do not commute. This prevents to resort to naive perturbative methods in the tunnel constant t to calculate $\chi_c(\omega)$, since divergences $\propto 1/\omega$ are then recovered in the subsequent $\omega \to 0$ limit for the dynamical charge susceptibility $\chi_c(\omega)$ [155, 156]. This requires to adopt non-perturbative methods for the calculation of the dynamical charge susceptibility. The spinless case, described by the Coulomb blockade model Eq. (iv), has been addressed in Refs. [68, 136]. The authors considered the Bethe-Salpeter equations for the dynamical charge susceptibility. The technical difficulties connected to their solution force them to use approximations killing quantum coherences. They thus obtained results which can be recovered from a master equation approach [68]. The spinful problem has also been addressed even in the case of fast quenches with real-time diagrammatic techniques [157, 158], highlighting the existence of different relaxation time-scales for the charge and the spin on the dot plus a third time scale which is independent of the level position and Coulomb interaction [67, 159]. An alternative approach would be to obtain the corrections to the general Korringa-Shiba relation Eq. (2.7) considering the finite temperatures corrections to the low energy effective Fermi liquid Hamiltonian provided in Eq. (2.10). Our analysis, relying on the generalized Korringa-Shiba relation Eq. (2.7), proves that the non-monotonous behaviors of R_q are caused by transitions to different ground-states of the quantum dot. Statistical mixtures of these states at finite temperatures are then supposed to weaken the dependence of R_q on the magnetic field. A quantitative analysis should consider the corrections to the Fermi liquid fixed point Hamiltonian Eq. (2.10) provided by Nozières' theory of the Kondo problem [121, 144, 160]. These appear as inelastic irrelevant contributions controlled by couplings $\propto \varepsilon/T_K$, ε being the energy of the incoming electrons. It is of interest to consider these terms in a perturbative approach and study how they would affect the universal quantization of the charge relaxation resistance. Would the suppression of the Kondo singlet at finite temperature be revealed by a giant peak in the charge relaxation resistance as in the case of the breaking of the SU(2) symmetry by a magnetic field? This question is interesting because, for static quantities, the temperature and the magnetic field play analog roles [61]. But R_q is a *dynamic* quantity and its universality relies on the effective non-interacting Fermi liquid theory valid for any magnetic field, but absolutely not for any temperature, which activates non-elastic processes for electrons scattering on the quantum dot.

Apart the problem of finite temperatures, the methods developed in this Thesis would find interesting applications to different situations. First of all it would be interesting to investigate in more detail situations in which non-Fermi liquid behaviors are possible as in the

two-channel case, close to charge degeneracy [70, 71] and in cases in which the Friedel sum rule does not hold. A low energy effective approach could still find fruitful application for new experiments which will soon find their realization in quantum devices. A first possibility could be found by considering charge relaxation dynamics in the case that lead electrons propagate in the edge states of a topological insulator. The case of the integer and fractional Hall effect have been already investigated [73, 74], and recent studies have considered quantum RC circuits in the quantum spin Hall regime [54]. The recent experimental realization of this topological insulator [27] has motivated a large effort in the study of quantum dot circuits predicting new exotic manifestations of Kondo physics [161] (which has been also recently predicted in 3D topological insulators [162]). It would be extremely interesting to investigate charge relaxation in the exotic low energies Kondo regimes discussed in the presence of interactions in the spin Hall edges [163]. In a completely different framework, recent experiments showing the possibility to probe quantum dot circuits by a microwave coherent signal [43, 44, 45, 46] give rise to new possibilities of research. The phase of the microwave signal has been shown to be sensitive to the manifestation of the Kondo ridge in the middle of the Coulomb diamond [43] and still requires a quantitative theory. This could be realized connecting our Fermi liquid approach for the quantum dot circuit with an input/output theory of the microwave signal [164]. Moreover, the transmitted classical signal in the resonator has been recently shown to be sensitive to the RC time of the quantum RC circuit [165]. The possibility to add artificial superconducting atoms with the resonators in these devices gives the possibility to synthesize quantum states of light in the resonator [41]. It would be then possible to study the driving of the quantum dot by a state in the gate which is not classical anymore. Moreover, it is also interesting to abandon the linear regime going towards purely out-of-equilibrium ones. The study of fast quenches on the gate voltage in the case of interacting dots it is still at its early stage [67, 159, 166] and it would constitute a necessary compendium of the studies dealing with non-interacting dots within Floquet's scattering theory [167]. This would be of interest to study the possibility of the emission of triggered fractional charges [168], in the edges of two-dimensional gases in the fractional quantum Hall regime, which has been for the moment predicted for Lorentzian voltage pulses in the edges [169].

APPENDIX

A Results of linear response theory

In this appendix we illustrate some further properties and results of linear response theory inspired by Ref. [170]. In A.1 we show that the real and the imaginary parts of the dynamical charge susceptibility Eq. (1.37) are respectively even and odd functions of the frequency, leading to Eq. (1.38). In A.2 we demonstrate that the power dissipation of the quantum RC circuit in the linear response regime is given by Eq. (2.2).

A.1 Parity of the dynamical charge susceptibility

The Lehman representation [98] of the dynamical charge susceptibility $\chi_c(\omega)$, defined in Eq. (1.37), readily access to its real and imaginary parts. This is obtained from the Fourier transform of Eq. (1.37)

$$\chi_c(\omega) = \frac{i}{\hbar}\int_{-\infty}^{\infty} d(t-t')e^{i(\omega+i0^+)(t-t')}\theta(t-t')\left\langle\left[\hat{n}(t),\hat{n}(t')\right]\right\rangle_0, \tag{A.1}$$

where the factor $i0^+$ must be inserted to regularize retarded functions. Inserting the closure relation with the eigenstates $|n\rangle$ of energy E_n of the time independent Hamiltonian H_0, the averages can be cast into the form

$$\langle\hat{n}(t)\hat{n}(t')\rangle_0 = \sum_{n,m} p_n e^{i\omega_{nm}(t-t')}N_{nm}N_{mn}, \tag{A.2}$$

where $p_n = e^{-\beta E_n}/Z$ is the Boltzmann weight, $\hbar\omega_{nm} = E_n - E_m$ and $N_{nm} = \langle n|\,\hat{n}\,|m\rangle$ the matrix elements of the dot occupation. In this representation, the Fourier transform in Eq. (A.1) is readily carried out giving

$$\chi_c(\omega) = -\frac{1}{\hbar}\sum_{nm} p_n N_{nm}N_{mn}\left(\frac{1}{\omega+i0^+ +\omega_{nm}} - \frac{1}{\omega+i0^+ -\omega_{nm}}\right). \tag{A.3}$$

Applying the relation

$$\frac{1}{x\pm i0^+} = \mathrm{P}\left[\frac{1}{x}\right] \mp i\pi\delta(x), \tag{A.4}$$

with $\mathrm{P}[f(x)]$ the principal value of the function $f(x)$, the real and imaginary part of $\chi_c(\omega)$ are readily obtained

$$\mathrm{Re}\left[\chi_c(\omega)\right] = -\frac{1}{\hbar}\sum_{nm} p_n N_{nm}N_{mn}\left\{\mathrm{P}\left[\frac{1}{\omega+\omega_{nm}}\right] - \mathrm{P}\left[\frac{1}{\omega-\omega_{nm}}\right]\right\}, \tag{A.5}$$

$$\mathrm{Im}\left[\chi_c(\omega)\right] = \frac{i\pi}{\hbar}\sum_{nm} p_n N_{nm}N_{mn}\Big\{\delta\big(\omega+\omega_{nm}\big) - \delta\big(\omega-\omega_{nm}\big)\Big\}, \tag{A.6}$$

which are respectively even and odd functions of ω.

A.2 Energy dissipation in the linear response regime

The time dependence of the Hamiltonian Eq. (1.31) is caused by the presence of an external drive, more precisely the gate potential $V_g(t)$. In the situation of Chapter 2, the time dependence of orbital energies in the dot is given by $\varepsilon_d(t) = \varepsilon_d^0 + \varepsilon_\omega \cos(\omega t)$. In the time unit, the systems dissipates the energy

$$\delta W = \delta \langle \hat{n} \rangle \, \varepsilon_\omega \cos\big(\omega t\big). \tag{A.7}$$

In the permanent regime the average power $\mathscr{P}$ dissipated by the system during the time period T is then

$$\mathscr{P} = \frac{\varepsilon_\omega}{T} \int_0^T dt \, \frac{d \langle \hat{n}(t) \rangle}{dt} \cos(\omega t). \tag{A.8}$$

Neglecting constant contributions, the average $\langle \hat{n}(t) \rangle$ is given by the dynamical charge susceptibility Eq. (1.37)

$$\langle \hat{n}(t) \rangle = \varepsilon_\omega \int_{-\infty}^{\infty} dt' \chi_c(t - t') \cos(\omega t). \tag{A.9}$$

Substituting this expression in Eq. (A.8), we obtain

$$\mathscr{P} = -i\omega \frac{\varepsilon_\omega^2}{4} \big[\chi_c(\omega) - \chi_c(-\omega)\big] + i\omega \frac{\varepsilon_\omega^2}{T} \int_0^T dt \frac{\chi_c(-\omega) e^{2i\omega t} - \chi_c(\omega) e^{-2i\omega t}}{4}. \tag{A.10}$$

Expressing $\chi_c(\omega) = \mathrm{Re}\big[\chi_c(\omega)\big] + i\mathrm{Im}\big[\chi_c(\omega)\big]$ as the sum of its real and imaginary part and applying the parity properties demonstrated in A.1, the first term recovers Eq. (2.2) for the dissipated power

$$\mathscr{P} = \frac{1}{2} \varepsilon_\omega^2 \omega \mathrm{Im}\big[\chi_c(\omega)\big], \tag{A.11}$$

while the second term in Eq. (A.10) reduces to vanishing integrals of $\sin(2\omega t)$ and $\cos(2\omega t)$ over their period. In the case of Section 2.4, we have the same problem with $\langle \delta \hat{n} \rangle$ in Eq. (A.7) replaced by $\langle \hat{A} \rangle$, with the operator $\hat{A}$ given in Eq. (2.53). Repeating the same steps of this discussion we obtain the power dissipated by the low energy effective Fermi liquid Eq. (2.51)

B Multi resonant level model

In this section we carry out the calculation of the quantum dot density of states in the case of a single channel and an infinity of levels in the quantum dot. The action of the system reads

$$S=\sum_{i\omega_n}\left\{-\sum_k c_k^\dagger G_k^{-1}(i\omega_n)c_k-\sum_l d_l^\dagger D_l^{-1}(i\omega_n)d_l+t\sum_{kl}\left[c_k^\dagger d_l+d_l^\dagger c_k\right]\right\}, \tag{B.1}$$

with

$$\begin{aligned} G_k^{-1}(i\omega_n)&=i\omega_n-\varepsilon_k\,,\\ D_l^{-1}(i\omega_n)&=i\omega_n-\varepsilon_l\,. \end{aligned} \tag{B.2}$$

The integration of the lead electron modes is Gaussian leading to the effective action

$$S'=\sum_{i\omega_n}\left\{-\sum_l d_l^\dagger(i\omega_n)D_l^{-1}(i\omega_n)d_l(i\omega_n)+t^2\sum_k G_k(i\omega_n)\sum_{ll'}d_l^\dagger(i\omega_n)d_{l'}(i\omega_n)\right\}. \tag{B.3}$$

Applying Wick's theorem the full propagator of the dot electrons is readily obtained

$$\mathscr{D}_{ll'}(i\omega_n)=\delta_{ll'}D_l(i\omega_n)+D_l(i\omega_n)D_{l'}(i\omega_n)\frac{\gamma(i\omega_n)}{1-\gamma(i\omega_n)\Theta(i\omega_n)}\,, \tag{B.4}$$

where we defined

$$\gamma(i\omega_n)=t^2\sum_k G_k(i\omega_n)\,,\qquad\qquad \Theta(i\omega_n)=\sum_l D_l(i\omega_n)\,. \tag{B.5}$$

In the wide band limit $\gamma(i\omega_n)=-i\Gamma\mathrm{sgn}(i\omega_n)$. Our aim is to calculate the static susceptibility χ_c of the charge on the dot. The charge on the dot is given by

$$\begin{aligned} \langle\hat{Q}\rangle=e\sum_l\langle d_l^\dagger d_l\rangle=\frac{e}{\beta}\sum_{l,i\omega_n}e^{i\omega_n 0^+}\mathscr{D}_{ll}(i\omega_n)=\\ =\frac{e}{2\pi i}\sum_l\int_{-\infty}^{\infty}d\varepsilon\, f(\varepsilon)\left[\mathscr{D}_{ll}(\varepsilon+i0^+)-\mathscr{D}_{ll}(\varepsilon-i0^+)\right]. \end{aligned} \tag{B.6}$$

We write the energy spectrum on the dot as $\varepsilon_l=-eV_g+l\Delta$, with $l\in\mathbb{Z}$ and Δ the level spacing. Eq. (B.4) is then a function of $\varepsilon+eV_g$. Shifting all energies by eV_g, the differential capacitance $C_0=-\partial\hat{Q}/\partial V_g$ is readily obtained at zero temperature

$$C_0=\frac{e^2}{2\pi i}\sum_l\left[\mathscr{D}_{ll}(eV_g+i0^+)-\mathscr{D}_{ll}(eV_g-i0^+)\right], \tag{B.7}$$

with

$$\begin{aligned}\mathscr{D}_{ll}(eV_g \pm i0^+) &= \frac{1}{eV_g - l\Delta} \mp \frac{1}{(eV_g - l\Delta)^2} \frac{i\Gamma}{1 \pm i\Gamma \left[\sum_p \frac{1}{eV_g - p\Delta}\right]} \\ &= \frac{1}{\Delta}\left\{\frac{1}{x+l} \mp \frac{i\Gamma/\Delta}{(x+l)^2} \frac{1}{1 \pm i\pi\frac{\Gamma}{\Delta}\coth(\pi x)}\right\},\end{aligned} \tag{B.8}$$

where $x = eV_g/\Delta$ and we exploited the following result

$$\sum_l \frac{1}{x+l} = \Psi_0(1-x) - \Psi_0(x) = \pi\coth(\pi x), \tag{B.9}$$

with $\Psi_0(x)$ the digamma function. Substituting this expression in Eq. (B.7), the sum over levels can be also carried out, leading to

$$C_0 = e^2\frac{\pi\Gamma}{2\Delta^2}\frac{1}{\sin^2\left(\pi\frac{eV_g}{\Delta}\right)}\left[\frac{1}{1+i\pi\frac{\Gamma}{\Delta}\coth\left(\pi\frac{eV_g}{\Delta}\right)} + \frac{1}{1-i\pi\frac{\Gamma}{\Delta}\coth\left(\pi\frac{eV_g}{\Delta}\right)}\right], \tag{B.10}$$

where the following identity has been used

$$\sum_l \frac{1}{(l+x)^2} = \Psi_1(1-x) - \Psi_1(x) = \frac{\pi^2}{\sin^2(\pi x)}, \tag{B.11}$$

with $\Psi_n(x)$ the polygamma function. Some algebra leads to

$$C_0 = \frac{e^2}{\Delta}\frac{2}{\frac{\Delta}{\pi\Gamma} + \frac{\pi\Gamma}{\Delta} - (\frac{\Delta}{\pi\Gamma} - \frac{\pi\Gamma}{\Delta})\cos\left(\frac{2\pi eV_g}{\Delta}\right)}, \tag{B.12}$$

that, identifying term by term with Eq. (1.25), leads to the mapping Eq. (1.59).

C Scattering theory and phase-shift

The T-matrix encodes all the information about the effects of the quantum dot on the propagation of lead electrons. It is an improper self-energy for the resolvent of the lead electrons appearing in a slightly modified form of the Dyson equation

$$G(z) = G^0(z) + G^0(z)\,T(z)\,G^0(z)\,, \tag{C.1}$$

$$G(z) = \frac{1}{z-H}\,, \tag{C.2}$$

where z is a complex number. G_0 is the free resolvent describing electrons unperturbed by potential scattering

$$G^0_{kk'}(z) = \langle k|\, G^0(z)\,\big|k'\rangle = \frac{\delta_{kk'}}{z-\varepsilon_k}, \tag{C.3}$$

the $|k\rangle$ states being the single particle eigenvectors of the unperturbed Hamiltonian. In the absence of electron-electron interactions, the resolvent and the retarded Green's function coincide and the definition of Eq. (C.1) implies Eq. (2.17).

The definition of the phase-shift in Eqs. (2.17) and (2.18) can be generalized as

$$\delta = \arg\left[T(\omega + i0^+)\right] \tag{C.4}$$

and it is clear within scattering theory [171, 172]. This describes the situation shown in Fig. C, in which an electron wave packet enters in the scattering region at time $t = 0$. We can approximate the time of emission and detection of this wave packet as the far past and future, respectively $t = -\infty$ and $t = +\infty$. Close to detection and emission, it is reasonable to assume that the wave packet does not feel the presence of the scatterer, whose interaction range is delimited inside the dashed line in Fig. C. In these situations, the electron wave function is an asymptotic superposition of *free* plane waves. If we define the IN and OUT states $\big|\Psi^{\pm}\rangle$, the eigenvectors of energy ε of the Hamiltonian of the whole system, including the scattering region, as the states coinciding asymptotically with free plane waves in the past and in the future respectively, the S matrix gives the overlap between the two

$$S_{kk'}(\varepsilon) = \langle \Psi^-_k \big|\, \Psi^+_{k'}\rangle\,, \tag{C.5}$$

where k and k' are the momenta of the OUT and IN states. The T matrix is related to the S matrix through [171, 172]

$$S_{kk'} = \delta_{kk'} - 2\pi i\delta(\varepsilon_k - \varepsilon_{k'})\,T_{kk'}. \tag{C.6}$$

The S matrix is unitary and in the single channel case it is given by a phase $S(\varepsilon) = e^{2i\delta(\varepsilon)}$. δ is then exactly the phase-shift caused by the scattering onto the impurity of the conduction

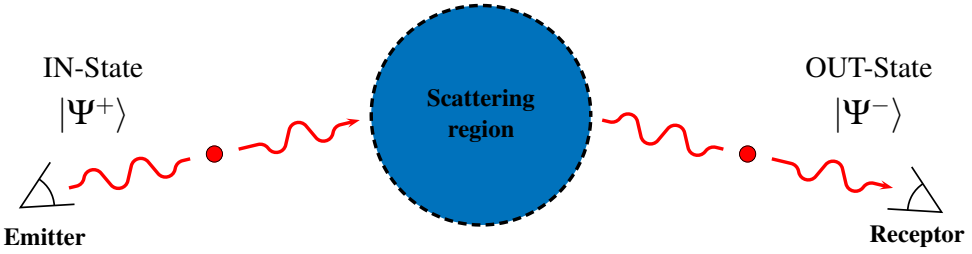

Figure C: Illustration of the physical situation described by the scattering formalism. Electron wave packets are emitted in the IN-State $|\Psi^+\rangle$ and then measured in the OUT-state $|\Psi^-\rangle$ once they have passed through the scattering region.

electrons. Switching then to the resolution in energy of the eigenstates of the system, Eq. (C.6) becomes

$$S(\varepsilon) = 1 - 2\pi i \nu_0 T(\varepsilon). \tag{C.7}$$

Applying this result for the resonant level model where the T-matrix is given by Eq. (2.17), we show that the δ defined in Eq. (2.18) coincides with the phase-shift of the OUT state with respect to the IN state

$$S(\omega) = e^{2i\delta} = \frac{\omega - \varepsilon_d - i\Gamma}{\omega - \varepsilon_d + i\Gamma}. \tag{C.8}$$

In Appendix D, we also check that the same kind of arguments applies for the potential scattering Hamiltonian Eq. (2.10). In general the condition $S(\varepsilon) = e^{2i\delta(\varepsilon)}$ is always verified if we take the definition of the phase-shift directly from the T-matrix

$$T = -\frac{1}{\pi \nu_0} \sin\delta e^{i\delta}. \tag{C.9}$$

D T-matrix in the potential scattering Hamiltonian

The potential scattering Hamiltonian Eq. (2.10) is non-interacting. In this case, the resolvent of the lead electrons coincides with their Green's function which can be easily obtained within the path integral formalism. Considering the action of the system

$$S = \sum_{i\omega_n,k,\sigma} c^\dagger_{k\sigma}(i\omega_n)(-i\omega_n + \varepsilon_k)c_{k\sigma}(i\omega_n) + W(\varepsilon_d)\sum_{k\neq k'} c^\dagger_{k\sigma}(i\omega_n)c_{k'\sigma}(i\omega_n)\,, \tag{D.1}$$

The Green's function is obtained by expanding the exponential of the action in the coupling W. One can notice that the series so obtained takes the form

$$G_{kk'} = \frac{\delta_{kk'}}{z-\epsilon_k} + \frac{1}{z-\epsilon_k}\frac{1}{z-\epsilon_{k'}}W(1+\Sigma(z)+\Sigma^2(z)+\Sigma^3(z)+\ldots)\,, \tag{D.2}$$

$$\Sigma(z) = \sum_k \frac{W}{z-\epsilon_k}. \tag{D.3}$$

The T-matrix reads then

$$T(z) = \frac{t}{1-\Sigma(z)}. \tag{D.4}$$

Taking the typical analytical continuation $z \to \omega + i0^+$ and a constant wide band density of states ν_0 for lead electrons we obtain

$$T(\omega+i0^+) = \frac{W}{1+i\pi\nu_0 W} = \frac{W}{\sqrt{1+(\pi\nu_0 W)^2}}e^{i\delta}\,, \tag{D.5}$$

with the phase-shift Eq. (2.21). Substituting Eq. (D.5) in Eq. (C.7), we find again $S = e^{2i\delta}$, accordingly with Eq. (C.8).

E Fundamental representation of the SU(N) group

The explicit form of the fundamental representation of the SU(4) group can be found in Ref. [173]:

$$\lambda_1 = \begin{pmatrix} 0 & 1 & 0 & 0 \\ 1 & 0 & 0 & 0 \\ 0 & 0 & 0 & 0 \\ 0 & 0 & 0 & 0 \end{pmatrix}, \quad \lambda_2 = \begin{pmatrix} 0 & -i & 0 & 0 \\ i & 0 & 0 & 0 \\ 0 & 0 & 0 & 0 \\ 0 & 0 & 0 & 0 \end{pmatrix}, \quad \lambda_1 = \begin{pmatrix} 1 & 0 & 0 & 0 \\ 0 & -1 & 0 & 0 \\ 0 & 0 & 0 & 0 \\ 0 & 0 & 0 & 0 \end{pmatrix},$$

$$\lambda_4 = \begin{pmatrix} 0 & 0 & 1 & 0 \\ 0 & 0 & 0 & 0 \\ 1 & 0 & 0 & 0 \\ 0 & 0 & 0 & 0 \end{pmatrix}, \quad \lambda_5 = \begin{pmatrix} 0 & 0 & -i & 0 \\ 0 & 0 & 0 & 0 \\ i & 0 & 0 & 0 \\ 0 & 0 & 0 & 0 \end{pmatrix}, \quad \lambda_6 = \begin{pmatrix} 0 & 0 & 0 & 0 \\ 0 & 0 & 1 & 0 \\ 0 & 1 & 0 & 0 \\ 0 & 0 & 0 & 0 \end{pmatrix},$$

$$\lambda_7 = \begin{pmatrix} 0 & 0 & 0 & 0 \\ 0 & 0 & -i & 0 \\ 0 & i & 0 & 0 \\ 0 & 0 & 0 & 0 \end{pmatrix}, \quad \lambda_8 = \frac{1}{\sqrt{3}} \begin{pmatrix} 1 & 0 & 0 & 0 \\ 0 & 1 & 0 & 0 \\ 0 & 0 & -2 & 0 \\ 0 & 0 & 0 & 0 \end{pmatrix}, \quad \lambda_9 = \begin{pmatrix} 0 & 0 & 0 & 1 \\ 0 & 0 & 0 & 0 \\ 0 & 0 & 0 & 0 \\ 1 & 0 & 0 & 0 \end{pmatrix}, \tag{E.1}$$

$$\lambda_{10} = \begin{pmatrix} 0 & 0 & 0 & -i \\ 0 & 0 & 0 & 0 \\ 0 & 0 & 0 & 0 \\ i & 0 & 0 & 0 \end{pmatrix}, \quad \lambda_{11} = \begin{pmatrix} 0 & 0 & 0 & 0 \\ 0 & 0 & 0 & 1 \\ 0 & 0 & 0 & 0 \\ 0 & 1 & 0 & 0 \end{pmatrix}, \quad \lambda_{12} = \begin{pmatrix} 0 & 0 & 0 & 0 \\ 0 & 0 & 0 & -i \\ 0 & 0 & 0 & 0 \\ 0 & i & 0 & 0 \end{pmatrix},$$

$$\lambda_{13} = \begin{pmatrix} 0 & 0 & 0 & 0 \\ 0 & 0 & 0 & 0 \\ 0 & 0 & 0 & 1 \\ 0 & 0 & 1 & 0 \end{pmatrix}, \quad \lambda_{14} = \begin{pmatrix} 0 & 0 & 0 & 0 \\ 0 & 0 & 0 & 0 \\ 0 & 0 & 0 & -i \\ 0 & 0 & i & 0 \end{pmatrix}, \quad \lambda_{15} = \frac{1}{\sqrt{6}} \begin{pmatrix} 1 & 0 & 0 & 0 \\ 0 & 1 & 0 & 0 \\ 0 & 0 & 1 & 0 \\ 0 & 0 & 0 & -3 \end{pmatrix}.$$

It is straightforward to check that

$$2 \sum_{\mu\mu'\nu\nu'} \mathbf{S}_{\nu\nu'} \cdot \mathbf{T}_{\mu\mu'} c^\dagger_\mu c_{\mu'} d^\dagger_\nu d_{\nu'} = \sum_{\mu\mu'} c^\dagger_\nu c_{\nu'} \left(d^\dagger_{\nu'} d_\nu - \frac{q}{N} \delta_{\nu\nu'} \right), \tag{E.2}$$

if one sets $\sum_\nu d^\dagger_\nu d_\nu = q$. The d and c operators are fermions. It is also useful to mention that the fundamental representation of the SU(N) group satisfies the following relation

$$T_a T_b = \frac{1}{2N} \delta_{ab} \mathbb{1} + \frac{1}{2} \left(i f_{abc} + d_{abc} \right) T_c, \tag{E.3}$$

where

$$d_{acd} d_{bcd} = \frac{N^2 - 4}{N} \delta_{ab}, \tag{E.4}$$

$$f_{acd} f_{bcd} = N \delta_{ab}, \tag{E.5}$$

with the following consequences

$$\begin{aligned} S_i S_j T_i T_j &= -\frac{1}{N}\mathbf{S}\cdot\mathbf{T} + \frac{N^2-1}{4N}\mathbb{1}, \\ S_i S_j T_j T_i &= \frac{N^2-2}{2N}\mathbf{S}\cdot\mathbf{T} + \frac{N^2-1}{4N}\mathbb{1}. \end{aligned} \tag{E.6}$$

F Contributions to $\mathcal{V}^R$ in the Coulomb blockade model

All the contributions corresponding to the diagrams of Figs. 3.7 and 3.10 are listed below (with $\mathscr{C} = N\nu_0^3 t^4$)

$$\begin{aligned}
\mathcal{V}_1 &= -\mathscr{C}\int d\varepsilon_1 d\varepsilon_2 \frac{\varepsilon_1}{(\varepsilon_2+E_1)^2(\varepsilon_1+\varepsilon_2)},\\
\mathcal{V}_2 &= \mathscr{C}\int d\varepsilon_1 d\varepsilon_2 \frac{\varepsilon_1}{(\varepsilon_1+E_1)^2(\varepsilon_1+\varepsilon_2)},\\
\mathcal{V}_3 &= \mathscr{C}\int d\varepsilon_1 d\varepsilon_2 \frac{\varepsilon_1}{(\varepsilon_2+E_{-1})^2(\varepsilon_1+\varepsilon_2)},\\
\mathcal{V}_4 &= -\mathscr{C}\int d\varepsilon_1 d\varepsilon_2 \frac{\varepsilon_1}{(\varepsilon_1+E_{-1})^2(\varepsilon_1+\varepsilon_2)},\\
\mathcal{V}_5 &= -2\mathscr{C}\int d\varepsilon_1 d\varepsilon_2 \frac{\varepsilon_1}{(\varepsilon_1+\varepsilon_2)(\varepsilon_2+E_1)(\varepsilon_1+E_{-1})},\\
\mathcal{V}_6 &= 2\mathscr{C}\int d\varepsilon_1 d\varepsilon_2 \frac{\varepsilon_1}{(\varepsilon_1+\varepsilon_2)(\varepsilon_1+E_1)(\varepsilon_2+E_{-1})},\\
\mathcal{V}_7 &= -\mathscr{C}\int d\varepsilon_1 d\varepsilon_2 \frac{\varepsilon_1}{(\varepsilon_2+E_1)^2(\varepsilon_1+\varepsilon_2+E_2)},\\
\mathcal{V}_8 &= -\mathscr{C}\int d\varepsilon_1 d\varepsilon_2 \frac{\varepsilon_1}{(\varepsilon_1+E_1)^2(\varepsilon_1+\varepsilon_2+E_2)},\\
\mathcal{V}_9 &= -2\mathscr{C}\int d\varepsilon_1 d\varepsilon_2 \frac{\varepsilon_1}{(\varepsilon_2+E_1)(\varepsilon_1+\varepsilon_2+E_2)(\varepsilon_1+E_1)},\\
\mathcal{V}_{10} &= \mathscr{C}\int d\varepsilon_1 d\varepsilon_2 \frac{\varepsilon_1}{(\varepsilon_2+E_{-1})^2(\varepsilon_1+\varepsilon_2+E_{-2})},\\
\mathcal{V}_{11} &= \mathscr{C}\int d\varepsilon_1 d\varepsilon_2 \frac{\varepsilon_1}{(\varepsilon_1+E_{-1})^2(\varepsilon_1+\varepsilon_2+E_{-2})},\\
\mathcal{V}_{12} &= 2\mathscr{C}\int d\varepsilon_1 d\varepsilon_2 \frac{\varepsilon_1}{(\varepsilon_1+E_{-1})(\varepsilon_1+\varepsilon_2+E_{-2})(\varepsilon_2+E_{-1})},
\end{aligned} \tag{F.1}$$

where integrals run over the $\varepsilon_{1,2} > 0$ domain, to which the contributions of Eq. (3.50) and Eq. (3.51) must be added. Whereas each term in Eqs. (3.50) and (3.51) suffers from an UV divergence, the summation over all contributions is finite and does not depend on the cutoff procedure. We shall adopt a sharp cutoff at energy D_0 in the following. Moreover, the calculation exhibits a particle-hole symmetry: for example, $\mathcal{V}_3$ can be viewed as the symmetric of $\mathcal{V}_1$, they have opposite sign and E_n exchanged with E_{-n}. The result will then be necessarily of the form $A[\varepsilon_d] - A[-\varepsilon_d]$, which implies that any constant independent of ε_d will be ignored during calculations. The dilogarithm function appears

$$Li_2(z) = \int_z^0 dt \frac{\ln(1-t)}{t}, \tag{F.2}$$

and the following equalities will be exploited

$$Li_2(x) + Li_2(1-x) = \frac{\pi^2}{6} - \ln x \ln(1-x), \tag{F.3a}$$

$$Li_2(x) + Li_2\left(\frac{1}{x}\right) = \frac{\pi^2}{3} - \frac{1}{2}\ln^2 x - i\pi \ln x, \ \ (x \geq 1). \tag{F.3b}$$

As an intermediate step, we find (we omit the $\mathscr{C} = N\nu_0^3 t^4$ factor)

$$\begin{aligned}
\mathcal{V}_1 + \mathcal{V}_2 &= -\frac{D_0}{E_1} - 2\ln E_1 \ln D_0 + \ln^2 D_0 \\
&\quad - 2\ln D_0 + \ln^2 E_1 + 2\ln E_1, \\
\mathcal{V}_7 + \mathcal{V}_8 &= -\frac{D_0}{E_1} + \frac{E_2}{E_1}\ln D_0 + \\
&\quad \frac{1}{E_1(E_2 - E_1)}(E_1 E_2 \ln E_1 - E_2^2 \ln E_2), \\
\mathcal{V}_5 + \mathcal{V}_6 + \mathcal{V}'' &= -\frac{\varepsilon_d}{E_c}\pi^2 - \frac{\varepsilon_d}{E_c}\ln^2\frac{E_1}{E_{-1}} + 2\ln\frac{E_1}{E_{-1}}, \\
\mathcal{V}_9 &= 2\ln E_1 \ln D_0 - \ln^2 D_0 + \frac{E_1}{E_c}\ln^2 E_1 \\
&\quad - \frac{E_1}{E_c}\frac{\pi^2}{2} + \frac{E_2}{E_c}\frac{\pi^2}{6} + \frac{E_2}{E_c} Li_2\left(\frac{E_2 - E_1}{E_2}\right) \\
&\quad + \frac{E_2}{2E_c}\ln^2 E_2 - \frac{E_2}{E_c}\ln E_1 \ln E_2,
\end{aligned}$$

with the contribution of Eq. (3.50)

$$\mathcal{V}' = \nu_0 t^2 \ln\frac{E_1}{E_{-1}} + N\nu_0^3 t^4 \left(\mathcal{V}'_a + \mathcal{V}'_b\right), \tag{F.4}$$

$$\begin{aligned}
\mathcal{V}'_a &= \int d\varepsilon_1 d\varepsilon_2 \frac{1}{(\varepsilon_2 + E_1)}\left(\frac{\varepsilon_1}{(\varepsilon_1 + E_1)} + \frac{\varepsilon_1}{(\varepsilon_1 + E_{-1})}\right) \\
&= \frac{2D_0}{E_1} - \ln D_0 - \frac{E_{-1}}{E_1}\ln D_0 + \ln E_1 + \frac{E_{-1}}{E_1}\ln E_{-1},
\end{aligned} \tag{F.5}$$

where $\mathcal{V}'_b$ is obtained from $\mathcal{V}'_a$ by particle-hole symmetry. It can be checked explicitly that the terms depending on the cutoff D_0 in the above expressions cancel out when the summation

over all contributions is carried out. One is left with

$$\begin{aligned}
\mathcal{V}_1 + \mathcal{V}_2 &= \ln^2 E_1 + 2\ln E_1, \\
\mathcal{V}_7 + \mathcal{V}_8 &= \frac{1}{E_1(E_2 - E_1)}(E_1 E_2 \ln E_1 - E_2^2 \ln E_2), \\
\mathcal{V}_a' &= \ln E_1 + \frac{E_{-1}}{E_1}\ln E_{-1}, \\
\mathcal{V}_5 + \mathcal{V}_6 + \mathcal{V}'' &= -\frac{\varepsilon_d}{E_c}\pi^2 - \frac{\varepsilon_d}{E_c}\ln^2\frac{E_1}{E_{-1}} + 2\ln\frac{E_1}{E_{-1}}, \\
\mathcal{V}_9 &= \frac{E_1}{E_c}\ln^2 E_1 - \frac{E_1}{E_c}\frac{\pi^2}{2} + \frac{E_2}{E_c}\frac{\pi^2}{6} + \frac{E_2}{2E_c}\ln^2 E_2 \\
&\quad + \frac{E_2}{E_c} Li_2\left(\frac{E_2 - E_1}{E_2}\right) - \frac{E_2}{E_c}\ln E_1 \ln E_2.
\end{aligned}$$

Adding the particle-hole symmetric terms ($\mathcal{V}_{3,4,10,11,12}$ and $\mathcal{V}_b'$), one finally arrives at Eq. (3.2).

G Bethe ansatz equations for the Anderson model

The system reads (we follow the notations of Ref. [139])

$$\rho(k)+g'(k)\int_{-\infty}^{B}dp\rho(p)R[g(k)-g(p)]+g'(k)\int_{-\infty}^{Q}d\lambda\sigma(\lambda)s[g(k)-\lambda]=\mathscr{S}^{\rho}(k), \tag{G.1}$$

$$\sigma(\lambda)-\int_{-\infty}^{Q}d\lambda'\sigma(\lambda')R(\lambda-\lambda')+\int_{-\infty}^{B}dk\rho(k)s[\lambda-g(k)]=\mathscr{S}^{\sigma}(\lambda), \tag{G.2}$$

with the source terms given by

$$\mathscr{S}^{\rho}(k)=\frac{1}{2\pi}\left\{1+g'(k)\int_{-\infty}^{\infty}dpR[g(k)-g(p)]\right\}+\frac{1}{L}\left\{\Delta(k)+g'(k)\int_{-\infty}^{\infty}dp\Delta(p)R[g(k)-g(p)]\right\}, \tag{G.3}$$

$$\mathscr{S}^{\sigma}(\lambda)=\int_{-\infty}^{\infty}dks(\lambda-g(k))\left[\frac{1}{2\pi}+\frac{\Delta(k)}{L}\right]. \tag{G.4}$$

We have introduced the functions

$$R(x)=\frac{1}{2\pi}\int_{-\infty}^{\infty}d\omega\frac{e^{-i\omega x}}{1+e^{|\omega|}}, \qquad s(x)=\frac{1}{2\cosh(\pi x)}, \tag{G.5}$$

$$g(k)=\frac{k-\varepsilon_d-U/2}{2U\Gamma}, \qquad \Delta(k)=\frac{\Gamma}{\pi}\frac{1}{(k-\varepsilon_d)^2+\Gamma^2}. \tag{G.6}$$

L is the size of the system and the spinon and holon densities can be split in a conduction and impurity (dot) part

$$\rho(k)=\rho_c(k)+\frac{\rho_i(k)}{L}, \qquad \sigma(\lambda)=\sigma_c(\lambda)+\frac{\sigma_i(\lambda)}{L}. \tag{G.7}$$

The linearity of Eqs. (G.1) and (G.2) implies that the conduction and impurity terms decouple. The former sets the macroscopic properties of the system, *i.e.* the global Zeeman energy H and the position of the valence level ε_d,

$$\frac{H}{2\pi}=\int_{-\infty}^{B}dk\rho_c(k), \qquad \frac{1}{\pi}\left(\varepsilon_d+\frac{U}{2}\right)=\int_{-\infty}^{Q}d\lambda\sigma_c(\lambda), \tag{G.8}$$

while the latter gives the occupancy $\langle\hat{n}\rangle$ and the magnetization $\langle\hat{m}\rangle$ of the dot, namely

$$\langle\hat{m}\rangle=\frac{1}{2}\int_{-\infty}^{B}dk\rho_i(k), \qquad \langle\hat{n}\rangle=1-\int_{-\infty}^{Q}d\lambda\sigma_i(\lambda). \tag{G.9}$$

These equations hold exclusively for $\varepsilon_d\geq -U/2$ and $H\geq 0$, while the results for $\varepsilon_d<-U/2$ are obtained by particle-hole symmetry. The zero magnetic field case $H=0$ and the particle-hole symmetric point $\varepsilon_d=-U/2$ are obtained by setting B and Q respectively to $-\infty$. In these cases, the Bethe ansatz equations for ρ and σ decouple and an analytical solution can be constructed on the basis of the Wiener-Hopf method [78]. This decoupling results in a complete separation of spin and charge degrees of freedom of the dot, see Eqs. (G.9), a striking feature of one dimensional quantum systems [174].

H Calculations for the SU(4) renormalized vertex

In this Appendix we give the details about the calculations carried out in Chapter 5 in the different charge sectors defined by the number q of charges blocked on the quantum dot.

H.1 Sector with $q = 1$

H.1.1 Mean-field analysis

Here we carry out the mean-field analysis of the last term in Eq. (5.30), quartic in the lead electron fields, leading to Eq. (5.33). The last term in Eq. (5.30) can be written explicitly in the frequency representation

$$t^4 \mathrm{Tr}\left[\mathbf{w}^\dagger \cdot B_2 \cdot \mathbf{A}_2 \cdot B_2 \cdot \mathbf{w}\right] = \frac{t^4}{\beta^2} \sum B_2(i\omega_1 + i\omega_2 - i\omega_3 + i\Omega_1 - i\Omega_2) D_3(i\omega_1 + i\omega_2 + i\Omega_1) B_2(i\omega_1 + i\Omega_1) \times c^\dagger_{k\alpha}(i\omega_D) c^\dagger_{k'\beta}(i\omega_3) c_{k''\gamma}(i\omega_2) c_{k'''\delta}(i\omega_1) f^\dagger_\nu(i\Omega_2) f_{\nu'}(i\Omega_1) . \quad \text{(H.1)}$$

The sum runs over all frequencies and momenta and $i\omega_D = i\omega_1 + i\omega_2 - i\omega_3 + i\Omega_1 - i\Omega_2$ to ensure energy conservation. The sum over orbital labels is set by the specific algebraic form of $\mathbf{A}_2$ and $\mathbf{w}$ in Eqs. (5.24) and (5.26) respectively. The mean-field analysis simply requires to contract two of the lead electron operators in Eq. (H.1) and replace them by their unperturbed propagator, for instance

$$\overbrace{c^\dagger_{k\alpha}(i\omega_D) c^\dagger_{k'\beta}(i\omega_3) c_{k''\gamma}(i\omega_2)} c_{k'''\delta}(i\omega_1) f^\dagger_\tau(i\Omega_2) f_{\tau'}(i\Omega_1) = - G_k(i\omega_2) c^\dagger_{k'\beta}(i\omega_1 + i\Omega_1 - i\Omega_2) c_{k'''\delta}(i\omega_1) f^\dagger_\nu(i\Omega_2) f_{\nu'}(i\Omega_1) \quad \text{(H.2)}$$

the minus coming from the commutation relations of Grassmann variables. Recalling the discussion in Section 3.3.3, we can expand the frequency dependence of the propagators appearing in Eq. (H.1) close to the fixed point frequencies $i\omega$ for lead electrons and $i\omega_\Lambda$ for dot para-fermions. To leading order, all frequency dependence is irrelevant and can be neglected. The result has always the form

$$V = A_n \times \frac{t^4}{\beta} \sum c^\dagger_{k\mu}(i\omega_1 + i\Omega_1 - i\Omega_2) c_{k'\mu'}(i\omega_1) f^\dagger_\nu(i\Omega_2) f_{\nu'}(i\Omega_1) , \quad \text{(H.3)}$$

with A_n depending on which lead electrons in Eq. (H.1) have been contracted

$$\begin{aligned}
\beta-\gamma \quad &\rightarrow \quad A_0 = \frac{B_2^2(i\omega+i\omega_\Lambda)}{\beta}\sum_{p,i\omega_n} G_p(i\omega_n)D_3(i\omega_n+i\omega\Lambda+i\omega) \\
&= \frac{\nu_0}{(\varepsilon_d+U)^2}\ln\frac{2\varepsilon_d+3U}{D_0}, \qquad \text{(H.4)} \\
\alpha-\gamma \text{ or } \beta-\delta \quad &\rightarrow \quad A_1 = -\frac{B_2(i\omega+i\omega_\Lambda)}{\beta}\sum_{p,i\omega_n} G_p(i\omega_n)D_3(i\omega_n+i\omega_\Lambda+i\omega)B_2(i\omega_n+i\omega_\Lambda) \\
&= \frac{\nu_0}{(\varepsilon_d+U)(\varepsilon_d+2U)}\left[\ln\frac{2\varepsilon_d+3U}{D_0}-\ln\frac{\varepsilon_d+U}{D_0}\right], \qquad \text{(H.5)} \\
\alpha-\delta \quad &\rightarrow \quad A_2 = \frac{1}{\beta}\sum_{p,i\omega_n} G_p(i\omega_n)D_3(i\omega_n+i\omega_\Lambda+i\omega)B_2^2(i\omega_n+i\omega_\Lambda) \\
&= -\frac{\nu_0}{(\varepsilon_d+U)(\varepsilon_d+2U)}+\frac{\nu_0}{(\varepsilon_d+2U)^2}\left[\ln\frac{2\varepsilon_d+3U}{D_0}-\ln\frac{\varepsilon_d+U}{D_0}\right]. \qquad \text{(H.6)}
\end{aligned}$$

The Matsubara sums were carried out first and the analytical continuations $i\omega \rightarrow 0$ and $i\omega_\Lambda \rightarrow \varepsilon_d+\lambda$ are done later. The cutoff D_0 must be introduced to prevent UV divergences and can be sent to infinity at the end of calculations. Notice that no infra-red divergence appears at this stage of calculations. Performing explicitly the spin summation one can show that the effective interaction can be cast into the form

$$\frac{t^2}{\beta}(4A_1-2A_0-2A_2)\left[\sum_{\mu\neq\mu',\nu\neq\nu'}-\sum_{\mu\neq\nu}\delta_{\nu\nu'}\delta_{\mu\mu'}\right]c_\mu^\dagger c_{\mu'}f_\nu^\dagger f_{\nu'}. \qquad \text{(H.7)}$$

Applying the projection property $\sum_\nu f_\nu^\dagger f_\nu = 1$ and Eq. (E.2) this recovers Eq. (5.33), realizing the mapping onto the form Eq. (5.19).

H.1.2 Calculation of the renormalized vertex

The steps required for the calculation of the renormalized vertex $\mathcal{V}^R$ are those summarized in the paragraph before Eq. (5.34): the calculation of the full renormalized para-fermion propagator, with the corrections to the pole and its quasi-particle weight, and the calculation of all diagrams up to fourth order in t contributing to the vertex function Eq. (5.32). The calculation of the full propagator $\mathscr{D}_1(i\omega_n) = -\langle f_\nu(i\omega_n)f_\nu^\dagger(i\omega_n)\rangle$ is completely analog to the one carried out for the para-fermions in the SU(2) Anderson model in Section 4.3. The Dyson equation allows us to write the propagator in the form

$$\mathscr{D}_1(i\omega_n) = \frac{1}{D_1^{-1}(i\omega_n)-\Sigma_1(i\omega_n)}, \qquad \text{(H.8)}$$

with, to leading order in Γ, the self-energy $\Sigma_1(i\omega_n)$ given by the same diagram of the SU(2) case, pictured in Fig. 4.9

$$\begin{aligned}\Sigma_1(i\omega) &= \frac{4}{\beta}\sum_{p,i\omega_n} G_p(i\omega_n)W_1(i\omega_n, i\omega_n, i\omega - i\omega_n) \\ &= \nu_0 t^2\left[\ln\frac{\lambda - i\omega}{D_0} + 3\ln\frac{2\varepsilon_d + U + \lambda - i\omega}{D_0}\right],\end{aligned} \tag{H.9}$$

where, the anti-symmetric properties of the SU(N) matrices **S** and **T**, imply that only $\mathscr{W}_1$ in Eq. (5.31), and not $\mathscr{J}_1$, contributes to the self energy. The full propagator can then be written in the form

$$\mathscr{D}_1(i\omega_n) = \frac{\mathscr{Z}_1}{i\omega_n - \tilde{\varepsilon}_{d1}}, \tag{H.10}$$

providing the corrected pole $\tilde{\varepsilon}_d$ and the quasi-particle weight $\mathscr{Z}_1$

$$\mathscr{Z}_1(\tilde{\varepsilon}_{d1}) = \frac{1}{1 - \Sigma_1'(\tilde{\varepsilon}_{d1})} = 1 + \nu_0 t^2\left[\frac{1}{\varepsilon_d} - \frac{3}{\varepsilon_d + U}\right], \tag{H.11}$$

$$\tilde{\varepsilon}_{d1} = \varepsilon_d + \lambda + \Sigma_1(\tilde{\varepsilon}_{d1}) \sim \varepsilon_d + \lambda + \nu_0 t^2\left(\ln\frac{-\varepsilon_d}{D_0} + 3\ln\frac{\varepsilon_d + U}{D_0}\right). \tag{H.12}$$

The same diagrams as in Fig. 4.8 have to be calculated using the $S_{\mathrm{SU(4)}}$ interaction appearing in Eq. (5.30). The first contribution to the renormalized vertex $\mathscr{V}^R$ is given by the first diagram of the series in Fig. 4.8 multiplied by the quasi-particle weight $\mathscr{Z}_1$ Eq. (H.11) and performing the analytical extension $i\omega_\Lambda \to \tilde{\varepsilon}_{d1}$ to the renormalized pole in Eq. (H.12). This contribution reads

$$\begin{aligned}\mathscr{V}_1 &= \mathscr{Z}_1\left[\mathscr{J}_1(i\omega, i\omega, i\omega_R - i\omega)\mathbf{S}\cdot\mathbf{T} + \mathscr{W}_1(i\omega, i\omega, i\omega_R - i\omega)\mathbb{1}\right]\Big|_{i\omega\to 0,\ i\omega_\Lambda\to\tilde{\varepsilon}_{d1}} \\ &= \mathbf{S}\cdot\mathbf{T}\left[J_1\mathscr{Z}_1 + 2\nu_0 t^4\left(\ln\frac{-\varepsilon_d}{D_0} + 3\ln\frac{\varepsilon_d + U}{D_0}\right)\left(\frac{1}{\varepsilon_d^2} + \frac{1}{(\varepsilon_d + U)^2}\right)\right] \\ &\quad + \mathbb{1}\left[W_1\mathscr{Z}_1 + \frac{\nu_0 t^4}{4}\left(\ln\frac{-\varepsilon_d}{D_0} + 3\ln\frac{\varepsilon_d + U}{D_0}\right)\left(\frac{1}{\varepsilon_d^2} - \frac{3}{(\varepsilon_d + U)^2}\right)\right],\end{aligned} \tag{H.13}$$

with J_1 and W_1 the couplings obtained by the Schrieffer-Wolff transformation in Eqs. (2.78) and (2.79) respectively.

The calculation of the diagrams of order t^4 in Fig. 4.8 contributing to the vertex function is also completely similar to those carried for the SU(2) Anderson model, the main difference is in the commutation relations between the SU(N) matrices given by the relations Eq. (E.6).

The results are analog Eqs. (4.35) and (4.41) and they read

$$\mathcal{V}^a = -\frac{1}{\beta}\sum_{pi\omega_n\alpha\beta} G_p(i\omega + i\omega_\Lambda - i\omega_n) D_1(i\omega_n)\left[\left(-\frac{1}{4}J_a^2 + 2J_a W_a\right)\mathbf{S}\cdot\mathbf{T} + \left(\frac{15}{64}J_a^2 + W_a^2\right)\mathbb{1}\right], \quad \text{(H.14)}$$

$$\mathcal{V}^b = -\frac{1}{\beta}\sum_{pi\omega_n\alpha\beta} G_p(i\omega + i\omega_n - i\omega_\Lambda) D_1(i\omega_n)\left[\left(\frac{7}{4}J_b^2 + 2J_b W_b\right)\mathbf{S}\cdot\mathbf{T} + \left(\frac{15}{64}J_b^2 + W_b^2\right)\mathbb{1}\right]. \quad \text{(H.15)}$$

In the contribution a, the frequency dependencies of the couplings J_a and W_a read

$$J_a = -2t^2\left[B_0(i\omega_n - i\omega) + B_2(i\omega + i\omega_\Lambda)\right], \quad \text{(H.16)}$$

$$W_a = -\frac{t^4}{4}\left[B_0(i\omega_n - i\omega) - 3B_2(i\omega + i\omega_\Lambda)\right], \quad \text{(H.17)}$$

while in $\mathcal{V}^b$

$$J_b = -2t^2\left[B_0(i\omega_\Lambda - i\omega) + B_2(i\omega + i\omega_n)\right], \quad \text{(H.18)}$$

$$W_b = -\frac{t^2}{4}\left[B_0(i\omega_\Lambda - i\omega) - 3B_2(i\omega + i\omega_n)\right]. \quad \text{(H.19)}$$

The same kind of integrals as in the SU(2) Anderson model have to be calculated

$$\begin{aligned}
I_{00} &= \frac{1}{\beta}\sum_{p,i\omega_n} G_p(i\omega + i\omega_\Lambda - i\omega_n) D_1(i\omega_n) B_0^2(i\omega_n - i\omega) = \frac{\nu_0}{\varepsilon_d^2}\left[\ln\frac{-\varepsilon_d}{\Lambda} - 1\right],\\
I_{02} &= \frac{1}{\beta}\sum_{p,i\omega_n} G_p(i\omega + i\omega_\Lambda - i\omega_n) D_1(i\omega_n) B_0(i\omega_n - i\omega) B_2(i\omega + i\omega_\Lambda) = \frac{\nu_0}{\varepsilon_d(\varepsilon_d + U)}\ln\frac{\Lambda}{-\varepsilon_d},\\
I_{22} &= \frac{1}{\beta}\sum_{p,i\omega_n} G_p(i\omega + i\omega_\Lambda - i\omega_n) D_1(i\omega_n) B_2^2(i\omega + i\omega_\Lambda) = -\frac{\nu_0}{(\varepsilon_d + U)^2}\ln\frac{\Lambda}{D_0},\\
L_{00} &= \frac{1}{\beta}\sum_{p,i\omega_n} G_p(i\omega + i\omega_n - i\omega_\Lambda) D_1(i\omega_n) B_0^2(i\omega_\Lambda - i\omega) = \frac{\nu_0}{\varepsilon_d^2}\ln\frac{\Lambda}{D_0},\\
L_{02} &= \frac{1}{\beta}\sum_{p,i\omega_n} G_p(i\omega + i\omega_n - i\omega_\Lambda) D_1(i\omega_n) B_0(i\omega_\Lambda - i\omega) B_2(i\omega + i\omega_n) = \frac{\nu_0}{\varepsilon_d(\varepsilon_d + U)}\ln\frac{\varepsilon_d + U}{\Lambda},\\
L_{22} &= \frac{1}{\beta}\sum_{p,i\omega_n} G_p(i\omega + i\omega_n - i\omega_\Lambda) D_1(i\omega_n) B_2^2(i\omega + i\omega_n) = \frac{\nu_0}{(\varepsilon_d + U)^2}\left[1 - \ln\frac{\varepsilon_d + U}{\Lambda}\right].
\end{aligned} \quad \text{(H.20)}$$

Notice that we directly applied Solyom's prescription [124], illustrated in Eq. (4.39), equivalent to introduce the infra-red cutoff Λ for sums over momenta. Only the integrals I_{22} and L_{00} depend on the high energy cut-off D_0, which must disappear as we will show later on. The contributions to the vertex function read

$$\mathcal{V}^a = t^4\left(4I_{02} + 4I_{22}\right)\mathbf{S}\cdot\mathbf{T} - t^4\left(I_{00} + \frac{3}{2}I_{22} + \frac{3}{2}I_{02}\right)\mathbb{1}, \quad \text{(H.21)}$$

$$\mathcal{V}^b = -t^4\left(8L_{00} + 12L_{02} + 4L_{22}\right)\mathbf{S}\cdot\mathbf{T} - t^4\left(L_{00} + \frac{3}{2}L_{22} + \frac{3}{2}L_{02}\right)\mathbb{1}. \quad \text{(H.22)}$$

These contributions, in contrast with the SU(2) case, even if summed with the leading contribution Eq. (H.13), do not allow to carry out the limit $D_0 \to \infty$. The contributions to the vertex function from the t^4 order interaction Eq. (5.33), derived in Section H.1.1, have to be taken into account to remove the D_0 dependence. Their summation leads to the final results Eq. (5.34) and (5.36).

H.2 Sector with $q = 2$

The steps of the previous calculation in the $q = 1$ case are repeated. To second order in t, the self-energy of the boson propagator $\mathscr{B}_2(i\nu) = -\langle b(i\nu) b^\dagger(i\nu)\rangle$ reads

$$\begin{aligned}\Sigma_2(i\nu) &= \frac{4}{\beta}\sum_{p,i\omega_n} \mathscr{W}_2(i\nu, i\omega_n, i\omega_n)\, G_p(i\omega_n) \\ &= \frac{2\Gamma}{\pi}\left[\ln\frac{-i\nu + 3\varepsilon_d + 3U + \lambda}{D_0} + \ln\frac{\varepsilon_d + \lambda - i\nu}{D_0}\right],\end{aligned} \tag{H.23}$$

with $\mathscr{W}_2$ in Eq. (5.47). The self-energy leads to the renormalized pole $i\nu_\Lambda$ and quasi-particle weight $\mathscr{Z}_2$

$$i\nu_\Lambda \to \tilde{\varepsilon}_{d2} = 2\varepsilon_d + U + \lambda + 2\frac{\Gamma}{\pi}\left[\ln\frac{\varepsilon_d + 2U}{D_0} + \ln\frac{-\varepsilon_d - U}{D_0}\right], \tag{H.24}$$

$$\mathscr{Z}_2 = 1 - \nu_0 J_2, \tag{H.25}$$

with J_2 given by the Schrieffer-Wolff transformation Eq. (2.78). Notice that the slave-states used to describe the quantum dot are now bosons, implying that their propagator $\mathscr{B}_2$ depends on bosonic Matsubara frequencies $i\nu_n$.

We calculate now all the contributions to the renormalized vertex $\mathscr{V}_2^R = \mathscr{Z}_2\mathscr{V}$, involving the four-point vertex function $\mathscr{V}$ defined in Eq. (5.51). The contributions corresponding to the first diagram of the series in Fig. 4.8 are readily obtained

$$\begin{aligned}\mathscr{V}_{1-2} = \mathbf{S}\cdot\mathbf{T}\Bigg[J_2 - \nu_0 J_2^2 + 2\nu_0\left(\frac{J_2^2}{4} + 4W_2^2\right)\ln\frac{(-\varepsilon_d - U)(\varepsilon_d + 2U)}{D_0^2}\Bigg] + \\ + \mathbb{1}\left[W_2 - \nu_0 J_2 W_2 + \nu_0 J_2 W_2 \ln\frac{(-\varepsilon_d - U)(\varepsilon_d + 2U)}{D_0^2}\right].\end{aligned} \tag{H.26}$$

These include the corrections to the pole Eq. (H.24) and the quasi-particle weight Eq. (H.25).

Then we have the contributions which are the analog of the contributions $\mathscr{V}^a$ and $\mathscr{V}^b$ in

the previous section

$$\mathcal{V}_2^a = -\frac{1}{\beta}\sum_{p,i\nu_n} G_p(i\omega + i\nu_\Lambda - i\nu_n) B_2(i\nu_n)\left[\left(-J_a^2 + 2J_a W_a\right)\mathbf{S}\cdot\mathbf{T} + \left(\frac{5}{16}J_a^2 + W_a^2\right)\mathbb{1}\right], \tag{H.27}$$

$$\mathcal{V}_2^b = -\frac{1}{\beta}\sum_{p,i\nu_n} G_p(i\omega + i\nu_n - i\nu_\Lambda) B_2(i\nu_n)\left[\left(J_b^2 + 2J_b W_b\right)\mathbf{S}\cdot\mathbf{T} + \left(\frac{5}{16}J_b^2 + W_b^2\right)\mathbb{1}\right]. \tag{H.28}$$

In the contribution a, the frequency dependencies of the couplings J_a and W_a read

$$J_a = -2t^2\left[F_1(i\nu_n - i\omega) + F_3(i\omega + i\nu_\Lambda)\right], \tag{H.29}$$

$$W_a = -\frac{t^4}{2}\left[F_1(i\nu_n - i\omega) - F_3(i\omega + i\nu_\Lambda)\right], \tag{H.30}$$

while in $\mathcal{V}^b$

$$J_b = -2t^2\left[F_1(i\nu_\Lambda - i\omega) + F_3(i\omega + i\nu_n)\right], \tag{H.31}$$

$$W_b = -\frac{t^2}{2}\left[F_1(i\nu_\Lambda - i\omega) - F_3(i\omega + i\nu_n)\right]. \tag{H.32}$$

Notice that the relations (E.6) do not to hold anymore. The reason is that the bosonic representation of the SU(4) symmetric product Eq. (5.48), is not given by matrices composing a fundamental representation of SU(4). These matrices obey different relations

$$\begin{aligned} S_i S_j T_i T_j &= -\mathbf{S}\cdot\mathbf{T} + \frac{5}{16}\mathbb{1}, \\ S_i S_j T_j T_i &= +\mathbf{S}\cdot\mathbf{T} + \frac{5}{16}\mathbb{1}. \end{aligned} \tag{H.33}$$

The calculation of the Matsubara sums and of the integrals over momenta leads to the following result

$$\begin{aligned} \mathcal{V}_2^a &= 2t^4\left(I_{11} + 3I_{33} + 4I_{13}\right)\mathbf{S}\cdot\mathbf{T} - \frac{t^4}{2}\left(3I_{11} + 3I_{33} + 4I_{13}\right)\mathbb{1}, \\ \mathcal{V}_2^b &= -2t^4\left(3L_{11} + L_{33} + 4L_{13}\right)\mathbf{S}\cdot\mathbf{T} - \frac{t^4}{2}\left(3L_{11} + 3L_{33} + 4L_{13}\right)\mathbb{1}, \end{aligned} \tag{H.34}$$

with

$$
\begin{aligned}
I_{11} &= \frac{1}{\beta}\sum_{p,i\nu_n} B_2(i\nu_n)G_p(i\omega+i\nu_\Lambda-i\nu_n)F_1^2(i\nu_n-i\omega) = -\frac{\nu_0}{(\varepsilon_d+U)^2}\left[1+\ln\frac{\Lambda}{-\varepsilon_d-U}\right],\\
I_{13} &= \frac{1}{\beta}\sum_{p,i\nu_n} B_2(i\nu_n)G_p(i\omega+i\nu_\Lambda-i\nu_n)F_1(i\nu_n-i\omega)F_3(i\omega+i\nu_\Lambda)\\
&= \frac{\nu_0}{(\varepsilon_d+U)(\varepsilon_d+2U)}\ln\frac{\Lambda}{-\varepsilon_d-U},\\
I_{33} &= \frac{1}{\beta}\sum_{p,i\nu_n} B_2(i\nu_n)G_p(i\omega+i\nu_\Lambda-i\nu_n)F_3^2(i\omega+i\nu_\Lambda) = -\frac{\nu_0}{(\varepsilon_d+2U)^2}\ln\frac{\Lambda}{D_0},\\
L_{11} &= \frac{1}{\beta}\sum_{p,i\nu_n} B_2(i\nu_n)G_p(i\omega+i\nu_n-i\nu_\Lambda)F_1^2(i\nu_\Lambda-i\omega) = \frac{\nu_0}{(\varepsilon_d+U)^2}\ln\frac{\Lambda}{D_0},\\
L_{13} &= \frac{1}{\beta}\sum_{p,i\nu_n} B_2(i\nu_n)G_p(i\omega+i\nu_n-i\nu_\Lambda)F_1(i\nu_\Lambda-i\omega)F_3(i\omega+i\nu_n)\\
&= -\frac{\nu_0}{(\varepsilon_d+U)(\varepsilon_d+2U)}\ln\frac{\Lambda}{\varepsilon_d+2U},\\
L_{33} &= \frac{1}{\beta}\sum_{p,i\nu_n} B_2(i\nu_n)G_p(i\omega+i\nu_n-i\nu_\Lambda)F_3^2(i\omega+i\nu_n) = \frac{\nu_0}{(\varepsilon_d+2U)^2}\left[1+\ln\frac{\Lambda}{\varepsilon_d+2U}\right].
\end{aligned}
\tag{H.35}
$$

Again, the summation of all these contributions with $\mathcal{V}_{1-2}$ in Eq. (H.26) does not allow for taking the $D_0\to\infty$, which still requires to consider the contribution to the vertex function of the two interactions term of order t^4 in Eq. (5.46). A mean-field analysis, analog to that carried out in Section H.1.1, leads to the following expression of their contribution to the action

$$
S_{t^4} = \left[2(\mathcal{V}_0-\mathcal{V}_4)\mathbf{S}\cdot\mathbf{T}+\frac{\mathcal{V}_0+\mathcal{V}_4}{2}\mathbb{1}\right]\mathrm{Tr}\left[c^\dagger c b^\dagger b\right]. \tag{H.36}
$$

$\mathcal{V}_0$ and $\mathcal{V}_4$ are the contributions to the vertex coming from the 0 and 4 charge sector respectively. They read

$$
\begin{aligned}
\mathcal{V}_0 &= A_0+A_2-2A_1,\\
\mathcal{V}_4 &= C_0+C_2-2C_1,
\end{aligned}
\tag{H.37}
$$

with

$$
\begin{aligned}
A_0 &= \frac{1}{\beta}\sum_{p,i\omega_n} G_p(-i\omega_n)F_1^2(i\nu - i\omega)B_0(i\nu - i\omega + i\omega_n) = -\frac{\nu_0}{(\varepsilon_d+U)^2}\ln\frac{-2\varepsilon_d - U}{D_0}\,,\\
A_2 &= \frac{1}{\beta}\sum_{p,i\omega_n} G_p(-i\omega_n)F_1^2(i\nu + i\omega_n)B_0(i\nu - i\omega + i\omega_n) = \frac{\nu_0}{\varepsilon_d(\varepsilon_d+U)} + \frac{\nu_0}{\varepsilon_d^2}\ln\frac{\varepsilon_d+U}{2\varepsilon_d+U}\,,\\
A_1 &= -\frac{1}{\beta}\sum_{p,i\omega_n} G_p(-i\omega_n)F_1(i\nu + i\omega_n)B_0(i\nu - i\omega + i\omega_n)F_1(i\nu - i\omega)\\
&= \frac{\nu_0}{\varepsilon_d(\varepsilon_d+U)}\ln\frac{\varepsilon_d+U}{2\varepsilon_d+U}\,,\\
C_0 &= \frac{1}{\beta}\sum_{p,i\omega_n} G_p(i\omega_n)F_3^2(i\nu + i\omega)B_0(i\nu + i\omega + i\omega_n) = \frac{\nu_0}{(\varepsilon_d+2U)^2}\ln\frac{2\varepsilon_d+5U}{D_0}\,, \qquad \text{(H.38)}\\
C_2 &= \frac{1}{\beta}\sum_{p,i\omega_n} G_p(i\omega_n)F_3^2(i\nu + i\omega_n)B_0(i\nu + i\omega + i\omega_n)\\
&= -\frac{\nu_0}{(\varepsilon_d+3U)(\varepsilon_d+2U)} + \frac{\nu_0}{(\varepsilon_d+3U)^2}\ln\frac{2\varepsilon_d+5U}{\varepsilon_d+2U}\,,\\
C_1 &= -\frac{1}{\beta}\sum_{p,i\omega_n} G_p(i\omega_n)F_1(i\nu + i\omega_n)B_0(i\nu + i\omega + i\omega_n)F_1(i\nu + i\omega)\\
&= \frac{\nu_0}{(\varepsilon_d+3U)(\varepsilon_d+2U)}\ln\frac{2\varepsilon_d+5U}{\varepsilon_d+2U}\,.
\end{aligned}
$$

The summation of all these contributions to the previous ones allows us to carry out safely the limit $D_0 \to \infty$ and obtain Eqs. (5.52) and (5.55) for the renormalized vertex in the sector $q = 2$.

BIBLIOGRAPHY

[1] E. Akkermans and G. Montambaux, *Mesoscopic physics of electrons and photons* (Cambridge University Press, 2007)

[2] B. L. Altshuler and A. G. Aronov, *Electron-electron interactions in disordered systems,* Modern Problems in Condensed Matter Physics, eds. AL Efros and M. Pollak (Elsevier, North Holland, 1985), 1(1985)

[3] F. Pierre, A. B. Gougam, A. Anthore, H. Pothier, D. Esteve, and Norman O. Birge, *Dephasing of electrons in mesoscopic metal wires,* Phys. Rev. B **68**, 085413 (2003)

[4] G. Göppert, Y. M. Galperin, B. L. Altshuler, and H. Grabert, *Magnetic-field effects in energy relaxation mediated by Kondo impurities in mesoscopic wires,* Phys. Rev. B **66**, 195328 (2002)

[5] B. Huard, A. Anthore, N. O. Birge, H. Pothier, and D. Esteve, *Effect of magnetic impurities on energy exchange between electrons,* Phys. Rev. Lett. **95**, 036802 (2005)

[6] T. Micklitz, A. Altland, T. A. Costi, and A. Rosch, *Universal Dephasing Rate due to Diluted Kondo Impurities,* Phys. Rev. Lett. **96**, 226601 (2006)

[7] J. Gabelli, G. Fève, J.-M. Berroir, B. Plaçais, A. Cavanna, B. Etienne, Y. Jin, and D. C. Glattli, *Violation of kirchhoff's laws for a coherent rc circuit,* Science **313**, 499–502 (2006)

[8] J. Gabelli, *Mise en évidence de la cohérence quantique des conducteurs en régime dynamique*, Ph.D. thesis, Université Pierre et Marie Curie-Paris VI (2006)

[9] B. L. Altshuler, A.G. Aronov, and D.E. Khmelnitsky, *Effects of electron-electron collisions with small energy transfers on quantum localisation,* J. Phys. C: Solid State Physics **15**, 7367 (1982)

[10] C. P. Umbach, S. Washburn, R. B. Laibowitz, and R. A. Webb, *Magnetoresistance of small, quasi-one-dimensional, normal-metal rings and lines,* Phys. Rev. B **30**, 4048–4051 (1984)

[11] R. A. Webb, S. Washburn, C. P. Umbach, and R. B. Laibowitz, *Observation of $\frac{h}{e}$ Aharonov-Bohm Oscillations in Normal-Metal Rings,* Phys. Rev. Lett. **54**, 2696–2699 (1985)

[12] C.P. Umbach, P. Santhanam, C. Van Haesendonck, and R.A. Webb, *Nonlocal electrical properties in mesoscopic devices,* Applied physics letters **50**, 1289–1291 (1987)

[13] M.A. Topinka, B.J. LeRoy, R.M. Westervelt, S.E.J. Shaw, R. Fleischmann, E.J. Heller, K.D. Maranowski, and A.C. Gossard, *Coherent branched flow in a two-dimensional electron gas,* Nature **410**, 183–186 (2001)

[14] B. Hackens, F. Martins, S. Faniel, C.A. Dutu, H. Sellier, S. Huant, M. Pala, L. Desplanque, X. Wallart, and V. Bayot, *Imaging Coulomb islands in a quantum Hall interferometer,* Nature Communications **1**, 39 (2010)

[15] S. Schnez, C. Rössler, T. Ihn, K. Ensslin, C. Reichl, and W. Wegscheider, *Imaging the lateral shift of a quantum point contact using scanning gate microscopy,* Phys. Rev. B **84**, 195322 (2011)

[16] T. Can, H. Dai, and D. K. Morr, *Current eigenmodes and dephasing in nanoscopic quantum networks,* Phys. Rev. B **85**, 195459 (2012)

[17] B. J. van Wees, H. van Houten, C. W. J. Beenakker, J. G. Williamson, L. P. Kouwenhoven, D. van der Marel, and C. T. Foxon, *Quantized conductance of point contacts in a two-dimensional electron gas,* Phys. Rev. Lett. **60**, 848–850 (1988)

[18] D.A. Wharam, M. Pepper, H. Ahmed, J.E.F. Frost, D.G. Hasko, D.C. Peacock, D.A. Ritchie, and G.A.C. Jones, *Addition of the one-dimensional quantised ballistic resistance,* J.Phys. C **21**, L887 (1988)

[19] E. Scheer, N. Agraït, J. C. Cuevas, A. Levy Yeyati, B. Ludoph, A. Martín-Rodero, G. R. Bollinger, J. M. van Ruitenbeek, and C. Urbina, *The signature of chemical valence in the electrical conduction through a single-atom contact,* Nature **394**, 154–157 (1998)

[20] D.P.E. Smith, *Quantum point contact switches,* Science **269**, 371–373 (1995)

[21] S. Frank, P. Poncharal, Z.L. Wang, and W. A. de Heer, *Carbon nanotube quantum resistors,* Science **280**, 1744–1746 (1998)

[22] M. Z. Hasan and C. L. Kane, *Colloquium: Topological insulators,* Rev. Mod. Phys. **82**, 3045–3067 (2010)

[23] D. J. Thouless, M. Kohmoto, M. P. Nightingale, and M. den Nijs, *Quantized Hall Conductance in a Two-Dimensional Periodic Potential,* Phys. Rev. Lett. **49**, 405–408 (1982)

[24] K. v. Klitzing, G. Dorda, and M. Pepper, *New Method for High-Accuracy Determination of the Fine-Structure Constant Based on Quantized Hall Resistance,* Phys. Rev. Lett. **45**, 494–497 (1980)

[25] D. C. Tsui, H. L. Stormer, and A. C. Gossard, *Two-Dimensional Magnetotransport in the Extreme Quantum Limit,* Phys. Rev. Lett. **48**, 1559–1562 (1982)

[26] B. A. Bernevig, T. L. Hughes, and S.-C. Zhang, *Quantum spin Hall effect and topological phase transition in HgTe quantum wells,* Science **314**, 1757–1761 (2006)

[27] M. König, S. Wiedmann, C. Brüne, A. Roth, H. Buhmann, L. W Molenkamp, X.-L. Qi, and S.-C. Zhang, *Quantum spin Hall insulator state in HgTe quantum wells,* Science **318**, 766–770 (2007)

[28] R. Landauer, *Electrical resistance of disordered one-dimensional lattices,* Phil. Mag. **21**, 863–867 (1970)

[29] M. Büttiker, Y. Imry, R. Landauer, and S. Pinhas, *Generalized many-channel conductance formula with application to small rings,* Phys. Rev. B **31**, 6207–6215 (1985)

[30] R. Landauer, *Spatial variation of currents and fields due to localized scatterers in metallic conduction,* IBM J. Res Dev. **32**, 306–316 (1988)

[31] L. Kouwenhoven and C. Marcus, *Quantum dots,* Physics World **11**, 35–39 (1998)

[32] S. J. Tans, M. H. Devoret, H. Dai, A. Thess, R. E. Smalley, L.J. Geerligs, and C. Dekker, *Individual single-wall carbon nanotubes as quantum wires,* Nature **386**, 474–477 (1997)

[33] M. Fuechsle, J. A. Miwa, S. Mahapatra, H. Ryu, S. Lee, O. Warschkow, L. C.L. Hollenberg, G. Klimeck, and M. Y. Simmons, *A single-atom transistor,* Nature Nanotechnology **7**, 242–246 (2012)

[34] D. Loss and D. P. DiVincenzo, *Quantum computation with quantum dots,* Phys. Rev. A **57**, 120–126 (1998)

[35] R.J. Schoelkopf, P. Wahlgren, A.A. Kozhevnikov, P. Delsing, and D.E. Prober, *The radio-frequency single-electron transistor (rf-set): a fast and ultrasensitive electrometer,* Science **280**, 1238–1242 (1998)

[36] J.R. Petta, A.C. Johnson, J.M. Taylor, E.A. Laird, A. Yacoby, M.D. Lukin, C.M. Marcus, M.P. Hanson, and A.C. Gossard, *Coherent manipulation of coupled electron spins in semiconductor quantum dots,* Science **309**, 2180–2184 (2005)

[37] A. Wallraff, D.I. Schuster, A. Blais, L. Frunzio, R.-S. Huang, J. Majer, S. Kumar, S.M. Girvin, and R.J. Schoelkopf, *Strong coupling of a single photon to a superconducting qubit using circuit quantum electrodynamics,* Nature **431**, 162–167 (2004)

[38] J. M. Raimond, M. Brune, and S. Haroche, *Manipulating quantum entanglement with atoms and photons in a cavity,* Rev. Mod. Phys. **73**, 565–582 (2001)

[39] S. Haroche and J.-M. Raimond, *Exploring the quantum: Atoms, cavities, and photons* (Oxford Univ. Press, 2006)

[40] H. Paik, D. I. Schuster, L. S. Bishop, G. Kirchmair, G. Catelani, A. P. Sears, B. R. Johnson, M. J. Reagor, L. Frunzio, L. I. Glazman, S. M. Girvin, M. H. Devoret, and R. J. Schoelkopf, *Observation of high coherence in josephson junction qubits measured in a three-dimensional circuit qed architecture,* Phys. Rev. Lett. **107**, 240501 (2011)

[41] M. Hofheinz, H. Wang, M. Ansmann, R.C. Bialczak, E. Lucero, M. Neeley, A.D. O'Connell, D. Sank, J. Wenner, J.M. Martinis, *et al., Synthesizing arbitrary quantum states in a superconducting resonator,* Nature **459**, 546–549 (2009)

[42] P. Campagne-Ibarcq, E. Flurin, N. Roch, D. Darson, P. Morfin, M. Mirrahimi, M. H. Devoret, F. Mallet, and B. Huard, *Stabilizing the trajectory of a superconducting qubit by projective measurement feedback,* arXiv preprint arXiv:1301.6095(2013)

[43] M. R. Delbecq, V. Schmitt, F. D. Parmentier, N. Roch, J. J. Viennot, G. Fève, B. Huard, C. Mora, A. Cottet, and T. Kontos, *Coupling a quantum dot, fermionic leads, and a microwave cavity on a chip,* Phys. Rev. Lett. **107**, 256804 (2011)

[44] T. Frey, P. J. Leek, M. Beck, A. Blais, T. Ihn, K. Ensslin, and A. Wallraff, *Dipole coupling of a double quantum dot to a microwave resonator,* Phys. Rev. Lett. **108**, 046807 (2012)

[45] K. D. Petersson, L. W. McFaul, M. D. Schroer, M. Jung, J. M. Taylor, A. A. Houck, and J. R. Petta, *Circuit quantum electrodynamics with a spin qubit,* Nature **490**, 380–383 (2012)

[46] M.R. Delbecq, L.E. Bruhat, J.J. Viennot, S. Datta, A. Cottet, and T. Kontos, *Photon-mediated interaction between distant quantum dot circuits,* Nature communications **4**, 1400 (2013)

[47] E. Bocquillon, V. Freulon, J.-M. Berroir, P. Degiovanni, B. Plaçais, A. Cavanna, Y. Jin, and G. Fève, *Coherence and indistinguishability of single electrons emitted by independent sources,* Science **339**, 1054–1057 (2013)

[48] M. Büttiker, *Role of scattering amplitudes in frequency-dependent current fluctuations in small conductors,* Phys. Rev. B **45**, 3807–3810 (1992)

[49] M. Büttiker, A. Prêtre, and H. Thomas, *Dynamic conductance and the scattering matrix of small conductors,* Phys. Rev. Lett. **70**, 4114–4117 (1993)

[50] M. Büttiker, H. Thomas, and A. Prêtre, *Mesoscopic capacitors,* Phys. Lett. A **180**, 364–369 (1993)

[51] A. Prêtre, H. Thomas, and M. Büttiker, *Dynamic admittance of mesoscopic conductors: Discrete-potential model,* Phys. Rev. B **54**, 8130–8143 (1996)

[52] J. Gabelli, G. Fève, J.-M. Berroir, and B. Plaçais, *A coherent rc circuit,* Rep. Prog. Phys. **75**, 126504 (2012)

[53] Simon E. Nigg and M. Büttiker, *Universal detector efficiency of a mesoscopic capacitor,* Phys. Rev. Lett. **102**, 236801 (2009)

[54] I. Garate and K. Le Hur, *Noninvasive probes of charge fractionalization in quantum spin hall insulators,* Phys. Rev. B **85**, 195465 (2012)

[55] A. Golub and E. Grosfeld, *Charge resistance in a majorana rc circuit,* Phys. Rev. B **86**, 241105 (2012)

[56] G. Fève, A. Mahé, J.-M. Berroir, T. Kontos, B. Plaçais, D. C. Glattli, A. Cavanna, B. Etienne, and Y. Jin, *An On-Demand Coherent Single-Electron Source,* Science **316**, 1169–1172 (2007)

[57] A. Mahé, F. D. Parmentier, E. Bocquillon, J.-M. Berroir, D. C. Glattli, T. Kontos, B. Plaçais, G. Fève, A. Cavanna, and Y. Jin, *Current correlations of an on-demand single-electron emitter,* Phys. Rev. B **82**, 201309 (2010)

[58] E. Bocquillon, F. D. Parmentier, C. Grenier, J.-M. Berroir, P. Degiovanni, D. C. Glattli, B. Plaçais, A. Cavanna, Y. Jin, and G. Fève, *Electron quantum optics: Partitioning electrons one by one,* Phys. Rev. Lett. **108**, 196803 (2012)

[59] I.L. Aleiner, P.W. Brouwer, and L.I. Glazman, *Quantum effects in coulomb blockade,* Physics Reports **358**, 309–440 (2002)

[60] K. A. Matveev, *Quantum fluctuations of the charge of a metal particle under the Coulomb blockade conditions,* Zh. Eksp. Teor. Fiz. **99**, 1598 (1990), [*Sov. Phys. JETP* **72,** 892 (1991)]

[61] A. C. Hewson, *The Kondo Problem to Heavy Fermions* (Cambridge University Press, Cambridge, 1993)

[62] L. Glazman and M.E. Raikh, *Resonant Kondo transparency of a barrier with quasilocal impurity states,* JETP Lett. **47**, 105 (1988)

[63] D. Goldhaber-Gordon, H. Shtrikman, D. Mahalu, D. Abusch-Magder, U. Meirav, and M.A. Kastner, *Kondo effect in a single-electron transistor,* Nature **391**, 156–159 (1998)

[64] W.G. Van der Wiel, S. De Franceschi, T. Fujisawa, J.M. Elzerman, S. Tarucha, and L.P. Kouwenhoven, *The Kondo effect in the unitary limit,* science **289**, 2105–2108 (2000)

[65] P. W. Brouwer, A. Lamacraft, and K. Flensberg, *Nonequilibrium theory of Coulomb blockade in open quantum dots,* Phys. Rev. B **72**, 075316 (2005)

[66] S. E. Nigg, R. López, and M. Büttiker, *Mesoscopic Charge Relaxation,* Phys. Rev. Lett. **97**, 206804 (2006)

[67] J. Splettstoesser, M. Governale, J. König, and M. Büttiker, *Charge and spin dynamics in interacting quantum dots,* Phys. Rev. B **81**, 165318 (2010)

[68] Y. I. Rodionov, I. S. Burmistrov, and A. S. Ioselevich, *Charge relaxation resistance in the Coulomb blockade problem,* Phys. Rev. B **80**, 035332 (2009)

[69] Y. Etzioni, B. Horovitz, and P. Le Doussal, *Rings and boxes in dissipative environments,* Phys. Rev. Lett. **106**, 166803 (2011)

[70] C. Mora and K. Le Hur, *Low-frequency admittance as probe of majorana fermions,* arXiv:1212.0650

[71] P. Dutt, T. L. Schmidt, C. Mora, and K. Le Hur, *Strongly correlated dynamics in multi-channel quantum RC circuits,* Phys. Rev. B **87**, 155134 (2013)

[72] C. Mora and K. Le Hur, *Universal Resistances of the Quantum RC Circuit,* Nat. Phys. **6**, 697 (2010)

[73] Y. Hamamoto, T. Jonckheere, T. Kato, and T. Martin, *Dynamic response of a mesoscopic capacitor in the presence of strong electron interactions,* Phys. Rev. B **81**, 153305 (2010)

[74] Y. Hamamoto, T. Jonckheere, T. Kato, and T. Martin, *Quantum phase transition of dynamical resistance in a mesoscopic capacitor,* Journal of Physics: Conference Series **334**, 012033 (2011)

[75] H. Shiba, *Korringa Relation for the Impurity Nuclear Spin-Lattice Relaxation in Dilute Kondo Alloys,* Prog. Theor. Phys. **54**, 967–981 (1975)

[76] M. Lee, R. López, M.-S. Choi, T. Jonckheere, and T. Martin, *Effect of many-body correlations on mesoscopic charge relaxation,* Phys. Rev. B **83**, 201304 (2011)

[77] J. Friedel, *On some electrical and magnetic properties of metallic solid solutions,* Can. J. Phys. **34**, 1190–1211 (1956)

[78] A.M. Tsvelick and P.B. Wiegmann, *Exact results in the theory of magnetic alloys,* Adv. Phys. **32**, 453–713 (1983)

[79] P.B. Wiegmann and A.M. Tsvelick, *Exact solution of the Anderson model: I,* J. Phys. C **16**, 2281 (1983)

[80] S. Datta, *Electronic transport in mesoscopic systems* (Cambridge university press, 1997)

[81] E. P. Wigner, *Lower Limit for the Energy Derivative of the Scattering Phase Shift,* Phys. Rev. **98**, 145–147 (1955)

[82] Z. Ringel, Y. Imry, and O. Entin-Wohlman, *Delayed currents and interaction effects in mesoscopic capacitors,* Phys. Rev. B **78**, 165304 (2008)

[83] J. Wang, B. Wang, and H. Guo, *Quantum inductance and negative electrochemical capacitance at finite frequency in a two-plate quantum capacitor,* Phys. Rev. B **75**, 155336 (2007)

[84] S. E. Nigg and M. Büttiker, *Quantum to classical transition of the charge relaxation resistance of a mesoscopic capacitor,* Phys. Rev. B **77**, 085312 (2008)

[85] M. Büttiker and S.E. Nigg, *Role of coherence in resistance quantization,* Eur. Phys. J. Special Topics **172**, 247–255 (2009)

[86] Y. Imry, *Directions in condensed matter physics, edited by g. grinstein and g. mazenco,* (1986)

[87] R. Landauer, *Electrical transport in open and closed systems,* Z. Phys. B **68**, 217–228 (1987)

[88] G. Fève, *Quantification du courant alternatif: la boîte quantique comme source d'électrons uniques subnanoseconde,* Ph.D. thesis, Université Pierre et Marie Curie-Paris VI (2006)

[89] R. Kubo, M. Toda, and N. Hashitsume, *Statistical physics: Nonequilibrium statistical mechanics*, Vol. 2 (Springer, 1992)

[90] C. Texier, *Physique statistique des systemes (faiblement) hors équilibre: formalisme de la réponse linéaire. Dissipation quantique. Transport électronique.* (http://lptms.u-psud.fr/christophe_texier/files/2010/03/coursrl_Ch_Texier.pdf, 2013)

[91] A. Altland and B. Simons, *Condensed matter field theory* (Cambridge University Press, 2006)

[92] I. L. Aleiner and L. I. Glazman, *Mesoscopic charge quantization,* Phys. Rev. B **57**, 9608–9641 (1998)

[93] F. D. M. Haldane, *Scaling Theory of the Asymmetric Anderson Model,* Phys. Rev. Lett. **40**, 416–419 (1978)

[94] P. Nozières and D. Pines, *The theory of quantum liquids* (Perseus books Reading, Massachusetts, 1999)

[95] P. Coleman, *Introduction to Many Body Physics* (http://www.physics.rutgers.edu/ coleman/620/mbody/pdf/bkx.pdf, 2013)

[96] D. C. Langreth, *Friedel Sum Rule for Anderson's Model of Localized Impurity States,* Phys. Rev. **150**, 516–518 (1966)

[97] M. Rontani, *Friedel sum rule for an interacting multiorbital quantum dot,* Phys. Rev. Lett. **97**, 076801 (2006)

[98] H. Bruus and K. Flensberg, *Many-Body Quantum Theory in Condensed Matter Physics. An Introduction* (Oxford University Press, USA, 2004)

[99] J. R. Schrieffer and P. A. Wolff, *Relation between the Anderson and Kondo Hamiltonians,* Phys. Rev. **149**, 491–492 (1966)

[100] B. Coqblin and J. R. Schrieffer, *Exchange Interaction in Alloys with Cerium Impurities,* Phys. Rev. **185**, 847–853 (1969)

[101] H. Grabert, *Charge fluctuations in the single-electron box: Perturbation expansion in the tunneling conductance,* Phys. Rev. B **50**, 17364–17377 (1994)

[102] H. Grabert, *Rounding of the Coulomb Staircase by the tunneling conductance,* Physica B: Condensed Matter **194**, 1011–1012 (1994)

[103] P. W. Anderson, *Localized Magnetic States in Metals,* Phys. Rev. **124**, 41–53 (1961)

[104] D.M. Cragg and P. Lloyd, *Potential Scattering and the Kondo Problem,* J. Phys. C **11**, L597 (1978)

[105] P. Lloyd and D. M. Cragg, *The Nozieres-Wilson relation in the low-temperature Kondo problem,* J. Phys. C **12**, 3289 (1979)

[106] D. M. Cragg and P. Lloyd, *Universality and the renormalisability of rotationally invariant Kondo Hamiltonians,* J. Phys. C **12**, 3301 (1979)

[107] B. Horvatić and V. Zlatić, *Equivalence of the perturbative and Bethe-Ansatz solution of the symmetric Anderson Hamiltonian,* J. Phys. (Paris) **46**, 1459–1467 (1985)

[108] H. R. Krishna-murthy, J. W. Wilkins, and K. G. Wilson, *Renormalization-group approach to the Anderson model of dilute magnetic alloys. II. Static properties for the asymmetric case,* Phys. Rev. B **21**, 1044–1083 (1980)

[109] K. G. Wilson, *The renormalization group: Critical phenomena and the Kondo problem,* Rev. Mod. Phys. **47**, 773–840 (1975)

[110] H. R. Krishna-murthy, J. W. Wilkins, and K. G. Wilson, *Renormalization-group approach to the Anderson model of dilute magnetic alloys. I. Static properties for the symmetric case,* Phys. Rev. B **21**, 1003–1043 (1980)

[111] F.D.M. Haldane, *Theory of the atomic limit of the Anderson model. I. Perturbation expansions re-examined,* J. Phys. C: Solid State Phys. **11**, 5015 (1978)

[112] L. Borda, G. Zaránd, W. Hofstetter, B. I. Halperin, and J. von Delft, *Su(4) Fermi Liquid State and Spin Filtering in a Double Quantum Dot System,* Phys. Rev. Lett. **90**, 026602 (2003)

[113] K. Le Hur and P. Simon, *Smearing of charge fluctuations in a grain by spin-flip assisted tunneling,* Phys. Rev. B **67**, 201308 (2003)

[114] G. Zaránd, A. Brataas, and D. Goldhaber-Gordon, *Kondo effect and spin filtering in triangular artificial atoms,* Solid State Commun. **126**, 463–466 (2003)

[115] R. López, D. Sánchez, M. Lee, M.-S. Choi, P. Simon, and K. Le Hur, *Probing spin and orbital Kondo effects with a mesoscopic interferometer,* Phys. Rev. B **71**, 115312 (2005)

[116] M.-S. Choi, R. López, and R. Aguado, *Su(4) Kondo Effect in Carbon Nanotubes,* Phys. Rev. Lett. **95**, 067204 (2005)

[117] P. Jarillo-Herrero, J. Kong, H.S.J. Van Der Zant, C. Dekker, L.P. Kouwenhoven, and S. De Franceschi, *Orbital Kondo effect in carbon nanotubes,* Nature **434**, 484–488 (2005)

[118] A. Makarovski, J. Liu, and G. Finkelstein, *Evolution of Transport Regimes in Carbon Nanotube Quantum Dots,* Phys. Rev. Lett. **99**, 066801 (2007)

[119] G.P. Lansbergen, G.C. Tettamanzi, J. Verduijn, N. Collaert, S. Biesemans, M. Blaauboer, and S. Rogge, *Tunable Kondo Effect in a Single Donor Atom,* Nano Letters **10**, 455–460 (2009)

[120] G. C. Tettamanzi, J. Verduijn, G. P. Lansbergen, M. Blaauboer, M. J. Calderón, R. Aguado, and S. Rogge, *Magnetic-Field Probing of an SU(4) Kondo Resonance in a Single-Atom Transistor,* Phys. Rev. Lett. **108**, 046803 (2012)

[121] C. Mora, P. Vitushinsky, X. Leyronas, A. A. Clerk, and K. Le Hur, *Theory of nonequilibrium transport in the SU(N) Kondo regime,* Phys. Rev. B **80**, 155322 (2009)

[122] A. A. Abrikosov, *Electron scattering on magnetic impurities in metals and anomalous resistivity effects,* Physics **2**, 5–20 (1965)

[123] A. A. Abrikosov and A. A. Migdal, *On the theory of the kondo effect,* J. Low Temp. Phys. **3**, 519–536 (1970)

[124] J. Solyom, *Renormalization and scaling in the X-ray absorption and Kondo problems,*

[125] N. Read and D.M. Newns, *On the solution of the Coqblin-Schreiffer Hamiltonian by the large-N expansion technique,* J. Phys. C: Solid State Phys. **16**, 3273 (1983)

[126] V. V. Bazhanov, S. L. Lukyanov, and A. M. Tsvelik, *Analytical results for the Coqblin-Schrieffer model with generalized magnetic fields,* Phys. Rev. B **68**, 094427 (2003)

[127] B. Delamotte, *A hint of renormalization,* Am. J. Phys. **72**, 170 (2004)

[128] N. Read and D.M. Newns, *A new functional integral formalism for the degenerate Anderson model,* J. Phys. C: Solid State Physics **16**, L1055 (1983)

[129] P. Coleman, *New approach to the mixed-valence problem,* Phys. Rev. B **29**, 3035–3044 (1984)

[130] A. Houghton, N. Read, and H. Won, *1/N expansion for the transport coefficients of the single-impurity Anderson model,* Phys. Rev. B **35**, 5123–5150 (1987)

[131] R. Shankar, *Renormalization-group approach to interacting fermions,* Rev. Mod. Phys. **66**, 129–192 (1994)

[132] W. Metzner, C. Castellani, and C. Di Castro, *Fermi systems with strong forward scattering,* Advances in Physics **47**, 317–445 (1998)

[133] A. A. Abrikosov, L. P. Gorkov, and I. E. Dzyaloshinski, *Methods of Quantum Field Theory in Statistical Physics* (Courier Dover Publications, 1975)

[134] L. Zhu and Q. Si, *Critical local-moment fluctuations in the Bose-Fermi Kondo model,* Phys. Rev. B **66**, 024426 (2002)

[135] G. Zaránd and E. Demler, *Quantum phase transitions in the Bose-Fermi Kondo model,* Phys. Rev. B **66**, 024427 (2002)

[136] Y. I. Rodionov, I. S. Burmistrov, and N. M. Chtchelkatchev, *Relaxation dynamics of the electron distribution in the Coulomb-blockade problem,* Phys. Rev. B **82**, 155317 (2010)

[137] N. Andrei and J. H. Lowenstein, *Scales and Scaling in the Kondo Model,* Phys. Rev. Lett. **46**, 356–360 (1981)

[138] A.M. Tsvelick and P.B. Wiegmann, *Exact solution of the Anderson model. ii. Thermodynamic properties at finite temperatures,* J. Phys. C **16**, 2321 (1983)

[139] N. Kawakami and A. Okiji, *Ground State of Asymmetric Anderson Hamiltonian,* J. Phys. Soc. Jpn. **51**, 2043 (1982)

[140] A. Okiji and N. Kawakami, *Thermodynamic properties of the anderson model,* Phys. Rev. Lett. **50**, 1157–1159 (1983)

[141] N. Kawakami and A. Okiji, *Density of states for elementary excitations in the Kondo problem,* Phys. Rev. B **42**, 2383–2392 (1990)

[142] H. Suhl, *Dispersion Theory of the Kondo Effect,* Phys. Rev. **138**, A515–A523 (1965)

[143] S. E. Barnes, *New method for the Anderson model,* J. Phys. F **6**, 1375 (1976)

[144] P. Nozieres, *A "Fermi-liquid" description of the Kondo problem at low temperatures,* J. Low Temp. Phys. **17**, 31–42 (1974)

[145] J. Kondo, *Effect of Ordinary Scattering on Exchange Scattering from Magnetic Impurity in Metals,* Phys. Rev. **169**, 437–440 (1968)

[146] K. Fischer, *Self-Consistent Treatment of the Kondo Effect,* Phys. Rev. **158**, 613–622 (1967)

[147] P.B. Wiegmann, *Towards an exact solution of the Anderson model,* Physics Letters A **80**, 163–167 (1980)

[148] P.B. Wiegmann, *Exact solution of the s-d exchange model (Kondo problem),* J. Phys. C **14**, 1463 (1981)

[149] K. Le Hur, *Zeeman smearing of the coulomb blockade,* Phys. Rev. B **64**, 161302 (2001)

[150] I. Affleck, *A current algebra approach to the Kondo effect,* Nucl. Phys. B **336**, 517–532 (1990)

[151] I. Affleck and A. W. W. Ludwig, *Exact conformal-field-theory results on the multichannel Kondo effect: Single-fermion Green's function, self-energy, and resistivity,* Phys. Rev. B **48**, 7297–7321 (1993)

[152] P. Coleman and N. Andrei, *Diagonalisation of the generalised Anderson model,* J. Phys. C **19**, 3211 (1986)

[153] C. M. Pascu and G. Zarand, *Private communication.*.

[154] O. Parcollet, A. Georges, G. Kotliar, and A. Sengupta, *Overscreened multichannel* SU(n) *Kondo model: Large-n solution and conformal field theory,* Phys. Rev. B **58**, 3794–3813 (1998)

[155] W. Götze and P. Wölfle, *Dynamical impurity spin susceptibility in metals,* J. Low Temp. Phys. **5**, 575–589 (1971)

[156] O. Parcollet and C. Hooley, *Perturbative expansion of the magnetization in the out-of-equilibrium Kondo model,* Phys. Rev. B **66**, 085315 (2002)

[157] J. König, H. Schoeller, and G. Schön, *Zero-Bias Anomalies and Boson-Assisted Tunneling Through Quantum Dots,* Phys. Rev. Lett. **76**, 1715–1718 (1996)

[158] J. König, J. Schmid, H. Schoeller, and G. Schön, *Resonant tunneling through ultrasmall quantum dots: Zero-bias anomalies, magnetic-field dependence, and boson-assisted transport,* Phys. Rev. B **54**, 16820–16837 (1996)

[159] L. D. Contreras-Pulido, J. Splettstoesser, M. Governale, J. König, and M. Büttiker, *Time scales in the dynamics of an interacting quantum dot,* Phys. Rev. B **85**, 075301 (2012)

[160] C. Mora, *Fermi-liquid theory for SU*(N) *Kondo model,* Phys. Rev. B **80**, 125304 (2009)

[161] I. Kuzmenko, A. Golub, and Y. Avishai, *Kondo tunneling into a quantum spin Hall insulator,* Phys. Rev. B **85**, 205313 (2012)

[162] A. K. Mitchell, D. Schuricht, M. Vojta, and L. Fritz, *Kondo effect on the surface of three-dimensional topological insulators: Signatures in scanning tunneling spectroscopy,* Phys. Rev. B **87**, 075430 (2013)

[163] J. Maciejko, C. Liu, Y. Oreg, X.-L. Qi, C. Wu, and S.-C. Zhang, *Kondo Effect in the Helical Edge Liquid of the Quantum Spin Hall State,* Phys. Rev. Lett. **102**, 256803 (2009)

[164] A. A. Clerk, M. H. Devoret, S. M. Girvin, F. Marquardt, and R. J. Schoelkopf, *Introduction to quantum noise, measurement, and amplification,* Rev. Mod. Phys. **82**, 1155–1208 (2010)

[165] A. Cottet, C. Mora, and T. Kontos, *Mesoscopic admittance of a double quantum dot,* Phys. Rev. B **83**, 121311 (2011)

[166] O. Kashuba, H. Schoeller, and J. Splettstoesser, *Nonlinear adiabatic response of interacting quantum dots,* EPL **98**, 57003 (2012)

[167] M. Moskalets and M. Büttiker, *Floquet scattering theory of quantum pumps,* Phys. Rev. B **66**, 205320 (2002)

[168] L. Saminadayar, D. C. Glattli, Y. Jin, and B. Etienne, *Observation of the e/3 Fractionally Charged Laughlin Quasiparticle,* Phys. Rev. Lett. **79**, 2526–2529 (1997)

[169] J. Keeling, I. Klich, and L. S. Levitov, *Minimal excitation states of electrons in one-dimensional wires,* Phys. Rev. Lett. **97**, 116403 (2006)

[170] C. Cohen-Tannoudji, J. Dupont-Roc, and G. Grynberg, *Photons and atoms: introduction to quantum electrodynamics* (Wiley, 1989)

[171] S. Weinberg, *The Quantum Theory of Fields: Foundations*, Vol. 1 (Cambridge University Press, 1996)

[172] R. G. Newton, *Scattering Theory of Waves and Particles* (Dover publications, 2002)

[173] W. Greiner and B. Muller, *Quantum Mechanics, Symmetries* (Springer, 2001)

[174] T. Giamarchi, *Quantum Physics in One Dimension*, Vol. 121 (Oxford University Press, USA, 2004)

Résumé

Cette thèse développe une théorie effective de liquide de Fermi pour décrire la dynamique électronique dans un circuit RC quantique dans des régimes de forte interaction. Ce dispositif est composé d'une boîte quantique connectée à un réservoir d'électrons par un point de contact quantique. La boîte quantique est aussi couplée capacitivement à une grille métallique. Ce dispositif n'admet pas de courant continu, mais seulement un courant alternatif. Son comportement est analogue à celui d'un circuit RC classique et ne respecte pas les lois de Kirchhoff si le transport est cohérent. La résistance de relaxation de charge est universellement fixée à $R_q = h/2e^2$, sans dépendre de l'ouverture du point de contact quantique, différement de ce qui est observé en transport direct. Nous étudions des régimes de blocage de Coulomb, provoqués par les fortes interactions électroniques. Nous démontrons que la dynamique électronique est sans interactions de façon effective à basse énergie. Nous prouvons la validité d'une formule de Korringa-Shiba généralisée, prédisant l'universalité de R_q même en présence de fortes interactions. Nous étudions aussi les comportements non universels de R_q causés par la présence d'un champ magnétique. Une attention particulière est dédiée à la physique Kondo. Nous démontrons l'existence d'un pic géant pour R_q, correspondant à la destruction du singulet Kondo. Notre approche est étendue à des dispositifs de symétrie SU(4), respectée par des boîtes quantiques avec dégénérescence orbitale. En appliquant les méthodes analytiques ici dévéloppées, nous dérivons l'expression exacte de la température Kondo dans le cas avec symétrie SU(4).

Mots clés : physique mésoscopique, dynamique électronique cohérente, circuit RC quantique, effet Kondo, blocage de Coulomb, liquide de Fermi.

Abstract

In this Thesis, we develop an effective low energy Fermi liquid formalism to describe the electron dynamics in the strongly interacting quantum RC circuit. This device is composed of a quantum dot connected to an electron reservoir by a quantum point contact. The dot is coupled capacitively to a top metallic gate. Direct current is forbidden and electron transport can be observed if the quantum dot is driven by a time dependent gate potential. Theoretical and experimental studies confirmed the analogy to a classical RC circuit and showed a violation of Kirchhoff's laws for phase-coherent transport: the charge relaxation resistance of the quantum RC circuit is universally quantized to $R_q = h/2e^2$, regardless of the quantum point contact transmission, in striking contrast to direct transport measurements. We consider Coulomb blockade regimes caused by strong electronic interactions on the dot. For both spinless and spinful electrons, we show electron dynamics to be effectively non-interacting at low temperature. We derive a generalized Korringa-Shiba relation, predicting universal quantization for the charge relaxation resistance even in the presence of strong interactions on the dot. We also study non-universal behaviors of R_q for spinful electrons in the presence of a magnetic field. We focus on the Kondo regime and show the emergence of a giant peak for R_q caused by the destruction of the Kondo singlet. We extend our approach to the SU(4) symmetric case, relevant in the case of further orbital degeneracy on the dot. The analytical methods developed in this work are applied to obtain the exact expression of the SU(4) Kondo temperature.

Keywords : mesoscopic physics, coherent electron dynamics, quantum RC circuit, Kondo effect, Coulomb blockade, Fermi liquid.